申报	系列：教师系列教学与科研并重型
	专业：农业机械化工程
	职称：副教授

业绩成果材料

（申报人的业绩成果材料包括论文、科研项目、获奖以及其他成果等）

单　位（二级单位）　工程学院

姓　名　林彩霞

材料核对人：　　单位盖章：

核对时间：

华南农业大学制

目　录

一、教学研究业绩

1.教育教学改革与研究项目：《汽车营销应用型课程与教学内容体系改革研究与实践》的申报书及立项批复..... 1

2.教学比赛证书：广东省高校教师教学创新大赛二等奖.. 14

3.编写教材：参编十一五规划教材《汽车运用技术》《汽车服务企业管理》、十二五规划教材《汽车市场营销学》，主编《汽车美容装饰工等级考试教材》 15

二、科研项目

1.主持：

1.1.十四五国家重点研发计划子课题“小粒/异形种子高效精量育苗播种生产线研制”任务书 45

1.2.广东省省级科技计划项目“山地果园运输车可发电式轮边缓速制动技术研究与示范”合同书 57

2.主参：

2.1.项目“适应丘陵山区农业作业的通用动力装备及高效作业机具攻关项目”研究任务书 70

2.2.国家重点研发计划“重型拖拉机无级变速传动技术研究与样机开发”课题合作协议 80

2.3.国家自然科学基金面上项目“轴承间隙粘弹性润滑剂的非线性动力学分析”计划书 84

三、论文、著作等

1.检索证明 92

2.以第一作者发表本专业论文情况

2.1. 基于量纲分析的液力缓速器制动性能试验分析 98

2.2. 基于台架检测汽车滚动阻力的修正模型 109

2.3. 液力缓速器能量耗散方程的建立 117

2.4. 液力缓速器制动系统的能效分析 126
2.5. 液力缓速器研究进展 134
2.6. 双转子摆线泵流量特性分析及优化设计 143
2.7. 在用车滑行检测台架与道路差异性研究 152
3.以通讯作者发表本专业论文情况
3.1. Nondestructive identification of Litchi Downy Blight at different stages based on spectroscopy analysis 160
3.2. A novel method for detecting missing seedlings based on UAV images and rice transplanter operation information ... 177
3.3. Analysis of radial electromagnetic force in claw pole alternator considering excitation current harmonics 188

四、科研成果

1.知识产权
1.1.实用新型专利授权证书：一种山地果园运输车可发电式轮边缓速装置 204
1.2.实用新型专利授权证书：基于舵机驱动的曲柄滑块式末端执行器及茶叶采摘机器 205
1.3.实用新型专利授权证书：减速器变速工况轴承力预测方法、装置、设备及介质 206

五、其他业绩

1.指导学生学科竞赛
1.1.第九届广东大学生科技学术节之节能减排工业设计大赛优胜奖证书 207
1.2. 第十五届全国大学生节能减排社会实践与科技竞赛校内选拔赛一等奖证书 208
1.3. 第九届广东省汽车与农机电子环保大赛三等奖 209
2.个人荣誉

2.1.工程学院优秀班主任证书 210
2.2.工程学院“十二五”工作先进个人证书..... 211
2.3.华南农业大学“优秀共产党员”证书..... 212
2.4.工程学院 “优秀共产党员”证书..... 213

JG11059

华南农业大学教育教学改革与研究项目

申　　报　　书

项目名称：汽车营销应用型课程与教学内容体系改革研究与实践

申 请 人：林彩霞

申请单位：工程学院

联系电话：

移动电话：[redacted]

电子邮箱：cxlin76@163.com

申报日期：2011.6.3

华南农业大学教务处　制

一、简表

<table>
<tr><td rowspan="3">项目简况</td><td>项目名称</td><td colspan="6">汽车营销应用型课程与教学内容体系改革研究与实践</td></tr>
<tr><td>项目类别</td><td colspan="6">A、招标项目　　B、重点项目　　C、√一般项目　　D、自筹项目</td></tr>
<tr><td>起止时间</td><td colspan="6">2011 年 12 月 —— 2013 年 12 月</td></tr>
<tr><td rowspan="11">项目申请人</td><td>姓名</td><td colspan="2">林彩霞</td><td>性别</td><td>女</td><td>出生年月</td><td></td></tr>
<tr><td colspan="2">专业技术职务</td><td colspan="2">讲师</td><td colspan="2">行政职务</td><td></td></tr>
<tr><td colspan="2">学历</td><td colspan="2">研究生</td><td colspan="2">最终学位</td><td>硕士</td></tr>
<tr><td rowspan="3">所在单位及联系方式</td><td>单位名称</td><td colspan="5">工程学院</td></tr>
<tr><td>电话</td><td colspan="5">（O）　　（H）
（手机）：</td></tr>
<tr><td>E－mail</td><td colspan="5">cxlin76@163.com</td></tr>
<tr><td rowspan="4">主要教学工作简历</td><td>时间</td><td>课程名称</td><td>授课对象</td><td>学时</td><td colspan="2">所在单位</td></tr>
<tr><td>2009 春</td><td>交通运输企业设计与管理</td><td>2006 交通运输</td><td>32</td><td colspan="2">工程学院</td></tr>
<tr><td>2009 秋</td><td>现代汽车营销</td><td>交通运输</td><td>32</td><td colspan="2">工程学院</td></tr>
<tr><td>2010 春</td><td>汽车概论</td><td>公选课</td><td>32</td><td colspan="2">全校</td></tr>
<tr><td rowspan="5">主要教学改革和科学研究工作简历</td><td>时间</td><td colspan="3">项目名称</td><td colspan="2">获奖情况</td></tr>
<tr><td>2004——2006</td><td colspan="3">汽车服务工程课程建设与教学改革方法的研究</td><td colspan="2"></td></tr>
<tr><td>2007——2009</td><td colspan="3">国家自然科学基金轴承间隙粘弹性润滑剂的非线性动力性分析</td><td colspan="2"></td></tr>
<tr><td>2009——2012</td><td colspan="3">基于模糊推理的驾驶疲劳机理及辨识方法研究　广东省自然科学基金</td><td colspan="2"></td></tr>
<tr><td></td><td colspan="3"></td><td colspan="2"></td></tr>
<tr><td rowspan="3">项目组</td><td>总人数</td><td>高级</td><td>中级</td><td>初级</td><td>博士后</td><td>博士</td><td>硕士</td><td></td></tr>
<tr><td>5</td><td>2</td><td>3</td><td></td><td></td><td></td><td></td><td></td></tr>
<tr><td>主要成员（不含申请者）</td><td>姓名</td><td>性别</td><td>出生年月</td><td>职称</td><td colspan="2">工作单位</td><td>分工</td><td>签名</td></tr>
<tr><td></td><td>王海林</td><td>男</td><td></td><td>教授</td><td colspan="2">工程学院</td><td>就业指导</td><td></td></tr>
</table>

2

		何效平	女	[illegible]	讲师	工程学院	多媒体课件制作	何效平
		赵新	男	[illegible]	副教授	工程学院	案例分析	赵新
		张建莉	女	[illegible]	讲师	工程学院	营销模拟平台的建立	张建莉

3

二、立项依据：（项目的意义、现状分析）

1、项目的意义

2007年，中国汽车产销量双双突破800万辆，近几年并保持每年近20%的增长速度，年产销1000万辆大关突破在即。亿万中国家庭已经为拥有汽车、进入汽车生活做好了准备。作为世界最大的汽车消费潜力市场和世界排名第二的汽车消费市场，中国汽车市场蕴藏的市场机遇是前所未有的。也正因此，中国汽车市场的竞争激烈程度也达到了空前激烈的境地。当前，众多的汽车厂家、众多的品牌和车型充斥市场，卖方市场已经完全进化为买方市场，汽车行业正在加快优胜劣汰的进程。作为一个潜力巨大、开发并不充分的消费市场，对于任何品牌和任何经营者都有胜出的机会。其前提是：必须卖好车，必须做好营销。对厂家是如此，对经销商更是如此。如何快速有效地提升企业经营业绩，取决于营销方略的科学与合理性，取决于企业营销人才与营销队伍的执行能力。汽车企业要在竞争中立于不败之地甚至占领先机，就必须拥有一流的汽车营销人才。但是，由于高级汽车营销人才的匮乏，相当比例的汽车企业并未能取得如期的经营效果，如2010年比亚迪汽车经销商退网事件，导致比亚迪去年业绩下滑，或使汽车企业处于亏损乃至倒闭的边缘。

因此各地区各企业对汽车营销人才的需求一直维持在较高水平。许多企业由于找不到合格的汽车营销人才而抱怨学校培养的优秀营销人才太少。而对营销人才教育方面，一些学校针对汽车市场的需求，开始了汽车营销的专业化教育。如复旦大学开办了汽车营销EMB专业；同济大学成立了汽车营销管理学院；高职高专院校开设汽车营销专业等等，这一切都表明汽车营销人员已经成为热门人才，汽车营销教育已经成为一个新兴的学科。

然而，高职学院汽车技术营销专业的毕业生又因基础理论短缺、专业领域过于狭窄，而无法在企业发挥作用。而综合性大学培养的应用型人才又具有明显的教育学术化倾向，在实践和动手能力上明显缺乏，因此，高等工程教育急需向更高层次延伸，而在当前，培养大量的具有一定的汽车

4

产品知识和营销理论知识基础，营销意识强，发现问题和解决问题能力强为主要特征的新型本科应用型人才，以实现把营销理论尽快地转化为现实生产力，是主动适应时代发展的要求，也是面向高新技术发展的迫切需要。因此，必须对目前的汽车营销课程进行改革，打造全新的以就业为导向的应用型汽车营销课程，培养适应社会需求的本科汽车营销人才。

2、现状分析

我校车辆工程系只有车辆工程专业和交通运输专业，这两个专业设置了现代汽车营销课程，培养目标偏向汽车维修、保养等方向；而经济管理学院的市场营销专业培养目标偏向市场营销人员，对汽车行业针对性不强。和其它院校的汽车营销专业相比，我系汽车营销人才培养目标欠明确，而且由于学生传统观念的影响，片面地认为汽车营销就是卖车，所以在就业上，出现普遍选择不做汽车营销。

在课程内容上，主要是汽车营销知识讲解和案例分析，学生分析问题的能力较强，但由于教学中社会实践活动安排较少，学生实际操作能力和解决实际问题的能力并不是很强，存在着课程学习的理论与实用性之间的矛盾问题。在教学方法中，主要采用老师讲解、学生提问、板书和多媒体结合的方式，针对实践性内容较少。

三、项目实施方案及实施计划

1.具体改革内容、改革目标和拟解决的关键问题

具体改革内容：

（1）教学指导思想的改革创新

以讲座或案例分析的形式，建立汽车营销理念，在一定程度上改变学生对汽车营销就业的传统观念，提高学生对汽车营销就业的认识。而且，市场营销观念：市场竞争、市场分析、购买者行为分析、目标市场、产品策略、定价策略、产品分销策略、产品促销策略与人生的职业规划有很大关系，人生面临着各种竞争，要对各种竞争和市场以及自身都要进行分析和定位，以谋划面对各种情况的策略。因此，可以利用市场营销观念进行职业规划。

（2）教学方法的改革创新

学生的学习能力、创新能力和在不可预见的情况发生时灵活处理问题的能力至关重要。这种能力不可能通过传统的“粉笔+讲课”的教学方法获得,而案例教学是培育学生学习能力、创新能力和磨练他们战略决策能力的最好方法。因此，在以案例分析学习汽车营销知识的基础上，进一步加强案例教学。任课老师首先通过各种视听媒体,对营销活动的典型事件展开情景描述和分析,其次要指定一个学生说明案例、分析问题并提出解决问题的手段,或定出实现公司目标的方法和途径。然后,其他同学从自己的角度来分析同一个案例,阐述自己的观点和采取的措施,以及指出自己在什么地方比前一个发言者更好。讨论一个案例需要 1-2 个学时。汽车营销基本内容针对每一章如：汽车市场竞争、汽车市场调研与分析、汽车购买者行为分析、汽车目标市场、汽车产品策略、汽车定价策略、汽车产品分销策略、汽车产品促销策略及战略规划，如每章一个案例共讨论 9 个案例,那么就需要 10-20 个学时,这样会影响到基础理论的讲授时间。为了在教学中既给学生讲授理论知识,又能讨论案例,在教学时间安排上需要作一些调整。增加学生在课前对课程的自学时间,教师在讲课时,对教学大纲中的重点内容仍系统讲授,对一般内容则讲授要点。这样,就可以把节省下来的讲课时间用于案例讨论。这样，就需要一个提供学生预习资料的平台——即汽车营销

6

课程网站建设。

同济大学建立汽车营销实训基地的培养模式,依托同济大学汽车专业软硬件优势,给学生提供了实践锻炼的机会。由于条件的限制，现在建立汽车营销实训基地很困难。借鉴经管学院的现代营销决策模拟系统，为提高学生处理实际问题的能力，拟在网站上开发汽车营销实战模拟平台。培养能够适应企业要求的高级汽车营销人才。

（3）教学内容的改革创新

在营销知识的基础上，增加言行举止礼仪规范、经济法律、谈判基本技巧方面的内容。同时借助汽车营销课程学习网站，给学生更多的学习机会。

改革目标：

提高学生对汽车营销职业的认识，进一步接受汽车营销职业；结合案例教学法、汽车营销课程网站以及汽车营销实战模拟平台，提高学生实际训练能力，培养适应企业需要的高级汽车营销人才。

拟解决的关键问题：

汽车营销课程网站以及汽车营销实战模拟平台建设。

2.实施方案、实施方法、具体实施计划（含年度进展情况）及可行性分析

实施方案、实施方法：

首先对用于教学的案例进行筛选，取自世界汽车企业的市场营销管理实践,尽量采用近年来发生的事情。为了保证这些案例的多样性和全面性,在把它用于正式教学之前,教师都要经过反复认真地分析。案例的正确答案只对学生们起某种提示或引导作用。因此,有时在案例制作时,故意漏了一些重要资料或数据,以免限制学生们的思维,妨碍答案的多元化,这样可以让学生针对环境变化寻找出更好的、更有效的解决方法。结合案例分析和视频、图片等资料编制多媒体课件，让学生上课更容易了解和掌握。

其次，对学生和老师以发放问卷的方式进行网站建设的调研，来获得网站建设的内容和式样，根据反馈意见把汽车营销课程网站和汽车营销实

7

战模拟平台建立起来。初步设想可以实现以下内容：

（1）案例教学区　　用于案例教学的案例和视听材料

（2）老师提问区　　教学难点和重点，让学生做好预习

（3）查询功能区

（4）交流论坛区　老师和学生互动平台

（5）营销实战模拟区　汽车营销实战模拟平台

（6）资料上载和下传区

具体实施计划：

2011.9-2011.12　案例分析、总结以及多媒体课件的开发；

2012.1-2012.6　网站建设调研分析以及网站建设；

2012.7-2012.12　汽车营销实战模拟平台建设；

2013.1-2013.6　情景化、实践化教学方法的实际应用；

2013.7-2013.12　对教学改革进行总结。

可行性分析：

1）符合国家政策和时代特色要求

教高[2007]2 号文件中要求高校深化教育改革、全面加强大学生素质培养，建立与社会经济发展相适应的教学体系，高度重视实践环节，提高大学生实践能力。

案例教学法、网络和实践教学在发达国家早已成熟，并深入开展，我国名牌大学也把这种教学模式用在高校人才培养上。

2）我校车辆工程系拥有高素质的队伍，师资力量较为雄厚，在教术教学方面有较强的实力。这些为本课题的开展提供实践基础。

3）有先进的基础设备

我校校园网采用光纤，迅速便捷的实现宿舍网络与校园网的互联，为大学生免费利用校内资源自主学习创造了条件，为开展网络与实践教学相结合的教学模式提供了报障。

4）丰富的校园网资源

网络教学资源库得到学校的重点建设，学校图书馆购买了大量专业数据库资源，为本课题的取材和资料提供了条件。

8

3.项目预期的成果和效果（包括成果形式，预期推广、应用范围、受益面等）

1）多媒体教学课件
2）汽车营销课程网站以及汽车营销实战模拟平台
3）把这种优质的教学模式应用在我系的教学实践中，为我校培养高水平人才
4）受益对象以后的车辆工程专业和交通运输专业的学生

4.本项目的特色与创新之处

1）教育指导思想创新，把市场营销理念应用于学生的就业规划

2）教学方法创新，案例分析教学方法、课程网络教育以及营销实战模拟平台，培养适应社会需要的人才

9

四、现有研究基础

1.与本项目有关的研究积累或已取得的教学改革工作成绩

1）项目主持人参编了林业出版社十二五规划教材《汽车营销》

2）已有基本内容的多媒体课件以及部分案例分析

3）学生就业质量的提高，有不少学生在本田、丰田等知名企业工作，他们为母校提供了很多信息和资源，为网站和实战模拟提供了第一手资料

2.单位已具备的教研基础和环境及项目的支持情况，尚缺少的条件和拟解决的途径

我系有自己的汽车运用实验室，并在省级重点实验中心申请建设时积累了大量的视听材料和教学资源。

3.申请者和项目组成员所承担的教学改革和科研项目情况

林彩霞，女。华南农业大学工程学院，讲师，硕士，研究方向为机械设计理论。先后参加了交通部西部交通科技项目“ASM 用汽车底盘综合性能测功机及控制系统的开发研究”（200139836576-2）、国家自然科学基金“轴承间隙粘弹性润滑剂的非线性动力性分析”（No：10602019）等课题的研究，硕士学位论文《在用车动力性检测台架与路试差异性研究》获得优秀硕士论文奖。2011年被评为校级骨干青年教师。

发表的论文：

[1] 刘浩学，林彩霞，马强骏，朱玉平. 基于台架检测汽车滑行距离的修正模型长安大学学报（自然科学版）. 2006,26（2）：88-90.

[2] 林彩霞，刘浩学. 基于台架检测汽车滚动阻力的修正模型. 汽车技术，2010,（4）：46-49.

[3] 林彩霞，张建莉. 三元催化器冷启动问题探讨.农机使用与维修，2009 .（4）：45-46.

[4] 林彩霞，张建莉，何效平. 液力缓速器制动性能影响因素分析. 2009 年农业工程学会会议论文集.

[5] 林彩霞，张建莉 ，何效平. 液力缓速器制动性能分析.汽车与安全，2009，（6）：63-66.

[6] 林彩霞.汽车服务工程. 多媒体课件的开发. 中国教育教学杂志，

10

2009. 06.

参编的教材：

[1] 汽车服务企业管理. 北京理工大学出版社. 高等学校“十一五”规划教材. 2008 年

[2] 汽车运用技术. 北京理工大学出版社. 高等学校“十一五”规划教材. 2007 年

[3] 汽车美容装饰工等级考试教材. 副主编. 机械工业出版社. 2009 年

参与的课题：

国家自然科学基金 No：10602019 轴承间隙粘弹性润滑剂的非线性动力性分析 2007-2009 排名第三 25 万

广东省自然科学基金 排名第三 No：9151802904000002 基于模糊推理的驾驶疲劳机理及辨识方法研究 2009-2012

11

五、经费预算

支出科目	金额（元）	计算根据及理由
合计	3000	
1. 调研	500	调研教改模式
2. 资料	1000	案例资料的收集
3. 多媒体课件开发	500	汽车营销上课需要的课件
4. 汽车营销实战模拟网站	1000	建立网站所需的资料
5.		
6.		

六、申请者所在单位评审、推荐意见

单位意见

同意申报

（公章）

单位领导签字：王海林

二〇一一年三月九日

12

七、评审小组意见

同意立项

评审小组长签字：

二〇一一年 8 月 30 日

八、学校意见

同意立项

签章：

二〇一一年 8 月 31 日

13

NATIONAL TEACHING INNOVATION CONTEST FOR COLLEGE TEACHERS 全国高校教师教学创新大赛

首届全国高校教师教学创新大赛广东分赛

暨广东省高校教师教学创新大赛

获奖证书

主讲教师： 王海林

团队成员： 赵新、林彩霞、周锡恩

主讲课程： 《汽车检测与诊断技术》

获奖等级： 二等奖（正高组）

证书编号： GDTIC2021026

广东省高等教育学会　华南师范大学

2021年4月

高等院校“十一五”规划教材·汽车类

汽车运用技术

王海林　迟瑞娟　主编　　朱余清　高爱云　副主编

QICHEYUNYONGJISHU

北京理工大学出版社
BEIJING INSTITUTE OF TECHNOLOGY PRESS

内 容 提 要

本书立足于汽车运用实践，以汽车使用、维护、服务为对象，主要介绍汽车使用条件的特性，汽车使用性能及评价指标，汽车运行材料及其合理使用，汽车节能技术，汽车安全技术，汽车公害及其预防，汽车在特殊条件下的使用，汽车技术状况及其变化与维护，汽车检测诊断技术，汽车试验技术，汽车使用寿命与鉴定，汽车运用服务系统等。在编写内容上注意了前瞻性、科学性、知识性，特别注重实用性。

本书可作为高等学校汽车服务工程、汽车运用工程、交通运输及交通工程专业的教材或教学参考书，也适用于高职高专汽车类各专业的教材，可作为汽车服务的培训教材，也可供汽车运用部门的技术管理人员学习参考。

图书在版编目（CIP）数据

汽车运用技术／王海林，迟瑞娟主编．—北京：北京理工大学出版社，2007.7

ISBN 978-7-5640-1223-6

Ⅰ.汽…　Ⅱ.①王…②迟…　Ⅲ.汽车-使用-高等学校-教材　Ⅳ.U471.2

中国版本图书馆 CIP 数据核字（2007）第 082513 号

出版发行／北京理工大学出版社
社　　址／北京市海淀区中关村南大街 5 号
邮　　编／100081
电　　话／(010)68914775(办公室) 68944990(批销中心) 68911084(读者服务部)
网　　址／http：// www.bitpress.com.cn
经　　销／全国各地新华书店
印　　刷／北京国马印刷厂
开　　本／787 毫米×1092 毫米　1/16
印　　张／22.5
字　　数／537 千字
版　　次／2007 年 7 月第 1 版　2007 年 7 月第 1 次印刷
印　　数／1～4000 册　　责任校对／张　宏
定　　价／35.00 元　　责任印制／母长新

前 言

汽车工业是国民经济的支柱产业之一，是高度专业化、自动化的综合性工业。我国加入WTO后，汽车工业迎来了新的机遇与挑战。近年来，中国汽车保有量和产销量快速增长，大大促进了交通运输及汽车运用与服务的发展。

汽车运用与服务涉及车辆使用性能、道路环境及服务等诸多因素，本书主要介绍汽车使用条件的特性，汽车使用性能及评价指标，汽车运行材料及其合理使用，汽车节能技术，汽车安全技术，汽车公害及其预防，汽车在特殊条件下的使用，汽车技术状况及其变化与维护，汽车检测诊断技术，汽车试验技术，汽车使用寿命与鉴定，汽车运用服务系统等。

本书是根据中国汽车工程学会教材出版委员会关于汽车服务工程教材建设会议精神，结合多年来的科学研究与教学实践，在参考国内外大量研究成果的基础上，本着前瞻性、科学性、知识性、实用性的原则编写的。

本书由华南农业大学王海林副教授和中国农业大学迟瑞娟副教授主编，参加编写的有：朱余清（华南农业大学，第1、3章）、王海林（第2、4章）、迟瑞娟（第5、6章）、张毅（黑龙江工程学院，第7、8章）、高爱云（河南科技大学，第9、10章）、林彩霞（华南农业大学，第11、12章）。全书由王海林、迟瑞娟统稿。林伟兰、罗文豪也参与了本书的修改工作。

本书可作为高等学校或高职高专汽车运用工程、汽车服务工程专业的教材，也可作为交通运输、车辆工程、交通工程等专业师生及汽车运用与服务技术工程人员的参考书。

在本书编写过程中，得到了许多领导及同事的指导和关注，并参考引用了大量的国内外文献资料，谨此深表感谢。

鉴于汽车运用技术的复杂性，许多问题尚待探索，加之编者水平有限，书中贻误和不妥之处，恳请使用本书的师生和读者批评指正。

编 者

目 录

第1章 汽车使用条件 …… (1)
1.1 概述 …… (1)
1.2 气候条件 …… (2)
1.3 道路条件 …… (3)
1.4 运输条件 …… (5)
1.5 汽车高速公路使用条件 …… (8)
1.6 汽车运用水平 …… (9)
1.7 汽车运行技术条件 …… (10)
1.8 汽车运行工况 …… (11)
思考题 …… (12)

第2章 汽车性能及评价指标 …… (13)
2.1 汽车的动力性 …… (13)
2.2 汽车燃油经济性及评价指标 …… (24)
2.3 汽车行驶的安全性 …… (26)
2.4 汽车的平顺性 …… (44)
2.5 汽车的通过性 …… (46)
2.6 汽车排放污染及其控制指标 …… (49)
2.7 汽车使用性能量标 …… (52)
思考题 …… (55)

第3章 汽车运行材料及其合理使用 …… (56)
3.1 汽车燃料及其合理使用 …… (56)
3.2 发动机油及其合理使用 …… (64)
3.3 车辆齿轮油及其合理使用 …… (73)
3.4 汽车润滑脂及其合理使用 …… (78)
3.5 汽车制动液及其合理使用 …… (82)
3.6 汽车液力传动油及其合理使用 …… (86)
3.7 汽车其他工作液及其合理使用 …… (90)
3.8 汽车轮胎及其合理使用 …… (94)
思考题 …… (104)

第4章 汽车节能技术 …… (106)
4.1 概述 …… (106)
4.2 汽车技术状况与节能的关系 …… (108)
4.3 汽车节能途径和技术 …… (111)
4.4 汽车新能源 …… (131)
思考题 …… (136)

第5章 汽车安全技术 …… (137)
5.1 概述 …… (137)
5.2 汽车安全技术法规与标准 …… (141)
5.3 汽车主动安全技术 …… (152)
5.4 汽车被动安全技术 …… (154)
5.5 汽车被动安全性试验 …… (169)
思考题 …… (176)

第6章 汽车公害 …… (177)
6.1 概述 …… (177)
6.2 汽车排气污染物的形成及试验 …… (181)
6.3 汽车噪声及试验 …… (193)
思考题 …… (206)

第7章 汽车在特殊条件下的使用 …… (207)
7.1 汽车走合期的使用 …… (207)
7.2 汽车在低温条件下的使用 …… (209)
7.3 汽车在高原和山区条件下的使用 …… (214)
7.4 汽车在高温条件下的使用 …… (217)
7.5 汽车在坏路和无路条件下的使用 …… (220)
思考题 …… (222)

第8章 汽车技术状况的变化 …… (223)
8.1 汽车技术状况与汽车运用性能的变化 …… (223)
8.2 影响汽车技术状况变化的因素 …… (225)
8.3 汽车技术状况变化规律 …… (229)
8.4 汽车技术状况的维护 …… (230)
思考题 …… (233)

第9章 汽车诊断与检测 …… (234)
9.1 概述 …… (234)
9.2 汽车故障及其诊断方法 …… (236)

9.3 汽车诊断参数 …… (239)
9.4 汽车检测制度 …… (242)
9.5 汽车常见的诊断与检测设备 …… (244)
9.6 汽车电控系统的诊断与检测 …… (254)
思考题 …… (267)

第 10 章 汽车试验技术 …… (268)
10.1 概述 …… (268)
10.2 汽车动力性试验 …… (271)
10.3 汽车燃油经济性试验 …… (275)
10.4 汽车制动性试验 …… (278)
10.5 汽车操纵稳定性试验 …… (281)
10.6 汽车平顺性试验 …… (287)
10.7 汽车可靠性试验 …… (291)
10.8 汽车通过性试验 …… (295)
思考题 …… (298)

第 11 章 汽车使用寿命及鉴定 …… (299)
11.1 概述 …… (299)
11.2 汽车使用寿命评价指标 …… (299)
11.3 汽车更新 …… (300)
11.4 在用车评估与鉴定 …… (308)
思考题 …… (323)

第 12 章 汽车运用服务 …… (324)
12.1 汽车维修 …… (324)
12.2 汽车美容 …… (327)
12.3 备件供应 …… (330)
12.4 人才培训 …… (333)
12.5 质量保证 …… (335)
12.6 旧车置换 …… (338)
12.7 报废回收 …… (342)
12.8 客户联系 …… (346)
思考题 …… (347)

主要参考文献 …… (348)

汽车文化
汽车公害控制
汽车运用技术
汽车服务工程
汽车试验技术
汽车测试技术
汽车诊断技术

汽车服务企业设计
汽车商品国际贸易
汽车物流与信息技术
二手车评估与交易实务
汽车装饰与车身修复技术
汽车服务工程毕业设计指导书

汽车维修工程
汽车专业英语
汽车营销策划
汽车再生技术
汽车金融服务
汽车保险与理赔
汽车服务企业管理

责任编辑／刘志实
封面设计／七星工作室

ISBN 978-7-5640-1223-6

9 787564 012236 >

定价：35.00元

高等院校“十一五”规划教材·汽车类

汽车服务企业管理

朱 刚 王海林 主编

QICHE FUWU QIYE GUANLI

北京理工大学出版社
BEIJING INSTITUTE OF TECHNOLOGY PRESS

内 容 简 介

本书根据汽车服务企业的特点，运用现代企业管理的理论和方法，对企业各项管理活动进行了系统的论述，其主要内容包括汽车服务行业管理概述、企业筹建与开业、人力资源与培训管理、全面质量管理、汽车服务企业财务与成本管理、汽车服务企业设备管理、服务企业的信息管理、汽车售后服务管理、服务企业的督察与处罚、汽车服务企业文化等。这些内容既适合一般汽车维修企业，又适合4S店、特约服务站。

图书在版编目（CIP）数据

汽车服务企业管理／朱刚，王海林主编．—北京：北京理工大学出版社，2008.5

高等院校“十一五”规划教材．汽车类

ISBN 978-7-5640-1399-8

Ⅰ.汽…　Ⅱ.①朱…②王…　Ⅲ.汽车工业-工业企业管理-高等学校-教材　Ⅳ.F407.471.6

中国版本图书馆CIP数据核字（2008）第043022号

出版发行／北京理工大学出版社
社　　址／北京市海淀区中关村南大街5号
邮　　编／100081
电　　话／(010)68914775(办公室) 68944990(批销中心) 68911084(读者服务部)
网　　址／http://www.bitpress.com.cn
经　　销／全国各地新华书店
印　　刷／保定市中画美凯印刷有限公司
开　　本／787毫米×1092毫米　1/16
印　　张／16.75
字　　数／391千字
版　　次／2008年5月第1版　2008年5月第1次印刷
印　　数／1~4000册　　责任校对／陈玉梅
定　　价／30.00元　　责任印制／吴皓云

前 言

由于汽车工业具有很强的产业关联度，因此被视为国家经济发展水平的一个重要标志。近10年来，我国汽车工业快速而稳步发展，汽车工业的繁荣，使汽车及其相关产业的人才需求量大幅度增长。尽管我国很多汽车服务企业已经初具规模，但未来几十年是一个对汽车服务行业充满挑战的时代，汽车技术的飞速发展，必然带来一场汽车服务行业的革命，传统的维修模式、经营方式、管理手段已经远远不能适应现代激烈的市场竞争的需要，汽车服务企业需要接受新的管理理念，需要一批业务全面的综合型管理人才。

本书根据汽车服务企业的特点，运用现代企业管理的理论和方法，对企业各项管理活动进行了系统的论述，其主要内容包括汽车服务行业管理概述、企业筹建与开业、人力资源与培训管理、全面质量管理、汽车服务企业财务与成本管理、汽车服务企业设备管理、服务企业的信息管理、汽车售后服务管理、服务企业的督察与处罚、汽车服务企业文化等。这些内容既适合一般汽车维修企业，又适合4S店、特约服务站。

本书主编为华南理工大学朱刚、华南农业大学王海林，章节分配如下：朱刚（华南理工大学）编写第1、2、4章，王海林、林彩霞（华南农业大学）编写第3、8、10章，杨守丽（辽宁工学院）编写第5、6章，重庆大学贺岩松编写第7、9章。

由于编者水平有限，书中难免有不当之处，敬请读者批评指正。

编 者

目 录

第1章 汽车服务企业管理概述 …… (1)
1.1 服务企业现代化管理 …… (1)
1.2 服务企业的管理素质 …… (6)
思考题 …… (18)

第2章 企业的筹建与开业 …… (19)
2.1 企业的筹建 …… (19)
2.2 开业标准 …… (29)
思考题 …… (39)

第3章 人力资源与培训管理 …… (40)
3.1 人力资源管理 …… (42)
3.2 员工培训管理 …… (51)
3.3 绩效评估 …… (56)
3.4 报酬与激励 …… (60)
思考题 …… (66)

第4章 全面质量管理 …… (67)
4.1 质量管理概述 …… (67)
4.2 质量的分析方法 …… (76)
4.3 维修质量的评价 …… (88)
思考题 …… (93)

第5章 汽车服务企业财务成本管理 …… (94)
5.1 汽车服务企业财务管理 …… (94)
5.2 汽车服务企业成本费用管理 …… (116)
思考题 …… (124)

第6章 汽车服务企业设备管理 …… (125)
6.1 设备管理概述 …… (125)
6.2 设备的选择与评价 …… (128)
6.3 设备的使用、维护与修理 …… (131)
6.4 汽车服务企业的设备更新与改造 …… (138)

思考题 …… (146)

第 7 章 服务企业的信息管理 …… (147)
7.1 信息管理系统 …… (147)
7.2 互联网络 …… (153)
7.3 电子商务 …… (163)
7.4 企业资源计划 …… (172)
思考题 …… (174)

第 8 章 汽车售后服务管理 …… (175)
8.1 汽车售后服务概述 …… (175)
8.2 信贷服务与购车 …… (175)
8.3 汽车保险与理赔 …… (177)
8.4 旧车交易服务 …… (182)
8.5 汽车配件供应 …… (193)
8.6 汽车维修与检测 …… (196)
8.7 汽车美容与装饰 …… (204)
思考题 …… (209)

第 9 章 汽车维修服务企业的督查与处罚 …… (210)
9.1 汽车维修行业与督查管理 …… (210)
9.2 汽车维修服务行业监督管理 …… (213)
9.3 汽车维修合同管理 …… (216)
9.4 汽车维修的违章与处罚 …… (221)
思考题 …… (231)

第 10 章 企业文化 …… (232)
10.1 企业文化概述 …… (232)
10.2 企业文化建设 …… (242)
10.3 企业形象 …… (247)
思考题 …… (255)

参考文献 …… (256)

封面设计／七星工作室
责任编辑／何 士娟

ISBN 978-7-5640-1399-8

定价：30.00 元

普通高等教育汽车与交通类专业“十二五”规划教材

汽车市场营销学

肖 艳 孙庆峰 主编

中国林业出版社

内 容 简 介

本书在国内外相关研究成果的基础上，运用文献分析和案例研究等方法，系统全面地阐述了汽车市场营销学的基本原理、方法及策略。主要内容包括汽车市场营销战略、汽车市场调查与预测、汽车市场营销组合策略、汽车品牌营销、二手车营销、汽车服务营销和汽车国际营销等。本书将理论上的探索性、知识上的实用性、操作上的写实性和技巧上的启示性相统一，突出实践性和系统性等特点。既能为读者提供完整的理论视角，又能为读者提供可借鉴的汽车营销运作技能。

本书可以作为高等院校交通运输、汽车运用工程、汽车服务工程等专业的本科教材，也可以作为相关专业的教学参考用书、汽车营销从业人员自学参考用书。

图书在版编目（CIP）数据

汽车市场营销学 / 肖艳，孙庆峰主编. —北京：中国林业出版社，2012.3
普通高等教育汽车与交通类专业“十二五”规划教材
ISBN 978-7-5038-6485-8

Ⅰ. ①汽… Ⅱ. ①肖… ②孙… Ⅲ. ①汽车—市场营销学—高等学校—教材
Ⅳ. ①F766

中国版本图书馆 CIP 数据核字（2012）第 020067 号

中国林业出版社·教材出版中心
策划编辑：牛玉莲 杜 娟
责任编辑：杜 娟
电 话：83221489 83220109 传真：83220109

出版发行：中国林业出版社（100009 北京西城区德内大街刘海胡同 7 号）
E-mail：jiaocaipublic@163.com 电话：（010）83224477
http://lycb.forestry.gov.cn
经 销：新华书店
印 刷：北京市昌平百善印刷厂
版 次：2012 年 3 月第 1 版
印 次：2012 年 3 月第 1 次印刷
开 本：787mm×1092mm 1/16
印 张：14.75
字 数：339 千字
定 价：29.00 元

本书编写人员名单

主　　编　肖　艳　孙庆峰

副 主 编　施继红　韩志刚　马振江

编写人员　（以拼音为序）

巴兴强　东北林业大学

陈来荣　北京林业大学

韩志刚　中南林业科技大学

林彩霞　华南农业大学

马振江　东北林业大学

施继红　吉林农业大学

孙庆峰　北华大学

肖　艳　北华大学

赵建光　北华大学

前　言

新中国汽车工业走过了半个多世纪的沧桑历程，经过几代汽车人的不懈努力，取得了举世瞩目的成就。但是，作为我国国民经济支柱产业的汽车工业，在创新能力、建设规模、市场培育、营销模式、营销策略等方面，与汽车工业强国相比仍存在较大差距，中国汽车人任重而道远。

本书作为高等院校交通运输、汽车服务工程、汽车运用工程等专业的规划教材，系统阐述了汽车市场营销基本原理、方法及策略，主要内容包括汽车市场营销战略、汽车市场调查与预测、汽车市场营销组合策略、汽车品牌营销、二手车营销、汽车服务营销和汽车国际营销等。本教材体现出以下特色：一是理论上凸显前瞻性，在理论阐释中引入网络营销、电子商务、品牌营销；二是案例上凸显适用性，紧密结合国际主要汽车公司的营销运作实际；三是篇章上凸显简约性，篇章结构模块化设计，尽量精简、浓缩。

为了满足教学的要求，教材编写过程中始终坚持明确的思路与定位。首先是在内容方面：传承和创新并重，把握经济社会发展脉搏，关注相关领域的最新进展。其次是在编写形式方面：注重教材表现形式的新颖性和多样性，激发学生学习积极性。每章均包括学习要点、本章小结、思考题和典型案例等。

本书由肖艳、孙庆峰担任主编，佟大新教授主审。第1章由巴兴强编写，第5章、第9章由施继红编写，第6章、第7章由韩志刚编写，第3章、第8章由陈来荣编写，第2章、第4章由林彩霞编写，

目 录

前 言

第1章 导 论 …… (1)

1.1 汽车市场与汽车市场营销 …… (2)

1.1.1 汽车市场的含义及分类 …… (2)

1.1.2 我国汽车市场的发展沿革 …… (3)

1.1.3 汽车市场营销的含义及功能 …… (5)

1.2 汽车市场营销学的研究内容和研究方法 …… (8)

1.2.1 汽车市场营销学的研究对象和内容 …… (8)

1.2.2 汽车市场营销学的研究方法 …… (9)

1.3 汽车市场营销观念的演变 …… (10)

1.3.1 生产观念 …… (10)

1.3.2 产品观念 …… (11)

1.3.3 推销观念 …… (11)

1.3.4 营销观念 …… (12)

1.3.5 社会营销观念 …… (13)

第2章 汽车市场营销战略 …… (19)

2.1 汽车市场营销战略概述 …… (19)

2.1.1 汽车市场营销战略的制定原则 …… (19)

2.1.2 汽车市场营销战略的制定程序 …… (20)

2.1.3 汽车市场营销战略的制定方法 …… (23)

2.2 汽车市场营销战略环境分析 …… (23)

2.2.1 汽车市场营销战略宏观环境分析 …… (24)

2.2.2 汽车市场营销战略微观环境分析 …… (29)

2.3 汽车目标市场营销战略 …… (32)

2.3.1 市场细分 …… (32)
2.3.2 目标市场选择 …… (36)
2.3.3 市场定位 …… (40)

第3章 汽车市场调查与预测 …… (43)
3.1 市场营销信息系统 …… (43)
3.1.1 市场信息概述 …… (43)
3.1.2 市场营销信息系统的构成 …… (44)
3.2 汽车市场营销调查 …… (45)
3.2.1 汽车市场营销调查的含义和作用 …… (45)
3.2.2 汽车市场营销调查的主要内容 …… (46)
3.2.3 汽车市场营销调查的步骤 …… (47)
3.2.4 汽车市场调查方法 …… (48)
3.2.5 市场调查资料整理与分析 …… (51)
3.3 汽车市场需求预测 …… (52)
3.3.1 汽车市场需求预测的内涵及作用 …… (52)
3.3.2 汽车市场需求预测的基本原则 …… (53)
3.3.3 影响汽车市场需求预测的因素 …… (54)
3.3.4 汽车市场需求预测的步骤 …… (54)
3.3.5 汽车市场需求预测方法 …… (55)

第4章 汽车产品策略 …… (64)
4.1 整体产品的含义 …… (64)
4.1.1 整体产品含义的三层次说 …… (64)
4.1.2 整体产品含义的五层次说 …… (65)
4.1.3 整体产品含义的两形态说 …… (66)
4.2 产品生命周期理论 …… (67)
4.2.1 产品生命周期含义 …… (67)
4.2.2 产品生命周期各阶段的判断 …… (68)
4.2.3 汽车产品生命周期的市场策略 …… (69)
4.3 产品组合策略 …… (73)
4.3.1 产品组合的含义 …… (73)
4.3.2 汽车产品组合的要素 …… (73)
4.3.3 汽车产品组合主要策略 …… (73)
4.4 新产品开发策略 …… (75)
4.4.1 汽车新产品的特点和类型 …… (75)
4.4.2 汽车新产品的开发 …… (76)

第 5 章 汽车价格策略 …… (83)
5.1 汽车价格含义及构成要素 …… (83)
5.1.1 汽车价格含义 …… (83)
5.1.2 汽车价格构成要素 …… (84)
5.2 影响汽车定价的因素 …… (84)
5.2.1 汽车定价目标 …… (85)
5.2.2 汽车产品成本 …… (85)
5.2.3 市场供需状况 …… (85)
5.2.4 市场竞争分析 …… (85)
5.2.5 其他因素 …… (86)
5.3 汽车定价方法 …… (87)
5.3.1 成本导向定价法 …… (87)
5.3.2 需求导向定价法 …… (90)
5.3.3 竞争导向定价法 …… (91)
5.4 汽车定价策略 …… (93)
5.4.1 汽车新产品定价策略 …… (93)
5.4.2 汽车产品组合定价策略 …… (95)
5.4.3 心理定价策略 …… (96)
5.4.4 折扣定价策略 …… (97)
5.4.5 竞争定价策略 …… (99)
5.4.6 地区定价策略 …… (99)
5.4.7 价格调整策略 …… (100)
5.5 汽车定价程序 …… (101)
5.5.1 研究目标市场，确定定价目标 …… (101)
5.5.2 分析影响产品定价的因素 …… (102)
5.5.3 选择定价方法 …… (103)
5.5.4 确定产品价格 …… (103)

第 6 章 汽车分销渠道策略 …… (107)
6.1 汽车分销渠道的含义与功能 …… (107)
6.1.1 汽车分销渠道的含义 …… (107)
6.1.2 汽车分销渠道的功能 …… (108)
6.2 国内外汽车分销渠道发展概况 …… (108)
6.2.1 国外汽车分销渠道发展概况 …… (109)
6.2.2 我国汽车分销渠道的演变过程及展望 …… (111)
6.3 汽车分销渠道设计 …… (114)
6.3.1 渠道设计要素 …… (114)
6.3.2 影响汽车分销渠道选择的因素 …… (118)

6.4 汽车分销渠道管理 …… (120)
6.4.1 选择分销渠道成员 …… (120)
6.4.2 激励分销渠道成员 …… (123)
6.4.3 评估分销渠道成员 …… (125)

第7章 汽车促销策略 …… (128)
7.1 促销策略概述 …… (128)
7.1.1 促销的含义及作用 …… (128)
7.1.2 促销的方式及特点 …… (129)
7.1.3 促销组合的含义 …… (131)
7.1.4 影响促销组合策略的因素 …… (131)
7.2 人员促销策略 …… (131)
7.2.1 人员促销的形式 …… (132)
7.2.2 人员促销的步骤 …… (132)
7.2.3 人员促销的基本方法 …… (133)
7.2.4 人员促销的技巧 …… (133)
7.2.5 促销人员的管理 …… (134)
7.3 广告促销策略 …… (139)
7.3.1 广告的作用 …… (139)
7.3.2 广告媒体的选择 …… (140)
7.3.3 广告策略 …… (141)
7.3.4 广告预算 …… (145)
7.3.5 广告效果评价 …… (147)
7.4 销售促进策略 …… (148)
7.4.1 销售促进的形式 …… (148)
7.4.2 销售促进策略 …… (152)
7.5 公共关系策略 …… (154)
7.5.1 公共关系的要素 …… (154)
7.5.2 公共关系的模式 …… (155)
7.5.3 公共关系的工作程序 …… (157)

第8章 汽车品牌营销 …… (161)
8.1 品牌概述 …… (161)
8.1.1 品牌的含义 …… (161)
8.1.2 品牌的要素 …… (162)
8.1.3 品牌的效应 …… (162)
8.1.4 品牌与商标的关系 …… (163)
8.2 品牌资产价值 …… (163)
8.2.1 品牌资产的含义 …… (164)

8.2.2 品牌资产价值的构成 (164)
8.2.3 品牌资产价值的评估 (164)
8.2.4 品牌资产增值的途径 (166)
8.3 品牌定位 (167)
8.3.1 品牌定位原则 (167)
8.3.2 品牌定位分析工具 (167)
8.4 品牌识别与推广 (168)
8.4.1 品牌识别模式与管理 (169)
8.4.2 品牌推广方式和策略 (170)
8.5 品牌延伸 (171)
8.5.1 品牌延伸的内涵 (171)
8.5.2 品牌延伸的策略及基本原则 (172)
8.5.3 品牌延伸的主要步骤 (173)
8.6 品牌管理 (173)
8.6.1 品牌诊断 (174)
8.6.2 品牌维系 (174)
8.6.3 品牌保护 (176)

第9章 二手车营销 (180)
9.1 二手车交易 (180)
9.1.1 二手车交易的含义 (180)
9.1.2 二手车交易的主要形式 (181)
9.1.3 二手车交易基本流程 (181)
9.1.4 二手车交易的税费 (183)
9.1.5 二手车交易过程中发生的费用 (183)
9.2 二手车置换 (184)
9.2.1 二手车置换的含义 (184)
9.2.2 二手车置换的作用 (184)
9.2.3 二手车置换的程序 (185)
9.2.4 二手车置换的方式 (185)
9.2.5 二手车置换申请文件的填写 (186)
9.3 二手车售后服务 (188)
9.3.1 售后服务体系的作用 (188)
9.3.2 售后服务体系的构成 (189)
9.3.3 售后服务体系建设 (189)

第10章 汽车服务营销 (194)
10.1 汽车服务营销概述 (194)
10.1.1 服务的内涵及分类 (194)

10.1.2 汽车服务的特点 …… (196)
10.1.3 服务营销的内涵与特点 …… (197)
10.1.4 汽车服务营销的内容 …… (198)
10.2 汽车服务营销策略 …… (200)
10.2.1 “四全”服务策略 …… (200)
10.2.2 提高让渡价值策略 …… (201)
10.2.3 超值服务策略 …… (201)
10.3 汽车服务营销策划 …… (202)
10.3.1 服务项目策划 …… (202)
10.3.2 服务承诺策划 …… (203)
10.3.3 服务规范策划 …… (203)
10.3.4 服务模式策划 …… (204)

第 11 章 汽车国际营销 …… (206)
11.1 国际汽车工业发展概况 …… (206)
11.1.1 世界汽车工业发展历程 …… (206)
11.1.2 各国汽车工业发展现状 …… (208)
11.1.3 国际汽车工业的发展趋势 …… (213)
11.2 国际汽车市场营销环境概述 …… (214)
11.2.1 政治环境 …… (214)
11.2.2 法律环境 …… (214)
11.2.3 经济环境 …… (215)
11.2.4 文化环境 …… (216)
11.3 国际汽车市场的营销方式 …… (217)
11.3.1 产品出口 …… (217)
11.3.2 国外生产 …… (218)
11.3.3 对销贸易 …… (219)
11.4 国际汽车市场的营销策略 …… (220)
11.4.1 产品策略 …… (220)
11.4.2 价格策略 …… (220)
11.4.3 渠道策略 …… (220)
11.4.4 促销策略 …… (220)

参考文献 …… (224)

责任编辑／杜　娟
封面设计／美光制版

普通高等教育汽车与交通类专业“十二五”规划教材

汽车构造
汽车电器及电子控制技术
汽车运用工程学
汽车试验学
汽车检测与故障诊断
汽车维修工程学
汽车物流
汽车市场营销学
交通事故工程概论
汽车评估
汽车保险与理赔
专用车辆
汽车运行材料
新能源汽车导论
汽车服务工程概论
汽车服务信息系统
汽车制造工艺及装备
交通工程概论
交通案例分析
道路建筑材料
路基路面工程
道路工程检测技术
交通工程设施设计
桥梁工程
土木工程概论
道路工程专业英语
交通工程专业英语
交通安全工程
交通运输工程概论

ISBN 978-7-5038-6485-8
9 787503 864858 >

中国林业出版社教材出版中心
CHINA FORESTRY PUBLISHING HOUSE TEXTBOOK CENTER

定价：29.00 元

全国汽车维修工等级考试配套教材

汽车美容装饰工等级考试教材

初级 中级 高级

何效平　林彩霞　编著

机械工业出版社
CHINA MACHINE PRESS

全国汽车维修工等级考试配套教材编委会

主任：刘仲国

成员：王海林　赵祚喜　刘庆庭　朱余清　赵　新
李　庆　何效平　罗　阔　杨均忠　黄燕娟
毛彩云　刘　星　林彩霞　武　涛　陈学深
张永博　张　毅　张建莉　李　君　吕恩利
黎　锋　黄伟强

本书是全国汽车维修工等级考试配套教材，汽车美容装饰工培训部分。本册共分为初级工、中级工、高级工三篇。主要内容有：汽车美容装饰与咨询服务、汽车外部清洗、发动机美容护理、汽车内室清洁护理、汽车漆面护理、汽车其他部位的美容及保养、汽车内部装饰、汽车车窗及车身装饰、汽车安全保护及防护装饰、车用电器装饰、汽车信息与控制装饰、日常经营管理。

本书可作为汽车美容装饰工等级考试培训教材，也可供相关从业人员学习参考使用。

图书在版编目(CIP)数据

汽车美容装饰工等级考试教材：初级、中级、高级/何效平，林彩霞编著. —北京：机械工业出版社，2009.1

全国汽车维修工等级考试配套教材

ISBN 978-7-111-25221-4

Ⅰ.汽… Ⅱ.①何…②林… Ⅲ.汽车—车辆保养—水平考试—教材 Ⅳ.U472

中国版本图书馆 CIP 数据核字(2008)第 152222 号

机械工业出版社(北京市百万庄大街 22 号 邮政编码 100037)

策划编辑：徐 巍 责任编辑：杜凡如 责任校对：李 婷

封面设计：姚 毅 责任印制：洪汉军

北京铭成印刷有限公司印刷

2009 年 1 月第 1 版第 1 次印刷

169mm×239mm · 16.25 印张 · 315 千字

0001—4000 册

标准书号：ISBN 978-7-111-25221-4

ISRC CN-M10-08-0115-0/V.T(光盘)

定价：45.00 元(含 1VCD)

凡购本书，如有缺页、倒页、脱页，由本社发行部调换

销售服务热线：(010)68326294

购书热线：(010)88379639 88379641 88379643

编辑热线：(010)88379368

封面无防伪标均为盗版

目　录

编者的话

第一篇　汽车美容装饰初级工

第一章　汽车美容装饰与咨询服务 …… 3
第一节　汽车美容装饰简介 …… 3
第二节　汽车美容基础知识 …… 4
第三节　汽车美容装饰需要的知识和技能 …… 9
第四节　汽车美容装饰从业人员接待礼仪规范 …… 10
第五节　客户咨询解答技巧与服务 …… 15

第二章　汽车外部清洗 …… 23
第一节　汽车清洗概述 …… 23
第二节　汽车清洗的方法 …… 33

第三章　发动机美容护理 …… 50
第一节　发动机外部的清洁护理 …… 50
第二节　发动机内部护理 …… 52

第四章　汽车内室清洁护理 …… 58
第一节　常见内室美容用品及设备简介 …… 58
第二节　汽车内室的清洗 …… 64
第三节　汽车内室的美容 …… 75
第四节　汽车内室的杀菌消毒与熏香 …… 76
第五节　部分车内饰件的恢复性美容 …… 81

第二篇　汽车美容装饰中级工

第五章　汽车漆面护理 …… 87
第一节　汽车漆面的基础知识 …… 87
第二节　汽车漆面研磨技术 …… 91

第三节　汽车喷漆的基础知识 …… 93
第四节　汽车漆面打蜡、封釉和镀膜 …… 98

第六章　汽车其他部位的美容及保养 …… 111
第一节　轮胎美容及保养 …… 111
第二节　汽车玻璃美容及保养 …… 116
第三节　灯具美容及保养 …… 118
第四节　保险杠的护理 …… 120
第五节　车身沥青处理 …… 121
第六节　车门饰板的漏水处理 …… 122

第七章　汽车内部装饰 …… 123
第一节　更换车内篷壁 …… 123
第二节　车内地毯与脚垫装饰 …… 128
第三节　车内木质装饰 …… 131
第四节　车内饰品装饰 …… 132
第五节　车内香品装饰 …… 134

第八章　汽车车窗及车身装饰 …… 136
第一节　车窗覆膜 …… 136
第二节　汽车天窗安装 …… 140
第三节　车身大包围 …… 142
第四节　车身装饰 …… 143
第五节　汽车保险杠 …… 147

第九章　汽车安全保护及防护装饰 …… 150
第一节　汽车安全带与安全气囊 …… 150
第二节　汽车防盗装置 …… 167
第三节　汽车电子门锁的安装 …… 173
第四节　汽车安全报警装置 …… 176

第三篇　汽车美容装饰高级工

第十章　车用电器装饰 …… 183
第一节　汽车音响 …… 183
第二节　其他车用电器装饰 …… 201

● ISBN 978-7-111-25221-4
ISRC CN-M10-08-0115-0/V·T(光盘)

封面设计/电脑制作：姚毅

全国汽车维修工等级考试配套教材

- 汽车维修工等级考试指南
- 汽车维修工等级考试教材(初级)
- 汽车维修工等级考试教材(中级)
- 汽车维修工等级考试教材(高级)
- 汽车维修工等级考试教材(技师　高级技师)
- 汽车维修电工等级考试教材(初级)
- 汽车维修电工等级考试教材(中级)
- 汽车维修电工等级考试教材(高级)
- 汽车维修电工等级考试教材(技师　高级技师)
- 汽车维修钣金工等级考试教材(初级　中级　高级)
- 汽车维修漆工等级考试教材(初级　中级　高级)
- 汽车美容装饰工等级考试教材(初级　中级　高级)
- 汽车空调维修工等级考试教材(初级　中级　高级)
- 汽车维修检验工等级考试教材(初级　中级　高级)

上架指导：交通运输/汽车修理/汽车整车修理

策划编辑：徐　巍

编辑热线：(010)88379368

地　址：北京市百万庄大街22号　邮政编码：100037
联系电话：(010)68326294　网址：http://www.cmpedu.com(机工教材网)
(010)68993821　E-mail:cmp@cmpedu.com
购书热线：(010)88379639　网址：http://www.cmpbook.com(机工门户网)
(010)88379641　E-mail:cmp@cmpbook.com
(010)88379643

ISBN 978-7-111-25221-4

9 787111 252214 >

定价：45.00元(含1VCD)

子课题编号：2024YFD2000601-4 **密　级：公开**

“十四五”国家重点研发计划
子课题任务书

子课题名称（编号）：	小粒/异形种子高效精量育苗播种生产线研制（2024YFD2000601-4）
子课题承担单位：	华南农业大学
子课题负责人：	林彩霞
课题名称（编号）：	小粒/异形种子高效精量育苗播种技术与装备研发（2024YFD2000601）
课题承担单位：	华南农业大学
项目名称（编号）：	设施蔬菜种苗智能化生产关键装备创制与应用（2024YFD2000600）
项目牵头单位：	华南农业大学
执行期限：	2024 年 12 月至 2027 年 11 月

中华人民共和国科学技术部制

2024 年 12 月 20 日

填 写 说 明

一、任务书甲方即课题牵头承担单位，乙方即子课题承担单位。

二、任务书中的单位名称，请按规范全称填写，并与单位公章一致。

三、任务书中文字须用宋体小四号字填写。

四、凡不填写内容的栏目，请用“无”表示。

一、目标及考核指标、评测方式/方法

子课题目标、成果与考核指标表

子课题目标[1]	预期成果				考核指标[2]				考核方式（方法）及评价手段[4]
	预期成果名称			预期成果类型	指标名称	立项时已有指标值/状态	中期指标值/状态[3]	完成时指标值/状态	
研制小粒/异形种子高效精量育苗播种生产线	**主要成果**	1	小粒/异形种子高效精量育苗播种生产线	☑新产品 ☑新技术 ☑论文 ☑发明专利	数量指标	无	申请发明专利 1 件，设计试制小粒/异形种子高效精量育苗播种生产线 1 套	申请发明专利 1 件；发表论文 1 篇；提供小粒/异形种子高效精量育苗播种生产线 1 套	发明专利受理通知书、论文录用通知、生产线。
					技术指标	【TRL6】育苗盘传送作业速度≥600 盘/小时、关键技术及自主化率≥93%	【TRL7】育苗盘传送作业速度≥800 盘/小时、关键技术及自主化率≥95%	【TRL8】提供小粒/异形种子高效精量育苗播种生产线 1 套，育苗盘传送作业速度≥1000 盘/小时、关键技术及自主化率≥97%	第三方检测机构检测并出具检测报告并提供用户使用证明。

科技报告考核指标	序号	报告类型[5]	数量	提交时间	公开类别及时限[6]
	1	年度执行报告	1	2025 年 11-12 月	延期公开
	2	中期执行情况报告	1	中期检查前	延期公开
	3	年度执行报告	1	2026 年 11-12 月	延期公开
	4	年度执行报告	1	2027 年 11-12 月	延期公开
	5	最终科技报告	1	2027 年 11-12 月	延期公开
	6	综合绩效评价报告	1	子课题执行期结束后 6 个月内	延期公开

二、子课题研究内容、研究方法及技术路线

（一）主要研究内容

拟解决的关键科学问题、关键技术问题，针对这些问题拟开展的主要研究内容。

2.1 拟解决的关键科学问题、或关键技术问题

基于机-电-气协同调控的育苗盘高效传送系统构建，以 PLC 为核心元件构建播种生产线控制系统，实现播种全环节育苗盘的高效传送作业。

2.2 拟开展的主要研究内容

开发以 PLC 为控制核心的机-电-气协同调控系统，协同调控播种生产线各环节高效配合作业，研发播种运行数据监控和运行参数调节的人机交互界面，开展多品种多形状小粒种子精播性能测试试验，实现设施蔬菜育苗播种智能化高效精量生产。

（二）采取的研究方法

针对研究拟解决的问题，拟采用的方法、原理、机理、算法、模型等。

运用多机构协同的设计方法，采用概率统计理论和多目标试验优化方法，寻找播种、补种、铺土、扫土、覆土、淋水等装置的最佳匹配作业速度，利用积累的准确测试数据驱动播种全环节协同工作，实现育苗盘高效传送作业。

三、主要创新点

围绕基础前沿、共性关键技术或应用示范等层面，简述课题的主要创新点。具体内容应包括该项创新的基本形态及其前沿性、时效性等，并说明是否具备方法、理论和知识产权特征。

基于机-电-气协同调控，以及利用积累的准确测试数据驱动播种全环节协同工作，实现小粒/异形精量播种生产线的育苗盘高效传送作业。

四、预期经济社会效益

子课题的科学、技术、产业预期指标及科学价值、社会、经济、生态效益。

1. 科学、技术、产业预期指标

子课题将基于机-电-气协同调控的育苗盘高效传送系统构建，以 PLC 为核心元件构建播种生产线控制系统，研制小粒/异形种子高效精量育苗播种生产线样机 1 套，关键技术及零部件自主化率达到 97%以上；申请发明专利 1 件、发表论文 1 篇。

2. 科学价值

子课题将明确数据优化管理、参数协同控制与性能指标评价等技术要求，为播种全环节的智能化管控提供数据基础，也为设施蔬菜育苗播种智能化高效精量生产提供性能试验平台。

3. 社会、经济、生态效益

子课题研究将显著提高小粒/异型种子播种生产全环节的育苗盘传送作业效率，为播种生产缓解用工难、用工贵等突出问题，有力支撑设施蔬菜种苗产业的高质量发展。另外，生产线研发制造的关键技术及装备自制化率可以达到97%以上，有效降低了播种设备的市场价格，为推广应用提供了保障。

五、子课题年度计划

按每6个月制定完成子课题的计划进度，应将子课题的考核指标分解落实到年度计划中。

年度	任务	考核指标	成果形式
2024年12月 — 2025年5月	开展机、电、气零部件选型，以及生产线控制系统方案设计	播种生产线设计方案	机械结构设计图纸
2025年6月 — 2025年11月	生产线模块化设计，生产线各环节装置的结构参数优化	申请专利1件	发明专利受理通知书、年度科技报告
2025年12月 — 2026年5月	机、电、气协同控制系统构建，初步研制播种生产线	关键技术及零部件自主化率达到95%以上	样机、中期报告
2026年6月 — 2026年11月	开发协同控制系统人机界面，研究生产线配套装置运行参数的协同方法，研制完成播种生产线	播种生产线1条、关键技术及零部件自主化率达到97%以上	播种生产线、年度报告
2026年12月 — 2027年5月	开展生产线育苗盘高效传送作业性能测试	发表论文1篇	论文录用通知书、第三方检测报告
2027年6月 — 2027年11月	总结研究成果，编写绩效报告； 准备项目结题材料	/	年度科技报告、最终科技报告、项目绩效报告

六、子课题组织实施机制及保障措施

1、内部组织管理方式、协调机制等。

1.1 子课题内部组织管理方式

（1）实行子课题负责人负责制

子课题执行团队由子课题负责人和子课题骨干构成，负责子课题的具体实施、管理、规划、协调、执行、检查，以及落实子课题执行进度，以及组织年度评估、中期检查和最终的子课题结题验收等关键环节。子课题负责人负责子课题任务分解，遵循已批准的计划和预算方案执行子课题任务，组织制定年度工作计划及经费执行，强化子课题内研讨沟通，以及与课题组的沟通和汇报，确保子课题整体进度按时推进，同时负责组织撰写年度工作总结，并确保经费的合法、合规使用，每年需提交子课题的年度进展报告和下一年度的研究计划。

（2）规范子课题经费管理和使用

子课题负责人依托执行单位财务管理部门单独设立专项经费账户，对子课题资金的分配、使用进行加强管理，保证子课题经费合理、合法使用，确保专款专用，并接受审计部门的监督和审查。

2、实施的相关政策，已有的组织、技术基础，支撑保障条件。

2.1．政策支撑

2023 年国家农业农村部等多部委联合推出《全国现代设施农业建设规划（2023—2030 年）》，规划指出以加快现代设施农业高质量发展为目标，以优化现代设施农业布局、适度扩大规模、升级技术装备为重点，明确指出以提升现代化设施蔬菜种苗产业为重点任务。本项目研究内容重点解决现有设施蔬菜种苗播种装备缺乏等问题，研发高效精量和精准定向育苗播种成套设备，研究成果为加快现代设施农业高质量发展提供了有力支撑，与国家战略目标一致，符合国家相关政策要求。

2.2．良好的课题相关研究平台

子课题承担单位华南农业大学建有农业装备技术全国重点实验室（共建）、农业农村部蔬菜（叶菜）全程机械化科研基地、 广东省农业人工智能重点实验室等 10 余个国家级及省部级科研平台，配套有设施加工、性能监测和机电测试等科研实验室等等。科研与生产高度融合，可以为本任务的实施提供最有力的人才技术、研发手段、设备仪器试验平台、生产加工和试验基地等方面保障。

2.3．组建实力雄厚和稳定的课题研究团队

子课题主持人长期从事农业机械研究工作，提供了有力的人才支撑。子课题研究团队主要成员为科研骨干，可确保子课题研究团队在子课题执行期间的稳定。

3、对实现项目总目标的支撑作用，及与项目内其他课题的协同机制，限 500 字以内。

本子课题主要针对高速作业下小粒/异形蔬菜种子播种不精量问题，突破稳量充种、组合清种、同步排种等播种关键技术，目标研发小粒/异形种子高效精量育苗播种生产线样机 1 套，关键技术及零部件自主化率达到 97%以上

也为本项目设施蔬菜种苗智能化生产中的移栽、嫁接、推广示范等提供技术与装备保障。申请发明专利 1 件、发表论文 1 篇。

七、知识产权对策、成果管理及合作权益分配

1. 按照国家科技成果相关规定，严格执行《科技成果登记办法》和《关于国家科研计划项目研究成果知识产权管理的若干规定》，实行国家科技计划重大成果报告制度。根据科技成果特点，按照法律法规的规定适时选择申请专利、进行著作权登记等适当方式予以保护。

2. 在子课题实施过程中，严禁弄虚作假、徇私舞弊、剽窃他人成果等科研不端行为。在不影响子课题的专利申请或其他知识产权保护的前提下，明确要求依托本子课题所取得的所有研究成果，包括但不限于论文、专著、样机、样品、报道、软件、数据库和奖项等，应标注“国家重点研发计划资助”字样及项目编号，英文标注：“National Key R&D Program of China”。第一标注的成果作为验收或评估的确认依据。

3. 子课题实施过程中形成的专利、技术和产品等知识产权依照国家相关规定进行管理。

4. 在不影响知识产权保护前提下，积极推动子课题产生的知识产权和科研成果的转移和运用，加快知识产权的商品化、科研成果的产业化。

5. 按照国家有关科技计划项目知识产权管理规定及联合申请协议中对知识产权的约定，建立成果和知识产权权益分配机制，加强课题共有知识产权保护。

八、需要约定的其他内容

无

九、子课题参加人员基本情况表

序号	姓名	性别	出生日期	身份证号码（军官证、护照）	技术职称	职务	学位	专业	投入本课题的全时工作时间（人月）	人员分类	是否有工资性收入	工作单位
1	林彩霞	女			中级	无	博士	农业机械化	18	项目骨干	是	华南农业大学
2	韦未	女			副教授	副院长	博士	水工结构工程	18	子课题骨干	是	华南农业大学
3	胡威	女			中级实验师	无	硕士	农业水土工程	18	子课题骨干	是	华南农业大学
4	姚志强	男			无	无	学士	机器人工程	30	其他研究人员	否	华南农业大学
5	杨金鹏	男			无	无	学士	农业工程与信息技术	30	其他研究人员	否	华南农业大学
固定研究人员合计									114	/	/	/

十、经费预算

子课题承担单位基本情况表

表 B1

<table>
<tr><td colspan="8">填表说明：1.组织机构代码指企事业单位国家标准代码，单位若已三证合一请填写单位社会信用代码，无组织机构代码的单位填写“000000000”；
2.单位公章名称必须与单位名称一致。</td></tr>
<tr><td colspan="2">子课题编号</td><td colspan="3">2024YFD2000601-4</td><td>执行周期（月）</td><td colspan="2">36</td></tr>
<tr><td colspan="2">子课题名称</td><td colspan="6">小粒/异形种子高效精量育苗播种生产线研制</td></tr>
<tr><td rowspan="11">子课题承担单位</td><td colspan="2">单位名称</td><td colspan="5">华南农业大学</td></tr>
<tr><td colspan="2">单位性质</td><td colspan="5">大专院校</td></tr>
<tr><td colspan="2">单位主管部门</td><td colspan="3">广东省教育厅</td><td>隶属关系</td><td>地方</td></tr>
<tr><td colspan="2">单位组织机构代码</td><td colspan="5">124400004554165634</td></tr>
<tr><td colspan="2">单位法定代表人姓名</td><td colspan="5">薛红卫</td></tr>
<tr><td colspan="2">单位所属地区</td><td>广东省</td><td colspan="2">广州市</td><td colspan="2">天河区</td></tr>
<tr><td colspan="2">联系邮箱</td><td colspan="5">无</td></tr>
<tr><td colspan="2">通信地址</td><td colspan="5">广州市天河区五山路 483 号</td></tr>
<tr><td colspan="2">邮政编码</td><td colspan="5">510642</td></tr>
<tr><td colspan="2">银行账号</td><td colspan="5">3602002609000310520</td></tr>
<tr><td colspan="2">单位开户名称</td><td colspan="5">华南农业大学</td></tr>
<tr><td colspan="2">开户银行（全称）</td><td colspan="5">中国工商银行股份有限公司 广州五山支行</td></tr>
<tr><td rowspan="10">相关责任人</td><td rowspan="6">子课题负责人</td><td>姓名</td><td colspan="5">林彩霞</td></tr>
<tr><td>身份证号码</td><td colspan="5"></td></tr>
<tr><td>工作单位</td><td colspan="5">华南农业大学</td></tr>
<tr><td>电话号码</td><td colspan="2"></td><td>手机号码</td><td colspan="2"></td></tr>
<tr><td>电子邮箱</td><td colspan="2">cxllin@scau.edu.cn</td><td>邮政编码</td><td colspan="2">510642</td></tr>
<tr><td>通信地址</td><td colspan="5">广州市天河区五山路 483 号华南农业大学工程学院</td></tr>
<tr><td rowspan="4">财务部门负责人</td><td>姓名</td><td colspan="5">龚浩</td></tr>
<tr><td>电话号码</td><td colspan="2"></td><td>手机号码</td><td colspan="2"></td></tr>
<tr><td>传真号码</td><td colspan="5"></td></tr>
<tr><td>电子邮箱</td><td colspan="5">gonghao@scau.edu.cn</td></tr>
</table>

子课题预算表

表 B2 子课题编号：2024YFD2000601-4

子课题名称：小粒/异形种子高效精量育苗播种生产线研制　　金额单位：万元

序号	预算科目名称	金额
	（1）	（2）
1	**一、中央财政专项资金**	**60.00**
2	（一）直接费用	**51.00**
3	1.设备费	**7.00**
4	（1）购置设备费	**7.00**
5	（2）试制设备费	**0.00**
6	（3）设备改造费	**0.00**
7	（4）设备租赁费	**0.00**
8	2.业务费	**32.00**
9	（1）材料费	14.00
10	（2）测试化验加工费	4.00
11	（3）燃料动力费	1.00
12	（4）出版/文献/信息传播/知识产权事务费	1.00
13	（5）会议/差旅/国际合作与交流	10.00
14	（6）其他支出	2.00
15	3.劳务费	**12.00**
16	（1）劳务性费用	10.00
17	（2）专家咨询费	2.00
18	（3）其他	0.00
19	（二）间接费用	**9.00**
20	**二、其他来源资金**	**0.00**
21	**三、合计**	**60.00**

注：1.间接费用无需编制预算说明；2.绩效支出在间接费用中无比例限制。承担单位在统筹安排间接费用时，要处理好合理分摊间接成本和对科研人员激励的关系，绩效支出安排与科研人员在子课题工作中的实际贡献挂钩。

任务书签署

甲乙双方根据《国务院印发关于深化中央财政科技计划（专项、基金）管理改革方案的通知》（国发〔2014〕64 号）、《国务院关于优化科研管理提升科研绩效若干措施的通知》（国发〔2018〕25 号）、《国务院办公厅关于改革完善中央财政科研经费管理的若干意见》（国办发〔2021〕32 号）、《科技部 财政部关于印发<国家重点研发计划管理暂行办法>的通知》（国科发资〔2017〕152 号）、《财政部 科技部关于印发<国家重点研发计划资金管理办法>的通知》（财教〔2021〕178 号）、《科学技术活动违规行为处理暂行规定》（科学技术部令第 19 号）、《科技部财政部关于印发<中央财政科技计划（专项、基金等）监督工作暂行规定>的通知》（国科发政〔2015〕471 号）、《科技部 自然科学基金委关于进一步压实国家科技计划（专项、基金等）任务承担单位科研作风学风和科研诚信主体责任的通知》(国科发监〔2020〕203 号)等有关文件规定，以及有关法律、政策和管理要求，依据项目立项通知，签署本任务书。

同时，本单位和子课题负责人**郑重承诺：**对本子课题所有成果产出（包括但不限于新产品、新技术、标准、论文、专利等）的真实性、与课题的关联性等负责，将按要求落实科研作风学风和科研诚信主体责任；课题经费全部用于与本课题研究工作相关的支出，不截留、挪用、侵占，不用于与科学研究无关的支出；接受并积极配合相关部门的监督检查。如有违反，本单位和子课题负责人以及相关成果产出者愿接受项目管理专业机构和相关部门做出的各项处理决定，包括但不限于终止课题执行、追回项目（课题）经费，取消一定期限国家科技计划项目申报资格，记入科研诚信严重失信行为数据库以及主要负责人接受相应党纪政纪处理等。

课题承担单位（甲方）：（公章）

课题负责人（签字）：

2024 年12 月30 日

子课题承担单位（乙方）：（公章）

子课题负责人（签字）：

2024 年12 月30 日

项目牵头承担单位（丙方）：（公章）

项目负责人签字（签字）：

2024年12月30 日

受理编号：c1630550100104

项目编号：2016A020210108

文件编号：粤科规财字〔2016〕47号

2016A020210108

广东省省级科技计划项目

合同书

项目名称：山地果园运输车可发电式轮边缓速制动技术研究与示范

计划类别：农村科技领域

项目起止时间：2016-07-01　至　2018-06-30

管理单位(甲方)：广东省科学技术厅

承担单位(乙方)：华南农业大学

乙方主管部门(丙方)：华南农业大学

通讯地址：广东省广州市天河区五山路483号

邮政编码：510642　　单位电话：020-38632819

项目负责人：林彩霞　　联系电话：020-85280752

项目联系人：林彩霞　　联系电话：[illegible]

广东省科学技术厅
二〇一四年制

一、项目实施内容

（1）可发电式轮边缓速器技术

根据电磁转换原理，以现有的果园运输车的基本尺寸为基础进行轮边缓速器的CAD设计，基本结构包括缓速盘的设计、电磁铁线圈铁芯和线圈绕组的设计、支撑支架的设计、发电装置的设计等。 为获得轮边缓速器最佳结构参数，在Solidworks建立了轮边缓速器的参数化模型，利用ANSYS进行数值模拟分析，以期获得在一定的缓速盘、电磁铁线圈等部件结构下的最大制动力。并进行相应的试验调试。

(2)主导产品技术优化与集成示范

在每年果园收获的时期将山地果园运输车提供给种植大户试用，同时让种植大户在其的果园中对村民进行山地运输车演示。与当地农机部门合作，宣传山地果园运输车对农药、化肥、水果采摘运输中的帮助。推销到户，分派团队队员，对大型农户进行上门推销。

（3）培养一批面向山地果园运输机械化发展的应用型人才。

二、项目考核指标

1.项目完成后提供的研究开发成果及形式（须明确产品、专利、版权、标准等成果的类型及数量）

成果形式		成果数量	成果形式		成果数量
发明专利	申请	1	引进人才(人)		
	授权		培养人才(人)		2
实用新型专利	申请	2	科技人才奖励(人)		
	授权		技术标准制定	牵头(个)	
外观设计专利	申请			参与(个)	
	授权		科技报告(篇)		
国外专利	PCT受理		软件著作权(项)		
	授权		论文论著(篇)		3
获得国家级奖项(项)			其中：被收录论文数(篇)	SCI	
获得省级奖项(项)				EI	3
新服务(项)				ISTP	
新产品（或新材料、新装备、新品种（系））			新工艺（或新方法、新模式、新技术）		
创新载体项目必填	技术服务数量（项）				
	服务企业数量（家）				
科技金融项目必填	开展培训宣讲活动场次(次)				
	服务企业数量(家)				
	帮助企业融资(万元)				
	引进专业机构(家)				
院士工作站项目必填	引进院士及其团队科技成果转化数量				
	院士开展的战略咨询和技术指导次数				
	院士年进站次数				
	院士及院士团队年进站时间				
软科学项目必填	决策咨询报告(篇)(至少1篇)				
	研究总报告(篇)(至少1篇)				
	研究中期报告(篇)				
	研究分报告(篇)				
	调研报告(篇)				
	专著(篇)[须注明“广东省软科学研究计划项目(项目编号：)资助”]				
	核心期刊论文(篇)[以第一作者发表，须注明“广东省软科学研究计划项目(项目编号：)资助”]				
	培养人才(人)				

	获国家级奖项(项)	
	获省级奖项(项)	
	其他（具体形式：用户填）	
其他成果及形式说明：		
2. 主要技术经济指标及社会效益		
累计新增销售收入（万元）		
累计新增利税（万元）		
其他主要技术经济指标及社会效益说明：		
/		
项目负责人（签章）：林新波 2016年 8 月 18 日		

三、项目进度和阶段目标

开始日期	结束日期	主要工作内容
2016-07-01	2016-12-30	1.成立项目组，制定项目总体技术方案。 2.以现有的果园运输车的基本尺寸为基础进行轮边缓速器的CAD设计，基本结构包括缓速盘的设计、电磁铁线圈、铁芯和线圈绕组的设计、支撑支架的设计、发电装置的设计等。 3.申请发明专利1件，实用新型专利2件。 4.发表期刊论文1篇。
2017-01-01	2017-06-30	1.为获得轮边缓速器最佳结构参数，在Solidworks建立了轮边缓速器的参数化模型，利用ANSYS进行数值模拟分析，以期获得在一定的缓速盘、电磁铁线圈等部件结构下的最大制动力。 2. 生产样机，试验调试。 3.申请实用新型专利1件。 4.发表期刊论文1篇。
2017-07-01	2017-12-30	1.主导产品技术优化与集成示范， 进行小批量生产，将山地果园运输车提供给种植大户试用，同时让种植大户在其的果园中对村民进行山地运输车演示。与当地农机部门合作，宣传山地果园运输车对农药、化肥、水果采摘运输中的帮助。推销到户，分派团队队员，对大型农户进行上门推销。培养一批面向山地果园运输机械化发展的应用型人才。 2.发表期刊论文1篇。
2018-01-01	2018-06-30	1.不断优化生产工艺，减低生产成本。 2.撰写结题报告，项目验收。

四、承担、参与单位工作分工及经费分配情况

承担/参与单位名称（盖章）	工作分工	总经费分摊（万元）	省科技厅经费分配（万元）
华南农业大学	全面负责山地果园运输车可发电式轮边缓速技术的研发设计及生产，研发过程中的调研、制动性能及安全性能研究。负责样机示范工作。在广东省大面积推广，收集用户使用情况的反馈信息。	15.00	15.00
	合计	15.00	15.00

五、项目总经费及省科技厅经费预算

<table>
<tr><td colspan="7">1.省科技厅经费下达总额：　（大写）壹拾伍万圆整；（小写　）15.00万元；</td></tr>
<tr><td colspan="7">2.省科技厅经费拨付方式：　一次性拨款</td></tr>
<tr><td colspan="7">3.省科技厅经费年度下达计划：总额15.00(万元)</td></tr>
<tr><td colspan="3">分期</td><td colspan="4">经费(万元)</td></tr>
<tr><td colspan="3">第1期</td><td colspan="4">15</td></tr>
<tr><td colspan="7">4.总经费开支预算计划：</td></tr>
<tr><td colspan="6">经费筹集情况：</td><td>（单位：万元）</td></tr>
<tr><td colspan="7">总投入经费：15.00</td></tr>
<tr><td rowspan="2"></td><td rowspan="2">省科技厅经费</td><td colspan="4">自筹资金</td><td rowspan="2">合计</td></tr>
<tr><td>自有资金</td><td>贷款</td><td>地方政府投入</td><td>其它</td></tr>
<tr><td>已投入经费：</td><td></td><td></td><td></td><td></td><td></td><td></td></tr>
<tr><td>新增经费：</td><td>15.00</td><td></td><td></td><td></td><td></td><td>15.00</td></tr>
<tr><td>政府部门、境外资金及其他资金投入情况说明：</td><td colspan="6"></td></tr>
</table>

新增经费预算：				（单位：万元）
	新增经费总额		省科技厅经费	
支出经费	经费额	用途说明	经费额	用途说明
基建费：				
1、直接费用：	14.25		14.25	
(1)设备费：	1.50	用于购置研究测试仪器设备	1.50	用于购置研究测试 仪器设备
(2)材料费：	2.50	用于购买试验材料费	2.50	用于购买试验材料费
(3)测试化验加工外协费：	2.25	材料的加工费，山地制动性能试验	2.25	材料的加工费，山地制动性能试验
(4)燃料动力费：	0.50	试验用油	0.50	试验用油
(5)差旅费：	1.50	山地果园试验的差旅费、交通费，会议交流	1.50	山地果园试验的差旅费、交通费，会议交流
(6)会议费：				
(7)国际合作与交流费：				
(8)出版/文献/信息传播/知识产权事务费：	2.00	论文版面费、专利受理费	2.00	论文版面费、专利受理费
(9)租赁费：				
(10)人员费：	4.00	劳务费	4.00	劳务费
(11)专家咨询费：				
(12)直接费用其他支出：				
(13)科技金融服务体系其他费用：	0.00		0.00	
①信用评级补贴：				
②大赛场租：				
③特派员奖励与补贴：				
2、间接费用：	0.75		0.75	
0.75：	0.75	科研管理费	0.75	科研管理费
合计：	15.00		15.00	

六、人员信息

项目负责人情况

姓名	年龄	性别	职称	职务	学历	在项目中承担的任务	所在单位	签名
林彩霞	[illegible]	女	讲师	无	博士研究生	制定技术路线，结构分析，样机示范推广	华南农业大学	林彩霞
吴伟斌	[illegible]	男	教授	无	博士研究生	方案的总体设计，样机示范推广	华南农业大学	吴伟斌

主要研究开发人员

姓名	年龄	性别	职称	职务	学历	在项目中承担的任务	所在单位	签名
张建莉	[illegible]	女	讲师	无	硕士研究生	数值分析，试验调试，样机示范推广	华南农业大学	张建莉
卿艳梅	[illegible]	女	副教授	无	博士研究生	机械结构设计	华南农业大学	卿艳梅
何效平	[illegible]	女	讲师	无	硕士研究生	专利申报	华南农业大学	何效平
杨均忠	[illegible]	男	工程师	无	本科	试验分析	华南农业大学	杨均忠
姬兴	[illegible]	男	未取得	硕士研究生	硕士研究生	结构设计、试验分析	华南农业大学	姬兴
廖劲威	[illegible]	男	未取得	无	本科	试验分析	华南农业大学	廖劲威

七、承担、参与单位合作协议（须与申报书中合作协议或意向书相一致）

承担单位华南农业大学全面负责山地果园运输车可发电式轮边缓速技术的研发设计及生产，研发过程中的调研、制动性能及安全性能研究。负责样机示范工作。在广东省大面积推广，收集用户使用情况的反馈信息。

八、合同条款

第一条 甲方与乙方根据《中华人民共和国合同法》及国家有关法规和规定，为顺利完成（2016）年**山地果园运输车可发电式轮边缓速制动技术研究与示范** 专项项目（项目编号： 2016A020210108 ）经协商一致，特订立本合同，作为甲乙双方在项目实施管理过程中共同遵守的依据。

第二条 甲方的权利义务：

1. 按合同书规定进行经费核拨的有关工作协调。

2. 根据甲方需要，在不影响乙方工作的前提下，定期或不定期对乙方项目的实施情况和经费使用情况进行检查或抽查。

3. 根据《广东省科技计划项目信用管理办法(试行)》对乙方进行科技计划信用管理。

第三条 乙方的权利义务：

1. 确保落实自筹经费及有关保障条件。

2. 按合同书规定，对甲方核拨的经费实行专款专用，单独列账，并随时配合甲方进行监督检查。

3. 使用财政资金采购设备、原材料等，按照《广东省实施〈中华人民共和国招标投标法〉办法》有关规定，符合招标条件的须进行招标。

4. 项目实施完成或实施到一定程度，须按照《广东省省级科技计划项目结题管理的实施细则（试行）》提出验收或终止结题的申请，并按甲方要求做好项目结题工作。

5. 在每年1月向甲方如实提交上年度工作情况报告，报告内容包含上年度项目进展情况、经费决算和取得的效果等。

6. 按照国家和省有关规定，每年须提交年度科技报告；项目验收时，须提交验收科技报告。

第四条 在履行本合同的过程中，如出现广东省相关政策法规重大改变等不可抗力情况，甲方有权对所核拨经费的数量和时间进行相应调整。

第五条 在履行本合同过程中，需要对项目起止时间、项目经费使用（包括自筹经费、经费分配及经费支出预算等）、项目内容（包括研发内容、技术指标、经济指标及成果指标等）、项目名称、项目承担单位（包括承担单位更名、承担单位替换）、参与单位、项目负责人和成员等进行变更的，甲乙双方按照《广东省省级科技计划项目合同书管理的
实施细则（试行）》有关规定执行。

第六条 在履行本合同的过程中，当事人一方发现可能导致项目整体或部分失败的情形时，应及时通知另一方，并采取适当措施减少损失，没有及时通知并采取适当措施，致使损失扩大的，应当就扩大的损失承担责任。

第七条 本项目技术成果的归属、转让和实施技术成果所产生的经济利益的分享，除双方另有约定外，按国家和广东省有关法规执行。

第八条 属技术保密的项目，甲乙双方应另行订立技术保密条款，作为本合同正式内容的一部分，与本合同具有同等效力。

第九条 根据项目具体情况，经双方另行协商订立的附加条款，作为本合同正式内容的一部分，与本合同具有同等效力。

第十条 本合同的争议应由双方本着协商一致的原则解决，如双方协商不成的，则应向甲方所在地法院提起诉讼。

第十一条 保密条款：

1. 本合同保密内容范围为：

   无

2. 本合同保密期限为：

   无

3. 乙方应与可能知悉保密内容的人员签订技术秘密保护协议。

4. 各方应建立技术秘密保护制度。

5. 属技术保密的项目必须经省负责技术保密部门审查后，确定可否发表或用于国际合作和交流。

第十二条 甲方可根据具体情况决定乙方是否需要单位担保，若需要保证单位，应订立担保条款，作为本合同正式内容一部分。当乙方不履行或不完全履行本合同，以及没有或没有完全承担违约责任时，乙方的保证单位承担连带保证责任。

第十三条 本合同一式六份，各份具有同等效力。甲方存三份，乙方存二份，丙方存一份，本合同自签字之日起生效，有效期至项目结题后一年内。各方均应负合同的法律责任，不应受机构、人事变动的影响。

说明：本合同书中，凡是当事人约定无需填写的内容，应在空白处划（/）。

九、本合同签约各方

管理单位（甲方）：　广东省科学技术厅　（盖章）

单位地址：　广东省广州市连新路171号

法定代表人（或授权代表）：　黄宁生　_____（签章）

联系人（经办人）姓名：　刘世伟　_____（签章）

Email：　liusw@gdstc.gov.cn

电话：　020-83163909

2016年 9月 1日
年　月　日

承担单位（乙方）：　华南农业大学　（盖章）

二级部门：　华南农业大学工程学院

单位地址：　广东省广州市天河区五山路483号

法定代表人（或法人代理）：　陈晓阳　_____（签章）

联系人（项目主管）姓名：　石睿　_____（签章）

Email：　77909213@qq.com

电话：　020-85283435

开户单位名称：　华南农业大学

开户银行及帐号：　广东广州工行五山支行　3602002609000310520

2016年 9月 1日
年　月　日

乙方主管部门（丙方）：　华南农业大学　（盖章）

单位地址：　广东省广州市天河区五山路483号

法定代表人（或法人代理）：　陈晓阳　_____（签章）

联系人（项目主管）姓名：　石睿　_____（签章）

Email：　77909213@qq.com

电话：　020-85283435

开户单位名称：　华南农业大学

开户银行及帐号：　广东广州工行五山支行　3602002609000310520

2016年 9月 1日
年　月　日

内部

2021 年适应丘陵山区农业作业的通用动力装备及高效作业机具攻关项目研究任务书

项目名称：适应丘陵山区农业作业的通用动力装备及高效作业机具攻关项目

项目管理单位：工业和信息化部装备工业一司

项目牵头单位（甲方）：重庆鑫源农机股份有限公司

项目参与单位（乙方）：华南农业大学

起止年限：2021 年 6 月 1 日 —— 2022 年 12 月 31 日

根据《中华人民共和国民法典》、《中华人民共和国招标投标法》等有关法规以及2021年适应丘陵山区农业作业的通用动力装备及高效作业机具攻关项目的招标结果和招标、投标文件要求，为顺利组织实施完成2021年适应丘陵山区农业作业的通用动力装备及高效作业机具攻关重点项目（招标编号：TC210H02V），经协商一致，特订立本合同，作为甲乙双方在合同执行中共同遵守的依据。

一、成员单位任务分工及考核指标

分工	单位名称	任务分工与考核指标
1	华南农业大学	协助项目申报和验收，牵头开展丘陵山区果园多功能轨道作业系统装备研发与产业化。具体包括：突破索轨结构融合与远程遥控、模块化快速换装等关键核心技术，创制多功能果园遥控双轨作业系统装备。遥控双轨作业系统装备最大爬坡能力≥40°，承载最大重量≥1t，可进行灌溉、植保、运输作业；申请发明专利2-3项。

除实施内容和成果要求外，关于其他未能在本合同列出的内容及指标，以本项目技术要求和联合申报投标文件内容为准。

二、项目实施时间和实施进度计划

甲方将根据乙方的年度进度和目标完成情况进行考核。任务书签署后，原则上乙方需按任务书签署的进度完成实施方案建设内容和实施目标，未经许可不得擅自调整，否则将可能影响后续资金安排。

项目实施进度计划：

起止时间	项目建设内容
2021 年 6 月 1 日-2021 年 12 月 31 日	完成多功能果园遥控双轨作业系统装备及配套作业机具的技术方案论证，完成关键部件设计，申请发明专利。
2022 年 1 月 1 日-2022 年 6 月 30 日	突破索轨结构融合与远程遥控、模块化快速换装等关键核心技术，创制多功能果园遥控双轨作业系统装备。
联合体中期检查时间节点 2022 年 6 月 20 日	
2022 年 7 月 1 日-2022 年 12 月 31 日	完成多功能果园遥控双轨作业系统装备及配套作业机具性能测试，协助开展推广应用。
联合体验收检查时间节点 2022 年 11 月 20 日	

三、项目团队研究人员

序号	姓名	性别	联系电话	职务/职称	所学专业	学位	项目中的职务及分担的任务
1	李　君	男	[illegible]	教　授	机械工程	博士	项目总体设计与协调
2	李　震	男	[illegible]	教　授	农业工程	博士	轨道装备电控开发
3	曾　山	男	[illegible]	副研究员	农业工程	博士	轨道装备机械开发
4	王慰祖	男	[illegible]	副教授	机械工程	博士	轨道装备结构优化
5	林彩霞	女	[illegible]	讲师	农业工程	博士	轨道装备及配套机具测试
6	吕石磊	男	[illegible]	副教授	无线电物理	博士	轨道装备通信优化
7	李　钊	男	[illegible]	博士生	农业工程	硕士	轨道装备搭载功能开发
8	熊世杰	男	[illegible]	硕士生	机械工程	本科	轨道装备牵引制动设计
9	徐怀伟	男	[illegible]	硕士生	农业工程	本科	模块化快速换装设计

四、经费预算（不含厂房、土建、土地、铺底流动资金、建设期利息等费用）及专项资金下达计划

（一）任务总投资

本任务总投资（不含厂房、土建、土地、铺底流动资金、建设期利息等费用）（大写）肆佰壹拾肆万元整，（小写）414 万元。其中，财政专项补助资金 414 万元，自筹资金 0 万元。

（二）专项资金下达计划

甲方按照乙方的年度和目标完成情况进行考核，拟拨付专项补助资金：不超过（大写）肆佰壹拾肆万元整，（小写）414 万元。任务书签署后将根据财政预算计划下达第一笔补助资金，在验收合格后根据项目执行情况，按有关规定下达第二笔补助资金。

牵头单位负责财政资金管理，参与单位应严格按照牵头单位的有关管理要求执行。项目合同约定的实施期满 6 个月后，每延期一个月扣减计划补助资金的 2%，不足 1 个月按 1 个月计算，延期时间以通过验收的时间为准计算。对于擅自调整、无故延期或拖期严重的项目，将酌情调减后补助资金额度，情节严重的不再下达后补助资金或收回已下达资金。具体按照相关管理办法执行。

本项目采取竞争实施机制。对承担同一任务的两个单位，率先通过验收的按计划补助额度 100%拨付补助资金，后通过验收的按计划补助额度 70%拨付补助资金。**因此要求乙方单位务必于 2022 年 12 月 31 日之前完成经费使用审计报告。**

（三）预算明细表

具体投资明细如下表。

序号	支出科目	支出金额（万元）
1	设备费（含软件）	273
2	测试化验加工费	53
3	材料费	88
4	燃料动力费	/
5	会议费	/
6	差旅费	/
7	合作与交流费	/
8	出版/文献/信息传播/知识产权事务费	/
9	劳务费	/
10	人员费	/
11	专家咨询费	/
12	管理费	/
13	项目总投资概算（不含厂房、土建、土地、铺底流动资金、建设期利息等费用）合计	414

四、双方在本项目中的义务

（一）甲方负责：

1．负责项目组织管理，加强对项目的日常监管。按合同规定进行经费核拨。

2．甲方及其委托授权机构有权在项目实施过程中对乙方专项资金使用情况和项目的执行情况开展监督检查。

（二）乙方负责：

1．严格按照项目招投标文件（实施方案）、合同或申报材料中确定的内容和要求组织项目实施。

2．按合同及有关规定，对甲方核拨的经费实行**专款专用，单独核算**，随时配合甲方或甲方所委托的监督机构进行检查。专项资金使用须严格执行相关管理办法规定。启动资金应当用于与项目相关的设备、材料、产品、软件等采购费用，以及与项目相关的设计、检测、评价服务等费用。

3．提供乙方自筹的项目配套资金到位情况证明及使用情况。

4．在每年7月5日前向甲方如实提交上半年项目实施情况、存在问题和解决措施，在每年12月5日前向甲方如实提交上年度项目实施情况、存在问题和解决措施、下一年度工作安排、部门预算和自筹资金使用的书面报告。

5．对由联合体承担的项目，牵头单位对项目实施负总责。牵头单位应建立项目管理制度，加强对各成员单位项目执行、财政资金使用等环节的监督管理，并对项目实施全过程绩效管理，确保项目按进度实施并完成预期目标。联合体参与单位应按照联合体单位合作协议按时完成项目任务并接受牵头单位的监督检查。

6．项目完成后，乙方需及时响应甲方的要求，按时提交验收材料，配合甲方完成项目管理单位要求的各项验收活动。

五、保密条款

（一）甲乙双方应当对本合同的内容、因履行本合同或在本合同期间获得的或收到的对方的商务、财务、技术、产品的信息、用户资料或其他标明保密的文件或信息的内容（简称“保密资料”）保守秘密，未经对方书面事先同意，不得向本合同以外的任何第三方披露。资料接受方可仅为本合同目的、向其确有知悉必要的雇员披露对方提供的保密资料，但同时须指示其雇员遵守本条规定的保密及不披露义

务。甲乙双方应仅为本合同目的而复制和使用保密资料。

（二）除非得到另一方的书面许可，甲乙双方均不得将本合同中的内容及在本合同执行过程中获得的对方的商业信息向任何第三方泄露。

（三）本保密义务在本合同期满、解除或终止后仍然有效。

六、风险责任的承担

（一）项目管理单位在履行本合同的过程中，如遇到财政计划改变等不可抗力情况，对所核拨经费的数额和时间进行了变更，则甲方作为牵头单位按照变更后相应资金比例及时间调整给乙方合作单位拨付。甲方有及时拨付乙方专项资金的义务，否则应承担项目延期的相关责任。

（二）乙方在履行本合同过程中，因实施环境和条件发生重大变化，需要对建设内容、投资额度、实施期限进行调整的，须按相关管理办法规定履行程序。

（三）乙方在履行本合同的过程中，如发现可能导致项目失败或部分失败的情形时，应及时通知甲方，并应及时采取适当措施减少损失，如未及时通知甲方及采取适当补救措施致使项目损失扩大的，乙方应当就扩大的损失承担相关责任。

七、项目管理和验收

（一）项目组织实施和验收按照相关管理办法要求执行。

（二）甲方有权委托授权相关机构参与对项目的实施进程进行跟踪检查和评估，以及经费使用情况的审计。

（三）乙方要积极配合甲方委托授权的机构对项目进行的跟踪检查、评估和绩效评价，以及经费使用情况的审计。

八、知识产权归属及成果管理

项目牵头单位与各参与单位之间本着相互合作的精神，就项目申请、实施过程中产生的知识产权达成以下共识：

（一）牵头单位与各参与单位在共同实施本项目期间，各自分别完成的成果所获得的知识产权及相应权益均归各自所有，不因共同申请、实施本项目而改变。

（二）因申请或实施本项目的需要，各自向对方提供的相关信息，不构成向对方授予任何关于专利、著作权、商标权等知识产权的许可行为。

（三）多家单位共同完成的同一成果，则相应知识产权和成果收益应属完成单位共同所有。

九、其他

本合同一式四份，甲方三份，乙方一份，双方签字盖章后生效。

（以下无正文。）

十、签约各方

联合体牵头单位（甲方）：重庆鑫源农机股份有限公司　　（盖章）

项目负责人：　　（签章）

2022 年 1 月 17 日

联合体参与单位（乙方）：华南农业大学　　（盖章）

项目负责人：　　（签章）

基本账户银行信息：

户　　名：华南农业大学

开户银行：广州工行五山支行

帐　　号：3602 0026 0900 0310 520

2022 年 1 月 20 日

重型拖拉机无级变速传动技术研究与样机开发

课题合作协议

协议签订地：南京农业大学

甲方：南京农业大学

乙方：华南农业大学

甲方为国家重点研发计划“重型拖拉机智能化关键技术研究与整机开发”项目课题3“重型拖拉机无级变速传动技术研究与样机开发”的主持单位，乙方作为参与单位参加“重型拖拉机无级变速传动技术研究与样机开发”课题的相关任务。为了保证课题的顺利实施，经友好协商，双方达成如下协议：

一、 共同条款

甲、乙双方严格执行国家重点研发项目申报书所承诺任务目标及考核内容，严格执行国家有关科技项目管理办法和科研经费管理规定。

二、 任务分工

1. 甲方作为课题主持单位，整体负责项目运行的组织、实施、协调与控制，负责对参与单位的子课题（课题任务）执行进度、运行质量的监督与考核。
2. 甲方负责无级变速技术的研究与开发，包括如下内容：
   1）等比式无级传动设计方案、中间轴式带弹性均载结构、双行星排汇流技术的研究。
   2）完成1-2台实验样机的设计、计算、建模、绘图、试制以及无级变速性能的台架测试试验。
   3）开发重型拖拉机无级变速箱和重型拖拉机无级变速液压控制系统。
   4）研究重型拖拉机无级变速箱的智能控制技术与开发TCU装置，
3. 乙方完成智能重型拖拉机无级变速器样机的轻量化优化设计与开发，针对传动系统的减振、降噪等问题开展研究。
4. 乙方参与对样机的试验测试工作，负责对3-4台样机的实验数据整理与分析工作。
5. 乙方负责完成“重型拖拉机无级变速箱”行业标准的起草。

三、 考核指标

项目完成时，甲方应完成如下目标：

一）中间轴式带弹性均载的双行星汇流技术

1. 技术指标，等比式传动、噪音≤82dBA

2. 技术指标，段位≥3，总传动比≥4，变速范围为0.05-40km/h

3. 应用指标，适用于100-260马力重型拖拉机

4. 发表论文3篇，申请专利2-3项

二）重型拖拉机无级变速液压控制系统

1. 技术指标，液压控制离合器的响应时间≤0.3s

2. 技术指标，阀体集成≥90%

3. 应用指标，适用于100-260马力重型拖拉机

4. 发表论文3篇，申请专利2-3项

三）重型拖拉机无级变速传动箱

1. 技术指标，平均首次故障时间≥50小时

2. 技术指标，传动效率≥82%

3. 应用指标，适用于100-260马力重型拖拉机

4. 数量指标，1-2台实验样机，完成台架测试实验不少于50次

5. 发表论文3-4篇，申请专利1-2项

项目完成时，乙方应完成如下目标：

一）实现无级变速传动系轻量化设计

1. 技术指标，实际样机重量比实验样机减少20%以上，噪音≤82dBA

2. 应用指标，适用于100-260马力重型拖拉机

3. 发表论文2-3篇，申请专利2项,制定行业标准2项

二）无级变速传动系集成在整机上后，须与甲方共同负责通过国家相关标准规定的田间试验考核

1. 技术指标，试验测试合格率在95%以上

2. 应用指标，适用于100-260马力重型拖拉机

3. 发表论文2-3篇

三）协助完成重型拖拉机智能化关键技术研究与整机开发项目的产品鉴定。

四、 经费分配

根据项目总体经费及各方在项目中所承担的工作任务，分配给乙方专项经费人民币80万元（捌拾万元整）。

五、 知识产权及保密约定

在项目申请和执行过程中涉及的知识产权按以下方式处理：

（一）双方在申请本项目之前各自获得、拥有的知识产权及相应权益均归各自所有，不因共同申请本项目而改变。

（二）双方应对项目执行过程中产生的科技成果方式提交及时采取知识产权保护措施：

1、根据项目任务分工（以项目申报书具体约定为准），在双方的工作范围内独立完成的科技成果及其形成的知识产权归各完成方独立所有，对方具有署名权。

2、在本项目执行过程中，由双方共同完成的科技成果及其形成的知识产权归双方共有。

（1）由双方共同完成的技术秘密成果及知识产权，双方均有独自使用的权利。未经双方同意，任何一方不得向对方以外的第三方转让技术秘密。一方转让其共有的专利权、专利申请权或著作权的，应及时通知并取得对方的同意，对方有以同等条件优先受让的权利。一方声明放弃申请共有的专利权、专利申请权或著作权的，对方不得单独申请专利或著作权。

（2）双方对共有科技成果实施许可、转让专利技术、非专利技术而获得的经济收益由双方共享。

3、共同完成的科技成果（包括但不限于论文、申请奖励、鉴定）的人身权利，如身份权（署名权、修改权、发表权、保护作品完整权）、依法取得荣誉称号等荣誉权归双方共有，署名顺序按贡献大小由双方商定。

4、因申请本项目的需要，双方彼此提供的相关信息，除非本协议另有明确规定，否则不构成向合作方授予任何关于专利、著作权、商标权等知识产权的许可行为或其他权利。

5、本协议不在本协议双方之间建立任何商业上的代理、合作关系，如合作方希望建立任何商业上的代理、合作关系的，应另行签订协议。

6、双方对于根据本协议而知悉或获得的对方的商业秘密（包括但不限于经

营信息、技术信息）等相关信息和资料，对方不得以任何方式向对方以外的第三方披露或提供给第三方使用，该保密义务不因本合同的变更、终止、无效而失去效力，合同各方仍应承担保密义务。

7、除依法律规定或事先征得对方书面同意外，合同双方同意不向任何第三方提供本协议内容。

8、双方在正常职责范围内接触本协议或参与履行本协议约定的职员应被告知承担保密责任，前述提及的任何一方职员泄密的，其责任应由违约方承担。

六、 违约责任

本协议签订后，双方共同遵守，不能全面、及时履行合同约定的即构成违约，守约方有权根据实际情况要求违约方继续履行合同或解除合同，同时违约方负责赔偿对方因此造成的全部损失。

七、 其它

1. 其它未尽事宜，在项目实施过程中由双方共同协商解决，并形成书面文件作为本协议的补充，补充协议与本协议具有同等法律效力。
2. 因本协议而产生的纠纷由合同双方协商解决，协商不成的，由合同签订地有管辖权的人民法院进行裁决。
3. 本协议一式十一份，其中甲乙双方各持一份，其余用于项目申报，自双方签字盖章之日起生效。

甲方：南京农业大学

法人签章：

2016 年 6 月 20 日

乙方：华南农业大学

法人签章：

2016 年 6 月 27 日

项目批准号	10602019
归口管理部门	
申请代码	A020301
收件日期	

国家自然科学基金委员会

资助项目计划书

资助类别：面上项目

亚类说明：青年科学基金项目

附注说明：

项目名称：轴承间隙粘弹性润滑剂的非线性动力学分析

资助经费： 25.00 万元 执行年限：2007.01-2009.12

负 责 人：王海林

通讯地址：广东省广州市天河区五山路 483 号

邮政编码： 510642 电话：020-85280752

电子邮件： wanghl302@126.com

依托单位：华南农业大学

联系人： 陈奕 电话： 020-85280070

填表日期： 2006年10月8日

国家自然科学基金委员会

国家自然科学基金委员会资助项目计划书填报说明

一、收到《国家自然科学基金委员会资助项目批准通知》（以下简称《批准通知》）后，请认真阅读本填报说明和自然科学基金相关项目及财务管理办法（查阅Http://www.nsfc.gov.cn/），按《批准通知》的要求认真填写《国家自然科学基金委员会资助项目计划书》（以下简称《计划书》）。

二、填写《计划书》时要求科学严谨、实事求是、表述清晰、准确。《计划书》经主管科学部审核批准后，将作为项目研究计划执行和检查、验收的依据。

三、《计划书》为个性化表格，简表部分自动生成，不同类别的项目按不同要求撰写。请按以下提纲撰写《计划书》：

1、各类获资助项目都必须撰写中、英文摘要及主题词，填报经费预算表。

2、对于基金面上项目，项目组成员和研究内容按申请书执行，一般不得修改。如果《批准通知》中明确要求调整研究内容，须在《计划书》报告正文中对修改的内容作详细说明。没有要求修改的内容时，只需在报告正文中填写“研究内容和研究目标按照申请书执行”即可。

3、重点、重大项目的项目组成员和研究内容根据批准项目的实际情况填报，不能自行降低、更改研究目标，或缩减关键的研究内容。此外，还要突出以下几点：

（1） 研究的难点和在实施过程中可能碰到的问题，拟采用的研究方案和技术路线；

（2） 项目组主要成员分工，并请说明课题及合作单位之间的关系与分工；

4、 国家杰出青年科学基金和海外青年学者合作研究基金的计划书正文按下列提纲撰写：

1) 研究方向
2) 结合国内外研究现状，说明研究工作的学术思想和科学意义（限两个页面）
3) 研究内容、研究方案及预期目标（限两个页面）
4) 分年度进度安排
5) 研究队伍的组成情况

简表

申请者信息	姓　　名	王海林	性 别	男	出生年月	年　月	民 族	汉族
	学　　位	博士			职称	副教授		
	电　　话	020-85280752		电子邮件		wanghl302@126.com		
	传　　真	020-85281885		个 人 网 页				
	工 作 单 位	华南农业大学						
	所 在 院 系 所	工程学院						
依托单位信息	名　　称	华南农业大学					代 码	51064201
	联 系 人	陈奕		电子邮件		kycjhk@scau.edu.cn		
	电　　话	020-85280070		网站地址				
合作单位信息	单 位 名 称							代　码
项目基本信息	项 目 名 称	轴承间隙粘弹性润滑剂的非线性动力学分析						
	资 助 类 别	面上项目			亚 类 说 明	青年科学基金项目		
	附 注 说 明							
	申 请 代 码	A020301:流动的稳定性			E051502:机械润滑、密封与控制			
	基 地 类 别							
	执 行 年 限	2007.01-2009.12			研究属性	基础研究		
	资助经费	25.00 万元						

项目摘要

中文摘要(500 字以内)：
集成现有有关理论、数值计算、实验分析等研究成果，基于微观分子动力学及非线性动力学理论建模，研究含高分子添加剂的润滑油(非牛顿流体)与基础油(牛顿流体)作为轴承间隙润滑介质时，轴承－转子系统动力学及其摩擦学特性，揭示非牛顿流体抑制高速转子滑动轴承间隙油膜流态失稳的机理以及高分子润滑油膜的形成机理，分析高分子聚合物湍流减阻的机理。

关键词(不超过 5 个，用分号分开)：粘弹性流体;非线性动力学;滑动轴承

Abstract(limited to 500 words)：
Integrated the related theoretical, numerical and experimental research results, based on the microcosmic molecule dynamics and nonlinear dynamics, the bearing- rotor system dynamics and tribological characteristics are studied, with the lubricant contained high molecule additives (non-Newtonian fluid) and based oil (Newtonian fluid) as lubrication medium respectively. The mechanism of the viscoelastic fluid delaying transition to turbulence of oil film in bearing clearance of high speed rotor is investigated. The lubrication mechanism of high molecular weight ubrication film is analyzed. And the turbulent drag reduction mechanism of high molecular polymer is studied.

Keywords(limited to 5 keywords,seperated by;):viscoelastic fluid; nonlinear dynamics; sliding bearing

经费预算表

（金额单位：万元）

预算编制说明：

１．在填报本表之前，请根据项目资助类别认真阅读相关的资助经费管理办法；经费预算的编制以申请书中的《经费申请表》为基础，以《国家自然科学基金项目资助批准通知书》中的资助金额为依据；

２．编制经费预算时，不考虑不可预见因素和前期投入；

购置与试制仪器设备在 5 万元以上（包括 5 万元）时，须在报告正文中逐项说明用途和必要性。

科　　目	预算经费	备 注（计算依据与说明）
一．研究经费	22.0000	
1．科研业务费	10.5000	
（1）测试/计算/分析费	4.0000	机时费、计算机耗材
（2）能源/动力费	1.5000	实验耗电、水等
（3）会议费/差旅费	2.5000	会务费、调研费、差旅费
（4）出版物/文献/信息传播事务费	2.5000	资料费、打印复印费、出版费、网络费
（5）其它		
2．实验材料费	4.0000	
（1）原材料/试剂/药品购置费	2.5000	基础油、添加剂等
（2）其它	1.5000	实验消耗品
3．仪器设备费	4.5000	自制可视化实验台、购置测试仪器
4．实验室改装费	3.0000	管线调整
5．协作费		
二．国际合作与交流费	0.0000	
1．项目组成员出国合作交流		
2．境外专家来华合作交流		
三．劳务费	1.7500	研究生助研费、误餐费
四．管理费	1.2500	按 5%计
合　　计	25.0000	

与本项目相关的其他经费来源	国家其他计划资助经费	
	其他经费资助（含部门匹配）	
	其他经费来源合计	0.0000

报告正文

研究内容和研究目标按照申请书执行。

国家自然科学基金资助项目签批审核表

<table>
<tr>
<td colspan="2">我接受国家自然科学基金的资助，将按照申请书、项目批准意见和计划书负责实施本项目（批准号：10602019），严格遵守国家自然科学基金委员会关于资助项目管理、财务等各项规定，切实保证研究工作时间，认真开展研究工作，按时报送有关材料，及时报告重大情况变动，对资助项目发表的论著和取得的研究成果按规定进行标注。

项目负责人（签章）：
年 月 日</td>
<td>我单位同意承担上述国家自然科学基金项目，将保证项目负责人及其研究队伍的稳定和研究项目实施所需的条件，严格遵守国家自然科学基金委员会有关资助项目管理、财务等各项规定，并督促实施。

依托单位（公章）
年 月 日</td>
</tr>
<tr>
<td rowspan="2">本栏目由基金委填写</td>
<td colspan="2">科学处审查意见：

建议年度拨款计划（本栏目为自动生成，单位：万元）：
<table>
<tr><td>年度</td><td>总 额</td><td>第一年</td><td>第二年</td><td>第三年</td><td>第四年</td><td>第五年</td></tr>
<tr><td>金额</td><td></td><td></td><td></td><td></td><td></td><td></td></tr>
</table>
负责人（签章）：
年 月 日</td>
</tr>
<tr>
<td colspan="2">科学部审查意见：

负责人（签章）：
年 月 日</td>
</tr>
<tr>
<td rowspan="2">本栏目主要用于重大项目等</td>
<td colspan="2">相关局室审核意见：

负责人（签章）：
年 月 日</td>
</tr>
<tr>
<td colspan="2">委领导审批意见：

委领导（签章）：
年 月 日</td>
</tr>
</table>

项目批准号：10602019

负责人：王海林

项目名称：轴承间隙粘弹性润滑剂的非线性动力学分析

项目基本信息 | 项目摘要 | 人员信息 | 研究成果 | 相关文件 | 间接费用拨款计划

序号	姓名	出生年月	电子邮箱	职称	单位名称	项目分工	角色
1	王海林		wanghl302@126.com	副教授	华南农业大学	项目负责人	主持人
2	何效平		hxp702@163.com	讲师	华南农业大学	润滑性能分析	参与人
3	林彩霞		cxllin@sohu.com	讲师	华南农业大学	动力学分析	参与人
4	罗阔		luokuo@163.com	讲师	华南农业大学	性能计算	参与人
5	雷跃峰		leiyuefeng280@163.com		华南农业大学	实验研究	参与人
6	徐勇飞		regal000@163.com		华南农业大学	实验研究	参与人

SCAULIB202515158

检索证明

根据委托人提供的论文材料，委托人**工程学院 林彩霞** 7 篇论文收录情况如下表。

序号	论文名称	发表刊物及发表的年月卷期/页码等	作者排名	论文等级	作者文中单位	收录情况	影响因子	中科院大类分区
1	基于量纲分析的液力缓速器制动性能试验分析	江苏大学学报(自然科学版) 出版年：2016 出版日期：2016-11-01 17:00 卷期：37 06 页码：645-649+656 文献号： 文献类型：期刊论文	1	B 类	华南农业大学	北大核心	无	无
2	基于台架检测汽车滚动阻力的修正模型	汽车技术 出版年：2010 出版日期：2010-04-24 卷期： 04 页码：46-49 文献号： 文献类型：期刊论文	1	C 类	华南农业大学	北大核心	无	无
3	液力缓速器能量耗散方程的建立	机械设计 出版年：2014 出版日期：2014-03-20 卷期：31 03 页码：80-84	1	B 类	华南农业大学	北大核心	无	无

		文献号： 文献类型：期刊论文						
4	液力缓速器制动系统的能效分析	机械设计 出版年：2015 出版日期：2015-08-20 卷期：32 08 页码：17-20 文献号： 文献类型：期刊论文	1	B 类	华南农业大学	北大核心	无	无
5	液力缓速器研究进展	机床与液压 出版年：2014 出版日期：2014-03-15 卷期：42 05 页码：177-179+184 文献号： 文献类型：期刊论文	1	C 类	华南农业大学	北大核心	无	无
6	双转子摆线泵流量特性分析及优化设计	机床与液压 出版年：2017 出版日期：2017-01-28 卷期：45 02 页码：79-80+87 文献号： 文献类型：期刊论文	1	C 类	华南农业大学	北大核心	无	无

7	在用车滑行检测台架与道路差异性研究	中国农机化 出版年：2011 出版日期：2011-11-25 卷期： 06 页码：106-109 文献号： 文献类型：期刊论文	1	C类	华南农业大学	北大核心	无	无

说明：论文等级和中科院大类分区按《华南农业大学学术论文评价方案（试行）》划分。

报告免责声明:如未盖章,报告无效

检索员：田成

华南农业大学图书馆

2025-07-14

SCAULIB202515405

检索证明

根据委托人提供的论文材料，委托人**工程学院 林彩霞** 1 篇论文收录情况如下表。

序号	论文名称	发表刊物及发表的年月卷期/页码等	作者排名	论文等级	作者文中单位	收录情况	影响因子	中科院大类分区	引用
1	Nondestructive Identification of Litchi Downy Blight at Different Stages Based on Spectroscopy Analysis	AGRICULTURE-BASEL 出版年：2022 出版日期：MAR 卷期：12 3 页码：- 文献号：402 文献类型：Article	通讯作者	B 类	华南农业大学	SCI	IF2-year=3.6 IF5-year=3.6 （2022）	农林科学 3 区 Top 期刊：否 （2022）	SCI 核心合集 总引：8

说明：论文等级和中科院大类分区按《华南农业大学学术论文评价方案（试行）》划分。

报告免责声明:如未盖章,报告无效

检索员：田成

华南农业大学图书馆

2025-03-26

SCAULIB202624886

检索证明

根据委托人提供的论文材料，委托人**华南农业大学工程学院 林彩霞(学科类型:自然科学)** 2 篇论文收录情况如下表。

序号	论文名称	发表刊物及发表的年月卷期/页码等	作者排名	论文等级	作者文中单位	收录情况	影响因子	中科院大类分区	引用
1	A novel method for detecting missing seedlings based on UAV images and rice transplanter operation information	COMPUTERS AND ELECTRONICS IN AGRICULTURE 出版年：2025 出版日期：FEB 卷期：229 页码：- 文献号：109789 文献类型：Article	共同通讯作者	T2 类	华南农业大学工程学院	SCI	IF2-year=8.9 IF5-year=9.3 （2024）	农林科学 1 区 Top 期刊：是 OA 期刊：否 （2025）	SCI 核心合集 总引：5
2	Analysis of Radial Electromagnetic Force in Claw Pole Alternator Considering Excitation Current Harmonics	JOURNAL OF ELECTRICAL ENGINEERING & TECHNOLOGY 出版年：2025 出版日期：NOV 卷期：20 8 页码：5199-5214 文献类型：Article	通讯作者	B 类	华南农业大学工程学院	SCI	IF2-year=1.6 IF5-year=1.6 （2024）	工程技术 4 区 Top 期刊：否 OA 期刊：否 （2025）	SCI 核心合集 总引：0

说明：论文等级和中科院大类分区按《华南农业大学学术论文评价方案（试行）》划分。

报告免责声明:如未盖章,报告无效

检索员：卢炳卫

ISSN 1671-7775
CODEN JDXZA6

江苏大学学报

自然科学版

JOURNAL OF JIANGSU UNIVERSITY
NATURAL SCIENCE EDITION

第37卷 第6期 Vol.37 No.6

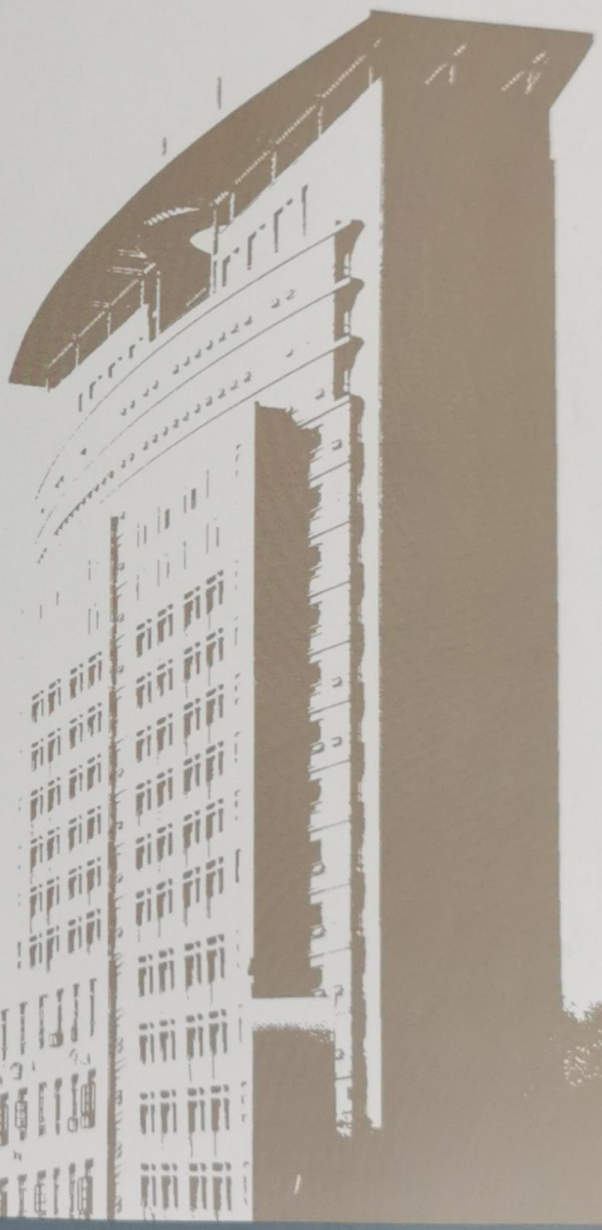

2016

江苏大学学报(自然科学版)
JOURNAL OF JIANGSU UNIVERSITY(Natural Science Edition)
2016年11月 Nov. 2016
第37卷 第6期 Vol. 37 No. 6

目 次

非充气车轮及其力学特性研究进展
赵又群，付宏勋，林 菜，李娅奇 621

并联式混合动力客车2参数换挡规律的分析与设计
田韶鹏，雷 蕾，伍 磊 628

结构参数对柴油机微粒捕集器捕集特性的影响
汤 东，王希凡，未建飞，赵 岑 634

双前桥转向三轴汽车的操纵稳定性
吴志成，陈 聪 640

基于量纲分析的液力缓速器制动性能试验分析
林彩霞 645

基于改进闭环子空间辨识的电动轮汽车纵向力估计
徐 兴，陈 特，陈 龙，王吴杰 650

并联混合动力汽车混合驱动模式的换挡规律
何 仁，徐益强 657

作物叶面图像自动分割方法
张连宽，PAUL Weckler，肖德琴 663

帘线钢盘条中大颗粒钛夹杂成因分析
雷家柳，薛正良 670

CaO-SiO_2-B_2O_3-硼泥渣系的熔化性能及渣系结构分析
王宏明，郭 亚，李桂荣 675

期刊基本参数：CN32-1668/N*1980*b*A4*128*zh*P*¥28.00*1500*21*2016-11*n

声波幅度对有限振幅声波传播畸变的影响
兰朝凤，隋雪梅，韩　闯，郭小霞，李凤臣　679

多台测量机器人在自动化监测中的开发应用
潘国荣，李　伟　684

飞轮储能用 Halbach 阵列定子无铁心无轴承永磁电机的设计
朱焜秋，陆荣华，胡亚民，黄建波　691

在线增量正交投影非负矩阵分解的目标跟踪算法
王海军，葛红娟，张圣燕　698

连续箱梁桥沥青混凝土铺装层间接触应力分析
王勋涛，封建湖，王　虎　706

不同荷载作用下膨胀土的膨胀率与膨胀潜势试验
武　科，吴昊天，张　文，王亚君　713

考虑桩自重及侧摩阻力影响的超长桩屈曲分析
李传勋，刘晓钊，吴文兵　719

LRB 隔震斜拉桥地震响应分析
陈水生，钟汉清，桂水荣　724

基于颗粒流程序的 ATB－30 下面层细观响应
吴　平　730

基于热成像的沥青混合料摊铺温度均匀性分析
胡力群，暴英波，王天林，张建伟，李　欢　735

改性沥青混合料施工温度的确定
张宜洛，郭　科，赵少宗，李　晨，杨自广　740

江苏大学学报(自然科学版)第 37 卷(2016 年)总目次
I

执行编辑　梁家峰　　英文校核　袁新华

JOURNAL OF JIANGSU UNIVERSITY (Natural Science Edition)
Vol. 37 No. 6
Nov. 2016

CONTENTS

Advancement of non-pneumatic wheels and mechanical characteristics
..... *ZHAO Youqun, FU Hongxun, LIN Fen, LI Yaqi* (621)
Analysis and design of two-parameter shifting schedule for parallel hybrid electric bus
..... *TIAN Shaopeng, LEI Lei, WU Lei* (628)
Effects of structural parameters on trapping characteristics of diesel particulate filter
..... *TANG Dong, WANG Xifan, WEI Jianfei, ZHAO Cen* (634)
Handling stability of three-axle vehicle with dual-front-axle-steering system
..... *WU Zhicheng, CHEN Cong* (640)
Experiment analysis of hydraulic retarder brake performance based on dimension analysis
..... *LIN Caixia* (645)
Longitudinal force estimation for motorized wheels driving electric vehicle based on improved closed-loop subspace identification ..... *XU Xing, CHEN Te, CHEN Long, WANG Wujie* (650)
Shift schedule of parallel hybrid electric vehicles under hybrid driving mode
..... *HE Ren, XU Yiqiang* (657)
Automtic leaf surface region segmentation from crop image
..... *ZHANG Liankuan, PAUL Weckler, XIAO Deqin* (663)
Cause analysis for large titanium inclusion in wire rod cord steel
..... *LEI Jialiu, XUE Zhengliang* (670)
Analyses of melting properties and structure of CaO-SiO_2-B_2O_3-boron mudslag system
..... *WANG Hongming, GUO Ya, LI Guirong* (675)
Influence of amplitude on propagation distortion of finite amplitude acoustic wave
..... *LAN Chaofeng, SUI Xuemei, HAN Chuang, GUO Xiaoxia, LI Fengchen* (679)
Development and application of several georobots in automatic monitoring
..... *PAN Guorong, LI Wei* (684)
Design of coreless-stator bearingless permanent magnet motor with Halbach array for flywheel energy storage system
..... *ZHU Huangqiu, LU Ronghua, HU Yamin, HUANG Jianbo* (691)
Object tracking algorithm via incremental orthogonal projective non-negative matrix factorization
..... *WANG Haijun, GE Hongjuan, ZHANG Shengyan* (698)
Stress analysis of asphalt concrete pavement for continuous box girder bridge under interfacial contact condition
..... *WANG Xuntao, FENG Jianhu, WANG Hu* (706)
Expansive ratio and expansive potentiality of expansive soil under different loadings
..... *WU Ke, WU Haotian, ZHANG Wen, WANG Yajun* (713)
Buckling analysis for super-long pile considering self-weight of pile and lateral frictional resistance
..... *LI Chuanxun, LIU Xiaozhao, WU Wenbing* (719)
Analysis on seismic response of lead rubber bearings in cable-stayed bridge
..... *CHEN Shuisheng, ZHONG Hanqing, GUI Shuirong* (724)
Mesoscopic response of ATB－30 sub-course based on particle flow code
..... *WU Ping* (730)
Temperature uniformity analysis of asphalt mixture paving based on thermal imaging
..... *HU Liqun, BAO Yingbo, WANG Tianlin, ZHANG Jianwei, LI Huan* (735)
Determination of construction temperature for modified asphalt mixture
..... *ZHANG Yiluo, LIU Ke, ZHAO Shaozong, LI Chen, YANG Ziguang* (740)

江苏大学学报(自然科学版)
JOURNAL OF JIANGSU UNIVERSITY(Natural Science Edition)
2016 年 11 月 Nov. 2016
第 37 卷 第 6 期 Vol. 37 No. 6
doi: 10.3969/j.issn.1671 -7775.2016.06.005

基于量纲分析的液力缓速器制动性能试验分析

林彩霞
(华南农业大学 工程学院，广东 广州 510642)

摘要： 为揭示液力缓速器制动性能诸影响因子的内在规律，基于量纲分析原理，通过台架试验，验证介质的物性参数、工作参数、缓速器结构参数等单值性条件对液力缓速器制动性能的作用效果，给出了由雷诺数、普朗特数、欧拉数、单位倾角和弦节比组成的液力缓速器准则函数. 理论分析和试验结果表明: 制动转矩受到油温的影响; 在工作介质一定时，转矩与普朗特数成反比，随着普朗特数增加而降低; 雷诺数越大，工作介质的受迫流动越剧烈，制动转矩随着雷诺数的增加而增大; 随着工作腔内油压增加，制动转矩增加，液力缓速器制动过程的驱动力来源于工作腔工作介质的压力差.

关键词： 液力缓速器; 制动性能; 量纲分析; 准则函数; 试验研究
中图分类号： U463.53 **文献标志码：** A **文章编号：** 1671 -7775(2016)06 -0645 -05
引文格式： 林彩霞. 基于量纲分析的液力缓速器制动性能试验分析[J]. 江苏大学学报(自然科学版)，2016，37(6)：645 -649，656.

Experiment analysis of hydraulic retarder brake performance based on dimension analysis

LIN Caixia
(College of Engineering, South China Agricultural University, Guangzhou, Guangdong 510642, China)

Abstract: To disclose the essential rule of influence factor on hydraulic retarder brake, the effects of working media physical parameters, working parameters and geometry parameters on hydraulic retarder brake performance were tested and verified based on dimension analysis. The criterion function of brake torque was deduced with parameters of *Re*, *Pr*, *Eu*, unit dip angle and chordal section length ratio. The theory and experiment research results show that the torque performance is affected by oil temperature. The torque is inversely proportional to *Pr* for the same working liquid, and the torque is decreased with the increasing of *Pr*. The larger the *Re* is, the more violent the working media flows with increased torque. The torque is increased with the increasing of oil pressure, and the torque driving force comes from the pressure difference of working media.

Key words: hydraulic retarder; braking performance; dimension analysis; criterion function; experiment research

液力缓速器是把汽车的动能转化为工作介质热能的辅助制动装置，因其具有制动件磨损小、寿命长、制动转矩大、过程平稳、不会产生热衰退和散热性能好等特点，其装置在国外普遍应用. 德国采埃孚、福伊特公司、美国通用汽车公司等公司生产的液力缓速器技术成熟，结构类型多样化.

液力缓速器在中国虽然也有应用，但基本上是国外的产品，价格昂贵. 过去中国生产的液力缓速

收稿日期: 2015 -12 -22
基金项目: 国家星火计划项目(2011E000040); 广东省科技计划项目(2016A020210108); 高等学校博士学科点专项科研基金资助项目(20114404110021)
作者简介: 林彩霞(1976—)，女，广东阳江人，讲师，博士研究生(cxlin76@163.com)，主要从事机械设计理论研究.

器，在相同参数和工况时，出现制动转矩比国外的产品低、密封性能不好、漏油等现象，阻碍了液力缓速器产业化进程的发展. 多年来，国内的专家、学者致力于液力缓速器的国产化，针对液力缓速器的结构、制动机理、设计方法等问题展开了诸多研究. 如基于1维束流，把油液在液力缓速器内部的3维流动简化为2维流动或者1维流动，再用试验的方法进行修正，建立相应的液力缓速器部分充液工况制动转矩液力计算数学模型[1-4]. 利用Fluent等流体力学软件对液力缓速器内部流场进行数值分析与计算发现，液力缓速器内部压力从循环圆中心到外环，压力逐渐增大，湍动能的分布在涡旋处较大，在流道固壁处较小[5-9]，以及在改变液力缓速器充液量、叶片数、叶片倾角、循环圆等参数的情况下进行数值分析，揭示不同情况下缓速器内部流动流场的变化规律[10-12]. 而现有对液力缓速器制动性能影响因子的内在相互规律的研究比较缺乏. 为了提高液力缓速器的制动性能，笔者基于量纲分析法推导出揭示各影响因子相互规律的准则函数，并利用样机进行台架试验分析.

1 液力缓速器准则函数的确定

根据白金汉 π 定理，如果在一个系统中有 q_1，q_2，…，q_n 共 n 个变量，这 n 个变量有一定的物理相关性，且只含有 k 个基本量纲，那么该系统就可以由 $J=(n-k)$ 个独立的量纲一的量来完全描述.

液力缓速器制动过程是由机械结构、工作介质和工作参数等因素影响的复杂过程，影响转矩的因素较多，有工作介质密度、黏性系数、温度、流动速度、流量、压力、循环圆直径、叶片倾角、定、动轮叶片数和动轮转速等. 依据前期试验研究的结果，选择了工作介质的物性参数：密度 ρ，量纲为 ML^{-3}；黏度 η，量纲为 $ML^{-1}T^{-1}$；导热系数 λ，量纲为 $ML\Theta^{-1}T^{-3}$；比定压热容 c_p，量纲为 $L^2\Theta^{-1}T^{-2}$. 工作参数：转速 n（以动轮的转速表征工作介质的流动速度），量纲为 T^{-1}；压力 p，量纲为 $ML^{-1}T^{-2}$. 几何参数：循环圆直径 D，量纲为L；叶片倾角 θ（考虑到液力缓速器倾角角度变化范围是 $0\sim\pi/2$，对倾角进行量纲一化为 $2\theta/\pi$，以下简称为单位倾角）；液力缓速器的弦长 l 为工作直径，节长为

$$b=(\pi D-xl_1-yl_2)/(x+y), \tag{1}$$

式中：x 为有进油口的叶片的个数，个；l_1 为有进油口的叶片的厚度，mm；y 为无进油口的叶片的个数，个；l_2 为无进油口的叶片的厚度，mm.

弦长与节长的比值称弦节比 l/b. 考核指标为制动转矩 T，量纲为 ML^2T^{-2}. 对于不带量纲的物理量，在 π 定理中直接当作量纲一的量来处理，用字母 π 表示，因此 $\pi_5=l/b$，$\pi_6=2\theta/\pi$. 以上共有8个变量，基本量纲：长度的量纲L、质量的量纲M、时间的量纲T、温度的量纲 Θ 共4个，根据 π 定理（8-4=4），可以推导出4个量纲为一的量. 制动转矩 T 的准则函数具体推导过程如下：

1）选定4个物理量作为基本物理量，该物理量的量纲必须包括上述4个基本物理量，基本物理量取为黏度 η、转速 n、循环圆直径 D 及导热系数 λ.

2）将基本物理量逐一与其余各量组成量纲一的量，量纲一的量采用幂指数形式表示，其中指数待定. 则有

$$\begin{cases}\pi_1=T\eta^{a_1}n^{b_1}D^{c_1}\lambda^{d_1},\\ \pi_2=\rho\eta^{a_2}n^{b_2}D^{c_2}\lambda^{d_2},\\ \pi_3=c_p\eta^{a_3}n^{b_3}D^{c_3}\lambda^{d_3},\\ \pi_4=p\eta^{a_4}n^{b_4}D^{c_4}\lambda^{d_4},\end{cases} \tag{2}$$

式中 a_1，a_2，a_3，a_4，b_1，b_2，b_3，b_4，c_1，c_2，c_3，c_4 为待定幂指数.

3）用量纲齐次原理来决定上述待定指数，以 π_1 为例，把 π_1 各项的量纲代入得

$$\pi_1=M^{1+a_1+d_1}L^{2-a_1+c_1+d_1}T^{-2-a_1-b_1-3d_1}\Theta^{-d_1}, \tag{3}$$

等号左边为量纲一的量，因而等号右边各量纲的指数必为0，算得：$a_1=-1$，$b_1=-1$，$c_1=-3$，$d_1=0$. 其他 π 项的指数同理算得，因此可得量纲一的量为

$$\begin{cases}\pi_1=\ =T\eta^{-1}n^{-1}D^{-3}=\dfrac{T}{\eta nD^3}=\dfrac{TRe}{\rho n^2D^5},\\ \pi_2=\dfrac{\rho nD^2}{\eta}=Re,\\ \pi_3=\dfrac{c_p\eta}{\lambda}=Pr,\\ \pi_4=\dfrac{p}{\eta n}=\dfrac{p}{\rho u^2}\dfrac{\rho u^2}{\eta n}=\dfrac{\pi^2}{3\ 600}EuRe,\end{cases} \tag{4}$$

10个变量中，除制动转矩 T 为因变量外，其余均为自变量. 所以，含有 T 的 π_1 可作为因变项，其他的为自变项，满足：

$$\pi_1=f(\pi_2,\pi_3,\pi_4,\pi_5,\pi_6). \tag{5}$$

把各 π 项代入式（5），即得液力缓速器准则函数：

$$\frac{TRe}{\rho n^2D^5}=f\left(Re,Pr,\frac{l}{b},\frac{2\theta}{\pi},\frac{p}{\eta n}\right). \tag{6}$$

令 $\lambda_T=f\left(Re,Pr,\dfrac{l}{b},\dfrac{2\theta}{\pi},\dfrac{p}{\eta n}\right)/Re$，定义为制动转

矩系数，式(6)变为

$$T=\lambda_T \rho n^2 D^5. \tag{7}$$

从式(6)，(7)可以看出：液力缓速器准则函数由雷诺数 Re、普朗特数 Pr、欧拉数 Eu、转速以及循环圆直径、弦节比和单位倾角等单值性条件组成，综合反映了工作介质性质、工作参数和结构参数对制动转矩的影响.

2　单值性条件对制动性能影响的试验

2.1　台架试验设备

液力缓速器试验台如图 1 所示，由液力缓速器、水温、油温传感器(型号：HSTL-PT1000，温度范围：-50 ~ 200 ℃，精度：±0.1% F.S)、压力传感器(型号：HSTL-2A，压力范围：0 ~ 25 MPa，精度：±0.25% F.S)、工况控制柜、模拟车辆惯性输入的驱动电动机(YSP315L2-2)、飞轮组(模拟 20 t 车辆减速的过程)、转矩、转速传感器(湘仪动力测试仪器有限公司 JC3A 型转矩、转速传感器，转矩测量精度：0.1 级，转速测量精度：±1 r·min^{-1})、转矩仪(湘仪动力测试仪器有限公司 JW-2A 型转矩仪)和散热水箱等组成.

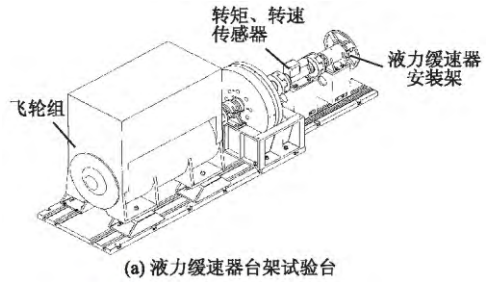

(a) 液力缓速器台架试验台

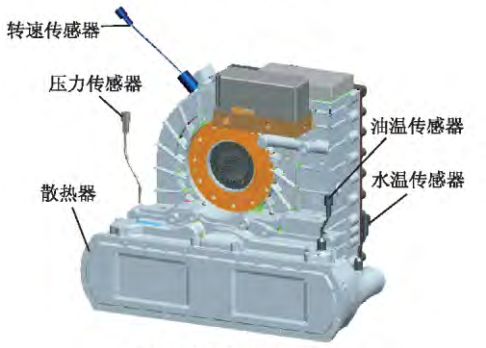

(b) 试验用液力缓速器

图 1　液力缓速器试验台示意图

2.2　试验用液力缓速器样机

试验采用 5 台液力缓速器样机，分别用 1，2，3，4，5 来表示. 样机 1 的循环圆直径为 298 mm，其他均为 308 mm；样机 3 的工作直径为 63 mm，其他均为 62 mm；定轮叶片数均为 33 片；动轮叶片数均为 36 片；样机 1，2，3 的叶片倾角均为 45°，样机 4 为 40°，样机 5 为 47°；有进油口的叶片厚度为 6.3 mm，无进油口的叶片厚度除了样机 1 为 2.7 mm 外，其他均为 2.5 mm；进油口均为 11 个.

2.3　试验方法

为验证不同工作介质对制动性能的影响，采用蓝喜力 HX7 5W-40 机油及空气进行制动试验. 进气压力为 0.5 MPa 时，采集制动过程中不同转速下转矩仪的数值为机油制动的转矩. 把液力缓速器的挡位置于空挡(即工作腔内完全不充油，进气压力为 0 MPa 的情况下)，采集制动过程中不同转速下转矩仪的数值为空气制动的转矩. 当转速稳定在1 100 r·min^{-1}，改变进气压力获得液力缓速器压力变化，测得的转矩用以验证工作参数的影响. 为验证结构参数对液力缓速器制动性能的影响，从式(6)可知液力缓速器制动转矩与循环圆直径成正比，因此采用样机 1，2 验证循环圆直径的影响；采用样机 2，4，5 验证单位倾角的影响；采用样机 2，3 验证弦节比的影响；试验过程与测机油的制动转矩的过程一致. 当转速分别稳定在(430 ± 10)，(510 ± 10)，(600 ± 10) r·min^{-1}时，样机 1 保持持续制动，进气压力为 0.5 MPa，记录相应转速下的转矩和油的温度，以分析温度对转矩的影响. 均以 3 次试验平均值作为最终分析结果.

3　试验结果与分析

3.1　工作介质与工作参数

采用机油进行制动的转矩曲线如图 2 所示.

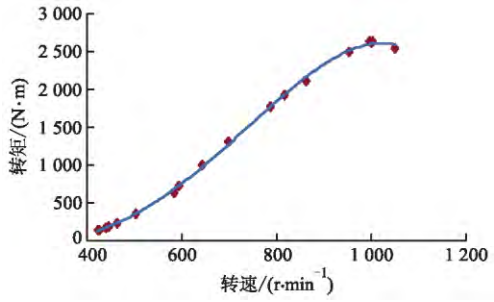

图 2　机油制动的转矩拟合曲线

液力缓速器的转矩是随着转速的增加而升高，在转速较低时，转矩上升比较慢，当转速大于 600 r·min^{-1}后，转矩上升较快.

空气制动即液力缓速器空转时产生制动转矩，转矩拟合曲线如图 3 所示. 空气有一定的黏度，空气

在液力缓速器空载时的运动是黏性运动，从图3中可以看出：随着转速的增加，该制动转矩也逐渐升高，在900 r·min^{-1}时制动转矩为70～80 N·m.

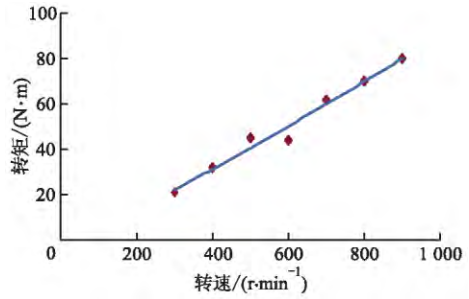

图3 空气制动的转矩拟合曲线

液力缓速器机油压力变化时，转矩变化如图4所示，当转速一定时，工作腔内油压为0时，制动转矩很小；随着工作腔内油压增加，制动转矩增加.

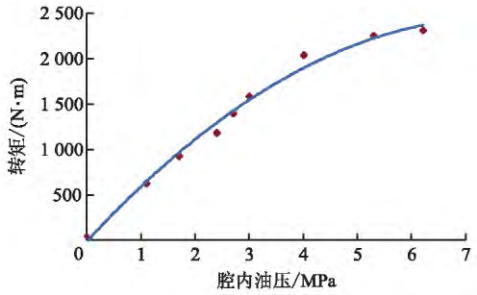

图4 油压变化的转矩拟合曲线

3.2 结构参数

3.2.1 循环圆直径

样机1，2的转矩拟合曲线如图5所示，拟合系数均达到0.9以上，相关性较高. 在相同转速下样机1的转矩比样机2的低，样机1，2结构参数主要不同是循环圆直径，故制动转矩与循环圆直径成正比.

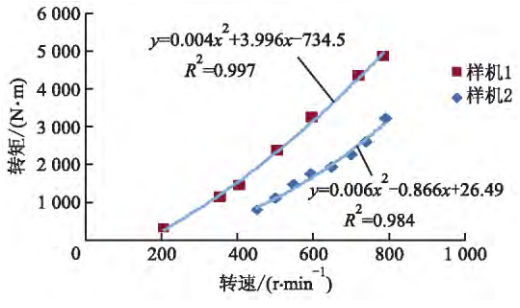

图5 样机1，2的转矩拟合曲线

3.2.2 单位倾角

样机2，4，5的单位倾角分别为0.500°，0.444°，0.520°. 在转速一定即(1 000±10) r·min^{-1}时，样机2，4，5的制动转矩如表1所示，不同单位倾角对制动转矩有影响.

表1 同一转速下样机2，4，5的制动转矩

样机	单位倾角/(°)	制动转矩/(N·m)
样机2	0.500	6 109.1
样机4	0.444	4 296.0
样机5	0.520	5 017.0

3.2.3 弦节比

根据式(1)计算可得样机2，3的弦节比分别为$l_2/b_2=1.13$，$l_3/b_3=1.148$. 样机2，3的转矩拟合曲线如图6所示，拟合系数均达到0.9以上，相关性较高. 从图6可以看出：在800 r·min^{-1}以下，样机2，3的转矩相差不大，超过800 r·min^{-1}后，在相同转速下，样机3的转矩比样机2的大. 样机2的弦节比比样机3的小，故弦节比大时，转矩较大.

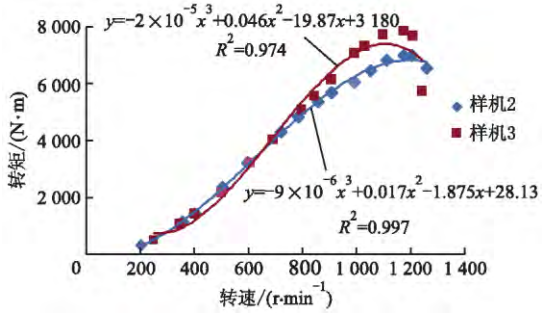

图6 样机2，3的转矩曲线

3.3 油 温

对温度t进行量纲一处理，$\frac{t}{t_0}$，t_0为油温变化范围，根据前期试验的结果油温的变化范围在所有工况下为30～130 ℃，故t_0的值为100. 不同转速下的量纲一油温的转矩曲线如图7所示，随着量纲一油温逐渐增加，转矩逐渐增加.

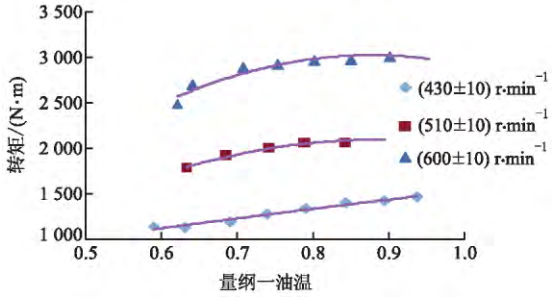

图7 量纲一油温的转矩散点图

4 各准则数与制动转矩的关系

根据样机1的转速与转矩试验，转矩与普朗特

数、雷诺数之间的关系分别如图 8 所示.

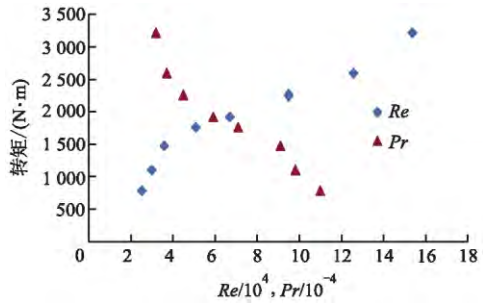

图 8　转矩与普朗特数、雷诺数的散点图

普朗特数是一个由流体物性参数组成的准则数，表征流体的物性对液力缓速器转矩的影响. 从图 8 可以看出：转矩与普朗特数成反比，随着普朗特数增加而降低.

雷诺数是表征流体受迫流动状态的准则，雷诺数越大，表明工作介质的受迫流动越剧烈，制动转矩越大. 从图 8 可以看出制动转矩是随着雷诺数的增加而增大的.

从图 4 可知随着工作腔内油压增加，制动转矩增加. 欧拉数主要反映压力对流体流动影响的准则数，流体的流动要有压差作为推动力，藉以克服流体阻力，故液力缓速器制动过程的驱动力来源于工作腔工作介质的压力差.

5　结　论

1）液力缓速器准则函数由雷诺数、普朗特数、欧拉数、单位倾角和弦节比组成.

2）通过试验可知：随着转速的增加，不同工作介质制动时制动转矩均增大；在相同转速下，机油的制动转矩比空气的制动转矩高；制动转矩与循环圆直径成正比；3 台样机中单位倾角为 0.500°时制动转矩最大；弦节比大，转矩较大；随着量纲一油温逐渐增加，转矩逐渐增加.

3）在工作介质一定的情况下，转矩与普朗特数成反比，随着普朗特数增加而降低；雷诺数越大，表明工作介质的受迫流动越剧烈，制动转矩随着雷诺数的增加而增大；随着工作腔内油压增加，制动转矩增加，液力缓速器制动过程的驱动力来源于工作腔工作介质的压力差.

参考文献(References)

[1] 姚寿文，王晓龙. 液力减速器叶栅系统优化及制动动力学仿真[J]. 机械设计，2007，24(12)：21－23，42.
YAO S W，WANG X L. Optimization on blade-grid system of hydraulic retarder braking dynamics simulation[J]. Journal of Machine Design，2007，24(12)：21－23，42.(in Chinese)

[2] 严军，过学迅，汪斌，等. 车辆液力缓速器内腔压力特性分析及建模[J]. 汽车工程，2010，32(4)：308－313.
YAN J，GUO X X，WANG B，et al. Analysis and modeling of internal pressure characteristics of vehicle hydraulic retarder[J]. Automotive Engineering，2010，32(4)：308－313.(in Chinese)

[3] 荆崇波，胡纪滨，鲁毅飞. 车用液力减速器制动性能试验研究[J]. 汽车技术，2005(12)：27－31.
JING C B，HU J B，LU Y F. Study on brake performance of automobile hydraulic retarder[J]. Aotomobile Technology，2005(12)：27－31.(in Chinese)

[4] 李涛. 车用电控液力缓速器现代设计方法研究[D]. 长春：吉林大学，2007.

[5] 何仁，严军，鲁明. 液力缓速器三维数值模拟及性能预测[J]. 汽车工程，2009，31(3)：250－252.
HE R，YAN J，LU M. 3D numerical simulation and performance prediction of hydraulic retarder[J]. Automotive Engineering，2009，31(3)：250－252.(in Chinese)

[6] 严军，何仁，鲁明. 液力缓速器变叶片数的三维数值模拟[J]. 江苏大学学报(自然科学版)，2009，30(1)：27－31.
YAN J，HE R，LU M. Numerical simulation of hydraulic retarder with different blade number[J]. Journal of Jiangsu University(Natural Science Edition)，2009，30(1)：27－31.(in Chinese)

[7] 何仁，严军，鲁明. 不同流道轴面形状的液力缓速器内流场的模拟[J]. 系统仿真学报，2009，21(24)：7743－7746.
HE R，YAN J，LU M. Simulation of inner flow field of the hydraulic retarder of different channel section shape[J]. Journal of System Simulation，2009，21(24)：7743－7746.(in Chinese)

[8] 严军，何仁. 液力缓速器叶片变角度的缓速性能分析[J]. 农业机械学报，2009，40(4)：206－210.
YAN J，HE R. Performance analysis for hydrodynamic retarder with different vanes[J]. Transactions of the Chinese Society for Agricultural Machinery，2009，40(4)：206－210.(in Chinese)

[9] 何仁，严军，鲁明. 叶片不同倾斜方式对液力缓速器缓速性能的影响分析[J]. 机械科学与技术，2009，28(8)：1056－1059.

(下转第 656 页)

LO-EKF algorithms [J]. Automotive Engineering, 2014, 36(11): 1316 - 1320. (in Chinese)

[5] 杨斯琦,解小华,陈虹. 一种新型的轮胎力级联估计方法 [J]. 信息与控制,2015,44(2): 203 - 214.
YANG S Q, XIE X H, CHEN H. Vehicle tire forces estimation using a novel cascade method [J]. Information and Control, 2015, 44(2): 203 - 214. (in Chinese)

[6] 赵海燕,陈虹,苏海涛,等. 基于滑模观测器的汽车轮胎力估计 [C] //第27届中国控制会议论文集. 北京:北京航空航天大学出版社, 2008: 691 - 695.

[7] JIN X J, YIN G D. Estimation of lateral tire-road forces and sideslip angle for electric vehicles using inte-racting multiple model filter approach [J]. Automatica Sinica Journal of the Franklin Institute, 2015, 352(2): 686 - 707.

[8] KENTA M, HORISHI F, YOICHI H. Four-wheel driving-force distribution method based on driving stiffness and slip ratio estimation for electric vehicle with in-wheel motors [C] //IEEE Vehicle Power and Propulsion Conference. USA: IEEE, 2012: 1286 - 1291.

[9] 王新,吕剑虹,向文国. 一种改进的子空间辨识方法在热工过程中的应用 [J]. 中国电机工程学报,2010, 30(32): 96 - 102.
WANG X, LYU J H, XIANG W G. A modified subspace identification method and its application in thermal process [J]. Proceedings of the CSEE, 2010, 30(32): 96 - 102. (in Chinese)

[10] 李顶根,刘刚. 基于PEM与子空间方法的汽油机空燃比动态模型辨识 [J]. 内燃机学报,2012,30(3): 248 - 253.
LI D G, LIU G. Air/fuel ratio control model of gasoline engine based on subspace identification and PEM methods [J]. Transactions of CSICE, 2012, 30(3): 248 - 253. (in Chinese)

[11] 刘昕明,高宪文,刘昕哲. 基于改进闭环子空间的集气管压力辨识方法 [J]. 仪器仪表学报,2014,35(5): 1079 - 1085.
LIU X M, GAO X W, LIU X Z. Gas collector pressure identification method based on improved closed-loop subspace [J]. Chinese Journal of Scientific Instrument, 2014, 35(5): 1079 - 1085. (in Chinese)

(责任编辑 贾国方)

(上接第649页)

HE R, YAN J, LU M. Performance analysis of a hydraulic retarder with different vane inclinations [J]. Mechanical Science and Technology for Aerospace Engineering, 2009, 28(8): 1056 - 1059. (in Chinese)

[10] 冯宜彬,过学迅. 液力减速器内流场的CFD数值模拟研究 [J]. 汽车工程,2009,31(4): 353 - 356.
FENG Y B, GUO X X. A study on the CFD numerical simulation of internal flow field in hydraulic retarder [J]. Automotive Engineering, 2009, 31(4): 353 - 356. (in Chinese)

[11] 王峰,闫清东,马越,等. 基于CFD技术的液力减速器性能预测研究 [J]. 系统仿真学报,2007,19(6): 1390 - 1392.
WANG F, YAN Q D, MA Y, et al. Prediction and analysis on hydraulic retarder performance based on CFD technology [J]. Journal of System Simulation, 2007, 19(6): 1390 - 1392. (in Chinese)

[12] 闫清东,邹波,唐正华,等. 车用液力减速器叶片数三维集成优化 [J]. 农业机械学报,2012,43(2): 21 - 25.
YAN Q D, ZOU B, TANG Z H, et al. 3-D integrated optimization of blade numbers for vehicular hydraulic retarder [J]. Transactions of the Chinese Society for Agricultural Machinery, 2012, 43(2): 21 - 25. (in Chinese)

(责任编辑 贾国方)

本刊被下列数据库列为来源期刊

荷兰《文摘与引文数据库》(SCOPUS)
英国《物理学、电技术、计算机与控制信息社数据库》(INSPEC)
美国《剑桥科学文摘》(CSA)
美国《化学文摘》(CA)
美国《数学评论》(MR)
俄罗斯《文摘杂志》(AJ)
德国《数学文摘》(ZBL MATH)
波兰《哥白尼索引》(IC)
英国《农业与生物科学研究中心文摘》(CABI)
中国科学引文数据库(CSCD)
中国学术期刊文摘(CSAC)

校名用字　赵朴初
封面设计　朱赢椿

本刊被《中文核心期刊要目总览》(2014年版)列为综合性科学技术类核心期刊,2013年被评为"RCCSE中国权威学术期刊"。被中国知网(www.cnki.net)、中国科技论文在线(www.paper.edu.cn)全文收录。

2002—2004年连获2届江苏期刊方阵优秀期刊奖。
2006—2014年连获5届中国高校优秀科技期刊奖。
2009年获第四届华东地区优秀期刊奖。
2011年获中国精品科技期刊奖。
2015年获江苏省精品科技期刊项目资助。

江苏大学学报(自然科学版)

JIANGSU DAXUE XUEBAO
(Ziran Kexue Ban)
1980年创刊,双月刊
第37卷　第6期　(总第191期)
2016年11月10日出版

JOURNAL OF JIANGSU UNIVERSITY
(Natural Science Edition)
Bimonthly, Started in 1980
Vol. 37 No.6 (Sum No.191)
Nov.10, 2016

主管单位　江苏省教育厅
主办单位　江 苏 大 学
主　　编　袁 寿 其
编辑出版　《江苏大学学报(自然科学版)》编辑部
地　　址　镇江市梦溪园巷30号
邮　　编　212003
电子信箱　xbbj@ujs.edu.cn
网　　址　http://zzs.ujs.edu.cn
电　　话　0511-84446612
印　　刷　江苏省邮电印刷厂
订　　阅　全国各地邮局
国内发行　镇江市邮局发行处
国外发行　中国国际图书贸易总公司

Administrated by Education Department of Jiangsu Province
Sponsored by Jiangsu University
Editor-in-Chief: Yuan Shouqi
Edited and Published by Editorial Department of Journal of Jiangsu University
Address: 30 Mengxiyuan Lane, Zhenjiang 212003, P.R.China
E-mail: xbbj@ujs.edu.cn
http://zzs.ujs.edu.cn
Telephone: 86-511-84446612
Distributed by China International Book Trading Corporation (P.O.Box 399, Beijing 100044, P.R.China)
Issue Number: BM5821

中国标准连续出版物号　ISSN 1671-7775 / CN 32-1668/N
邮发代号　28-83
国内定价　28.00元

ISSN 1671-7775
9 771671 777164 11>

汽车行业一等期刊　国家中文核心期刊
中国汽车工程学会　长春汽车研究所　主办
ISSN 1000-3703
CODEN: QJISEX

汽车技术

4
2010
QICHE JISHU

Automobile Technology

9 771000 370004 04>

汽车技术(月刊)　2010 年第 4 期(总第 415 期)

1970 年创刊
国内外公开发行

主　　管：国有资产监督管理委员会
主　　办：中国汽车工程学会
　　长春汽车研究所
编 辑 出 版：《汽车技术》杂志编辑部
主　　编：朱　兴　泽
电　　话：(0431)85789857
传　　真：(0431)85789810
地　　址：长春市创业大街 1063 号
邮 政 编 码：130011
电 子 信 箱：bjb_qy@faw.com.cn
国内统一刊号：CN22-1113/U
广告经营许可证：2201005050129
印　　刷：长春一汽四环汽研
　　印刷有限公司
发　行　号：国内 12-2　国外 M521
总 发 行 处：吉林省报刊发行局
订　阅　处：全国各地邮局,8 元/册
国外总发行处：中国国际图书贸易总公司
　　(北京 399 信箱)
本期出版日期：4 月 24 日

目　次

设计·计算·研究

悬架衬套安装方向优化设计 …… 郭孔辉　等　(1)
基于应力优化的大客车结构多目标优化 …… 丁炜琦　等　(4)
基于 BOOST 软件对某款汽油机
　排气歧管的优化 …… 周　毅　等　(8)
轿车柴油机气门正时和喷油嘴流量
　仿真与试验研究 …… 周岳康　等　(12)
优化设计方法在整车早期
　开发中的对比研究 …… 姜　欣　等　(17)
利用蜂窝结构改善汽车耐撞性的仿真研究 …… 简坚得　等　(21)
优化设计在汽车零部件轻量化中的应用 …… 蔡　锋　等　(25)
空气弹簧刚度特性模型及气体
　非理想化修正方法研究 …… 陈　龙　等　(29)
带复杂花纹的轮胎滑水
　显式动力学分析 …… 赵珍辉　等　(34)
燃油 2 次喷射对柴油机
　性能的影响研究 …… 姚　勇　等　(39)
液力机械自动变速器动力性
　换挡点算法研究 …… 李春芾　等　(42)

试验·测试

基于台架检测汽车滚动阻力的修正模型 …… 林彩霞　等　(46)
基于 CFD 的柴油机进气流动瞬态
　数值模拟与试验研究 …… 胡云萍　等　(50)

材料·工艺·设备

球墨铸铁转向节柱疲劳性能研究 …… 高秋金　等　(54)
基于变形镁合金的座椅靠背
　骨架轻量化设计 …… 高云凯　等　(57)

广　告

彩色广告目次 …… (33)
汕头市富力机械制造有限公司广告 …… (62)

Automobile Technology (Monthly) No.4,2010 (Serial No.415)

Department Responsible for:
State-owned Assets Supervision and Administration Commission
Sponsors:
The Society of Automotive Engineers of China; Changchun Automotive Research Institute
Publisher:
《Automobile Technology》Magazine Editorial Board
Managing Editor:
Zhu Xingze
Address:
1063 Chuang Ye Avenue, Changchun of China
Post Code:
130011
E-mail:
bjb_qy@faw.com.cn
Tel:
(0431)85789857
Fax:
(0431)85789810
Overseas Distributor:
China International Book Trading Co. (P.O.Box399, Beijing)
Code:
M521

CONTENTS

·DESIGN·CALCULATION·RESEARCH·

The Optimization of Suspension Bushing Mounting Direction ····· Guo Konghui et al (1)
Multi-objective Optimization on Bus Structure based on Optimized Stress ····· Ding Weiqi et al (4)
Optimization for A Gasoline Engine Exhaust Manifold based on BOOST Software ····· Zhou Yi et al (8)
Simulation and Test Study of the Valve Timing and Injector Flow Rate of Diesel Engine for Passenger Car ····· Zhou Yuekang et al (12)
Comparative Study of Optimization Design Method in the Early Stage of Vehicle Development ····· Jiang Xin et al (17)
A Simulation Study on Improving Vehicle Crashworthiness with Honeycomb Structure ····· Jian Jiande et al (21)
Application of Optimization Design in the Lightweight of Automotive Components ····· Cai Feng et al (25)
Study on Air Spring Stiffness Characteristic Model and Amendment to the Non-ideal Gas ····· Chen Long et al (29)
Explicit Dynamic Analysis of Hydroplaning for Tire with Complex Tread Pattern ····· Zhao Zhenhui et al (34)
Investigation on Influence of Secondary Fuel Injection on Diesel Engine Performance ····· Yao Yong et al (39)
Study on the Calculation Method of the Power Shift Point of Hydro-mechanical Automatic Transmission ····· Li Chunfu et al (42)

·TEST·MEASUREMENT·

Revising Model of Automobile Rolling Resistance based on Bench Test ····· Lin Caixia et al (46)
Transient value Simulation and Experimental Study on Air Intake Flow of Diesel Engine based on CFD ····· Hu Yunping et al (50)

·MATERIAL·TECHNOLOGY·EQUIPMENT·

Research on Fatigue Performance of Ductile Iron Steering Knuckle ····· Gao Qiujin et al (54)
Light-weight Design of Seat Backrest Frame based on Wrought Magnesium-alloy ····· Gao Yunkai et al (57)

基于台架检测汽车滚动阻力的修正模型

林彩霞[1]　刘浩学[2]　杨小刚[3]

（1.华南农业大学；2.长安大学；3.邢台职业技术学院）

【摘要】通过研究底盘测功机台架与实际道路的滚动阻力之间存在的差异，以及对车轮在台架上滚动阻力的分析，建立了车辆台架检测滚动阻力修正模型。以某型汽车为例，对该模型进行了台架对比试验验证。利用该模型求得检测车辆在任意滚筒直径的底盘测功机上的加载功率，其精度满足测功机检测规程中的规定。

主题词：滚动阻力　底盘测功机　修正模型

中图分类号：U467.1+2　文献标识码：A　文章编号：1000-3703(2010)04-0046-04

Revising Model of Automobile Rolling Resistance based on Bench Test

Lin Caixia[1], Liu Haoxue[2]

(1.South China Agricultural University; 2. Chang'an University; 3.Xingtai Polytechnic College)

【Abstract】By studying the difference of rolling resistance between chassis dynamometer bench and road, and analyzing the rolling resistance of wheels on bench, a revising model to test rolling resistance of vehicle bench is built. The paper takes a vehicle as example to compare and test the model with stand. With the aid of this model, loading power of the tested vehicle on the chassis dynamometer with random barrel diameter is obtained with accuracy in compliance with the requirement of dynamometer test regulation.

Key words: Rolling resistance, Dynamometer, Revising model

1　前言

汽车底盘测功机是一种根据相似理论模拟车辆在道路上实际行驶工况、进行不解体检验车辆性能的室内台架检测设备。该设备利用滚筒代替路面，由加载装置模拟车辆在平直道路上行驶时受到的空气阻力和滚动阻力；当汽车加速或滑行时，用惯性模拟系统即飞轮或交直流电机来模拟惯性阻力。因此，在底盘测功机上能测试汽车底盘输出功率、最高车速、加速时间和滑行距离等，以此判定汽车的动力性及底盘技术状况。同时由于底盘测功机可模拟道路行驶工况及方便地对试验车辆加载，故可在测量尾气排放和燃油消耗时作为车辆的外部负荷。为使底盘测功机检测结果更接近车辆实际运行情况，本文针对在台架上进行排放检测时滚动阻力存在的问题，在对台架和道路的滚动阻力分析的基础上，建立了滚动阻力修正模型，减小了测试数据误差。

2　工况法加载中存在的问题

GB18285—2000《在用车排气污染物限值及测试方法》中要求采用加速模拟工况试验法（ASM 法）测试汽车排放性能，用该方法检测时需对测功机进行加载计算，该标准给出了滚筒直径为 218 mm（下称小滚筒）时，在 ASM5025 工况与 ASM2540 工况下测功机的加载量，分别用 P_{5025-2} 和 P_{2540-2} 表示。对于同一辆被检测车辆来说，在滚筒直径不同的测功机上加载量的大小差异主要反应在滚动阻力损耗上，因此任意滚筒直径的测功机以滚筒直径为 218 mm 为基准进行加载，计算如下：

$$P_{5025}=P_{5025-2}+P_{f5025-2}-P_{f5025} \quad (1)$$

$$P_{2540}=P_{2540-2}+P_{f2540-2}-P_{f2540} \quad (2)$$

式中，P_{5025}、P_{2540} 分别为任意滚筒直径的测功机在 ASM5025 工况和 ASM2540 工况下设定的功率值；$P_{f5025-2}$、$P_{f2540-2}$ 分别为小滚筒的测功机在 ASM5025 工况和 ASM2540 工况下与滚筒表面摩擦损失功率；P_{f5025}、P_{f2540} 分别为任意滚筒直径的测功机在 ASM5025 工况和 ASM2540 工况下与滚筒表面摩擦损失功率。

上两式中，P_{5025-2}、P_{2540-2} 为已知量，为了计算出任意滚筒直径的加载量，在 GB18285—2000《在用车排气污染物限值及测试方法》中给出了某型号轮胎在任意直径滚筒表面滚动损失功率的计算公式。但是利用此公式计算时，对不同轮胎型号有不同的系数值，需要利用反拖或滑行的方法进行现场测试以确定系数，制约了检测线的检测效率，实际应用意义不大。为提高设备的检测精度及降低成本，必须探

索简易、方便且能满足一定精度要求的加载方法，这是本文的主要论述内容。

3 滚动阻力修正模型

3.1 滚动阻力分析

车轮在道路和滚筒上滚动时，轮胎与道路和滚筒接触区域产生法向、切向的相互作用及相应的轮胎变形力。此时由于轮胎有内摩擦产生弹性迟滞损失，使轮胎所做的功不能全部回收。

如图 1 所示，$\overset{\frown}{OCA}$、$\overset{\frown}{ADE}$分别为加载变形曲线和卸载变形曲线，显然两曲线并不重合，面积之差则为加载与卸载过程的能量损失。此能量消耗在轮胎各组成部分相互之间的摩擦以及橡胶、帘线等物质的分子间的摩擦，最后转化为热能而消失在大气中，这种损失即为弹性物质的迟滞损失，表现为阻碍车轮滚动的一种阻力偶，也就是汽车的滚动阻力。

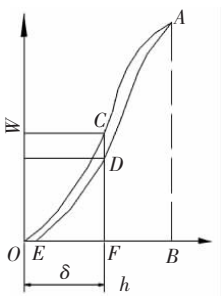

图 1 轮胎弹性迟滞曲线

3.1.1 汽车在台架上的滚动阻力分析

当车轮在台架上不滚动时，滚筒对车轮的法向反作用力的分布是前后对称的；但当车轮滚动时，在连线 O_1O_2（见图 2）前后作用力相对应点 d 和 d'的变形虽然相同，但由于存在弹性迟滞现象，处于压缩过程的前部点 d 的法向反作用力就大于处于恢复过程的后部点 d'的法向反力，如图 2 所示。从图 1 也可看出，设同一变形量为 δ，压缩时的受力为 CF，恢复时的受力为 DF，而 CF 大于 DF，这样使得前、后滚筒对轮胎法向反作用力的分布并不对称，反作用力的合力 F_{N1} 和 F_{N2} 以滚筒中心为原点向前偏斜了一定角度。设前滚筒偏斜了 γ 角，后滚筒偏斜了 β 角，其偏斜角度的大小与轮胎的结构、材料、气压、载荷、磨损程度和车速有关。当轮胎变形增大时，滚筒偏斜角也随着轮胎弹性迟滞损失的增大而增大。由于偏斜角的存在使接触面上的合力 F_{N1} 和 F_{N2} 的作用点相对于 O_1O_2 和 O_1O_3 连线向前移动的距离分别为 $l_1=\gamma\cdot r$ 和 $l_2=\beta\cdot r$[1]（见图 3）。

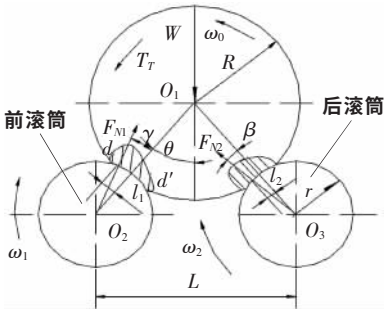

图 2 车轮在滚筒上滚动时接触面上压力分布示意

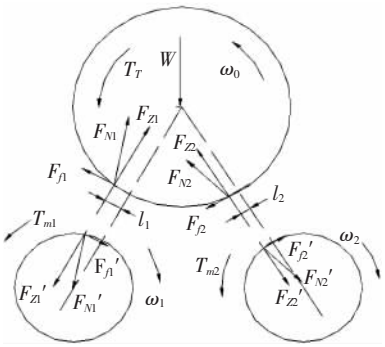

图 3 驱动轮与滚筒的受力示意

为分析方便，将研究对象取分离体，即将合力 F_{N1} 和 F_{N2} 分别分解成平行于 O_1O_2 和 O_1O_3 连线的支反力 F_{Z1} 和 F_{Z2}（见图 3），以及垂直于 O_1O_2 和 O_1O_3 连线的滚动阻力 F_{f1} 和 F_{f2}。为使车轮能在滚筒上匀速滚动，必须在车轮上施加驱动力矩 T_T 以克服滚动阻力和支反力对车轮造成的阻力矩。

由平衡条件[2]得：

对 O_1 取矩有：

$$T_T=F_{f1}\cdot R+F_{Z1}\cdot l_1+F_{f2}\cdot R+F_{Z2}\cdot R \tag{3}$$

对 O_2 取矩有：

$$F_{Z1}'l_1=F_{f1}'\cdot r \tag{4}$$

对 O_3 取矩有：

$$F_{Z2}'\cdot l_2=F_{f2}'\cdot r \tag{5}$$

又

$$F_{f1}=-F_{f1}',F_{f2}=-F_{f2}',F_{Z1}=-F_{Z1}',F_{Z2}=-F_{Z2}' \tag{6}$$

对上述方程联立求解得

$$T_T=(F_{f1}+F_{f2})\cdot(R+r) \tag{7}$$

令 $(F_{f1}+F_{f2})=F_f'$ 为车轮滚动的总阻力，根据汽车理论，汽车在滚筒上受到的滚动阻力为：

$$F_f'=(F_{Z1}+F_{Z2})\cdot f' \tag{8}$$

支反力与轴重有如下关系：

$$F_{Z1}=F_{Z2}=W/2\cos\theta \tag{9}$$

而

$$\theta=\arccos\sqrt{1-(\frac{L}{2(R+r)})^2} \tag{10}$$

则

$$F_f'=W\cdot f'/\sqrt{1-(\frac{L}{2(R+r)})^2} \quad (11)$$

式中，W 为轴重；L 为滚筒中心距；R 为轮胎静力半径；r 为滚筒半径；θ 为滚筒中心距与滚筒径向载荷作用方向之间的夹角，即安置角；f' 为台架滚动阻力系数。

3.1.2 汽车在道路上的滚动阻力分析

由汽车理论得滚动阻力 $F_f=W\cdot f$[3]，又因道路的曲率半径很大，可近似看成平面，因此汽车在道路上受到的滚动阻力不受安置角的影响。由于路面材料和滚筒材料不同，因此同一轮胎在相同轴载的情况下，在道路和滚筒上的滚动阻力系数不同。安置角、滚动阻力系数的不同是造成台架与道路滚动阻力不同的根本原因。因此，在实际应用中不能简单地用汽车在道路上的流动阻力代替台架上的滚动阻力。

3.2 修正模型的建立

在检测汽车排放性能过程中，检测结果受到多方面因素的影响，为了提高检测精度必须考虑不同因素的影响程度。汽车在台架上检测时，一般都是空载，且轴荷一定，则主要影响因素是轮胎气压，而轮胎气压的增加会使滚动阻力和行驶阻力均减小。因此为保证台架检测结果的精度，在进行动力性检测时，必须保证汽车具有标准轮胎气压。但是在检测站上不可能保证所有检测车辆都是标准轮胎气压，因此对非标准轮胎气压应给以修正[4,5]。

在台架上，滚动阻力系数随轮胎气压和车速变化的经验关系式为：

$$f'=(8.575\times10^{-3}-1.625\times10^{-7}p)+(2.195\times10^{-4}-2.72\times10^{-7}p)\cdot v \quad (12)$$

式中，p 为检测轮胎气压；v 为车速。

式(12)表明，滚动阻力系数由 2 部分组成：第 1 部分 $(8.575\times10^{-3}-1.625\times10^{-7}p)$ 表示低速时阻力系数与轮胎气压成反比，第 2 部分 $(2.195\times10^{-4}-2.72\times10^{-7}p)\cdot v$ 表示阻力系数在既定的轮胎气压时随车速变化的增量，在给定的轮胎气压下，滚动阻力系数随车速的增加而增大。对任一车辆，若已知轮胎气压和检测时的车速即可求出当时的滚动阻力系数，然后代入式(11)可得到滚动阻力的修正模型：

$$F'_f=W[(8.575\times10^{-3}-1.625\times10^{-7}p)+(2.195\times10^{-4}-2.72\times10^{-7}p)\cdot v]\Big/\sqrt{1-(\frac{L}{2(R+r)})^2} \quad (13)$$

为验证该模型的有效性，以金龙 XML6402 车为例进行试验，其轮胎气压为 300 kPa，轴重为 585 kg，用反拖法和模型计算得到的滚动阻力值如表 1 所列[6]。

表 1 反拖法和模型计算得到的金龙 XML6402 车滚动阻力

车速/km·h^{-1}		20	30	40	50	60	70	80	90
滚动阻力/N	反拖法	86.6	92.9	100.3	108.0	9 120.4	131.9	143.3	154.8
	模型计算	82.9	93.1	103.2	113.4	123.5	133.7	143.8	153.9
	差值	3.7	0.2	2.9	4.5	3.1	1.8	0.5	0.9

由表 1 可知，2 种计算结果相差最大值为 4.5 N，除在车速为 20 km/h 和 50 km/h 时两者相差较大外，其它车速下均相差不大，计算结果均满足精度要求，证明了该模型的可行性。

4 修正模型的应用

将式(13)代入式(1)和式(2)，则得出任意滚筒直径的测功机在 ASM5025 工况和 ASM2540 工况下的加载功率计算公式：

$$P_{5025}=P_{5025-2}+\frac{W\cdot v}{3\,600}f'[\frac{1}{\sqrt{1-(\frac{L_1}{2(R_1+r)^2})}}-\frac{1}{\sqrt{1-(\frac{L_2}{2(R_2+r)^2})}}] \quad (14)$$

$$P_{2540}=P_{2540-2}+\frac{W\cdot v}{3\,600}f'[\frac{1}{\sqrt{1-(\frac{L_1}{2(R_1+r)^2})}}-\frac{1}{\sqrt{1-(\frac{L_2}{2(R_2+r)^2})}}] \quad (15)$$

式中，L_1、R_1 分别为小滚筒的中心距和半径；L_2、R_2 分别为其它滚筒的中心距和半径。

式(14)和式(15)的物理意义为：公式中第 1 部分 P_{5025-2} 和 P_{2540-2} 为小滚筒时需加载的功率；第 2 部分为检测车辆在小滚筒上受到滚动阻力的损耗功率与在任意滚筒直径上的差值。当已知汽车的基准质量(即汽车的整备质量加上 100 kg)、轴重 W(在检测线上可以用轴重仪测出)、测功机给定的已知参数(L_1、R_1，L_2、R_2)、气压 p(用气压表测出)、车速 v(转速表测得)、轮胎半径 r(由轮胎规格计算得)时，根据式(14)和式(15)可求出所有检测车辆在任意滚筒直径的底盘测功机上的加载功率。因此，在工况法测试汽车排放时，可不用现场反拖或滑行，利用上述方法即可快速、方便地求解加载功率，极大地提高了检测效率。

5 结束语

本文以金龙 XML6402 车为试验对象进行台架试验，建立了台架检测滚动阻力修正模型，其精度满

足测功机检测规程中的规定。该模型对一般车辆检测具有同样的参考价值，利用该模型可确定工况法测试汽车尾气排放时在不同底盘测功机上的加载功率，方法简便、准确，对汽车检测站的尾气检测具有较好的实用性。

参 考 文 献

1 王建强.台试轮胎滚动阻力特性研究:[博士论文].长春:吉林大学,2001.

2 邱宗敏. 汽车动力性台架检测与评定方法的研究:[硕士论文].西安:长安大学,2006.

3 余志生.汽车理论.北京:机械工业出版社,2000.

4 田国华,张学利,何勇,等.汽车动力性检测.北京:人民交通出版社,2002.

5 王建强,何凤江,张立斌,等.汽车动力性检测模型的建立.中国公路学报,2001,14(3):109~112.

6 沈恒范.概率论与数理统计教程.北京:高等教育出版社,1995.

（责任编辑 文 楫）

修改稿收到日期为 2010 年 1 月 17 日。

（上接第 11 页）

5 修改前、后排气系统与试验结果对比

修改前、后排气系统分别如图 19 和图 20 所示。

图 19 修改前排气系统示意

图 20 修改后排气系统示意

按改进方案 2 设计排气系统并进行试验，测得该汽油机的外特性功率和扭矩曲线，并与原方案进行比较，发现该发动机的外特性功率和扭矩确实有所提高，结果如图 21 和图 22 所示。此外，与原方案相比，改进方案燃油消耗率曲线更加平坦，低油耗范围扩大，尤其是在高转速范围内，油耗上升不大，如图 23 所示。

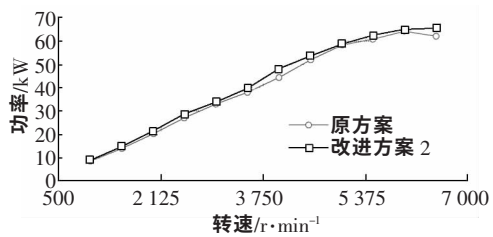

图 21 改进方案 2 与原方案功率对比曲线

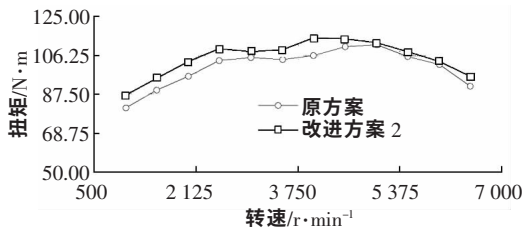

图 22 改进方案 2 与原方案扭矩对比曲线

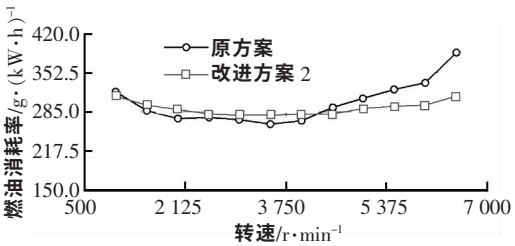

图 23 改进方案 2 与原方案燃油消耗率对比曲线

6 结束语

利用 AVL BOOST 软件对某汽油机建立了一维不稳定模拟计算模型，并对原方案进行了模拟计算。发现原方案未能达到预期性能目标，将排气歧管的连接方式由 4–1 接法改为 4–2–1 接法。经过模拟计算发现，主要工作段内发动机进气歧管气体流量有了显著增加，且排气背压增加不大。试验验证表明该发动机的外特性功率和扭矩确实有所上升，达到了预期目标值，达到优化目的。

参 考 文 献

1 刘永长. 内燃机热力过程模拟. 北京: 机械工业出版社, 1996.

2 沈运红.492Q 汽油机排气系统改型设计及模拟计算中若干问题的讨论.内燃机,1995(3).

3 Liu J P ,et al. Study On the Intake Pressure Wave Actions and Volumetric Eficiency –Speed Characteristics of Multi – Cylinder Engines. 内燃机学报, 1997.

4 Isaka Y, et al. Development of Yamaha Tumble Induction Control System(YTIS), SAE950201

5 Pearson R J, et al The simulation of gas dynamics in engine manifolds using nonlinear symmetric difference schemes, C06196 IMechE 1997.

（责任编辑 学 林）

修改稿收到日期为 2010 年 3 月 25 日。

北京天海工业有限公司

BEI JING TIANHAI INDUSTRY CO.,LTD.

地 址：北京市朝阳区天盈北路9号　　邮 编：100121
电 话：010-67383444　　传 真：010-67367022
网 址：www.btic.cn　　邮 箱：market@btic.com.cn

● 中国机械工程学会机械设计分会会刊 ● 中文核心期刊

ISSN 1001-2354
CN 12-1120/TH

机械设计®

JIXIE SHEJI
JOURNAL OF MACHINE DESIGN

3
2014
第31卷 第3期

9 771001 235142 03>

机械设计

JIXIE SHEJI

第 31 卷第 3 期 （总第 293 期）
（月刊 1983 年创刊）
2014 年 3 月 20 日出版

★中国机械工程学会机械设计分会会刊
★中国科学引文数据库(CSCD)来源期刊
★中文核心期刊
★中国科技论文统计源期刊
★学位与研究生教育指定中文重要期刊
“中国核心期刊(遴选)数据库”收录刊源
“中国科技期刊精品数据库”收录刊源
“中国期刊网”收录刊源
“中国学术期刊(光盘版)”收录刊源
“中国学术期刊综合评价数据库”收录刊源

主管单位:中国科学技术协会
主办单位:中国机械工程学会
天津市机械工程学会
天津市机电工业科技信息研究所
承办单位:天津市机电工业科技信息研究所
编辑出版:《机械设计》杂志社
社　　长:孙薇
名誉主编:王祖强
主　　编:孙薇
执行副主编:王莹
副 主 编:卜炎(兼)

地　　址:天津市河北区南口路 40 号
邮政编码:300232
电　　话:(022)27343427
传　　真:(022)27350969
http://jxsj.chinajournal.net.cn
E-mail:jxsj@chinajournal.net.cn(机械设计)
jxsj_id@163.com(工业设计)

责任编辑:陈虹　郭菊芹
英文编辑:刘国春(兼)　鲁林平(兼)
广告策划:苗冬丽
广告部电话:(022)27350969

刊号:ISSN 1001-2354
CN 12-1120/TH
国内总发行:天津市邮政报刊发行局
国外总发行:中国国际图书贸易总公司
订购处:全国各地邮局
国内邮发代号:6-59
国外邮发代号:M7315
广告经营许可证:津工商红广经许字(2013)7 号
商标注册证号:300166
印刷:天津市恒远印刷有限公司
定价:10.00 元

刊名题字:何光远

目　次

§设计领域综述§

集中电机驱动车辆动力传动系统 NVH 性能研究现状与展望 …… 于蓬,贺立钊,章桐,等(1)

§专题论文§

基于层次分析法的机械元件失效率预计 …… 谭世勇,索双富,陈绍仁(6)
基于 TRIZ 和 AD 的集成创新设计模型及其应用 …… 付敏,范德林,李锐(10)
基于模糊推理的零件特征加工方案决策研究 …… 马淑梅,刘春杰,孙运,等(15)
单台式机载电子设备的结构设计方法及应用 …… 向泽锐,徐伯初,朱先辉,等(19)
平面多自由度柔性机械手应用矢量法动力学建模及仿真 …… 田颖,张明路,张建华(25)
三关节机械臂运动精度的误差分析及补偿策略 …… 刘永青,袁祖强,戴加全,等(29)
基于变胞理论的欠驱动多指节灵巧手指的构态分析 …… 何竞飞,徐超,潘祺,等(34)
某薄板动力减振器振动特性研究 …… 李方方,李志远,王飞(39)
基于动力学仿真及非线性阻尼优化的商用车驾驶室悬置系统改进 …… 唐天柱,谢小平,白云志,等(42)
3-UPS/S 并联平台结构设计与运动学分析 …… 杨冬,李铁军,刘今越,等(47)
基于多尺度分析的截面线特征点自动提取及 B 样条曲线拟合 …… 李奇敏,蔡旭(51)
粒子群算法参数选择对动压滑动轴承优化设计的影响 …… 李佳琪,王晓红,孙军(55)
载重汽车复合悬架力学特性有限元分析 …… 庞辉,刘家连,彭威(59)
赛车转向梯形建模及优化设计 …… 向铁明,周水庭,沈理真(63)
陀飞轮在竖直位置时的摩擦力分析 …… 傅裕,王慧莹,薛超君,等(67)
利用变心齿轮传动的无碳小车的机构创新设计 …… 季元进,任利惠,顾建(71)
人工智能磁流变汽车智能制动技术研究 …… 任芸丹,芮延年(75)

§现代装备制造技术与实例分析§

液力缓速器能量耗散方程的建立 …… 林彩霞,赵旭飞(80)
基于 Unity3D 的加油车虚拟训练系统设计 …… 郭芮,蒋明,郑劼恒,等(84)
振动筛综合检测系统的设计 …… 王明新,陈纪学(88)
发动机振动评价研究 …… 徐中明,马坤,汪先国,等(90)
加工超细长轴的切削刀盘设计 …… 毛江峰,冯永刚(95)

§工业设计论坛与资讯§

产品竞争力系统性结构分析研究 …… 王华斌,郑建启(97)
针对 SOHO 族的多功能办公椅设计研究 …… 王珏,郭涵,高锐涛(101)
产品造型基因意向模型的建立及其应用 …… 侯冠华(105)
数控机床色彩设计研究 …… 赵玺,邓茜(109)
基于交互体验的智能家居控制面板设计研究 …… 熊喜秋,江文萍(113)
基于文化符号意向的手机造型设计研究 …… 杨文发,周振,许丽丽(116)
手枪式电动螺丝刀造型设计研究 …… 邬琦姝(119)
机械传动性能测试实验台原型优化设计 …… 钟蜀津,杨玉维,张磊,等(122)
轨道交通车辆内室的人性化设计 …… 王智勇,李洋,李娟(125)

工业设计作品欣赏索引:

掘进机造型设计 …… 付治国,栾丽君,张艳平(彩页 1)
摩托车尾箱设计 …… 胡俊(彩页 2)
儿童护眼台灯造型设计 …… 姚善良(彩页 3)

CONTENTS

§Summaries of designing domains§

NVH performance study of centralized motor driven vehicle power train ····· YU Peng, HE Li-zhao, ZHANG Tong, et al(1)

§Theses on special topics§

Failure rate prediction of mechanical components based on analytic hierarchy process ····· TAN Shi-yong, SUO Shuang-fu, CHEN Shao-ren(6)

Integrated innovation method based on TRIZ and AD and its application ····· FU Min, FAN De-lin, LI Rui(10)

Research on decision-making of part feature machining program based on fuzzy reasoning ····· MA Shu-mei, LIU Chun-jie, SUN Yun, et al(15)

Structural design method for single-installation airborne electronic equipment and application ····· XIANG Ze-rui, XU Bo-chu, ZHU Xian-hui, et al(19)

Modeling and simulation of planar MDOF flexible manipulator by applying vector method and dynamics ····· TIAN Ying, ZHANG Ming-lu, ZHANG Jian-hua(25)

Error analyze and compensation strategy of three-joint robot arm motion precision ····· LIU Yong-qing, YUAN Zu-qiang, DAI Jia-quan, et al(29)

Configuration analysis of under-actuated multi-phalanx dexterous finger based on metamorphic mechanisms ····· HE Jing-fei, XU Chao, PAN Qi, et al(34)

Study on vibration characteristic of sheet metal dynamic vibration absorber ····· LI Fang-fang, LI Zhi-yuan, WANG Fei(39)

Commercial vehicle cab suspensions' improvement based on dynamics simulation and nonlinear damping optimization ····· TANG Tian-zhu, XIE Xiao-ping, BAI Yun-zhi, et al(42)

Design and kinematic analysis of 3-UPS/S parallel mechanism ····· YANG Dong, LI Tie-jun, LIU Jin-yue, et al(47)

B-spline curve fitting based on multi-scale coexist automatic recognition feature point ····· LI Qi-min, CAI Xu(51)

Effect on optimization design of dynamic journal bearing by parameter choice of particle swarm algorithm ····· LI Jia-qi, WANG Xiao-hong, SUN Jun(55)

Finite element analysis of mechanical characteristics on composite rubber suspension of heavy vehicle ····· PANG Hui, LIU Jia-lian, PENG Wei(59)

Modeling and optimal design for racing car's steering trapezoid ····· XIANG Tie-ming, ZHOU Shui-ting, SHEN Li-zhen(63)

Friction analysis of a tourbillon in vertical positions ····· FU Yu, WANG Hui-ying, XUE Chao-jun, et al(67)

Innovational structure design of carbon-free car by using center-changed gear technique ····· JI Yuan-jin, REN Li-hui, GU Jian(71)

Research of vehicle intelligent brake control based on neural network and magneto-rheological fluid ····· REN Yun-dan, RUI Yan-nian(75)

§Mordern equipment manufacturing technology and analysis of examples§

Setting of hydraulic retarder energy dissipating formula ····· LIN Cai-xia, ZHAO Xu-fei(80)

Design of virtual training system for off-road group fueling vehicle based Unity3D ····· GUO Rui, JIANG Ming, ZHENG Jie-heng, et al(84)

Design of a comprehensive testing system for a vibrating screen ····· WANG Ming-xin, CHEN Ji-xue(88)

Research on vibration evaluation of engine ····· XU Zhong-ming, MA Kun, WANG Xian-guo, et al(90)

Design of cutting cutter to process ultra slender shaft part ····· MAO Jiang-feng, FENG Yong-gang(95)

§Forun and information of industrial design§

Study on systematic structural analysis of product competitiveness ····· WANG Hua-bin, ZHENG Jian-qi(97)

Research on design of multifunctional office chair for SOHO clan ····· WANG Jue, GUO Han, Gao Rui-tao(101)

Establishment and application of product appearance gene intentional model ····· HOU Guan-hua(105)

Study on color design of CNC machine ····· ZHAO Xi, DENG Qian(109)

Study of intelligent home furnishing control panel design based on interactive experience ····· XIONG Xi-qiu, JIANG Wen-ping(113)

Research of mobile phone modeling design based on culture symbolic intention ····· YANG Wen-fa, ZHOU Zhen, XU Li-li(116)

Study on modeling design of pistol-style electric screwdriver ····· WU Qi-shu(119)

Optimization design to the prototype of mechanical transmission performance tester ····· ZHONG Shu-jin, YANG Yu-wei, ZHANG Lei, et al(122)

Humanization design on interiors of the railcar ····· WANG Zhi-yong, LI Yang, LI Juan(125)

JOURNAL OF MACHINE DESIGN

M.(Since 1983)
Vol.31 No.3(Serial No.293)
2014-03-20

Responsible Department:
China Association for Science and Technology
Sponsored by:
Chinese Mechanical Engineering Society, et al
Undertaking unit:
Institute of Science & Technology Information of Mechatronic Industry, Tianjin
Edited and published by:
"Jixie Sheji" Magazine Society
Director: SUN Wei
Honorary chief editor: WANG Zu-qiang
Chief editor: SUN Wei
Executive vice chief editor: WANG Ying
Deputy chief editor: BU Yan

Address:
No. 40 Nan Kou Road,
Hebei District, Tianjin, China
Post code: 300232
Tel: 0086-22-27343427
Fax: 0086-22-27350969
http://jxsj.chinajournal.net.cn
E-mail: jxsj@chinajournal.net.cn

Responsible: CHEN Hong GUO Ju-qin
English editor: LIU Guo-chun(concurrent)
LU Lin-ping(concurrent)
Advertisement planner: MIAO Dong-li
Telephone number of advertisemet section:
0086-22-27350969

Periodical number:
ISSN 1001-2354
CN 12-1120/TH
Domestic general distributor:
Tianjin Newspaper and Magazine Publishing Bureau
Distributed abroad by:
China International Book Trade.Co.
Subscripting place:
All the post offices in China
Post distributing code:
Domestic: 6-59 Abroad: M7315
Trade mark registration number: 300166
Printed by: Hengyuan Press Ltd. Company
Price: 10.00 (CNY)

液力缓速器能量耗散方程的建立*

林彩霞，赵旭飞

（华南农业大学 工程学院，广东 广州 510642）

摘要：液力缓速器是把车辆的动能转化为工作介质的热能，实现平稳刹车的一种辅助制动装置。因其作用过程制动转矩大、过程平稳、寿命长、散热性能好等特点，在重载、高速运行的车辆上应用广泛。文中通过分析液力缓速器工作介质的流动特性，对工作介质微团所受的作用力进行分析，基于欧拉束流理论建立液力缓速器能量耗散方程，得出液力缓速器制动转矩的值取决于摩擦功的大小，而摩擦功与工作介质的粘度及应变速率的平方成正比。最后指出液力缓速器机械设计的核心在于限制工作介质的流态，为液力缓速器设计计算奠定理论基础。

关键词：液力缓速器；内部流动特性；能量耗散方程

中图分类号：U463.53 **文献标识码**：A **文章编号**：1001-2354(2014)03-0080-05

DOI:10.13841/j.cnki.jxsj.2014.03.019

在大卡车、频繁制动的公交车中，由于摩擦式制动器长时间连续制动产生热衰退导致制动失效和制动性能大幅下降，并引发事故，该事故占所有事故的比例分别超过20%和40%。如何在最大能量区把车辆的能量消耗掉，汽车需要辅助制动器。目前，汽车上安装的辅助制动器有电涡流缓速器和液力缓速器，电涡流由于同样会产生热衰退而导致制动力下降，满足不了车辆高速、重载制动的需要，因此逐渐被液力缓速器所取代。液力缓速器因其制动件磨损小、寿命长、制动转矩大、过程平稳、不会产生热衰退、散热性能好等特点，其技术装置在国外普遍应用。

我国从20世纪80年代开始，就有众多的专家学者对液力缓速器进行了理论和试验研究，如吉林大学陈波[1]、高博麟[2]、李涛[3]、李雪松[4]，北京理工大学魏巍等人[5]、闫清东等人[6]，江苏大学何仁等人[7]、严军等人[8]，武汉理工大学冯宜彬等人[9]对液力缓速器进行了试验、仿真、数值模拟分析计算和设计。近20年在国内也形成了多家液力缓速器制造商，但国内生产的液力缓速器，在相同参数和工况的情况下，出现制动转矩比国外的产品低、密封性能不好、漏油等现象，阻碍了液力缓速器产业化进程的发展。其根本原因是由于对液力缓速器制动过程中的机理等仍不清楚，缺乏对液力缓速器设计计算的正确指导理论。因此，文中通过分析液力缓速器工作介质的流动特性，建立液力缓速器能量耗散方程，为液力缓速器设计计算奠定了理论基础。

1 液力缓速器的结构及工作原理

液力缓速器的结构主要由定轮、动轮、工作介质、油池、供油管路、热交换器及比例阀等组成，安装在后桥与变速箱之间，液力缓速器的结构如图1所示。

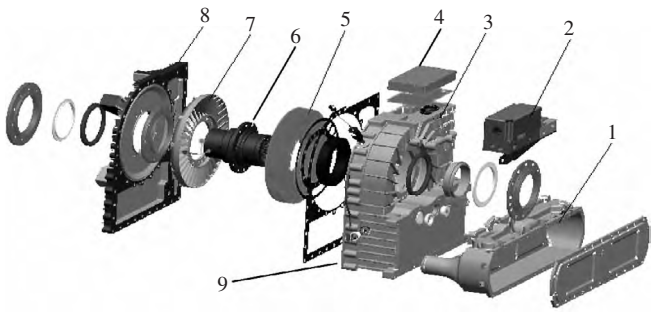

1 热交换器；2 比例阀；3 壳体；4 排气阀；5 定轮；
6 传动轴与法兰盘；7 动轮；8 前盖；9 油池

图1 液力缓速器结构示意图

定轮和动轮对置，形成工作腔经阀门和供油管路相通。液力缓速器的控制介质是压缩空气，由控制器进行控制，比例阀根据控制器给予的信号强弱对油池产生一个气动压力，该压力会根据工作状况向动轮和定轮之间的工作腔压入一定量的工作介质，工作介质通过动轮的转动而进入运动状态，在动轮和定轮之间以闭合的循环流动方式旋转，组成循环圆。工作介质有两个方向的运动——绕变速箱输出轴的轴向“公转”和绕循环圆的径向“自转”，工作介质甩向定轮时，工作介质

* 收稿日期：2013-01-30；修订日期：2013-09-10
基金项目：星火计划资助项目（2011E000040）
作者简介：林彩霞（1976—），女，广东阳江人，讲师，博士，研究方向：机械设计理论，已发表论文2篇。

的“公转”对定轮叶片产生冲击作用，将动轮作用于工作介质的动量矩传递到定轮叶片上，同时，固定的定轮叶片会对工作介质产生一个反向作用的动量矩，工作介质流出定轮再流入动轮时，对动轮产生一个反作用力，该反作用力在限制动轮转动的同时，产生热量使工作介质温度升高，从而实现对车辆的减速作用，该过程遵循能量守恒原理。

2　工作介质的流动特性

根据牛顿粘性应力公式[10]：

$$\tau_{xy}=\eta\dot{\gamma} \tag{1}$$

式中：τ_{xy}——切应力，N；

η——粘度，Pa·s；

$\dot{\gamma}$——切应变速率。

从式(1)中可以看出，切应力 τ_{xy} 与粘度 η 及切应变速率 $\dot{\gamma}$ 成正比，液体粘性愈大，切应变速率愈大，其流动所需的力愈大，流动时产生切应力也愈大，停止流动也愈快。液力缓速器的工作介质一般为机油，在标准大气压下机油的粘度如表 1 所示。

表 1　标准大气压力下机油的粘度

t/℃	η/(Pa·s)
0	3.848 23
20	0.799 41
40	0.210 25
60	0.072 49
80	0.031 95
100	0.017 05

机油为石油产品，在压力不高的情况下，其体积变化十分微小，基本可以忽略不计，一般可以认为机油是不可压缩的。因此，机油在液力缓速器内部的流动是不可压缩的粘性流动，液力缓速器能实现制动，就是由于机油的粘性流动产生的切应力。

3　液力缓速器能量耗散方程的建立

3.1　工作介质微团内部的受力分析

基于欧拉束流理论，由于工作介质在液力缓速器里的流动是受迫流动，重力作用的影响较之压力作用的影响要小得多，因此忽略重力的影响，只考虑作用在微团界面上的力。从工作介质中取出正六面微元体，如图 2 所示。

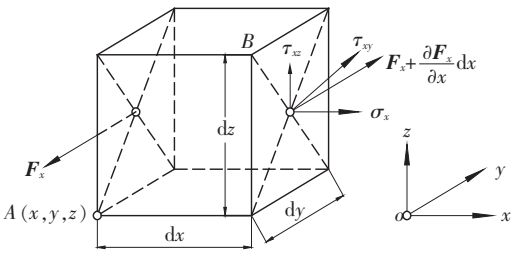

图 2　工作介质微元体的受力分布图

在垂直于 x 轴的两个外表面上，分别作用有应力 $\boldsymbol{F}_x$ 和 $\boldsymbol{F}_x+\frac{\partial \boldsymbol{F}_x}{\partial x}\mathrm{d}x$，下标 x 表示应力向量 $\boldsymbol{F}$ 作用在与 x 轴垂直的微元面上。由此可得分别作用在垂直于 x 轴、y 轴和 z 轴的微元面上的表面力的合力为：$\frac{\partial \boldsymbol{F}_x}{\partial x}\mathrm{d}x\mathrm{d}y\mathrm{d}z$，$\frac{\partial \boldsymbol{F}_y}{\partial y}\mathrm{d}x\mathrm{d}y\mathrm{d}z$，$\frac{\partial \boldsymbol{F}_z}{\partial z}\mathrm{d}x\mathrm{d}y\mathrm{d}z$，于是可得作用于单位容积的表面力的合力为：

$$\boldsymbol{F}=\frac{\partial \boldsymbol{F}_x}{\partial x}+\frac{\partial \boldsymbol{F}_y}{\partial y}+\frac{\partial \boldsymbol{F}_z}{\partial z} \tag{2}$$

式(2)中 $\boldsymbol{F}_x$，$\boldsymbol{F}_y$，$\boldsymbol{F}_z$ 都是向量，还可以把它们沿 3 个坐标方向分解，即分解成正应力 σ 和平行于各微元面的切应力 τ，则分别作用于与 x 轴、y 轴和 z 轴垂直的微元面上的应力 $\boldsymbol{F}_x$ 可分解为：

$$\begin{aligned}\boldsymbol{F}_x&=\sigma_x\boldsymbol{i}+\tau_{xy}\boldsymbol{j}+\tau_{xz}\boldsymbol{k}\\ \boldsymbol{F}_y&=\tau_{yx}\boldsymbol{i}+\sigma_y\boldsymbol{j}+\tau_{yz}\boldsymbol{k}\\ \boldsymbol{F}_z&=\tau_{zx}\boldsymbol{i}+\tau_{zy}\boldsymbol{j}+\sigma_z\boldsymbol{k}\end{aligned} \tag{3}$$

式中：$\boldsymbol{i}$，$\boldsymbol{j}$，$\boldsymbol{k}$——单位向量。

下标规定如下：正应力 σ 的下标代表应力的方向，切应力 τ 的第 1 个下标代表切应力所在平面的外法线方向，第 2 个下标代表切应力的方向，如 τ_{xy} 表示作用在与 x 轴垂直的平面上沿 y 向的切应力。由式(3)可以看出，要完全描述微元体的应力，需要有 9 个分量，表示为：

$$\boldsymbol{\pi}_{ij}=\begin{bmatrix}\sigma_x & \tau_{xy} & \tau_{xz}\\ \tau_{yx} & \sigma_y & \tau_{yz}\\ \tau_{zx} & \tau_{zy} & \sigma_z\end{bmatrix} \tag{4}$$

由式(2)、式(3)和式(4)得微元体的表面力公式如下：

$$\begin{aligned}\boldsymbol{F}=&\left(\frac{\partial\sigma_x}{\partial x}+\frac{\partial\tau_{yx}}{\partial y}+\frac{\partial\tau_{zx}}{\partial z}\right)\boldsymbol{i}+\left(\frac{\partial\tau_{xy}}{\partial x}+\frac{\partial\sigma_y}{\partial y}+\frac{\partial\tau_{zy}}{\partial z}\right)\boldsymbol{j}+\\ &\left(\frac{\partial\tau_{xz}}{\partial x}+\frac{\partial\tau_{yz}}{\partial y}+\frac{\partial\sigma_z}{\partial z}\right)\boldsymbol{k}\end{aligned} \tag{5}$$

3.2　工作介质微团的速度分析

工作介质微团 $A(x,y,z)$ 在 t 时刻的速度向量为：

$$\boldsymbol{v}_A(x,y,z,t)=\boldsymbol{u}_A(x,y,z,t)\boldsymbol{i}+\boldsymbol{v}_A(x,y,z,t)\boldsymbol{j}+\boldsymbol{w}_A(x,y,z,t)\boldsymbol{k}$$

式中：$\boldsymbol{u}$，$\boldsymbol{v}$，$\boldsymbol{w}$——$\boldsymbol{i}$，$\boldsymbol{j}$，$\boldsymbol{k}$ 三个方向的速度分量。

同一时刻在另一点 $B(x+\mathrm{d}x,y+\mathrm{d}y,z+\mathrm{d}z)$ 的速度可以用泰勒级数对点 $A(x,y,z)$ 展开：

$$\begin{aligned}&\boldsymbol{v}_B(x+\mathrm{d}x,y+\mathrm{d}y,z+\mathrm{d}z,t)=\boldsymbol{v}_A(x,y,z,t)+\\&\left(\frac{\partial \boldsymbol{V}}{\partial x}\right)_A\mathrm{d}x+\left(\frac{\partial \boldsymbol{V}}{\partial y}\right)_A\mathrm{d}y+\left(\frac{\partial \boldsymbol{V}}{\partial z}\right)_A\mathrm{d}z=\\&\left[\boldsymbol{u}_A+\left(\frac{\partial \boldsymbol{u}}{\partial x}\right)_A\mathrm{d}x+\left(\frac{\partial \boldsymbol{u}}{\partial y}\right)_A\mathrm{d}y+\left(\frac{\partial \boldsymbol{u}}{\partial z}\right)_A\mathrm{d}z\right]\boldsymbol{i}+\\&\left[\boldsymbol{v}_A+\left(\frac{\partial \boldsymbol{v}}{\partial x}\right)_A\mathrm{d}x+\left(\frac{\partial \boldsymbol{v}}{\partial y}\right)_A\mathrm{d}y+\left(\frac{\partial \boldsymbol{v}}{\partial z}\right)_A\mathrm{d}z\right]\boldsymbol{j}+\\&\left[\boldsymbol{w}_A+\left(\frac{\partial \boldsymbol{w}}{\partial x}\right)_A\mathrm{d}x+\left(\frac{\partial \boldsymbol{w}}{\partial y}\right)_A\mathrm{d}y+\left(\frac{\partial \boldsymbol{w}}{\partial z}\right)_A\mathrm{d}z\right]\boldsymbol{k}\end{aligned}\tag{6}$$

可见，B 点的速度可以用 A 点的速度及 9 个速度分量的偏导数来表示，这 9 个量组成速度导数张量，用 $\boldsymbol{D}$ 表示，即：

$$\boldsymbol{D}=\begin{bmatrix}\dfrac{\partial \boldsymbol{u}}{\partial x} & \dfrac{\partial \boldsymbol{u}}{\partial y} & \dfrac{\partial \boldsymbol{u}}{\partial z}\\ \dfrac{\partial \boldsymbol{v}}{\partial x} & \dfrac{\partial \boldsymbol{v}}{\partial y} & \dfrac{\partial \boldsymbol{v}}{\partial z}\\ \dfrac{\partial \boldsymbol{w}}{\partial x} & \dfrac{\partial \boldsymbol{w}}{\partial y} & \dfrac{\partial \boldsymbol{w}}{\partial z}\end{bmatrix}\tag{7}$$

将 3 个速度分量 $(\boldsymbol{u},\boldsymbol{v},\boldsymbol{w})$ 分别记为 $\boldsymbol{u}_1,\boldsymbol{u}_2,\boldsymbol{u}_3$，坐标轴 (x,y,z) 分别记为 x_1,x_2,x_3，则式(7)表示为：

$$\boldsymbol{d}_{ij}=\frac{\partial \boldsymbol{u}_i}{\partial x_j}\qquad(i,j=1,2,3)\tag{8}$$

根据张量分解定理[11]，可将此张量分解为一对称张量 $\boldsymbol{S}$ 与一反对称张量 $\boldsymbol{C}$ 之和，即

$$\boldsymbol{d}_{ij}=\boldsymbol{S}_{ij}+\boldsymbol{C}_{ij}\qquad(i,j=1,2,3)$$

式中：$$\boldsymbol{S}_{ij}=\frac{1}{2}\left(\frac{\partial \boldsymbol{u}_i}{\partial x_j}+\frac{\partial \boldsymbol{u}_j}{\partial x_i}\right)\qquad(i,j=1,2,3)\tag{9}$$

$\boldsymbol{S}_{ij}$ 称为应变变化率张量，式(1)可表示为：

$$\tau_{xy}=2\eta s_{yx}\tag{10}$$

由于不可压缩流体广义牛顿粘性应力公式[12]为：

$$\boldsymbol{\pi}_{ij}=\begin{cases}\eta\left(\dfrac{\partial \boldsymbol{u}_i}{\partial x_j}+\dfrac{\partial \boldsymbol{u}_j}{\partial x_i}\right) & (i\neq j)\\ 2\eta\dfrac{\partial \boldsymbol{u}_i}{\partial x_j}-P & (i=j)\end{cases}\tag{11}$$

式中：P——工作介质微团受到的压力，Pa。

又因粘性应力张量 $\boldsymbol{m}_{ij}=2\eta\boldsymbol{s}_{ij}(i,j=1,2,3)$，$\boldsymbol{\pi}_{ij}$ 用 $\boldsymbol{m}_{ij}$ 表示得：

$$\boldsymbol{\pi}_{ij}=\boldsymbol{m}_{ij}-p\delta_{ij},\delta_{ij}=\begin{cases}1 & (i\neq j)\\ 0 & (i=j)\end{cases}(i,j=1,2,3)\tag{12}$$

将式(4)和式(11)进行比较，可写出各应力分量的公式：

$$\begin{cases}\sigma_x=2\eta\dfrac{\partial \boldsymbol{u}}{\partial x}-P\\ \sigma_y=2\eta\dfrac{\partial \boldsymbol{v}}{\partial y}-P\\ \sigma_z=2\eta\dfrac{\partial \boldsymbol{w}}{\partial z}-P\end{cases}$$

$$\begin{cases}\tau_{xy}=\tau_{yx}=\eta\left(\dfrac{\partial \boldsymbol{u}}{\partial y}+\dfrac{\partial \boldsymbol{v}}{\partial x}\right)\\ \tau_{xz}=\tau_{zx}=\eta\left(\dfrac{\partial \boldsymbol{u}}{\partial z}+\dfrac{\partial \boldsymbol{w}}{\partial x}\right)\\ \tau_{zy}=\tau_{yz}=\eta\left(\dfrac{\partial \boldsymbol{v}}{\partial z}+\dfrac{\partial \boldsymbol{w}}{\partial y}\right)\end{cases}\tag{13}$$

3.3 液力缓速器能量耗散方程的建立

在以上分析的基础上，建立液力缓速器能量耗散方程。以单位质量工作介质作为研究对象，工作介质是不可压缩流体，体积膨胀率 $\dfrac{\partial \boldsymbol{u}_i}{\partial x_i}=0$，单位时间的膨胀功为零。由牛顿第二定律：在惯性系中，流体微元的质量与加速度的乘积等于该微元体所受外力的合力，则运动方程可写成向量的形式：

$$\rho\frac{\mathrm{d}\boldsymbol{V}}{\mathrm{d}t}=\boldsymbol{F}\tag{14}$$

式中：ρ——密度，$\mathrm{kg/m^3}$。

把式(2)代入上式，得：

$$\begin{cases}\rho\dfrac{\mathrm{d}\boldsymbol{u}}{\mathrm{d}t}=\dfrac{\partial \sigma_x}{\partial x}+\dfrac{\partial \tau_{yx}}{\partial y}+\dfrac{\partial \tau_{zx}}{\partial z}\\ \rho\dfrac{\mathrm{d}\boldsymbol{v}}{\mathrm{d}t}=\dfrac{\partial \sigma_y}{\partial y}+\dfrac{\partial \tau_{xy}}{\partial x}+\dfrac{\partial \tau_{zy}}{\partial z}\\ \rho\dfrac{\mathrm{d}\boldsymbol{w}}{\mathrm{d}t}=\dfrac{\partial \sigma_z}{\partial z}+\dfrac{\partial \tau_{xz}}{\partial x}+\dfrac{\partial \tau_{yz}}{\partial y}\end{cases}\tag{15}$$

因此，单位质量工作介质的动能随时间的变化率为：

$$\begin{aligned}&\rho\frac{\mathrm{d}}{\mathrm{d}t}\left(\rho\frac{\boldsymbol{u}^2+\boldsymbol{v}^2+\boldsymbol{w}^2}{2}\right)=\boldsymbol{u}\left(\frac{\partial \sigma_x}{\partial x}+\frac{\partial \tau_{yx}}{\partial y}+\frac{\partial \tau_{zx}}{\partial z}\right)+\\&\boldsymbol{v}\left(\frac{\partial \sigma_y}{\partial y}+\frac{\partial \tau_{xy}}{\partial x}+\frac{\partial \tau_{zy}}{\partial z}\right)+\boldsymbol{w}\left(\frac{\partial \sigma_z}{\partial z}+\frac{\partial \tau_{xz}}{\partial x}+\frac{\partial \tau_{yz}}{\partial y}\right)\end{aligned}\tag{16}$$

同样将 3 个速度分量 $(\boldsymbol{u},\boldsymbol{v},\boldsymbol{w})$ 分别记为 $\boldsymbol{u}_1,\boldsymbol{u}_2,\boldsymbol{u}_3$，坐标轴 (x,y,z) 分别记为 x_1,x_2,x_3，则式(16)可变为：

$$\frac{\mathrm{d}}{\mathrm{d}t}\left(\frac{1}{2}\sum_{i=1}^{3}\boldsymbol{u}_i^2\right)=\frac{1}{\rho}\sum_{i,j=1}^{3}\boldsymbol{u}_i\sum_{i,j=1}^{3}\frac{\partial \boldsymbol{\pi}_{ij}}{\partial x_j}\tag{17}$$

又根据 $\boldsymbol{u}_i\sum_{i,j=1}^{3}\dfrac{\partial \boldsymbol{\pi}_{ij}}{\partial x_j}=\dfrac{\partial(\boldsymbol{\pi}_{ij}\boldsymbol{u}_i)}{\partial x_j}-\boldsymbol{\pi}_{ij}\dfrac{\partial \boldsymbol{u}_i}{\partial x_j}$ 和式(12)，上式(17)可写成：

$$\frac{\mathrm{d}}{\mathrm{d}t}\left(\frac{1}{2}\sum_{i=1}^{3}\boldsymbol{u}_i^2\right)=\frac{1}{\rho}\sum_{i,j=1}^{3}\left[\frac{\partial(\boldsymbol{m}_{ji}\boldsymbol{u}_i)}{\partial x_j}-\frac{\partial(p\boldsymbol{u}_i)}{\partial x_i}-\boldsymbol{m}_{ji}\frac{\partial \boldsymbol{u}_i}{\partial x_j}\right]\tag{18}$$

式(18)即为液力缓速器的能量耗散方程，右边第 1 项是单位时间内切应力对运动着的单位质量工作介质所输运的机械能，该机械能由车辆的惯性能量输入；第 2 项是单位时间内压力对单位质量工作介质所做的功，即流动功；第 3 项是单位时间内切应力所做的摩擦功 $m_{ji}\dfrac{\partial \boldsymbol{u}_i}{\partial x_j}$。由于摩擦功的存在，使车辆的惯性能量不断消耗。又由于 $\dfrac{\partial \boldsymbol{u}_i}{\partial x_i}=0$，故摩擦功为：

$$m_{ji}\frac{\partial u_i}{\partial x_j}=\frac{\eta}{2}\left(\frac{\partial u_i}{\partial x_j}+\frac{\partial u_i}{\partial x_j}\right)^2 \quad (j,i=1,2,3) \tag{19}$$

式中：m_{ji}——粘性应力张量。

从式(19)可以看出，摩擦功与工作介质的粘度及应变速率的平方成正比，液力缓速器制动转矩的值取决于摩擦功的大小。

4　台架试验验证

4.1　台架试验装置

液力缓速器工况试验台的组成：液力缓速器；工况控制柜；模拟车辆惯性输入的驱动电机（长沙电机厂 YSP315L2-2）和飞轮组，该飞轮组可以模拟 20 t 车辆减速的过程；转矩转速传感器（湘仪动力测试仪器有限公司 JC3A 型转矩转速传感器）；散热水箱等。分别采用机油和空气进行制动。

4.2　试验结果分析

图 3 是采用机油进行制动的转矩曲线，从图3 可以看出液力缓速器的转矩随着转速的增加而升高，在转速为 226~400 r/min 时，转矩上升比较慢，当转速大于 400 r/min 后，转矩上升较快。随着转速的增加，制动转矩愈高。

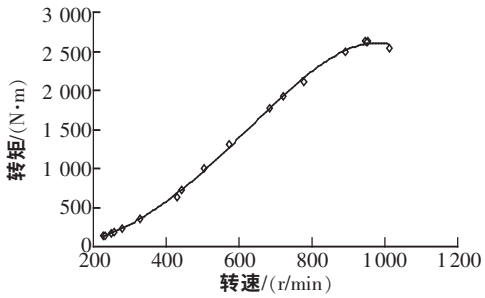

图 3　机油制动的转矩曲线

空气制动即液力缓速器空转时产生的制动转矩，如图 4 所示。空气有一定的粘度，故空气在液力缓速器空载时的运动也是粘性运动，从图 4 中可以看出，随着转速的增加，该制动转矩也是逐渐升高的，在900 r/min 时制动转矩在 70~80 N·m 之间。

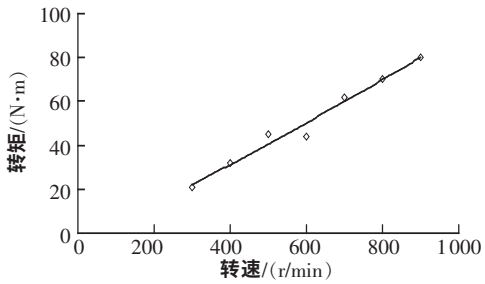

图 4　空气制动的转矩曲线

由上面的试验结果可以看出液力缓速器的制动转矩与工作介质的粘度及转速有关，其值取决于摩擦功的大小。当转速较低时，对工作介质的扰动较小，工作介质的流动速率小，摩擦功较小，故耗散的机械能少。工作介质的流动速率逐渐增大，摩擦功增大，故耗散的机械能愈多。

5　结论

液力缓速器的能量耗散方程揭示了液力缓速器制动的根本原因就是工作介质的切应力所做的摩擦功，把流体运动的机械能不可逆地转换为热能而消耗。在制动过程中，基于能量守恒原理，工作介质的温度必然升高，而粘度随着温度的升高而变得很小，因此，液力缓速器产生的制动转矩主要受切应变速率即工作介质运动速率的影响，与工作介质形成的运动密切相关。在高速时制动，工作介质运动速率高，应变速率大，摩擦功大，制动转矩高；而在低速时，应变速率小，制动转矩也小。故机械设计的核心在于限制工作介质的流态。

参考文献

[1] 陈波. 电控液力缓速器性能试验方法的研究[D]. 长春：吉林大学，2007.

[2] 高博麟. 重型车与液力缓速器匹配特性的仿真研究[D]. 长春：吉林大学，2009.

[3] 李涛.车用电控液力缓速器现代设计方法研究[D]. 长春：吉林大学，2007.

[4] 李雪松. 车辆液力缓速器三维流场分析与特性计算[D]. 长春：吉林大学，2006.

[5] 魏巍，李慧渊，邹波. 液力减速器制动性能及其两相流分析方法研究[J]. 北京理工大学学报，2010，30(11)：1281-1284.

[6] 闫清东，邹波，唐正华，等. 车用液力减速器叶片数三维集成优化[J]. 农业机械学报，2012，43(2)：21-25.

[7] 何仁，严军. 液力缓速器三维数值模拟及性能预测[J]. 汽车工程，2009，31(3)：250-252.

[8] 严军，何仁. 液力缓速器叶片变角度的缓速性能分析[J]. 农业机械学报，2009，40(4)：206-210.

[9] 冯宜彬，过学迅. 液力减速器内流场的 CFD 数值模拟研究[J]. 汽车工程，2009，31(4)：353-356.

[10] 杨明韶. 农业物料流变学[M]. 北京：中国农业出版社，2010：96-99.

基于 Unity3D 的加油车虚拟训练系统设计*

郭芮[1],蒋明[1],郑劼恒[1],杨宝锋[2]

(1.后勤工程学院 军事供油工程系,重庆 401311;2.92872 部队,辽宁 绥中 125200)

摘要:为提高越野群车加油车操作人员培训的效率和水平,节约训练成本,运用三维建模软件和 Unity3D 游戏制作引擎对加油车虚拟训练系统进行设计。设计过程包括系统整体框架规划,以加油车后操纵室操作面板的仪表驱动为例探讨了此系统的实现机制,包括三维建模、模型导入、环境设置、脚本驱动等,阐明了此系统发布运行和运用局域网互联的原理。从整体上设计了单机平台、支持局域网互联的虚拟训练系统。该系统以加油系统理论和数学模型为基础,综合运用三维建模软件和游戏制作引擎,不仅满足了后勤保障人员虚拟训练的要求,也可以为其他装备的虚拟训练研究提供借鉴意义。

关键词:加油车;Unity3D;虚拟训练

中图分类号:TP391.9 **文献标识码**:A **文章编号**:1001-2354(2014)03-0084-04

DOI:10.13841/j.cnki.jxsj.2014.03.020

越野群车加油车是我军油料加注骨干装备,具有展开撤收方便、机动能力强、加油迅速等优点。但是其实装训练的效果往往因受到场地、天气、经费、安全等因素制约而难以保证。在新时期我军大力推进现代化建设的背景下,探索更加科学有效的训练方法意义重大[1-3]。

模拟训练是装备训练的新途径新方法,在油料装备领域,已经有野战输油管线模拟训练系统研制成功,该系统是半实物仿真训练系统,提高了野战输油管线教学训练的水平和效益[4]。但是加油车体积大,操作部位、操作人员、操作环节多,采用半实物仿真成本高,不能实现费效比最小化。因此有必要研制基于 PC 平台的虚拟训练系统,使得受训者可以"足不出户"在机房里完成训练。

近年来"光荣使命"等 FPS 类游戏在部队官兵中产生了轰动效应和良好的沉浸式训练效果。如果能够运用游戏制作引擎开发加油车训练系统,模拟第 1 人称视角控制等游戏操作方式,官兵可以在近似实战的虚拟环境中完成装备的训练,既能体验类似游戏的愉悦,又能提高训练水平。而 Unity3D 是一款跨平台的专业游戏引擎,用它创建的游戏可以在浏览器、移动设备乃至游戏机等几乎所有常见的平台上运行。其简洁易用的界面和强大的功能,以及近年来对 iPhone 和 iPad 平台的支持使其成为业界主流游戏引擎[5]。

文中以 Unity3D 为平台,结合三维建模软件,阐述加油车虚拟训练系统的实现机制。

[11] 陈懋章. 粘性流体动力学基础[M]. 北京:高等教育出版社,2004:68-72.

[12] 董曾南,章梓雄. 粘性流体力学[M]. 北京:清华大学出版社,2011:56-62.

Setting of hydraulic retarder energy dissipating formula

LIN Cai-xia, ZHAO Xu-fei

(College of Engineering, South China Agricultural University, Guangzhou 510642, China)

Abstract: The hydraulic retarder is auxiliary brake equipment that turns the moving energy to the heat to brake placidity. It has the advantage of big torque, placidity, good heat disperse and long life so it is widely used in heavy, high speed vehicle. Energy dissipating formula of hydraulic retarder was set up in the paper by analyzing the working medium flow characteristic and the force of the working medium micro point, on the base of Eula theory, which drew a conclusion that the torque of hydraulic retarder was decided by the friction work which had relation with the working medium and the strain rate square. Last the paper points to the core of the mechanism design is to limit the flow form of working medium and settles the theory foundation of the hydraulic retarder design.

Key words: hydraulic retarder; inner flow characteristic; energy dissipating formula

Fig 4 Tab 1 Ref 12 "Jixie Sheji"3074

* 收稿日期:2013-10-08;修订日期:2013-12-10

基金项目:后勤工程学院学术创新资助项目(YZ08-43601)

作者简介:郭芮(1989—),男,山东聊城人,硕士研究生,主要从事油料输送技术与装备研究。

主办单位：中国机械工程学会、天津市机械工程学会、天津市机电工业科技信息研究所

报刊代号：6-59
定价：10.00元

● 中国机械工程学会机械设计分会会刊 ● 中文核心期刊

ISSN 1001-2354
CN 12-1120/TH

机械设计®

JIXIE SHEJI
JOURNAL OF MACHINE DESIGN

8
2015
第32卷 第8期

08
9 771001 235159

机械设计

JIXIE SHEJI

第 32 卷第 8 期 （总第 310 期）
（月刊 1983 年创刊）
2015 年 8 月 20 日出版

★中国机械工程学会机械设计分会会刊
★中国科学引文数据库(CSCD)来源期刊
★中文核心期刊
★中国科技论文统计源期刊
★学位与研究生教育指定中文重要期刊
“中国核心期刊(遴选)数据库”收录刊源
“中国科技期刊精品数据库”收录刊源
“中国期刊网”收录刊源
“中国学术期刊(光盘版)”收录刊源
“中国学术期刊综合评价数据库”收录刊源

主管单位：中国科学技术协会
主办单位：中国机械工程学会
天津市机械工程学会
天津市机电工业科技信息研究所
承办单位：天津市机电工业科技信息研究所
编辑出版：《机械设计》杂志社
社　　长：冯志伟
名誉主编：左斌
主　　编：孙薇
执行副主编：王莹
副 主 编：卜炎(兼)

地　　址：天津市河北区南口路 40 号
邮政编码：300232
电　　话：(022)27343427
传　　真：(022)27350969
http：//jxsj.chinajournal.net.cn
E-mail：jxsj@chinajournal.net.cn(机械设计)
jxsj_id@163.com(工业设计)

责任编辑：李娜　郭菊芹
英文编辑：李巨韬(兼)　鲁林平(兼)
广告策划：苗冬丽
广告部电话：(022)27350969

刊号：ISSN 1001-2354
CN 12-1120/TH
国内总发行：天津市邮政报刊发行局
国外总发行：中国国际图书贸易总公司
订购处：全国各地邮局
国内邮发代号：6-59
国外邮发代号：M7315
广告经营许可证：津工商红广经许字(2013)7 号
商标注册证号：300166
印刷：天津市恒远印刷有限公司
定价：12.50 元

刊名题字：何光远

目　次

§设计领域综述§

基于 CTT 的企业专利布局分析研究 …… 张换高，贾丽臻，张鹏，等(1)

§专题论文§

基于均匀压力法的某制动盘瞬态温度场研究 …… 夏德茂，奚鹰，王永健，等(7)
基于液电馈能式悬架的整车道路仿真研究 …… 彭明，过学迅，张杰，等(12)
液力缓速器制动系统的能效分析 …… 林彩霞，李长友，赵旭飞(17)
新能源汽车用无刷直流电机控制器性能测试平台设计 ……
…… 齐海军，陈黎卿，刘立超，等(21)
基于 Monte Carlo 法的应力-强度总体干涉模型建立 ……
…… 胡启国，庹奎，罗天洪，等(26)
蠕动式缆索机器人模糊故障树分析与应用 …… 陈霞(31)
基于 ADAMS 的折臂式随车起重机工作机构优化设计 ……
…… 李自贵，马俊，晋民杰，等(36)
浅析基于可变传动比齿轮-五杆机构的跳跃机构的特性 ……
…… 刘亦洋，姚亚峰，宋海涛，等(41)
基于设计矩阵和熵的可再制造性量化评价方法 …… 赵旭，张闻雷，陈东，等(46)
摆线转子泵瞬时流量及参数优化计算方法 …… 王敏(51)

§现代装备制造技术与实例分析§

含凸台连接整体加筋壁板结构的稳定性分析 …… 苏少普，陈先民，董登科(57)
基于瞬态动力学的铸造起重机桥架疲劳裂纹形成寿命研究 ……
…… 肖正明，项载毓，伍星，等(62)
锥直形喷嘴喷射角度对钻杆清洗质量的影响研究 ……
…… 张安琪，刘清友，黄本生(69)
叶片参数对导叶式旋风分离管性能的影响 …… 韩传军，陈飞，杨雪，等(72)
基于孤单翼理论矿用除尘风机叶轮设计及强度校核 …… 朱会东(78)
一种新型链传动推弹机推弹全行程仿真分析 …… 刘海涛，高跃飞，柯彪，等(83)
金属带式无级变速器金属块间接触特性研究 …… 郭卫，柴华，张武，等(88)
基于回转支承齿圈径向综合误差检测的莫氏锥度轴力学分析 ……
…… 汪叶青，汪永明(92)
锚杆钻车举升机构铰点位置优化设计 …… 吕继双，宋明江(96)
厚圆环弯曲振动特性研究 …… 张宁宁，吴胜举(100)

§工业设计论坛与资讯§

一款新型三轮摩托车车架设计及整体造型开发 …… 刘志锋，刘建军，李强(105)
基于产品识别的矿山机械造型设计研究 …… 王沈策(109)
基于 Kano 模型的家庭健身车改良设计研究 …… 冯蔚蔚，李宇晟，辛向阳(113)
基于感性工学的产品材质意象研究 …… 赵艳云，边放，李巨韬(117)
堆高设备的产品族设计评价方法研究 …… 苏晨，陈智伟，周红宇，等(122)
基于用户需求建模的血压计造型设计 …… 梁浩，刘卓，张芳燕(126)

工业设计作品欣赏索引：

医用眼部治疗仪造型设计 …… 王丹(彩页 1)
家用吸氧机造型设计 …… 赵争强，何东(彩页 2)
电动早餐车设计 …… 任文营，孟贺(彩页 3)

CONTENTS

§Summaries of designing domains§

Analysis research of patent layout for enterprise based on CTT ····· ZHANG Huan-gao, JIA Li-zhen, ZHANG Peng, et al(1)

§Theses on special topics§

Transient thermal analysis of the wheel-mounted disc brake based on uniform pressure ····· XIA De-mao, XI Ying, WANG Yong-jian, et al(7)

Vehicle road test simulation based on the hydraulic electromagnetic energy-regenerative suspension ····· PENG Ming, GUO Xue-xun, ZHANG Jie, et al(12)

Energy efficiency analysis of hydrodynamics retarder brake system ····· LIN Cai-xia, LI Chang-you, ZHAO Xu-fei(17)

Test platform design for performance of BLDC motor controller for new energy vehicles ····· QI Hai-jun, CHEN Li-qing, LIU Li-chao, et al(21)

Stress-strength population interference model based on Monte Carlo method ····· HU Qi-guo, TUO Kui, LUO Tian-hong, et al(26)

Analysis and application of the worming cable robot fuzzy fault tree ····· CHEN Xia(31)

Optimal design of working mechanism in the articulating boom crane based on ADAMS ····· LI Zi-gui, MA Jun, JIN Min-jie, et al(36)

Analysis the characteristics of hopping mechanism based on changes the transmission ratio of geared five-bar mechanism ····· LIU Yi-yang, YAO Ya-feng, SONG Hai-tao, et al(41)

Quantitative Assessment Method of Remanufacturability Based on Design Structure Matrices and Entropy ····· ZHAO Xu, ZHANG Wen-lei, CHEN Dong, et al(46)

Calculation of instantaneous flow rate of cycloid rotor pump and the method of parameters optimization ····· WANG Min(51)

§Mordern equipment manufacturing technology and analysis of examples§

Buckling analysis of integral stiffened panels with filleted junction ····· SU Shao-pu, CHEN Xian-min, DONG Deng-ke(57)

Research on fatigue crack initiation life of casting crane bridge base on transient dynamic analysis ····· XIAO Zheng-ming, XIANG Zai-yu, WU Xing, et al(62)

Influence study of spray angle of conical nozzle on the drillpipe cleaning quality ····· ZHANG An-qi, LIU Qing-you, HUANG Ben-sheng(69)

Effects of blade's parameters on performance for guide vane cyclone tube ····· HAN Chuan-jun, CHEN Fei, YANG Xue, et al(72)

Design and strength check of mine-used dust fan impeller based on lonely airfoil theory ····· ZHU Hui-dong(78)

Simulation and analysis of the ramming process of a new chain drive rammer device ····· LIU Hai-tao, GAO Yue-fei, KE Biao, et al(83)

Research on contact characteristics between metal blocks of metal belt continuously variable transmission ····· CHAI Hua, GUO Wei, ZHANG Wu, et al(88)

Morse's taper shaft mechanical analysis based on rotary bearing ring gear radial composite error detection ····· WANG Ye-qing, WANG Yong-ming(92)

Joint location optimized design of the roof bolting lifting mechanism ····· LV Ji-shuang, SONG Ming-jiang(96)

Research on bending vibration characteristics of thick ring ····· ZHANG Ning-ning, WU Sheng-ju(100)

§Forun and information of industrial design§

Frame design and overall modeling development of a new three-wheeled motorcycle ····· LIU Zhi-feng, LIU Jian-jun, LI Qiang(105)

Modeling design of mining machinery based on product identity ····· WANG Shen-ce(109)

Improvement design of family exercise bike based on Kano model ····· FENG Wei-wei, LI Yu-sheng, XIN Xiang-yang(113)

Image research of product material based on kansei engineering ····· ZHAO Yan-yun, BIAN Fang, LI Ju-tao(117)

Study on evaluation method to product family design of forklift equipment ····· SU Chen, CHEN Zhi-wei, ZHOU Hong-yu, et al(122)

Shape design of blood pressure meter based on user requirement modeling ····· LIANG Hao, LIU Zhuo, ZHANG Ling-yan(126)

JOURNAL OF MACHINE DESIGN

M.(Since 1983)
Vol.32 No.8(Serial No.310)
2015-8-20

Responsible Department:
China Association for Science and Technology
Sponsored by:
Chinese Mechanical Engineering Society, et al
Undertaking unit:
Institute of Science & Technology Information of Mechatronic Industry, Tianjin
Edited and published by:
"Jixie Sheji" Magazine Society
Director: FENG Zhi-wei
Honorary chief editor: ZUO Bin
Chief editor: SUN Wei
Executive vice chief editor: WANG Ying
Deputy chief editor: BU Yan

Address:
No. 40 Nan Kou Road,
Hebei District, Tianjin, China
Post code: 300232
Tel: 0086-22-27343427
Fax: 0086-22-27350969
http: //jxsj.chinajournal.net.cn
E-mail: jxsj@chinajournal.net.cn

Responsible: LI Na GUO Ju-qin
English editor: LI Ju-tao(concurrent)
LU Lin-ping(concurrent)
Advertisement planner: MIAO Dong-li
Telephone number of advertisemet section:
0086-22-27350969

Periodical number:
ISSN 1001-2354
CN 12-1120/TH
Domestic general distributor:
Tianjin Newspaper and Magazine Publishing Bureau
Distributed abroad by:
China International Book Trade.Co.
Subscripting place:
All the post offices in China
Post distributing code:
Domestic: 6-59 Abroad: M7315
Trade mark registration number: 300166
Printed by: Hengyuan Press Ltd. Company
Price: 12.50 (CNY)

液力缓速器制动系统的能效分析*

林彩霞,李长友,赵旭飞
(华南农业大学 工程学院,广东 广州 510642)

摘要:针对液力缓速器能量耗散特征,建立液力制动系统㶲平衡方程,通过㶲效率分析,揭示液力缓速器内流场能量转换与传递,为液力缓速器制动性能的优化设计提供能效分析方法及理论基础。

关键词:液力缓速器;制动系统;㶲平衡方程;能效分析
中图分类号:U463.53 文献标识码:A 文章编号:1001-2354(2015)08-0017-04
DOI:10.13841/j.cnki.jxsj.2015.08.004

Energy efficiency analysis of hydrodynamics retarder brake system

LIN Cai-xia, LI Chang-you, ZHAO Xu-fei
(College of Engineering, South China Agricultural University, Guangzhou, 510642)

Abstract: In view of the energy dissipation characteristics of hydraulic retarder brake system, this paper establishes an exergy balance foundations for analysis of exergy efficiency. The analysis reveals the essence of hydrodynamics retarder inner fluent field energy transferring nature, provides energy efficiency analysis method and theory foundation for improving the braking performance and optimizing design of hydrodynamics retarder.

Key words: hydrodynamics retarder; brake system; exergy balance foundations; energy efficiency analysis

液力缓速器是把汽车的动能转化为工作介质热能的辅助制动装置,因其制动件磨损小、寿命长、制动转矩大、过程平稳、不会产生热衰退、散热性能好等特点,其技术装置在国外普遍应用[1]。在我国虽然也有应用,但基本上是国外的产品,价格昂贵。

多年来,国内的专家、学者致力于液力缓速器的国产化,针对液力缓速器的结构、制动机理、设计方法等问题展开了诸多研究。如基于一维束流,把油液在液力缓速器内部的三维流动简化为二维流动或者一维流动,再用试验的方法进行修正,建立相应的液力缓速器部分充液工况制动转矩液力计算数学模型[2-5]。利用Fluent等流体力学软件对液力缓速器内部流场进行数值分析与计算发现,液力缓速器内部压力从循环圆中心到外环,压力逐渐增大,湍动能的分布在涡旋处较大,在流道固壁处较小[6-7],以及在改变液力缓速器充液量、叶片数、叶片倾角、循环圆等参数的情况下进行数值分析,揭示不同情况下缓速器内部流动流场的变化规律[8-10]。而现有研究在评价方法还有待进一步深入,国产液力缓速器在性能上与国外产品相距较大。为揭示液力缓速器能量转换与传递的本质,文中基于㶲分析法考证液力缓速器制动系统的能效。

㶲是指热力系统由任意状态可逆地变化到与环境状态相平衡时所做的最大有用功,㶲作为一种分析方法,在能量转换系统优化设计得到广泛的应用,能够全面深刻地揭示系统在各环节的损耗特征[11]。基于㶲分析法考察柴油机工作循环热力过程发现,柴油机工作循环过程中存在诸多不可逆因素所产生的㶲损失[12]。近年,系统的状态参数,㶲基准点,㶲效率分析,揭示能量损耗本质方面取得了较大的研究进展[13],通过对汽车散热器因传热温差及粘性流动阻力引起的不可逆㶲损失进行热力学分析,提出以更易于量化的㶲效率作为汽车散热器热力性能的评价指标[14]。

1 液力缓速系统㶲基准点

液力缓速器制动系统是给液力缓速器输入、输出

* 收稿日期:2013-10-28 修订日期:2015-02-17
基金项目:高等学校博士学科点专项科研基金资助项目(20114404110021)

油液，实现制动的多因素共同作用的复合系统。从系统的流动特征来看，归属连续的开口流动系统，油液通过油路、在换热器和液力缓速器之间循环流动，不断耗散了液力缓速器动轮的功。

假设液力缓速器的油液储存在一个无限大的油箱，那么，油箱中的油液在稳态时的能位状态即就是液力缓速系统的热量源和动量源最终的平衡状态。即为液力缓速系统的零参考点，此时油液的温度 T_0 和压力 P_0 为状态参数。

2 㶲流分析

从㶲的来源看，该系统㶲源于车辆的惯性及外部充液流动能。传递的过程是车辆的动能从半轴传递给液力缓速器的动轮，动轮传递给油液，然后由油液的粘性流动转换为热能耗散，传递过程受时间和空间条件的约束，其过程属于非稳态㶲传递。液力缓速器制动系统能流和㶲流如图 1 所示。

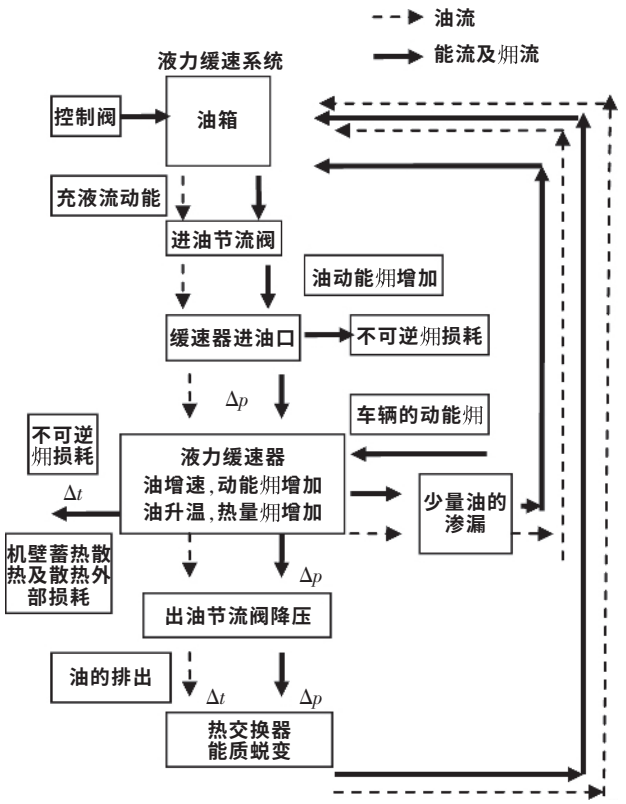

图 1 液力缓速系统能流图

图 1 中车辆的动能㶲被转化为液体的热㶲，热㶲以系统中的温差为载体而向外界耗散，流动㶲以油液压差为载体沿进油口向出油口传递。在该系统中，油液在高压气体的作用下，获得一定的流动能，即与给定的油箱环境基准态相比，油液具有了流动㶲，为尽快和动轮的转速一致，在进油节流阀的节流作用下，动能进一步提高，经液力缓速器总进油口流入缓速器定轮背部的进油槽，经进油口流入定动轮组成的工作腔。进入工作腔内的油液在动轮的带动下，形成涡旋，使其动能增加及温度升高。在温差作用下一部分用于机壁蓄热升温和耗散到环境，其余的在不可逆摩擦过程中耗散。在工作循环中不断地有部分油从出油口流出工作腔，高温、高压的油液首先进入出油节流阀，进行降压，然后流入热交换器进行二次节流降压和冷却，经过二次降压的油压力回复到基准状态，动轮携带的机械㶲全部被油液转化为热耗散。

3 㶲平衡方程

系统的㶲流可以划分成 3 个环节：第 1 为控制阀—进油节流阀—进油口；第 2 为液力缓速器—热交换器；第 3 为液力缓速器—出油节流阀—热交换器。下面分别从这 3 个环节建立其相应的㶲平衡方程。

(1)第 1 环节：控制阀—进油节流阀—进油口。

油箱内的油液处于环境基准态，温度和压力分别为 T_0，P_0。设控制阀施加的压力为 P_f，在压力作用下油液获得初速度 v_0，由于进油节流，油液的速度提高到 v_1，油液的压力降低为 P_1，油液的体积不变，流动过程中由于摩擦不可逆过程产生㶲损 I_1，因此该环节㶲平衡方程为：

$$(P_f-P_1)V=(\frac{1}{2}mv_1^2-\frac{1}{2}mv_0^2)+I_1 \tag{1}$$

式中：m——油液的质量，kg；

V——油液的体积，L。

(2)第 2 环节：液力缓速器—热交换器。

动轮的机械能为㶲源 E_M，即：

$$E_M=\frac{1}{2}\delta J\cdot\omega^2 \tag{2}$$

式中：δJ——车辆旋转质量，kg；

ω——转速，r/min。

在此环节，油液的温度、压力和速度变化到 T_2，P_2，v_2，故油液获得的动能㶲为：

$$E_{M1}=m\frac{v_2^2-v_1^2}{2} \tag{3}$$

油液不可压缩，膨胀功为零，因此忽略温度增加而引起的体积膨胀，油液获得的热量为其增加的内能，为：

$$Q'=\Delta U \tag{4}$$

该内能㶲为：

$$E_{Q'}=(1-\frac{T_0}{T_2})Q' \tag{5}$$

机壁温度变为 T_k，蓄热及向环境扩散的热量设为 Q''，其㶲值为：

$$E_w=(1-T_0/T_k)Q'' \tag{6}$$

在向环境扩散热量的过程中，存在外部㶲损失 $\sum E_{loss}$。油液以一定的液流角进入缓速器腔体，在进口处产生冲击阻力造成冲击损耗，用 E_l 表示。此外，还有油渗漏的损失 E_s 及摩擦阻力等产生的不可逆内部㶲耗散 I_2。因此，该环节的㶲平衡方程为：

$$E_M=(1-\frac{T_0}{T_2})Q'+m\frac{v_2^2-v_1^2}{2}+(1-T_0/T_k)Q''+E_l+\sum E_{loss}+E_s+I_2 \tag{7}$$

从式(7)可以看出，液力缓速器动轮的动能转化为油液的内能和动能，由于㶲损失的存在，油液内能和动能的增加量少于动轮动能的减少量，这意味着功热转换能力的减少，这是由于冲击阻力、摩擦阻力、渗漏及过程不可逆等引起的㶲损失而造成的。

(3)第 3 环节：液力缓速器—出油节流阀—热交换器。

以状态 (T_2,P_2,v_2) 的油液流进出油节流阀进行降压后流入热交换器，利用发动机的冷却液对油液进行冷却，油液的温度和压力最终恢复到基准态 (T_0,P_0)，油液的速度降低到 v'，重新进入油路进行循环。油液在前一环节获得的㶲增量在该环节将随油液被作为废物而排出，因此，此环节完全是排油㶲损。油液排出的热量为 Q_h，该热量㶲损为 $E_h=(1-\frac{T_0}{T_2})Q_h$，完全蜕变到大气环境中。该环节全部的排油㶲损 $E_{x,l}$ 为：

$$E_{x,l}=(P_2-P_0)V+(\frac{1}{2}mv_2^2-\frac{1}{2}mv'^2)+(1-\frac{T_0}{T_2})Q_h+I_1 \tag{8}$$

4　能量匹配的分析及相应的措施

4.1　系统的㶲效率及相应措施

(1)第 1 环节：控制阀—进油节流阀—进油口。

$$\eta_{ex1}=\frac{\frac{1}{2}mv_1^2-\frac{1}{2}mv_0^2}{(P_f-P_0)V} \tag{9}$$

从式(9)中可以看出，要使 η_{ex1} 达到最大，须尽量减少进油油路中的流动阻力，保证节流阀的提速作用。

(2)第 2 环节：液力缓速器—热交换器。

$$\eta_{ex2}=\frac{(1-\frac{T_0}{T_2})Q'+m\frac{v_2^2-v_1^2}{2}+(1-T_0/T_k)Q''}{E_M} \tag{10}$$

要提高该环节的㶲效率，必须使油液的动能、内能最大及机壁吸热、散热最多，尽量减少各种阻力和油的渗漏。提高油液的动能可以在不改变动轮输入速度的情况下，通过改变缓速器各结构参数来实现；还可以通过改变不同齿轮的啮合来实现。

(3)第 3 环节：液力缓速器—出油节流阀—热交换器。

$$\eta_{ex3}=\frac{0}{(P_2-P_0)V+(\frac{1}{2}mv_2^2-\frac{1}{2}mv'^2)+(1-\frac{T_0}{T_2})Q_h+I_1}=0 \tag{11}$$

由于热交换器的节流降压和降温作用，油液携带的热量㶲、压㶲和动能㶲完全蜕变到最初的平衡状态，因此，该环节㶲效率为 0，㶲损系数为 1。要保证液力缓速器稳定的制动转矩，必须在系统中有阻尼装置设计——出油节流阀和热交换器。

4.2　能量匹配分析

对整个液力缓速器辅助制动系统的㶲效率进行评价。以液力缓速器额定工况计算，在额定工况下即在转速为 1 000 r/min 时，液力缓速器施加的最大制动转矩为 4 000 N·m，制动功率为 418.8 kW，若 7 s 内使车辆减速至停止，此时，动轮的机械能等于制动能量，该机械能完全转化为热量，可生成 418.8 kJ 的热量，其中㶲值为 $\sum E_x$=418.8 kJ，其折合能质系数为 λ_n=1。工作油液吸收的热量经过热交换器被冷却水带走完全退化到环境，输出㶲值为 0，故能质系数 λ'_n=0。能质系数的差值 $\Delta\lambda'=(\lambda_n-\lambda'_n)=1$，计算系统的㶲效率为 0，㶲损系数为 1。液力缓速器输入的机械能为可无限转换的能量，是高级能量，而热量是可有限转换的热量，是低级能量，工作油液对液力缓速器所做的功完全变为热量㶲损耗，故系统的㶲效率必然为 0。因此，液力缓速器辅助制动系统优化设计须提高热量㶲损耗。

4.3　试验分析

提高热量㶲损耗的途径之一是让换热器的节流散热能力增大，油液恢复到基准状态。下面利用试验来对能量匹配分析的结果进行验证。

4.3.1　台架试验设备

液力缓速器工况试验台的组成：液力缓速器，水温、油温和压力传感器(基本误差：±0.1%)，工况控制柜，模拟车辆惯性输入的驱动电机（长沙电机厂 YSP315L2-2）和飞轮组，该飞轮组可以模拟 20 t 车辆减速的过程，转矩转速传感器(湘仪动力测试仪器有限公司 JC3A 型转矩转速传感器，转矩测量精度为 0.1 级，转速测量精度为±1 r/min)，散热水箱等。采用两种不同的热交换器进行试验，分别如图 2 所示。图 2a 的散热性能比图 2b 好。在进气压力为 0.5 MPa 时，将电机置于不同的转速，采集制动过程中转矩仪的数据，每做完 1 次试验，等待 10 min 左右，进行 3 次试验，取平均值。

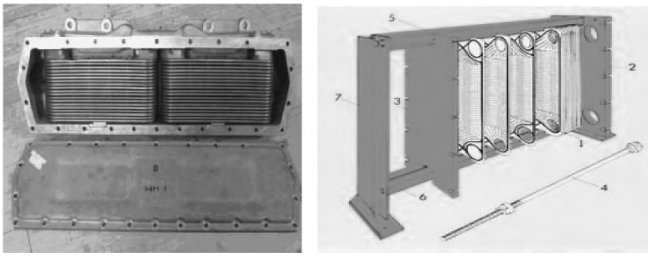

(a)散热片 19 片、并联板翅式热交换器　(b)水道 18 片、油道 7 片的板式热交换器

图 2　两种换热器的结构简图

4.3.2　试验及结果分析

试验数据如图 3 所示。从图 3 中可以看出，安装了图 2a 所示热交换器的液力缓速器的制动转矩明显比装了图 2b 所示热交换器的高。

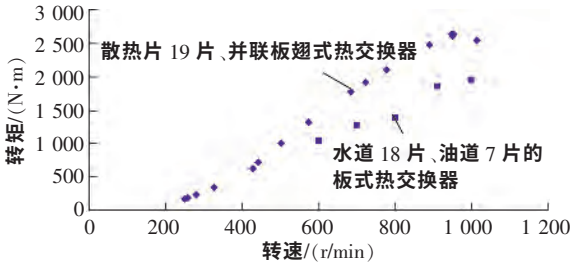

图 3　两种换热器的制动转矩

该试验结果表明图 2a 所示热交换器水路的压降低，使热量较快地通过发动机散热系统散热，热交换器散热量增加，即使式(8)中油液排出的热量增加，油液的温度、压力和速度却越接近基准态，因此使第 3 环节的排油㶲损耗增加，故使液力缓速器的制动转矩增加，从而验证了理论分析是正确的。

5　结论

(1)液力缓速制动系统是功热自发转换与传递的过程，过程的终态可以用油液在环境态时的状态点为计算㶲的基准点。

(2) 动能㶲及热量㶲是液力缓速器功转换的主体，提高其制动性能的途径在于有效提高液体的流动速度。

(3)提高系统热量㶲损耗率的途径是强化各节流环节的散热效能。

参考文献

[1] Timothy J, Cooney E J, Paubo Roberto, et al. Development of a hydraulic retarder for the allison AT545R transmission [J]. SAE, 1995, 952606: 18–22.

[2] 姚寿文，王晓龙. 液力减速器叶栅系统优化及制动动力学仿真[J]. 机械设计，2007，24(12)：21–23.

[3] 闫清东，邹波，魏巍. 液力减速器部分充液工况制动性能计算方法研究[J]. 北京理工大学学报，2011，31(12)：1396–1400.

[4] 严军，过学迅，汪斌，等. 车辆液力缓速器内腔压力特性分析及建模[J]. 汽车工程，2010，32(4)：308–313.

[5] 荆崇波，胡纪滨，鲁毅飞.车用液力减速器制动性能试验研究[J]. 汽车技术，2005，(12)：27–31.

[6] 何仁，严军，鲁明. 液力缓速器三维数值模拟及性能预测[J]. 汽车工程，2009，31(3)：250–252.

[7] 魏巍，李慧渊，邹波，等. 液力减速器制动性能及其两相流分析方法研究[J]. 北京理工大学学报，2010，30(11)：1281–1284.

[8] 严军，何仁，鲁明. 液力缓速器叶片变叶片数的三维数值模拟[J]. 江苏大学学报，2009，30(1)：27–31.

[9] 严军，何仁. 液力缓速器叶片变角度的缓速性能分析[J]. 农业机械学报，2009，40(4)：206–209.

[10] 闫清东，邹波，唐正华，等. 车用液力减速器叶片数三维集成优化[J]. 农业机械学报，2012，43(2)：21–25.

[11] 朱明善. 能量系统的㶲分析[M]. 北京：清华大学出版社，1988.

[12] 恽瑛安，齐红，孙平. 柴油机工作循环热力过程的㶲分析[J]. 农业工程学报，1994，10(3)：61–65.

[13] 李长友. 粮食热风干燥系统㶲评价理论研究[J]. 农业工程学报，2012，28(12)：1–6.

[14] 张秀琴，苏清祖，王忠. 汽车散热器性能评价的㶲分析法[J]. 汽车工程，2005，27(6)：751–753.

作者简介 林彩霞(1976—)，女，讲师，博士，研究方向 机械设计理论。
E-mail：cxlin76@163.com
李长友(通信作者)(1958—)，男，教授，研究方向 机械设计。
E-mail：lichyx@scau.edu.cn

主办单位：中国机械工程学会、天津市机械工程学会、天津市机电工业科技信息研究所

报刊代号：6-59
定价：12.50元

机床与液压

MACHINE TOOL&HYDRAULICS

中文核心期刊

www.jcyyy.com.cn

半月刊

2014·5 42卷 总第359期

中国科技期刊精品数据库收录期刊　中国科技论文统计源期刊　《中国学术期刊文摘》源刊

1973年创刊 • CN44-1259/TH　ISSN 1001-3881　CODE JYYEEV

机床与液压
JICHUANG YU YEYA

1973 年创刊
第 42 卷第 5 期（总第 359 期） 2014 年 3 月
半月刊（每月 15 日、28 日出版）
www. jcyyy. com. cn

主　　管：中国科学技术协会
主　　办：中国机械工程学会
　　广州机械科学研究院有限公司
编辑出版：《机床与液压》编辑部
地址：广州市黄埔区茅岗路 828 号（510700）

电话：020 - 32385312　传真：020 - 32389600
电子邮箱：jcy@ gmeri. com
英文专版采编中心（重庆理工大学期刊社）
电话：023 - 68667984，E - mail: jdygcyw@ 126. com

广告发行部
广告策划：梁万前　曹懿莎　冯晓兰
　　陈　望　黎文勤　李颖欣
美术编辑：陈卉子
电话：020 - 32385311　传真：020 - 32389600
电子邮箱：webmaster@ gmeri. com
发　　行：麦丽菊　发行热线：020 - 32389676
发行范围：国内外发行
国内发行：广东省报刊发行局
订 购 处：全国各地邮局
国外发行：中国国际图书贸易集团有限公司
广告经营许可证：440000100115
印　　刷：广州市新怡印务有限公司

ISSN1001 - 3881
CN44 - 1259/TH

国内邮发代号：46 - 40
国外发行代号：BM 550
定价：8 元/期，192 元/年

目　　次

◀ 试验与研究 ▶

板状阀芯旋转式四通换向阀
…… 韩冬　龚国芳　刘毅　廖湘平（1）
一种电液控制综合实验系统研究
…… 曹恒　周为民　孙波　吴帅　徐展　朱钧（4）
基于回归正交试验的皮质骨钻削力试验研究
…… 张青云　胡亚辉　何志祥　尹成君（8）
基于可适应产品平台的产品族配置方法研究
…… 程贤福　吴国栋　兰光英（11）
大型风力机动态载荷控制方法研究
…… 海几哲　孙文磊　吴安（15）
海洋废弃平台桩基拆除绳锯机夹紧齿优化设计研究
…… 王海波　张岚　孟庆鑫　王喆（21）
基于 SPSS 软件的消失模表面质量数控切削工艺优化分析
…… 左健民　周少龙　汪木兰　陈建（24）
液动力对锥阀振动特性的影响
…… 李光飞　刘桓龙　邓斌　王国志　晏静江（28）
液压多路阀灰铸铁阀体材料组织与性能研究
…… 王守仁　刘延利　朱艳华　郭培全　王敏（31）
滑片泵特性试验及性能曲线拟合
…… 李涛　张伟明　蒋明　徐洋（35）
精密成形数值模拟中弹性变形的测量方法
…… 陈淑婉　黄胜　詹艳然（38）
基于虚拟仪器的数控机床超声检测系统研究
…… 陈肖芬　张吉堂（41）
直驱泵控伺服液压机节能分析及试验研究
…… 冼灿标　齐水冰　孙友松
　　李连和　李可　李惠萌（45）
电液比例阀独立颤振的叠加方法研究
…… 刘国平　夏五星　齐大伟　胡瑢华（49）
视觉数控安全监控技术研究
…… 惠国保　李东波　童一飞　王引（52）

期刊基本参数：CN44 - 1259/TH* 1973* S* 16* 188* zh* P* ￥8.00＊ ＊49* 2014 - 03

基于小波变换与均值滤波的成形力信号处理研究
…… 蔡改贫　廖强　姜志宏　李龙茂（56）
电阻应变计在轧机伺服液压缸测试中的应用
… 尹丹　陈新元　邓江洪　李鹏　李涛（60）
RSSI 融合 RBF 改善测距精度的研究
…… 路继军　马松龄　贾昭（63）
干磨新工艺的试验研究
…… 严勇　郭力（66）
关于建立自由曲面测量－建模闭环系统的研究
…… 薛莹　何雪明（69）
履带起重机液压起升系统动态特性分析与实验研究
…… 高玉侠（73）

◀ 设计与开发 ▶

水下机器人外形优化设计
…… 王妹婷　齐永锋　汤方平　戴志光　陆柳延　吕学智（76）
双变量施肥液压调速系统的设计及仿真
…… 吴金林　张立新　喻俊志　王卫兵　张家华（80）
合模机构移模行程的 Taguchi 稳健设计
…… 吴磊　徐银　赵翼翔　左亚军（85）
具有远程无线监控功能的铝隔条折弯机控制系统设计
…… 张从鹏　李东旭（90）
双牛头电火花机床平滑枕的轻量化设计
…… 牛金磊　李锻能　丰树礼（93）
基于 EtherCAT 总线的发动机压装闭环控制系统的研究
…… 黄公安　高伟强　潘云龙　阎秋生　邹敏清（95）
基于 AMESim 的排土机司机室自动调平系统设计与研究
…… 肖艳军　韩静粉　石亚茹　关玉明（99）
基于 dsPIC30F6014A 的普通外圆磨床在线测控系统设计
…… 殷苏民　赵梁楠　许潮锋（103）
机夹刀片工作面激光熔覆工艺制定
…… 李淑玉　李成彪（108）
内部轮廓超声成像系统的设计
…… 李勇峰　张艳花　杨录（111）
小型船用油水分离器的创新设计与实现
…… 刘邵宏　童伟（116）
锯盘磨削机气动控制系统设计
…… 闫莉敏　吴青松（119）

◀ 建模与仿真 ▶

并联式磁流变阻尼器磁场分布分析
…… 郑佳佳　杨哲　黄林　王炅（121）
复合式镗铣加工中心铣削部分空间误差建模研究
…… 曲月　舒启林（125）
基于 AEMSim 的掘进机液压系统参数优化分析
…… 杨文林　闫炳雷　王忠宾（129）
基于 MATLAB 的沟槽型节流缓冲装置仿真与分析
…… 孟尧　刘忠　李晶晶（132）
离散辅助闭环偏心补偿法的建模与仿真
…… 杨阳　陈刚　王益群（136）
航空发动机叶片修复机床传动系动态建模及仿真
…… 龚淼　张涛（141）
轴向柱塞泵流量脉动特性的仿真研究
…… 王海燕　魏秀业（144）
一种新型插装式水压电磁换向阀的仿真研究
…… 苏龙龙　刘忠　聂松林　陈明辉（149）
可逆式四辊轧机液压 AGC 系统的仿真与分析
…… 李玉贵　包野　郭亚栋　侯成（154）
液压系统故障注入仿真研究
…… 丁遥　陈小虎　阳能军　高淑祥（157）

◀ 综述与分析 ▶

磁流变阀结构优化设计及性能分析研究现状
…… 胡国良　李海燕　喻理梵　黄敏　龙铭（160）
电液比例阀的结构原理与研究现状
…… 卢文辉　李胜　吕敏健（166）
现代设备故障智能诊断研究进展
…… 熊国良　黄文艺　张龙（173）
液力缓速器研究进展
…… 林彩霞　赵旭飞（177）

◀ 故障诊断与可靠性 ▶

面向最小维修的数控机床可靠性评估
…… 张根保　刘杰　杨毅　高琦樑（180）
飞机液压系统使用故障数据库系统登录界面的设计开发
…… 梁广辉　胡良谋　唐锋　胡飞　曹克强（185）
信息 ……（7）、（27）、（172）

MACHINE TOOL & HYDRAULICS
Half – Monthly
Vol. 42 No. 5 Mar. 2014

Authorities in Charge: China Association for Science and Technology
Sponsor: Chinese Mechanical Engineering Society
Guangzhou Mechanical Engineering Research Institute Co., Ltd
Editor & Publisher: 《MACHINE TOOL & HYDRAULICS》 Editorial Department
Add: No. 828 Maogang Road, Huangpu District, Guangzhou, China

Tel: (8620) 32385312
Fax: (8620) 32389600
Web: www.jcyyy.com.cn
E-mail: jcy@gmeri.com
English Special-Edition Editorial Center (Periodicals Office of Chongqing University of Technology)
Tel: (8623) 68667984
E-mail: jdygcyw@126.com
Distributed Range: Distribution at home and abroad
Domestic Distributor: Newspapers and Publications Board of Guangdong
Overseas Distributor: China International Book Trading Corporation
Post Distribution Code: 46 – 40
International Code: BM 550

CONTENTS

TEST & RESEARCH

A Rotary Reversing Valve with Plate Spool
…… HAN Dong GONG Guofang LIU Yi LIAO Xiangping (1)
Research on a Comprehensive Test Bed for Electro-hydraulic Control System
…… CAO Heng ZHOU Weimin SUN Bo WU Shuai XU Zhan ZHU Jun (4)
Experimental Study on Drilling Forces of Cortical Based on Orthogonal Regression
…… ZHANG Qingyun HU Yahui HE Zhixiang YIN Chengjun (8)
Adaptable Product Platform-based Product Family Configuration Method
… CHENG Xianfu WU Guodong LAN Guangying (11)
Study on Dynamic Load Control Method for Large Scale Wind Turbine
…… HAI Jizhe SUN Wenlei WU An (15)
Optimization Design of Clamping Teeth of Offshore Discarded Platform Piles Removal Wire Saw
…… WANG Haibo ZHANG Lan MENG Qingxin WANG Zhe (21)
CNC Cutting Process Optimization for the Surface Quality of the EPS Based on SPSS Software
…… ZUO Jianmin ZHOU Shaolong WANG Mulan CHEN Jian (24)
Effect of Flow Force to the Poppet Valve Vibration
…… LI Guangfei LIU Huanlong DENG Bin WANG Guozhi YAN Jingjiang (28)
Mechanical Properties and Microstructure of Gray Graphite Cast Iron for Cartridge Valve
…… WANG Shouren LIU Yanli ZHU Yanhua GUO Peiquan WANG Min (31)
Performance Test on Sliding-vane Pump and Performance Curve Fitting
LI Tao ZHANG Weiming JIANG Ming XU Yang (35)
Method for Measuring the Amount of Elastic Deformation in Numerical Simulation of Precision Forming
…… CHEN Shuwan HUANG Sheng ZHAN Yanran (38)
Research of Ultrasonic Testing System for NC Machine Tool Based on Virtual Instrument
…… CHEN Xiaofen ZHANG Jitang (41)
Analysis and Experiment Research on Energy-saving Mechanism of Direct Drive Pump-controlled Servo Hydraulic Press
…… XIAN Canbiao QI Shuibing SUN Yousong LI Lianhe LI Ke LI Huimeng (45)
Method Study of Superimposing Independent Dither to Electro-hydraulic Proportional Valve
LIU Guoping XIA Wuxing QI Dawei HU Ronghua (49)

Research on CNC Security Processing Based on Computer Vision
…… HUI Guobao LI Dongbo TONG Yifei WANG Yin (52)
Research of Incremental Forming Force Signals Processing Based on Wavelet Transform and Mean Filtering
…… CAI Gaipin LIAO Qiang JIANG Zhihong LI Longmao (56)
Application of Resistance Strain Gage in Rolling Mill Servo Cylinder Testing
…… YIN Dan CHEN Xinyuan DENG Jianghong LI Peng LI Tao (60)
Study on Ranging Accuracy Improvement Based on RSSI Fusing RBF
…… LU Jijun MA Songling JIA Zhao (63)
Experiment Research of Dry Grinding
…… YAN Yong GUO Li (66)
Research on Establishing the Closed-loop System of Measuring and Modeling for Free-form Surface
…… XUE Ying HE Xueming (69)
Dynamic Characteristics Analysis and Experimental Research for Crawler Crane Hydraulic Lifting System
…… GAO Yuxia (73)

DESIGN & DEVELOPMENT

Shape Optimal Design of Underwater Robot
…… WANG Meiting QI Yongfeng TANG Fangping DAI Zhiguang LU Liuyan LV Xuezhi (76)
Design and Simulation for Hydraulic Sleepless Speed Regulation System of Bivariable Fertilizing Application
…… WU Jinlin ZHANG Lixin YU Junzhi WANG Weibing ZHANG Jiahua (80)
Taguchi Robust Design for the Stroking of a Clamping Mechanism
…… WU Lei XU Yin ZHAO Yixiang ZUO Yajun (85)
Design of Control System for Aluminum Spacer Bending Machine with Remote Wireless Monitoring Function
…… ZHANG Congpeng LI Dongxu (90)
A Lightweight Design of Smooth Pillow in Double Tauren EDM Machine
…… NIU Jinlei LI Duanneng FENG Shuli (93)
Research on Engine Press-fit Closed-loop Control System Based on EtherCAT Bus
…… HUANG Gong'an GAO Weiqiang PAN Yunlong YAN Qiusheng ZOU Minqing (95)
Research and Design on the Automatic Tuning System of Spreader Cab Based on AMESim
XIAO Yanjun HAN Jingfen SHI Yaru GUAN Yuming (99)
Design of On-line Measurement and Control System for Plain External Grinder Based on dsPIC30F6014A
…… YIN Sumin ZHAO Liangnan XU Chaofeng (103)
Process Formulation of the Laser Cladding on Machine Clip Blade
…… LI Shuyu LI Chengbiao (108)
Design of Internal Contour Ultrasound Imaging System
…… LI Yongfeng ZHANG Yanhua YANG Lu (111)
Innovation Design and Implementation of a Small-sized Marine Oil-Water Separator
…… LIU Shaohong TONG Wei (116)
Design of Pneumatic Control System for Saw Disc Grinding Machine
…… YAN Limin WU Qingsong (119)

MODELING & SIMULATION

A New Type of MR Damper Magnetic Circuit Analysis
…… ZHENG Jiajia YANG Zhe HUANG Lin WANG Jiong (121)
Research on Volumetric Error Modeling for the Milling Part of Composite Boring and Milling Machine Center
…… QU Yue SHU Qilin (125)
Parameter Optimization for Hydraulic System of Roadheader Based on AMESim
… YANG Wenlin YAN Binglei WANG Zhongbin (129)
Simulation and Analysis of Grooved Type Cushion Structure Based on MATLAB
…… MENG Yao LIU Zhong LI Jingjing (132)
Modeling and Simulation of Discrete Assistant Closed-loop System for Eccentricity Compensation
…… YANG Yang CHEN Gang WANG Yiqun (136)
Dynamic Modeling and Simulation about Driveline of Aircraft Engine Blade Repair Machine
…… GONG Miao ZHANG Tao (141)
Simulation Study on the Flow Pulsation Characteristics of Axial Piston Pump
…… WANG Haiyan WEI Xiuye (144)
Simulation Study on a New Type of Water Hydraulic Cartridge Solenoid Directional Valve
…… SU Longlong LIU Zhong NIE Songlin CHEN Minghui (149)
Simulation and Analysis of Hydraulic AGC System in Reversing Four-high Mill
LI Yugui BAO Ye GOU Yadong HOU Cheng (154)
Simulation Study on the Hydraulic System Fault Injection
…… DING Yao CHEN Xiaohu YANG Nengjun GAO Shuxiang (157)

REVIEW & ANALYSIS

Research Status of Structure Optimization Design and Characteristics Analysis of Magnetorheological Valve
…… HU Guoliang LI Haiyan YU Lifan HUANG Min LONG Ming (160)
Fundamental Working Principles of Electro-hydraulic Proportional Valves and Review on Their Development
…… LU Wenhui LI Sheng LV Minjian (166)
Development of Modern Equipment Fault Intelligent Diagnosis
XIONG Guoliang HUANG Wenyi ZHANG Long (173)
Research Development of Hydraulic Retarder
…… LIN Caixia ZHAO Xufei (177)

FAULT DIAGNOSIS & RELIABILITY

Reliability Assessment for Multiple NC Machine Tools Oriented to Minimal Repair
…… ZHANG Genbao LIU Jie YANG Yi GAO Qiliang (180)
Entry Interface Design for Operational Fault Database System of Airplane Hydraulic System
…… LIANG Guanghui HU Liangmou TANG Feng HU Fei CAO Keqiang (185)

DOI: 10.3969/j.issn.1001 - 3881.2014.05.047

液力缓速器研究进展

林彩霞，赵旭飞
（华南农业大学工程学院，广东广州 510640）

摘要： 综述近年来国内外液力缓速器的设计理论、试验技术等研究现状，包括液力缓速器国内获得的专利、基于逆向工程的设计研究、一维束流理论的理论计算研究、CFD 数值研究、基于流固体耦合技术的结构强度研究等在液力缓速器设计理论上的应用，总结相应的研究进展和取得的成果。

关键词： 液力缓速器；设计理论；试验技术；研究进展
中图分类号： U463.53 **文献标识码：** A **文章编号：** 1001 - 3881（2014）5 - 177 - 3

Research Development of Hydraulic Retarder

LIN Caixia，ZHAO Xufei
（College of Engineering，South China Agricultural University，Guangzhou Guangdong 510640，China）

Abstract: The situations of domestic and foreign research on hydraulic retarder design theory and test technology in recent years were summarized，which included domestic patent，design theory based on reversing solution，theory calculation based on Eula theory，CFD numerical research and structure strength analysis based on coupling of flow field and solid，all kinds of test means and experimental technique. The related research progress and achievements were also analyzed and summarized.

Keywords: Hydraulic retarder; Design theory; Test technology; Research development

液力减速器为液力偶合器的一个分支，具有制动扭矩大、持续制动能力强、过程平稳、制动件的磨损极小、散热性能好、不会产生制动热衰退问题等优点[1]，因此，随着技术的不断发展，液力缓速器得到了广泛的应用，特别在重载、高速运行的汽车上其应用更为广泛，液力缓速器的重要性日益突出。

1 国外研究进展

国外对液力缓速器研究和应用较早，液力缓速器在大型公共汽车、旅游车、载货车以及军用车辆、坦克等车辆上已经得到较为普遍的应用。国外的液力缓速器技术成熟，结构类型多样化，随着其应用的广泛性，出现了很多生产液力缓速器的公司。德国采埃孚公司、德国福伊特公司、美国通用汽车公司等公司的产品以其成熟的技术及适用于各种车型，成为当今汽车液力缓速器行业发展水平的代表。由于各公司对技术的保密，国外关于液力缓速器的研究文献很少，国外的文献主要是对液力缓速器的工作原理、结构和维修进行介绍。如 Helmut SCHRECK 等[2]对液力缓速器商用车的应用进行了介绍，BERGMANN 等[3]分析了液力缓速器在商用车制动的发展前景。

2 国内研究进展

2.1 液力缓速器专利

国内检索到的液力缓速器多数为应用型装置，国家专利局颁布有关液力缓速器装置和机构的专利情况如下[4]：

一种能消除泵气损失的液力缓速器结构，专利号：200810020498，特征：在车辆正常行驶不需要制动时，采用离合器使液力缓速器转子处于静止状态，不会形成气流，彻底消除泵气损失。

液力缓速器的发电方法及装置，专利号：201010145781，特征：实现汽车制动能量回收和再生，达到汽车节能的目的。

液力减速制动器，专利号：02278294，特征：具有减小空气阻力损失装置。

开式前倾叶片双腔液力缓速器，专利号：201210243755，特征：双腔型，适用于公路客车和大吨位载货汽车。

液力缓速器用换热器，专利号：201220226807，特征：把原有的钎焊板式换热器单边进出拓展为对角进出。

矿车用液力减速器，专利号：201220076767。

一种可以恒速控制车辆的液力缓速器，专利号：200820216110，特征：能实现车辆的分级控制，而且可恒速控制。

液力缓速器，专利号：200720120163。

液力缓速器油道，专利号：200720120166。

收稿日期：2013 - 03 - 03
基金项目：高等学校博士学科点专项科研基金资助项目（20060564003）；星火计划项目（2011E000040）
作者简介：林彩霞（1976—），女，博士研究生，讲师，研究方向为机械设计理论。E - mail: cxlin76@163.com。

液力缓速器，专利号：201220174714。

这 4 种液力缓速器基本上是仿制福伊特设计生产的，目前市面上还没有成熟的产品在使用。

2.2 液力缓速器研究方法

2.2.1 基于逆向工程的设计研究

基于逆向工程的设计方法是对某一样机进行快速仿形测绘，反求设计参数，采用曲面重构的方法实现逆向设计。江苏大学刘凯等人[5]结合液力缓速器关键零部件叶轮的结构特点，利用精密光学三坐标测量仪对其进行扫描，并利用 CATIA 软件进行数据处理和模型构建，得到零件的三维模型和设计图纸，进而通过流场分析软件 Fluent 对液力缓速器内流场进行分析，这大大缩短了液力缓速器的设计开发周期，提高了设计效率。基于逆向工程的设计方法为以后的产品改型提供了很大便利，可以加快液力缓速器的国产化进程，尽快打破国外对于液力缓速器技术的垄断。

2.2.2 基于一维束流理论的理论计算研究

工作介质在液力缓速器内部的流动是一种在复杂空间的三维黏性流动，在分析工作介质在流道中的流动状况时，必须引入一些假设，把三维流动简化为二维流动或者一维流动，再用实验的方法进行修正，以解决液力缓速器流道结构的设计计算问题。目前对于叶片式机械，广泛应用的是一维束流理论，即欧拉束流理论。欧拉束流理论是传统设计方法的主要理论依据，为简化流场、便于研究，朱经昌等[6]通过理论计算的方法探讨了如何选择液力缓速器的设计功率与布置位置问题。长安大学赵鹏[7]、施凯男[8]基于该方法对液力缓速器进行了设计计算。北京理工大学杨凯华等[9]基于束流理论建立了液力缓速器设计计算的数学模型，用 MATLAB 作为仿真工具，建立了液力缓速器和车辆传动系统的动力学仿真模型。王峰等人[10]基于束流理论归纳分析了液力缓速器稳态工况制动扭矩计算的 3 种方法，并通过与实验结果的对比，阐述了各种方法的优、缺点和适用性。姚寿文等[11]在经验设计的基础上，结合一维束流理论和多岛遗传算法进行了叶栅系统的优化，开发了虚拟样机。闫清东等[12]分别基于两种液力缓速器内腔气液两相流动假设，采用均匀密度法和气液分层法建立了相应的液力缓速器部分充液工况制动转矩液力计算数学模型。严军等人[13]在 600 r/min 以下的速度范围内对液力缓速器流动速度与压降分布进行试验测定，并基于神经网络建立了内腔压力模型，该模型较为正确地外推高转速、高制动扭矩工况下的内腔压力走势与数值。

一维束流理论具有物理概念明确、参数调节简单的优点，在液力传动元件的设计研发中得到广泛应用。但实际上，工作液体在液力元件工作叶轮中的流动呈黏性、三维、不可压缩、非稳定的复杂流动，显然基于一维束流理论并包含有很多经验系数的设计计算方法无法计算其内部流动，并且在叶片和流道设计以及对外特性预测中存在很大误差。20 世纪 80 年代末至 90 年代初提出了液力传动二维流动理论和基于 S_1、S_2 流面的准三维流动理论，但因条件限制并未发展成为指导液力元件设计的成熟理论和方法。近年来，随着计算机技术、计算流体动力学（CFD）及其商业理论与方法研究和流动测量技术的飞速发展，对液力传动的研究又有了新的突破，同时也带动了液力传动理论与实际应用的长足发展。

2.2.3 基于 CFD 技术的数值研究

液力减速器叶栅系统叶片一般采用倾斜、等厚直叶片，结构相对于液力变矩器简单，叶片角度和叶片数目的确定一直是叶栅系统设计的重点。

华南农业大学的学者们在试验研究福伊特原型机的基础上，研制了液力缓速器样机，结合理论计算和数值模拟分析，并进行试验验证，取得了一定的研究成果。如沈文浩[14]采用单流道、满充液状态以及工作介质性质为常量，进行数值模拟分析，讨论了液力缓速器整机性能以及定轮、动轮机构内部流场分布特性，并进行了试验验证。黄俊刚等[15]研究了全流道满充液状态下，工作介质性质同样为常量，液力缓速器内部流场的压力和速度分布，以及对液力缓速器的结构参数如：循环圆的直径、几何形状、叶片倾角、进油口的分布等进行了数值分析。

吉林大学李雪松等[16]研究了全流道在部分和满充液状态下稳态和非稳态时液力缓速器内部流场的压力和速度分布；采用大涡模拟法求解液力缓速器三维流动控制方程，对液力缓速器油气混合现象进行分析；并对液力缓速器结构参数的选择进行了数值模拟分析。

北京理工大学李慧渊[17]基于三维流场理论对液力缓速器的设计进行了研究。魏巍等人[18]对于无内环的液力元件采用混合入、出口的边界条件处理方法，对充液率分别为 100%、80%、60%、40% 及 20% 时的工况分别进行 CFD 液力减速器内流场数值模拟，获取不同充液率和不同转速下的制动性能曲线，并得到对应不同工况的速度和压力场分布特性。闫清东等[19]基于瞬态流场计算方法，建立了某型液力减速器相应的仿真模型。结合实际车用工况确定了入、出油口的流速，设置了精确的初始流场作为边界和初始条件，运用 CFD 技术对液力减速器紧急制动工况的充液过程进行流场分析及制动外特性仿真计算。

江苏大学何仁等人[20-21]利用 Fluent 软件基于标准 $k-\varepsilon$ 模型和 SIMPLEC 算法，对液力减速器在不同

叶片数下，倾角为 50°、55°、60°时循环圆形状和半径不同时的内流场进行数值模拟，揭示了不同叶片数、不同叶片倾角和不同循环圆下叶轮内流动速度分布、压力分布的变化规律，从流道内湍流流动的速度分布、压力分布和湍动能分布规律 3 个方面分析该型叶轮流动的特点。

武汉理工大学冯宜彬等[22]应用 CFD 数值模拟技术，采用 Fluent 软件对液力缓速器内部流场进行研究，得到了不同工况下液力缓速器内流场的压力和速度分布特性与制动扭矩的大小。北方车辆研究所郭刘洋等[23]通过建立多个三维 CFD 计算模型，利用 CFD 软件对液力缓速器原始特性进行仿真，分析得出增加动轮出口和改变叶片角度对液力缓速器的制动性能和降低空转功率损失的影响。

2.2.4　基于流固耦合技术的结构强度研究

对液力缓速器的结构分析不再限定于单纯的有限元分析，必将基于流固耦合技术，将三维流场分析和有限元结构分析相结合，对不同压力场下液力元件叶栅及工作轮的应力分布以及形变位移进行求解分析。北京理工大学王峰等人[24]对某型液力减速器内流场，采用 CFD 数值模拟技术获得其流道内部压力场，运用坐标变换、曲面拟合等方法，得到叶片表面的压力随局部坐标变化的二元函数; 利用 ANSYS 软件的 APDL 程序将叶片的压力载荷加载到有限元分析模型中，实现了流体压力作用下的叶片强度问题较为精确的液力减速器叶片强度分析。杨涛[25]利用有限元软件 ANSYS 对液力缓速器动轮和定轮进行强度和模态分析。ZHAO 等[26]利用有限元对液力缓速器的壳体进行了震动分析并进行了相应的试验。

3　试验研究

液力缓速器的传动外特性、制动特性性能测试试验方面，一般是通过搭建传动试验台进行测试。北京理工大学荆崇波等[27]对某型液力减速器进行了制动性能试验研究，分别对液力减速器不同转速、不同充液率工况下的基本特性和制动特性进行了试验。试验结果表明，该液力减速器在高转速和大充油量的条件下制动效果较好。武汉理工大学过学迅等[28]进行了台架试验，对液力减速器空气鼓风损失进行了研究，通过鼓风损失理论计算设计出新的减损结构阀片，将液力减速器安装阀片和不安装阀片的试验结果进行对比，表明所设计的液力减速器减损结构措施具有理想的效果，且实验值和理论计算值基本吻合。

随着流动测试技术和计算机技术的发展，1996 年以来，在液力变矩器内流场的测量方面取得了很多成果，主要体现在对各叶轮流道内及叶片上速度和压力的测量，测量速度的较多。吉林大学于清海等[29]采用 PIV 技术对 YJ380 有机玻璃变矩器样机进行了流动测试研究，实现了液力变矩器内部流动可视化，并对测试结果进行了量化处理和分析，实验结果与理论分析吻合，证明了此实验方法的可行性和实验结果的正确性。因此，将 PIV 与 CT 技术相结合，是对液力缓速器内部流场进行研究的主要测试手段，是今后促进液力缓速器发展的主要手段之一。

4　结论

(1) 国外的液力缓速器技术成熟，结构类型多样化。国内液力缓速器的研究较晚，技术比较落后，因此，基于逆向工程的设计方法为以后的产品改型提供了很大便利，可以加快液力缓速器的国产化进程，尽快打破国外对于液力缓速器技术的垄断。

(2) 一维束流理论具有物理概念明确、参数调节简单的优点，简化流场便于研究。

(3) 在概念设计阶段，通过 CFD 这种虚拟设计对液力缓速器进行研究，可以获得大量的流动和换热的细节数据; 利用计算数据对设计方案进行评价，选择优化方案。但是还需要通过样机制造及对原型机和样机的试验分析，对 CFD 计算的结果进行验证，从而对设计结果进行修正。

(4) 基于流固耦合技术，将三维流场分析和有限元结构分析相结合，对不同压力场下液力元件叶栅及工作轮的应力分布以及形变位移进行求解分析，对使用在不同环境下的液力缓速器的结构强度分析是非常有必要的。

(5) 通过理论计算的方法描述液力缓速器结构设计及性能难度较大、并且精度较低，所以采取先进的流动测试技术对液力缓速器进行试验研究，是研究液力缓速器性能、探索其内部流动规律非常有效的方法。

参考文献:

【1】黄榕清，李刚营，胡宏. 液力缓速器和电涡流缓速器[J]. 机电工程技术，2005(10): 82 - 85.

【2】SCHRECK Helmut，KUCHER Heinz，REISCH Bernhard. ZF Retarder in Commercial Vehicles [R]. SAE 922452，1992.

【3】BERGMANN Uwe，KAHLAU Gerhard E，VOGELSANG Klaus，et al. State of Development and Future Prospects of Hydrodynamic Brakes for Trucks and Buses [R]. SAE 922454，1992.

【4】中国应用技术网. http://www.aptchina.com/faming/2219987/.

【5】刘凯，鲁明，严军. 基于逆向工程和流场分析的液力缓速器叶轮设计[J]. 拖拉机与农用运输车，2009，36(4): 55 - 57.

【6】朱经昌，魏宸官，郑慕侨. 车辆液力传动[M]. 北京: 国防工业出版社，1982.

(下转第 184 页)

年后的故障趋势可能会发生变化，需要更多的故障数据来进行建模；并且，模型需要利用分段 PLP[14] 或是混合 PLP[15]，这也是接下研究的方向之一。

参考文献:

【1】WECKAN G R,SHELL R L,MARVEL J H. Modeling the Reliability of Repairable Systems in the Aviation Industry [J]. Computers and Industrial Engineering,2001,40(1/2):51 – 63.

【2】de OLIVEIRA Maristela Dias,COLOSIMO Enrico A,GILARDONI Gustavo L. Bayesian Inference for Power Law Processes with Applications in Repairable Systems [J]. Journal of Statistical Planning and Inference,2012,142(5):1151 – 1160.

【3】张英芝,申桂香,薛玉霞,等. 随机截尾数控机床故障过程 [J]. 吉林大学学报,2007,37(6):1346 – 1348.

【4】王智明,杨建国,王国强,等. 多台数控机床最小维修的可靠性评估 [J]. 哈尔滨工业大学学报,2011,43(7):127 – 130.

【5】CROW L H. Confidence Interval Procedures for the Weibull Process With Applications to Reliability Growth [J]. Technometrics,1982,24(1):67 – 72.

【6】CROW L H. Reliability Analysis for Complex,Repairable Systems,AD1R765706M541 [R]. Maryland: U. S. Army Materiel System Analysis Activity,1975.

【7】NELSON W. Accelerated Testing: Statistical Methods,Test Plans,and Data Analysis [M]. NewYork: John Wiley & Sons,1990.

【8】MEEKER W Q,ESCOBAR L A. Statistical Methods for Reliability Data [M]. NewYork: John Wiley & Sons,1998.

【9】ASCHER H. Repairable Systems Reliability: Modeling, Inference,Misconceptions and Their Causes [M]. NewYork: Marcel Dekker,1984.

【10】KVALøY JT,LINDQVIST B. TTT-based Tests for Trend in Repairable Systems Data [J]. Reliability Engineering and System Saftey,1998,60(1):13 – 28.

【11】LEWIS P A,ROBINSON D W. Testing for Monotone Trend in a Modulated Renewal Process [C] //Reliability and biometry,Philadelphia: SIAM,1974: 163 – 182.

【12】LEE L. Comparing Rates of Several Independent Weibull Process [J]. Technometrics,1980,22: 427 – 430.

【13】ASCHER H. Different Insights for Improving Part and System Reliability Obtained from Exactly Same DFOM "Failure Numbers" [J]. Reliability Engineering and System Safety,2007,92(5):552 – 559.

【14】GUO Huairui,METTAS A,SARAKAKIS G,et al. Piecewise NHPP Models with Maximum Likelihood Estimation for Repairable Systems [C] //Reliability and Maintainability Symposium,San Jose,CA: IEEE,2010: 1 – 7.

【15】PULCINI G. Modeling the Failure Data of A Repairable Equipment with Bathtub Type Failure Intensity [J]. Reliability Engineering and System Safety,2001,72(1):209 – 218.

(上接第 179 页)

【7】赵鹏. 汽车液力缓速器开发技术研究 [D]. 西安: 长安大学,2008.

【8】施凯男. 汽车液力缓速器辅助制动性能研究 [D]. 西安: 长安大学,2009.

【9】杨凯华,阎清东. 车辆液力减速器仿真计算研究 [J]. 液压与气动,2002(7):50 – 51.

【10】王峰,阎清东,乔建刚. 液力减速器制动性能的计算方法 [J]. 起重运输机械,2006(5):24 – 27.

【11】姚寿文,王晓龙. 液力减速器叶栅系统优化及制动动力学仿真 [J]. 机械设计,2007,24(12):21 – 23.

【12】闫清东,邹波,魏巍. 液力减速器部分充液工况制动性能计算方法研究 [J]. 北京理工大学学报,2011,31(12):1396 – 1400.

【13】严军,过学迅,汪斌,等. 车辆液力缓速器内腔压力特性分析及建模 [J]. 汽车工程,2010,32(4):308 – 313.

【14】沈文浩. 液力缓速器制动过程的理论与实验研究 [D]. 广州: 华南农业大学,2009.

【15】黄俊刚,李长友,沈文浩. 液力缓速器定转子工作腔的三维流场数值模拟 [J]. 机床与液压,2010,40(3):1 – 7.

【16】李雪松,程秀生,苗丽影. 液力缓速器内流场三维瞬态数值模拟及特性预测 [J]. 汽车技术,2009(10):34 – 39.

【17】李慧渊. 基于三维流场理论的液力减速器设计研究 [D]. 北京: 北京理工大学,2009.

【18】魏巍,李慧渊,邹波. 液力减速器制动性能及其两相流分析方法研究 [J]. 北京理工大学学报,2010,30(11):1281 – 1284.

【19】闫清东,邹波,魏巍. 液力减速器部分充液工况制动性能计算方法研究 [J]. 北京理工大学学报,2011,31(12):1396 – 1400.

【20】何仁,严军,鲁明. 叶片不同倾斜方式对液力缓速器缓速性能的影响分析 [J]. 机械科学与技术,2009,28(8):1056 – 1059.

【21】严军,何仁. 液力缓速器叶片变角度的缓速性能分析 [J]. 农业机械学报,2009,40(4):206 – 210.

【22】冯宜彬,过学迅. 液力减速器内流场的 CFD 数值模拟研究 [J]. 汽车工程,2009,31(4):353 – 356.

【23】郭刘洋,杜明刚. CFD 为基础的液力减速器结构优化仿真 [J]. 现代制造工程,2009(1):104 – 106.

【24】王峰,阎清东,王书灵. 基于 CFD 和 FEA 的液力减速器叶片强度分析 [J]. 北京理工大学学报,2006,26(12):1052 – 1055.

【25】杨涛. 液力缓速器流场仿真及有限元分析 [D]. 武汉: 武汉理工大学,2009.

【26】ZHAO Xufei,LI Changyou,LI Xiaowen. Modal Analysis of the Hydraulic Retarder Shell [J]. Advanced Materials Research,2011,418: 2195 – 2199.

【27】荆崇波,胡纪滨,鲁毅飞. 车用液力减速器制动性能试验研究 [J]. 汽车技术,2005(12):27 – 31.

【28】过学迅,时军. 车辆液力缓速器设计和试验研究 [J]. 汽车工程,2003,25(3):140 – 142.

【29】于清海,王辉,马文星,等. PIV 技术在液力变矩器内部流场实验研究中的应用 [J]. 实验技术与管理,2004,21(5):31 – 34.

机床与液压

MACHINE TOOL&HYDRAULICS

ISSN 1001-3881
CN44-1259/TH

2017.02
半月刊 第45卷 总第428期
www.jcyyy.com.cn

中文核心期刊 中国科技期刊精品数据库收录期刊 中国科技论文统计源期刊 CODE JYYEEV 1973年创刊
主办：中国机械工程学会 广州机械科学研究院有限公司 协办：国家机器人检测与评定中心（广州）

机床与液压

JICHUANG YU YEYA

1973 年创刊

第 45 卷第 2 期（总第 428 期）2017 年 1 月

半月刊（每月 15 日、28 日出版）

www. jcyyy. com. cn

主　　管：中国科学技术协会

主　　办：中国机械工程学会
广州机械科学研究院有限公司

协　　办：国家机器人检测与评定中心(广州)

编辑出版：《机床与液压》编辑部

地址：广州市黄埔区茅岗路 828 号（510700）

电话：020-32385312　传真：020-32389600

电子邮箱：jcy@ gmeri. com

英文专版采编中心（重庆理工大学期刊社）

电话：023-68667984,E-mail:jdygcyw@ 126. com

广告发行部

广告策划：曹懿莎　黎文勤　徐瑾瑾

美术编辑：陈卉子

电话：020-32385311　传真：020-32389600

电子邮箱：adv@ gmeri. com

发　　行：麦丽菊　发行热线：020-32389676

网　　站：郭汝叙　网站热线：020-82496580

发行范围：国内外发行

国内发行：广东省报刊发行局

订 购 处：全国各地邮局

国外发行：中国国际图书贸易集团有限公司

广告经营许可证：440000100115

印　　刷：广州市新怡印务有限公司

ISSN1001-3881
CN44-1259/TH

国内邮发代号：46-40

国外发行代号：BM 550

定价：20 元/期，480 元/年

目　　次

◀ 制造与装备 ▶

六圆弧齿廓齿轮的设计及承载能力分析
…… 任重义　段建中　姜碧琼（1）

基于 NX 的径流式叶轮工序集中五轴制造工艺研究
…… 吴雁　吕博鑫　吕仕强　郑刚　张杰人（4）

MW 级风机齿轮箱故障模拟实验台设计
…… 张伟　李向阳　张树忠（9）

基于模态试验的螺栓联接刚度识别与应用
…… 桂林　刘彩章　徐妍妍　蔡涛（12）

石油钻杆螺纹修复技术研究
…… 万法伟　赵军友　曹清园
王富涛　曹建明　韩学义（15）

精密气浮工作台动态特性仿真与优化
…… 文明　姚勇　何康昊　陈华明
杨雷　邓立　李佩龙　姜飞（20）

高速电主轴单元-主轴箱体结合面模态分析与研究
…… 梁兆顺　李积元　苟卫东　白向娟（25）

五轴联动 BC 型木工雕刻机床结构与数控系统设计
…… 林砺宗　顾浩炜　韩帅（29）

金属外圆表面超声振动滚压加工技术的研究
…… 朱林　潘德术（35）

锚具夹片连续锯削加工工艺研究
…… 张晓东　赖玉活　李健
李新　李志敏　支凯宁（38）

移动式压板的创新设计及应用
…… 王道林（41）

一种高精重型数控铣床长导轨副方案设计
…… 王东　黄刚强　林健（43）

自动化车床在燃油泵盖加工中的应用
…… 武欣竹　杨继盛（46）

本刊已入编“万方数据——数字化期刊群”，“中国核心期刊(遴选) 数据库”，“中国期刊全文数据库（CJFD）”，“中文科技期刊数据库”及 CNKI 系列数据库，作者如不同意将文章入编，投稿时敬请说明。

期刊基本参数： CN44-1259/TH * 1973 * S * 16 * 164 * zh * P * ¥20.00 *　* 45 * 2017-1

五轴加工 RTCP 与非 RTCP 编程的比较
…… 刘旭华　詹华西（48）
钻孔刀架在数控车削加工中的运用
…… 陈向荣（52）

◀ 液压与气动 ▶

摆式波能发电装置 PTO 系统蓄能器特性研究
…… 黄英珂　陈东（54）
基于 AMESim 的摇臂式清仓机液压系统动态特性的研究
…… 邵明辉　韩跃进（59）
变速恒频风力发电机组液压变桨距系统的设计与仿真
…… 梁云峰　谷凤民　陈宇　郭学东（63）
SK40P 数控车床尾座数控化改造方法及实现
…… 刘凌云　罗敏　陈志楚　吴岳敏（69）
全液压驱动高架作业车设计与滑转性能仿真
…… 种东风　王万章　朱晨辉
秦伟桦　王宝山　王淼森（74）
双转子摆线泵流量特性分析及优化设计
…… 林彩霞　李健辉　苏佩坤　王海林（79）
A2F10 柱塞泵台架评定液压油氧化寿命的应用
…… 王月行　闫龙龙　郑东东（81）
压湿式制动器液压系统的设计
…… 缪丹云（84）
基于模型参考自适应控制的四轮独立驱动技术研究
…… 王海英　阮祺　常肖　邱喜华（88）
变频调速技术在液压自动夹紧系统中的应用研究
…… 张政泼　范贤龙
陈静　赖显渺　蒋桂平（92）
基于 AMESim 节流调速回路仿真及实验研究
… 陶柳　朱石沙　王云　雷雄　王竞（96）
自卸车液压系统对转向系统性能影响分析
…… 刘华洲　吴新佳（100）
基于 PLC 的建筑砌块成型机液压系统设计
…… 刘晓丽　李晓红（106）
叠加 U 形槽过流面积分析与计算
…… 周永飞　初长祥
高名乾　郭小龙　高英达（110）
机构往复直线运动行程控制液压系统的设计
…… 姚薇　吴海丹（113）
电动汽车液压再生制动系统模糊控制策略的研究
…… 徐东　苏世卿　梁永利（115）
一种收缩射流管的结构设计
…… 徐杰　李丙乾　李健（119）
基于 SimoDrive 611U/Ue 的液压精密控制系统设计与实现
…… 尤东升（123）

◀ 控制与检测 ▶

基于小波包-Haar 小波变换的漏磁检测信号降噪数据压缩方法
…… 宋志强　张莹　吴江（126）
一种机械结合面贴合率检测技术研究
…… 江晖　徐东鸣　王立朋（130）
基于传感网络的数控机床故障监控系统的设计
…… 吴蕾（133）
基于 ARM9 的齿轮加工数控系统的研究
…… 刁修慧　王慧（136）
光学精磨抛光机床性能参数的优化设计
…… 刘旸　朱成俊（139）

◀ 改造与维修 ▶

真空结晶机搅拌装置结构优化设计
…… 王建军　赵晶文（143）
FS41M15 数控铣床的技术升级改造
…… 范芳洪（147）
基于故障树的公路运输车气压制动系统故障诊断
…… 于文凯　陈艳　邵小平　傅乐平（152）
数控车床动力头故障维修
…… 黄贤超　王志鹏　余刚（155）
高压大流量液压压力机液压系统原理及常见故障分析
…… 禹智慧（157）
数控加工中心 ATC 装置的控制分析与故障排除
…… 晁晓圆（160）
某液压缸活塞杆连续抖动故障分析与排除
…… 蒋玲玲　张莉（163）
信息……（58）、（68）、（73）、（122）、（125）、（129）、（146）、（151）、（159）

MACHINE TOOL & HYDRAULICS
Half-Monthly
Vol. 45 No. 2 Jan. 2017

Authorities in Charge: China Association for Science and Technology
Sponsor: Chinese Mechanical Engineering Society
Guangzhou Mechanical Engineering Research Institute Co., Ltd
Co-organizor: National Robot Test and Assessment Center (Guangzhou)
Editor & Publisher: 《MACHINE TOOL & HYDRAULICS》 Editorial Department
Add: No. 828 Maogang Road, Huangpu District, Guangzhou, China

Tel: (8620) 32385312
Fax: (8620) 32389600
Web: www.jcyyy.com.cn
E-mail: jcy@gmeri.com
English Special-Edition Editorial Center (Periodicals Office of Chongqing University of Technology)
Tel: (8623) 68667984
E-mail: jdygcyw@126.com
Distributed Range: Distribution at home and abroad
Domestic Distributor: Newspapers and Publications Board of Guangdong
Overseas Distributor: China International Book Trading Corporation
Post Distribution Code: 46-40
International Code: BM 550

CONTENTS

MANUFACTURING TECHNOLOGY & EQUIPMENT

Sextuple-arc Gear Tooth Profile Design and Carrying Capacity Analysis ····· REN Zhongyi DUAN Jianzhong JIANG Biqiong (1)
Study on Five-axis Centralized Manufacturing of Radial Flow Impeller Based on NX ····· WU Yan LV Boxin LV Shiqiang ZHENG Gang ZHANG Jieren (4)
Design of Fault Simulation Test Bench for MW Grade Wind Turbine Gearbox ····· ZHANG Wei LI Xiangyang ZHANG Shuzhong (9)
Identification and Application of the Stiffness of Bolted Joint Based on Modal Test ····· GUI Lin LIU Caizhang XU Yanyan CAI Tao (12)
Research on Repairing Technology for Drill Pipe Thread WAN Fawei ZHAO Junyou CAO Qingyuan WANG Futao CAO Jianming HAN Xueyi (15)
Simulation and Dynamic Characteristic Optimization of the Ultra-precision Stage with Air-bearing ····· WEN Ming YAO Yong HE Kanghao CHEN Huaming YANG Lei DENG Li LI Peilong JIANG Fei (20)
Modal Analysis and Research on Joint Surface of High Speed Motorized Spindle Unit-Spindle Box ····· LIANG Zhaoshun LI Jiyuan GOU Weidong BAI Xiangjuan (25)
Design of BC Mode Five-axis Wood Engraving Machine Structure and CNC Control System ····· LIN Lizong GU Haowei HAN Shuai (29)
Study on the Ultrasonic Vibration Finishing Technology for the Metallic Outer Cylindrical Surface ····· ZHU Lin PAN Deshu (35)
Study on Continuous Sawing Process for Anchorage Clip ····· ZHANG Xiaodong LAI Yuhuo LI Jian LI Xin LI Zhimin ZHI Kaining (38)
Innovation Design and Application of the Mobile Clamp Plate ····· WANG Daolin (41)
Design of Long Guide Rail for High-precision CNC Milling Machine ····· WANG Dong HUANG Gangqiang LIN Jian (43)
The Application of the Fuel Pump in Automatic Lathe Processing ····· WU Xinzhu YANG Jisheng (46)
Comparison between RTCP Programming and Non RTCP Programming for Five-axis Machining ····· LIU Xuhua ZHAN Huaxi (48)

Application of Drilling Tool Post in the NC Turning Processing ····· CHEN Xiangrong (52)

HYDRAULICS & PNEUMATICS

Research on Characteristics of Storage Power Plant of Pendulum Wave Energy PTO System ····· HUANG Yingke CHEN Dong (54)
Research on Dynamic Characteristic of Hydraulic System for Rocker Arm Type Clearing Machine Based on AMESim ····· SHAO Minghui HAN Yuejin (59)
Design and Simulation for Hydraulic Variable Pitch System of Wind Turbine with Variable Speed and Constant Frequency ····· LIANG Yunfeng GU Fengmin CHEN Yu GUO Xuedong (63)
NC Transformation Method and Implementation for Tailstock of NC Lathe SK40P ····· LIU Lingyun LUO Min CHEN Zhichu WU Yuemin (69)
Design and Slip Performance Simulation for Three Wheeled High Frame Field Operation Vehicle with Full Hydraulic Driving ····· CHONG Dongfeng WANG Wanzhang ZHU Chenhui QIN Weihua WANG Baoshan WANG Miaosen (74)
Analysis and Optimal Design for Flow Characteristics of the Cycloidal Duplex Rotor Pump ····· LIN Caixia LI Jianhui SU Peikun WANG Hailin (79)
Application of A2F10 Piston Pump Bench for Evaluating the Oxidation Life of Hydraulic Fluids ····· WANG Yuexing YAN Longlong ZHENG Dongdong (81)
Design of the Press Wet Brake Hydraulic System ····· MIAO Danyun (84)
Research on Four Wheel Independent Driving Technology Based on Model Reference Adaptive Control ····· WANG Haiying RUAN Qi CHANG Xiao QIU Xihua (88)
Application Research of Frequency Control Technology in Hydraulic Automatic Clamping System ····· ZHANG Zhengpo FAN Xianlong CHEN Jing LAI Xianmiao JIANG Guiping (92)
Simulation of Throttle Velocity Modulation Circuit Based on AMESim and Experimental Research ····· TAO Liu ZHU Shisha WANG Yun LEI Xiong WANG Jin (96)
Performance Effect Analysis of Hydraulic System on Steering System in Dump Truck ····· LIU Huazhou WU Xinjia (100)
Design on Hydraulic System of Building Block Molding Machine Based on PLC ····· LIU Xiaoli LI Xiaohong (106)
Analysis and Calculation of the Orifice Area of Spool with U+U-type Notches ····· ZHOU Yongfei CHU Changxiang GAO Mingqian GUO Xiaolong GAO Yingda (110)
Design of a Hydraulic Actuated System for Reciprocating Linear Motion Control Mechanism ····· YAO Wei WU Haidan (113)
Research on Fuzzy Control Strategy for Electric Vehicle Hydraulic Regenerative Braking System ····· XU Dong SU Shiqing LIANG Yongli (115)
Structure Design of a Kind of Contraction Jet Pipe ····· XU Jie LI Bingqian LI Jian (119)
Design of Hydraulic Precision Control System Based on SimoDrive 611U/Ue ····· YOU Dongsheng (123)

CONTROL & MEASUREMENT

MFL Signal Denoise and Data Compression Method Based on Wavelet Packet-Haar Wavelet Transform Algorithm SONG Zhiqiang ZHANG Ying WU Jiang (126)
Study on the Joint Rate Measurement for the Machine Contact Surface ····· JIANG Hui XU Dongming WANG Lipeng (130)
Design of NC Machine Tool Fault Monitoring System Based on Sensor Network ····· WU Lei (133)
Research on Gear Machining CNC System Based on ARM9 ····· DIAO Xiuhui WANG Hui (136)
Optimization Design of Performance Parameters for Optical Accurate Grinding and Polishing Machine ····· LIU Yang ZHU Chengjun (139)

RECONSTRUCTION & MAINTENANCE

Structure Optimization Design for the Mixing Device of the Air Crystal Machine ····· WANG Jianjun ZHAO Jingwen (143)
Technological Upgrading of FS41M15 Numerical Control Milling Machine ····· FAN Fanghong (147)
Failure Diagnosis for Air Brake System of Some Truck Based on Fault Tree Analysis ····· YU Wenkai CHEN Yan SHAO Xiaoping FU Leping (152)
Failure Maintenance for Power Tool Turret of CNC Lathe HUANG Xianchao WANG Zhipeng YU Gang (155)
Principle and Common Faults Analysis for Hydraulic System of Press with Large Flow and High Pressure ····· YU Zhihui (157)
Control Mechanism Analysis and Trouble Shooting for ATC Device in CNC Machining Center ····· CHAO Xiaoyuan (160)
Fault Analysis and Elimination on Continuous Jitter of the Piston Rod of a Hydraulic Cylinder ····· JIANG Lingling ZHANG Li (163)

DOI: 10.3969/j. issn. 1001-3881. 2017. 02. 021

双转子摆线泵流量特性分析及优化设计

林彩霞，李健辉，苏佩坤，王海林
（华南农业大学工程学院，广东广州 510642）

摘要： 基于传统的单转子摆线泵流量特性分析思路，确定了双转子摆线泵的基本流量特性曲线。针对泵体的流量脉动特性，对双转子摆线泵的设计进行优化，进一步减少双转子摆线泵的流量脉动，使泵体工作更加平稳。

关键词： 双转子摆线泵；流量脉动；差动角；优化
中图分类号： TH122 **文献标志码：** A **文章编号：** 1001-3881（2017）02-079-2

Analysis and Optimal Design for Flow Characteristics of the Cycloidal Duplex Rotor Pump

LIN Caixia，LI Jianhui，SU Peikun，WANG Hailin
（College of Engineering，South China Agricultural University，Guangzhou Guangdong 510642，China）

Abstract： Based on the analysis about flow characteristic of single rotor cycloid pump，the flow characteristic curve of the cycloidal duplex rotor pump was gotten. Aiming at the flow pulsation，the cycloidal duplex rotor pump structure was optimized，to further reduce the flow pulsation of the pump.

Keywords： Duplex rotor cycloid pump；Flow pulsation；Differential angle；Optimization

摆线转子泵是一种特殊齿形的内啮合齿轮泵，又称摆线内啮合齿轮泵。摆线转子泵以其结构紧凑、体积小、运转平稳、噪声小、不易产生气穴、工作效率高等优点广泛应用于汽车、航空、石油、化工等领域。

流量的均匀性是评价泵体工作性能的重要参数。若泵体的流量脉动大，将会引起泵系统压力脉动，从而使系统产生噪声和震动。作者将对双转子摆线泵的流量特性进行分析，并通过分析数据，对泵体进行相关的优化设计。

1 基本几何参数

摆线转子泵的基本几何参数主要有以下 4 个：齿数、偏心距、创成圆半径、齿形圆半径等。一般情况下，齿数越大，流量与流量脉动越小。而偏心距的大小决定着齿轮节圆半径的大小，从而决定着泵的流量。

在设计中，一般需要根据流量等相关设计要求，首先确定以上 4 个独立的设计参数。待以上的基本参数确定后，便可通过计算，确定出其他的几何尺寸参数[1-3]。

2 流量特性计算

2.1 流量计算的数学模型

根据流量的定义和流量与排量的关系，可以将流量计算的数学模型简化为求排量的数学模型。即当内转子转动一周完成的一个工作循环所排出的液体体积。

式子表达为：

$$V = 2 \cdot B(S_{max} - S_{min}) \tag{1}$$

若不考虑泄漏情况，则双转子泵排量

$$q = z \cdot V \tag{2}$$

式中：B 为转子宽度；S_{max}、S_{min} 分别为单转子最大、最小密封腔面积；z 为内转子齿数。

关于最大、最小密封腔面积的计算，可参考文献[3]。下面简单介绍两种利用绘图软件快速求解的方法。

利用 SolidWorks 的测量功能求解。在建立三维模型后，导入 SolidWorks 的测量模块，点击测量工具选取需要测量的对象，然后调出详细参数列表即能找到相关的面积数据。

利用 AutoCAD 的计算区域面积功能求解。利用 AutoCAD 中提供的 Autolisp 二次开发功能绘制出摆线泵的齿廓曲线，然后对内外转子齿廓曲线所围成的相应区域进行面积计算，便能得到相应的面积数据。

2.2 瞬时流量计算

所谓的瞬时流量，是指泵体在某一时刻所排出的液体体积。由于内外转子所围成的总体积为一固定常数，根据摆线泵的工作原理可知，在任一时刻，进排油腔的体积变化率相等[4]。

瞬时流量计算公式：

收稿日期：2015-12-25
基金项目：广东省科技计划项目（2016A020210108）
作者简介：林彩霞（1976—），女，博士，讲师，研究方向为机械设计理论。E-mail：cxlin76@163.com。

$$Q_s = \frac{dV}{dt} = \frac{B\omega dS}{d\phi} \tag{3}$$

式中：ω 为内转子角速度。

2.3 平均流量

所谓的平均流量，是指泵体在单位时间所排出的液体体积。即：

$$Q_m = q \cdot n \tag{4}$$

式中：n 为转子转速。

2.4 流量脉动率

所谓的流量脉动率，是指泵体的最大瞬时流量差与平流流量的比值。用式子表达为：

$$\sigma_Q = \frac{Q_{smax} - Q_{smin}}{Q_m} \tag{5}$$

一般地，用流量脉动率来评价瞬时流量脉动。

3 流量脉动影响因素分析

对于摆线转子泵，影响流量脉动的因素主要分为转子参数对流量脉动的影响和泵体结构参数对流量脉动的影响[5-6]。

3.1 转子参数对流量脉动的影响

（1）齿数

齿数越小，流量脉动越大；齿数越大，流量脉动越小。增大齿数，单位体积排量相对减少。内转子齿数为偶数时，其流量脉动明显小于奇数齿。

（2）创成系数和弧径系数

增大创成系数、减少弧径系数均能降低摆线泵的流量脉动。与此同时，泵的排量、体积也相应增大。

3.2 泵体结构参数对流量脉动的影响

根据对双转子摆线泵进行的运动分析，双转子的差动角对泵体的流量脉动有较大的影响。下文将就双转子的差动角对泵体的流量脉动影响进行分析与相关的优化设计。

4 双转子摆线泵的流量脉动优化分析设计

关于摆线泵转子基本参数的优化计算，由于目前已经有较多十分完善的研究成果和优化方法，在此不再具体讨论，建议参考文献[7]。

下面将针对双转子摆线泵特有的结构参数“差动角”进行优化计算。

由于双转子摆线泵两个相互独立的转子其结构参数完全相同，因此，当差动角 $\theta = 0°$ 时，可以将两个转子看作是一个宽度叠加的独立转子，即 $B' = 2B$。

根据流量脉动率的计算公式

$$\sigma_Q = \frac{Q_{smax} - Q_{smin}}{Q_m} = \frac{V_{max} - V_{min}}{V_m} = \frac{BS_{max} - BS_{min}}{BS_m} = \frac{S_{max} - S_{min}}{S_m} \tag{6}$$

当转子其他参数不变，单一改变转子宽度 B，其流量脉动率不变。下面利用 MATLAB 分别对单转子和差动角 $\theta = 0°$ 时的双转子摆线泵的瞬时流量进行仿真计算，见图 1、2。

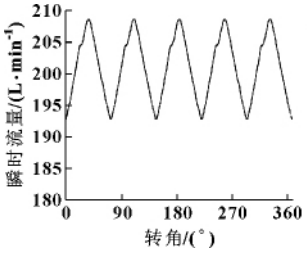

图 1 单转子摆线泵瞬时流量曲线图

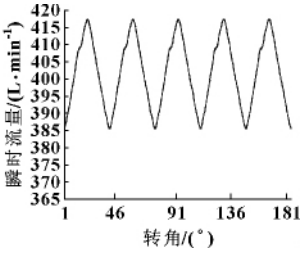

图 2 双转子摆线泵瞬时流量曲线图（$\theta = 0°$ 时）

对比图 1 和图 2，尽管双转子摆线泵在某一时刻的瞬时流量是单转子摆线泵在相同时刻瞬时流量的两倍，但其流量脉动率却没有发生变化，均为 0.078 9。

由于文中分析的双转子摆线泵其内转子齿数为 5，即当内转子每转过 72° 时，泵体输出流量特性进入一个周期循环。因此，下面将以 0.2° 的差动角递增速率，利用 MATLAB 对泵体的瞬时流量进行仿真计算，并求算出差动角 θ 在 0～72° 内所对应的流量脉动率曲线，从而优化出最佳的差动角。图 3 为不同差动角所对应的流量脉动率曲线。

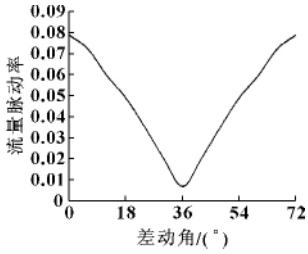

图 3 流量脉动率曲线

从图 3 可以看出：当双转子摆线泵的差动角 $\theta = 36°$ 时，其流量脉动率最小，$\sigma_{Q36} = 0.006\ 8$。

利用 MATLAB 再次对双转子摆线泵差动角优化前后的瞬时流量进行仿真计算。

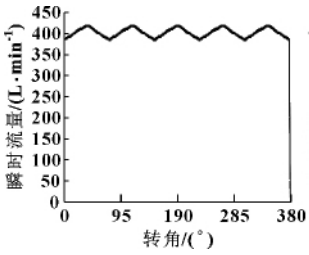

图 4 差动角优化前的瞬时流量曲线

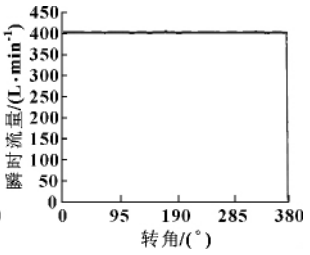

图 5 差动角优化后的瞬时流量曲线

如图 4—5 所示：差动角优化后，双转子摆线泵流量输出相当平稳，且其流量脉动率是优化前的 1/12，远少于相同排量的单转子摆线泵。

4 结论

经过差动角优化后的双转子摆线泵相比于单转子摆线泵更具有开发应用价值。

（下转第 87 页）

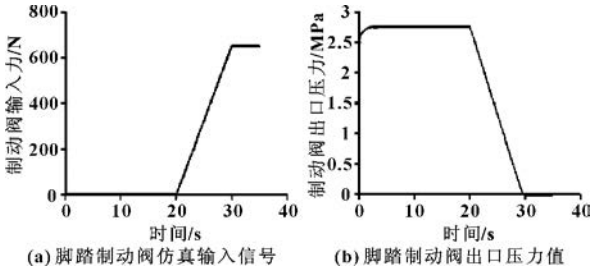

(a) 脚踏制动阀仿真输入信号　(b) 脚踏制动阀出口压力值

图 3　脚踏制动阀性能图

从图 3 可以看出：在前 20 s 制动压力为零输入的情况下，脚踏制动阀的出口输出压力值被稳定在 2.76 MPa，可充分满足矿用胶轮车的使用要求，胶轮车也可正常行驶；在 $t=20\sim30$ s，当制动力急剧增加时，脚踏制动阀的内部阀芯也将在内部作用力下移动，从而导致脚踏制动阀出口压力值的大幅降低，压湿式制动器的油压也相应下降，并实现胶轮车的制动控制。从图 3 中还可看出：脚踏制动阀的动态仿真输入压力与出口压力值之间呈现良好的线性关系，这也验证了所选用的脚踏制动阀的性能，能充分满足压湿式制动器制动控制的需要。

4　总结

压湿式制动器作为一种新型的安全性制动系统，在当前各类大型工程机械、矿用机械中都有着广泛的普及与应用。然而，当前压湿式制动器的设计与相关技术仍处于初步阶段。针对这种现状，结合某矿用胶轮车的设计实例，设计与选型了与该胶轮车压湿式制动器相配套的液压控制系统，并通过 AMESim10.0 仿真软件，对液压系统各主要元件的设计选型结果进行了分析与验证。结果证明该压湿式制动器液压系统的性能良好，能充分满足矿用胶轮车正常行驶与制动控制的需要。

参考文献:

[1] 袁喜悦，赵治国，王晨，等.新型 e-CVT 的湿式制动器液压系统的设计及控制 [J].机床与液压，2015，43(17)：118-120.
YUAN X Y，ZHAO Z G，WANG C，et al.Control and Design of Hydraulic System of Wet Brake for Novel Electric Continuous Variable Transmission [J].Machine Tool & Hydraulics，2015，43(17)：118-120.

[2] 曹秀洪.一种带式输送机盘式制动器液压控制系统的设计 [J].煤炭技术，2013(6)：30-31.
CAO X H.Design of a Disk Brake for Belt Conveyor Hydraulic Control System Design [J].Coal Technology，2013(6)：30-31.

[3] 刘旭，杨寅威.带式输送机盘式制动器液压系统设计 [J].液压与气动，2011(4)：91-92.
LIU X，YANG Y W.Design of Hydraulic System of Disk Brake for Belt Conveyor [J].Chinese Hydraulics & Pneumatics，2011(4)：91-92.

[4] 刘灿杰，贾跃虎，刘志奇.下运带式输送机盘式制动器液压系统设计与分析 [J].机床与液压，2011，39(18)：72-74.
LIU C J，JIA Y H，LIU Z Q.Design and Analysis of Hydraulic System of Disc Brake for Downward Belt Conveyor [J].Machine Tool & Hydraulics，2011，39(18)：72-74.

(上接第 80 页)

参考文献:

[1] 徐学忠.摆线泵几何参数选择及齿廓不产生根切的条件 [J].机床与液压，2004(12)：203-205.
XU X Z.The Selecting of Design Parameter and the Un-undercutting Condition in Cycloidal Pump [J].Machine Tool & Hydraulics，2004(12)：203-205.

[2] 闵荣，王永军.摆线转子泵结构参数优化技术研究 [J].机械科学与技术，2010(3)：333-336.
MIN R，WANG Y J.Optimizing the Structural Parameters of Cycloidal Pump [J].Mechanical Science and Technology for Aerospace Engineering，2010(3)：333-336.

[3] 毛华永，李国祥.摆线转子泵进、排油腔的设计计算 [J].山东大学学报(工学版)，2005(5)：19-23.
MAO H Y，LI G X.Design and Calculation for Oil Chambers of Cycloidal Rotor Pump [J].Journal of Shandong University(Engineering Science)，2005(5)：19-23.

[4] 徐学忠.摆线泵流量特性分析及计算机仿真 [J].机械传动，2006(6)：42-44.
XU X Z.Analysis and Simulation of Flow Characteristics of Cycloidal Pump [J].Journal of Mechanical Transmission，2006(6)：42-44.

[5] 杨明海，杨曦.影响内啮合摆线齿轮泵性能因素 [J].机械工程师，2009(7)：27-29.
YANG M H，YANG X.The Impact of Internal Cycloidal Gear Pump Performance Factors [J].Mechanical Engineer，2009(7)：27-29.

[6] 黄康，王昭，邱明明.多齿差摆线泵流量脉动及其影响因素研究.机床与液压，2014，42(7)：4-8.
HUANG K，WANG Z，QIU M M.Research on Flow Pulsation and Influence Factors of Cycloidal Gear Pump with Multi-tooth Number Difference [J].Machine Tool & Hydraulics，2014，42(7)：4-8.

[7] 徐学忠.摆线泵基本参数的优化设计 [J].液压与气动，2003(12)：6-7.
XU X Z.Optimization Design of Basic Parameter in Cycloidal Pump [J].Chinese Hydraulics & Pneumatics，2003(12)：6-7.

ISSN 1001-3881
CN44-1259/TH

广告经营许可证：440000100115　邮发代号：46-40　定价：20.00元

9 771001 388176 02

CHINESE AGRICULTURAL MECHANIZATION

中国农机化

全国中文核心期刊
中华人民共和国农业部主管
农业部南京农业机械化研究所主办

ISSN 1006-7205
CN 11-4440/S
9 771006 720117

2011 6

中国农机化

2011 年第 6 期

（双月刊，总第 238 期）

社长　王利民

主编　易中懿

主　　管　中华人民共和国农业部

主　　办　农业部南京农业机械化研究所

出　　版　中国农机化杂志社

编　　辑　《中国农机化》编辑部

地　　址　南京市柳营 100 号

邮　　编　210014

电　　话　(025)84346270

传　　真　(025)84346271

电子信箱　cnnnhgxx@public1.ptt.js.cn

印　　刷　南京四彩印刷有限公司

发　　行　全国各地邮局

出版日期　2011 年 11 月 25 日

刊　　号　ISSN 1006-7205 / CN32-1123/S

广告证号　3201004950023

每册定价　12.00 元

全年定价　72.00 元

目　次

■*发展研究*

我国不同区域农机田间作业油耗差异的初步研究 …… 宋英 等 3

农业机械化发展战略规划的指标体系及建构研究 …… 刘超 等 7

基于 OLS 和 HP 滤波的中国八大区域农业装备宏观投入态势研究 …… 吴晓涛 10

吉林省西部生态建设与农业机械化发展对策研究 …… 孙晓东 16

我国甘薯生产机械化技术路线研究 …… 胡良龙 等 20

走绿色农业道路　发展低碳农机 …… 李刚 26

中央级农业科研机构财政投入分析研究 …… 张晓泉 等 29

循环经济发展中的中央与地方政府博弈分析 …… 王磊 等 33

精细农业与信息化技术的研究现状与发展趋势 …… 耿爱军 等 38

■*管理研究*

我国机械化秸秆还田联合作业机的现状与发展 …… 戴飞 等 42

新疆兵团农一师农业机械化发展现状与水平分析 …… 弋晓康 等 46

都市农业与城市生态系统保护 …… 叶军 等 49

基于模糊评判法的我国企业管理人员自我效能感评价研究 …… 李文杰 等 53

农业建设项目过程绩效评价研究 …… 白俊峰 等 57

■*基础研究*

丘陵旱稻机械化种植品种筛选研究 …… 李艳大 61

我国花生主产区种植模式概况 …… 陈有庆 等 66

分段红薯机械化收获模式实验研究 …… 夏阳 等 70

农机事故关系因素的动态灰色关联分析 …… 陈聪 等 73

■*应用研究*

果树施药仿形控制系统的设计 …… 尤丽华 等 76

我国食用菌工厂化生产技术 …… 宋卫东 等 80

4MF-3 型指杆式棉花收获机的设计及试验研究 …… 沐森林 83

膜下滴灌多功能玉米精量播种机的研制 …… 赵炳南 等 87

基于 Solidworks 的移动苗床架设计与应用 …… 戴有华 等 91

基于 FLUENT 的小麦籽粒对辊粉磨流场模拟 …… 张克平 等 95

拖拉机气门套冷挤压工艺及模具设计 …… 陈红杰 98

微型多功能作业机在我国发展现状及其在丘陵山地推广前景 …… 闵启超 等 102

在用车滑行检测台架与道路差异性研究 …… 林彩霞 106

农机车载智能终端及监管服务平台的设计探讨 …… 吴崇友 等 110

新型水产养殖增氧机的设计 …… 王波 等 114

基于单片机控制的虚拟汽车自动空调实验台架的设计 …… 龚文资 118

数控线切割加工模具曲面装置的改造研究 …… 任成高 等 122

脱硫石膏改良碱化土壤试验研究 …… 许清涛 等 126

超声波辅助提取桔子皮中多糖的研究 …… 岳贤田 131

农用 AGV 综合通信系统设计 …… 尚婕 等 134

■*教育培训*

关于校企社联合农机培训模式的研究 …… 张晓辉 138

关于农机培训模式的探讨 …… 杨春华 142

高等教育和谐生态系统“生向标”的就业通络研究 …… 刘冬梅 等 146

本期责任编辑　凌小燕　王新　杨建平

Chinese Agricultural Mechanization
No. 6 2011 (Total No. 238)

Contents

Development Research
Preliminary study on difference of oil consumption of agricultural machine in field working in different areas of China ..... SONG Ying, YANG Lin, ZHANG Chuan-sheng, ZHANG Jian, CHU Wei-wen 3
Studies of system of guide line and configuration on stratagem programming of agricultural mechanization development ..... LIU Chao, WU Jian-Hua, BAI Ling 7
Research on the gross input of agricultural equipment of eight regions in China based on OLS and HP filter ..... WU Xiao-tao 10
Study on the Ecological Construction and Development Countermeasure of Agricultural Mechanization in the Western of Jilin Province ..... SUN Xiao-dong 16
Study on the route of mechanization ofsweet potato(ipomoea batatas lam.) production technology in China ..... HU Liang-long, HU Zhi-chao, XIE Yi-zhi, TIAN Li-jia, JI Fu-lai, WANG Bing 20
Study on the development of green agriculture and low carbon agricultural machinery in Xuzhou city ..... LI Gang 26
Analysis and study on fiscal input of central agriculture scientific research institutions ··· ZHANG Xiao-quan, ZHAO Run, CHENG Mei 29
Game analysis of developing recycling economy between central government and local government ..... WANG Lei, WANG Bo 33
Research status and developing direction of precision agriculture ..... GENG Ai-jun, ZHANG Xiao-hui, SONG Tao, MA Min 38
Management Research
Development present situation of straw returned combined machine used in China ..... DAI Fei, HAN Zheng-sheng, ZHANG Ke-ping, HU Jing-ming, FENG Yong-zhong, ZHANG Feng-wei 42
Analysis on Present Situation and Level of Agricultural Mechanization Development in Division Production and Construction Corps of Xinjiang ..... YI Xiao-kang , LIU Xiao-rui 46
Urban agriculture and protection of urban ecosystem ..... YE Jun,ZHAO Shu-ming 49
Fuzzy Judgement Based Study on Self-efficacy Evaluation of Domestic Enterprise Administrators ..... LI Wen-jie, ZHAO Run 53
Research on agriculture construction project process performance measurement ..... BAI Jun-feng, YIN Yi-lin 57
Basic Research
Study on cultivars screening of early rice mechanization planting in hilly area ..... LI Yan-da, YE Hou-zhuan, SHEN Xian-hua, GU Xin-xu, YAO Lin-tao, SHU Shi-fu, WAN Peng 61
Overview of Peanut Cropping Patterns in Main Production Area in China ..... CHEN You-qing, WANG Hai-ou, PENG Bao-liang, HU Zhi-chao. LIU Ming-ji 66
Experiment on the multiple step mechanized sweet potato harvest ..... XIA Yang, HE Yu-jing, WANG Wan-zhang, QIN Xian-zheng 70
Research the relation factors of farm machinery accident with the grey correlated analysis ··· CHEN Cong,CAO Lei,WANG Zhong-qun 73
Application Research
Design of orchard spraying profiling control system ..... YOU Li-hua, FANG Kai-tuo, LU Yao-cheng, ZHOU Liang-fu, FU Xi-min 76
Technologies of edible fungi industrial production in China ..... SONG Wei-dong , WANG Ming-you, XIAO Hong-ru, SONG Zhi-yu, DING Wen-qin 80
Design and experiment on the 4MF-3 Finger-type Cotton Picker ..... MU Sen-lin, ZHANG Yu-tong, SHI Lei, WU Chong-you, CHEN Chang-lin 83
Development of multipurpose maize precision seeder with drip irrigation ..... ZHAO Bing-nan, ZHU Feng-wen, ZHU Xiang-yu,ZHAO Xin-zi,YANG Sheng-bin,LIU Ying,YANG Wei,LIU Peng 87
Design and application of mobile seedbed frame based on Solidworks ..... DAI You-hua, CHEN Zhi-ming, LIU Yong-hua, YU Hong 91
Simulation of flow field of wheat milling based on fluent softwear ..... ZHANG Ke-ping, HUANG Jian-long, ZHANG Zhen-chuan, ZHAO Chun-hua, HUANG Xiao-peng 95
Cold extrusion process and die design of tractor valve cover ..... CHEN Hong-jie 98
Current situation and popularizing prospect in hilly mountains of mini multifunctional machine ..... Min Qi-chao, LIANG Su-ning, CHEN Chang-lin, JIN Mei 102
Research of the difference in automobile coast-down test between bench and road ..... LIN Cai-xia 106
Exploration on design intelligent terminal for agricultural vehicles and the supervision services platform ..... WU Chong-you, QIAN guo-ming, Wang Su-zhen 110
Design of new aquacultural aerator ..... WANG Bo,SHU Su 114
A virtual experimental platform design of automobile automatic air-conditioner on base of single-chip control ..... GONG Wen-zi 118
Transform research on processing mould surface device by WEDM ..... REN Cheng-Gao, SHEN Xiao-Long,PI Zhi-Mou 122
Optimal application rate of desulfurized gypsum in ameliorating soils moderate in sodic salinity - XU Qing-tao, LI Yu-bo, LI Xiao-dong 126
Extraction of polysaccharides with supersonic wave from Orange peel ..... YUE Xian-tian 131
Design of integrated communication system for agricultural AGV ..... SHANG Jie, JIANG Wen-gang, CAI Lan-tu 134
Education and Training
Research on the agricultural machine training mode of joint cooperatives, schools and enterprises ..... ZHANG Xiao-hui 138
Study with regard to the training mode of agricultural machinery ..... YANG Chun-hua 142
Research on employment vein ralaxing based on "student vane" of the harmonious ecosystem of higher education ..... LIU Dong-mei, WANG Bo, Zhang Jin 146

The duty editor LING Xiao-yan WANG Xin YANG Jian-ping

在用车滑行检测台架与道路差异性研究

林彩霞
(华南农业大学工程学院,广州市,510640)

摘要:研究了底盘测功机台架与道路滑行距离检测之间存在的差异,选用金龙汽车,在台架和道路进行滑行距离的对比试验,指出两者的结果存在差异。其主要原因是由于汽车在台架和道路所受到的阻力不同,并对各种阻力进行了分析,最后建立滑行距离修正模型,以减少测试数据误差,合理反映汽车实际的滑行距离。

关键词:在用车;滑行距离;道路与台架;差异特性;
中图分类号:U463.32　　文献标识码:A　　doi:10.3969/j.issn.1006-7205. 2011.06.027

林彩霞. 在用车滑行检测台架与道路差异性研究[J]. 中国农机化, 2011, (6): 106~109
LIN Cai-xia. Research of the difference in automobile coast-down test between bench and road [J]. Chinese Agricultural Mechanization, 2011, (6): 106~109

0 引言

汽车底盘测功机是最重要的汽车台架检测设备之一,在汽车工程中用于对技术状况的总体检验。在用车检测用底盘测功机要求在造价低的前提下保证一定的精度并兼容多种功能,但是目前底盘测功机还存在诸多问题:如测量数据准确度低;因机械结构不同形成内部阻力差异造成测量数据的可靠性差;难以对车辆的动力性做出正确评价,难以和检测排放用的测功机兼容;不易准确模拟道路阻力等。因此为使底盘测功机检测结果更接近车辆实际运行情况,本文针对室内台架进行滑行检测时存在的问题,力图在试验的基础上,分析造成台架与道路滑行距离存在差异的原因,并指出应建立相应的数学模型进行修正,以减少测试数据误差,合理反映汽车实际的滑行距离。

1 底盘测功机基本原理

汽车底盘测功机是一种根据相似理论模拟车辆在道路上实际行驶工况、进行不解体检验车辆性能的室内台架检测设备。根据相似理论第一定理,彼此相似的现象必定具有数值相同的相似准则。汽车在道路或台架上运行时,所做的运动可用牛顿第二定律来描述,因此,它们具有相同的相似准则 N_e 即牛顿准则,保证两者运动相似。

$$N_e=Ft/mv \tag{1}$$

这样根据相似第二定理,该设备利用滚筒代替路面,而车辆在平直道路上加速行驶时受到的空气阻力、滚动阻力由加载装置进行模拟。

车辆在平直道路上行驶受到的阻力为[1]:

$$F_t=Gf+\frac{C_wAv^2}{21.15}+\delta m\frac{dv}{dt} \tag{2}$$

式中:G——汽车动力,N;
f——滚动阻力系数;
d——汽车旋转质量换算系数;
m——汽车质量,kg;
dv/dt——行驶加速度,kg/s^2。

车辆在台架上受到的阻力为

$$F'=a+bv+m'\frac{\triangle v}{\triangle t} \tag{3}$$

式中:a——常数;
b——初速度影响系数;
m'——台架惯性质量,kg。

这样涡流机加载的阻力为两者的差值,即:

$$F_{dy}=F_t-F'=\left(Gf+\frac{C_wAv^2}{21.15}+\delta m\frac{dv}{dt}\right)-\left(a+bv+m'\frac{\triangle v}{\triangle t}\right) \tag{4}$$

当汽车滑行时,用惯性模拟系统即飞轮或交直流电机来模拟惯性阻力。路试时的动能 W 为(后轮为驱动车轮):

$$W=\frac{1}{2}mv^2+\frac{1}{2}(J_k+J_r)\omega^2+W_0 \tag{5}$$

式中:ω——车轮角速度,rad/s;

收稿日期:2010 年 6 月 23 日　　修回日期:2010 年 9 月 13 日
林彩霞,女,汉族,1976 年生,广东阳江人,华南农业大学工程学院讲师;研究方向为地面车辆机械设计理论与方法。

J_k,J_r——前后车轮转动惯量,kg·m²;

W_0——汽车传动系统旋转动能,w;

台架的动能 W'(同一车速)为:

$$W'=\frac{1}{2}J\omega_f^2+\frac{1}{2}J_0\omega_0^2+\frac{1}{2}J_h\omega_h^2+\frac{1}{2}J_r\omega^2+W_0 \quad (6)$$

式中:J、ω_f——飞轮的转动惯量、角速度,kg·m²、rad/s;

J_0、ω_0——滚筒的转动惯量、角速度,kg·m²、rad/s;

J_h、ω_h——加载装置转子的转动惯量、角速度,kg·m²、rad/s。

底盘测功机为模拟汽车道路行驶时的动能必须满足的条件为:$W'=W$。这样令:

$\omega_0/\omega=R/r=k_0$,$\omega_f/\omega=k_f$,$\omega_h/\omega=k_h$

式中:R——车轮半径;

r——滚筒半径。

并将 $v=R\omega$ 代入,则得飞轮的转动惯量为:

$$J=\frac{mR^2+J_k-J_0k_0^2-J_hk_hk_0^2}{k_f^2k_0^2} \quad (7)$$

因此在底盘测功机上能测试汽车底盘输出功率、最高车速、加速时间和滑行距离,以此判定汽车的动力性及底盘技术状况;同时由于可模拟道路行驶工况以及方便地对试验车辆加载,故可在测量尾气排放和燃油消耗时作为车辆的外部负荷。

2　台架与道路滑行对比试验

对 XML6402 汽车分别在道路和风冷式电涡流测功机 KDCG—10G(Φ369.2×1100)测功机上进行滑行距离对比试验,两者具有相同的滑行初速度。在道路上滑行时来回方向各进行两次,取均值,同时注意了相关因素的影响。KDCG—10G 测功机有两级飞轮,转动惯量分别为 14.8(kg·m²)和 49.6(kg·m²)。在控制相关因素的情况下,试验数据见表 1。

表 1　金龙道路和台架滑行试验结果(单位:m)

初速度(km/h)		20	30	40	50
道路	1	106.61	212.83	334.275	469.05
	2	110.415	222.485	352.865	481.99
	平均	108.513	217.658	343.57	475.52
台架	飞轮 1	73	140	200	258.6
	飞轮 2	67	136.5	206.4	260
	平均	70	138.25	203.2	259.3

从上表中可以看出道路和台架滑行距离随着滑行初速度的增加而增大,道路的滑行距离比测功机的滑行距离要长,两者存在差异。

3　滑行检测结果的差异原因分析

3.1　台架阻力分析

台架阻力是底盘测功机台架传递力时存在的内部阻力,主要是由各运动件在相对运动中存在机械磨擦引起的机械阻力构成,是台架本身的机械阻力,与车型无关[2]。根据实验测得的数据,KDCG-10G 测功机损耗功率在汽车发动机功率中所占的比例分别如表 2 所示。

表 2　KDCG—10G 测功机损耗功率

速度(km/h)	占金龙的比例(%)
20	1.11
30	2.00
40	2.94
50	3.61
60	4.72
70	5.67
80	7.22
90	8.69

从表中可见,台架损耗功率占发动机功率比例的最大值达 8.69%,说明这一数值是不应忽略的,其消耗了汽车滑行时的部分能量,而汽车在道路上滑行时是没有这一部分能量损耗的。加载公式(3)是对台架阻力的计算,但从中可以看出,该公式只考虑了台架的滚动阻力和惯性阻力的影响。因此,为提高检测结果的精确度,底盘测功机应该带反拖装置以测试出台架的内部损耗。

3.2　传动系阻力分析

汽车行驶时,传动系阻力的大小与传动系润滑油温密切相关,随润滑油温升高而降低。行驶中受迎面气流的影响,驱动桥的润滑油温度可能低于标准值,有试验指出,若稍微提高 8×8 汽车轮边减速器的油温 20K,就使液力阻力减少一半。而在台架上汽车处于静止状态,润滑油温度一般比道路行驶时高。汽车在道路上行驶时,还存在轮毂轴承摩擦阻力和车轮定位前束阻力,在台架上只有驱动轮的轮毂轴承摩擦阻力,不存在车轮定位前束阻力。因此,在台架与道路上的传动系阻力是不同的。

3.3　滚动阻力的差异性分析

1) 汽车在台架上的滚动阻力分析

在台架上当车轮不滚动时,滚筒对车轮的法向反作用力的分布是前后对称的,但当车轮滚动时,在线

O_1O_2 前后相对应点 d 和 d' 变形虽然相同，但由于弹性迟滞现象，处于压缩过程的前部点 d 的法向反力就大于处于恢复过程的后部点 d' 的法向反力，如图 1 所示(图中 O_2 为前滚筒，O_3 为后滚筒)。这样使得滚筒对轮胎法向反作用力的分布前后并不对称，反作用力的合力 F_{N1} 和 F_{N2} 以滚筒中心为原点向前偏斜了一定角度。设前滚筒偏斜了 γ 角，后滚筒偏偏斜了 β 角，其偏斜角度的大小与轮胎结构、材料、气压、载荷、轮胎磨损程度和运转车速有关。当轮胎变形增大时偏斜角也随着轮胎弹性迟滞损失的增大而变大。因此，F_{N1} 和 F_{N2} 的作用点相对于 O_1O_2 和 O_1O_3 连线向前移动的距离分别为 $l_1=\gamma\cdot r$ 和 $l_2=\beta\cdot r$[3]。

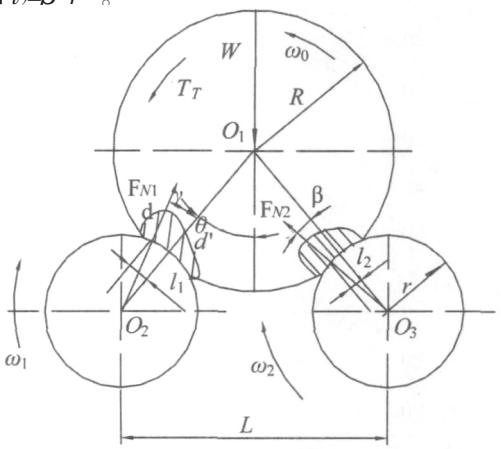

图 1 车轮在滚筒上滚动时接触面上压力分布图

为分析方便，将研究对象取分离体，见图 2，将合力 F_{N1} 和 F_{N2} 分别分解成平行于 O_1O_2 和 O_1O_3 连线的支反力 F_{Z1} 和 F_{Z2}，以及垂直于 O_1O_2 和 O_1O_3 连线的滚动阻力 F_{f1} 和 F_{f2}，为使车轮能在滚筒上匀速滚动，必须在车轮上施加驱动力矩 T_T 以克服上述的滚动阻力和支反力对车轮造成的阻力矩。

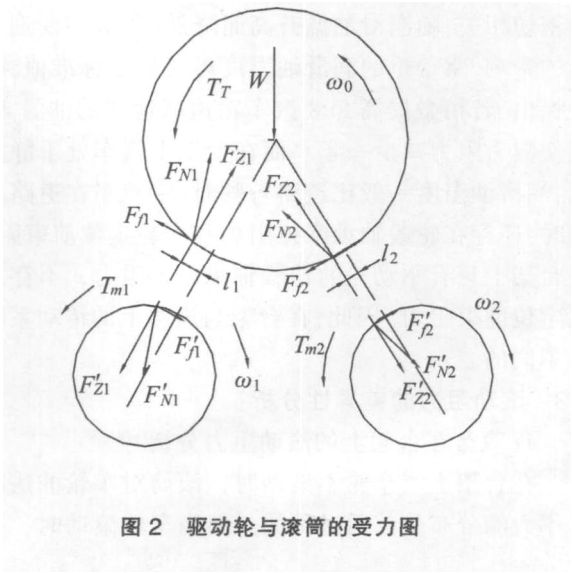

图 2 驱动轮与滚筒的受力图

由平衡条件得：

对 O_1 取矩：

$$T_T=F_{f1}R+F_{Z1}l_1+F_{f2}R+F_{Z2}l2 \tag{8}$$

对 O_2 取矩：

$$F'_{Z1}l_1=F'_{f1}r \tag{9}$$

对 O_3 取矩：

$$F'_{Z2}l_2=F'_{f2}r \tag{10}$$

又：

$$F_{f1}=-F'_{f1},F_{f2}=-F'_{f2},F_{Z1}=-F'_{Z1},F_{Z2}=-F'_{Z2} \tag{11}$$

对上述方程联立求解得：

$$T_T=(F_{f1}+F_{f2})(R+r) \tag{12}$$

令 $(F_{f1}+F_{f2})=F'f$ 为车轮滚动的总阻力。根据汽车理论，汽车在滚筒上受到的滚动阻力为：

$$F'f=(F_{Z1}+F_{Z2})f' \tag{13}$$

支反力与轴重有如下关系：

$$F_{Z1}=F_{Z2}=W/2\cos\theta \tag{14}$$

而 $$\theta=\arccos\sqrt{1-\left(\frac{L}{2(R+r)}\right)^2} \tag{15}$$

则 $$F_f'=\frac{Wf'}{\sqrt{1-\left(\frac{L}{2(R+r)}\right)^2}} \tag{16}$$

式中：W——轴重，N；

L——滚筒中心距，mm；

R——轮胎静力半径，mm；

r——滚筒半径，mm；

θ——滚筒中心距与滚筒径向载荷作用方向之间夹角的余角，即安置角，“°”；

f'——台架滚动阻力系数。

3.4 空气阻力的差异性分析

汽车在台架上是静止的，没有受到空气阻力的作用，而在道路上行驶时，空气阻力与车速的平方成正比，随着速度的增加，空气阻力增加很快，在较高速度时，空气阻力很大，远远超过滚动阻力，在道路上行驶阻力高于台架的行驶阻力，这是主要的原因。在台架上可以用加载的方法模拟空气阻力，但由于空气阻力是车速的二次函数，且涡流机加载存在滞后特性，因此模拟加载的空气阻力往往滞后于所设定的道路空气阻力。

3.5 惯性阻力的差异性分析

惯性阻力在滑行距离时表现为做功状态，能量的释放。滑行距离的大小虽然受台架阻力和行驶阻力的影响，但主要取决于滑行时惯性阻力释放能量的大小。惯性阻力大，释放能量就大。而惯性阻力的大小，取决于飞轮系统、滚筒及台架旋转部件的转动惯量是否与路试时汽车在相应车速下的转动惯量一致。在本试验

中所用的台架 $\omega_0=\omega_f=\omega_h$,故 $k_f=k_h=1$,由式 7 得本台架的转动惯量为[7]:

$$J=mr^2+\frac{J_h r^2}{R^2}-J_0-J_h \tag{17}$$

底盘测功机定型后,滚筒转动惯量 J_0 和加载涡流机转子的转动惯量 J_h 均为已知值,如西班牙产 F16-160 电涡流转子转动惯量为 1.86kg·m^2,被测汽车的质量和车轮转动惯量也为定值,故可据上式算得所设飞轮的转动惯量 J。

由于机械制造成本和安装体积的限制,一般在检测站中用的底盘测功机不可能配备太多的飞轮,而采用电机模拟惯量的成本太高,一般不采用。在本试验中的台架用两个飞轮,台架本身转动惯量为 18.33kg·m^2 模拟平移质量为 532.03kg,第一飞轮 14.8kg·m^2 模拟平移质量为 434.3kg,第二级飞轮为 49.6kg·m^2 模拟的平移质量为 1455.52kg。其模拟的平移质量和所检测的车型平移质量不能匹配,因此导致台架和道路惯性阻力的不同,因此使滑行距离检测结果的差异较大。为了减少差异,使台架滑行距离检测结果更接近实际,必须建立数学模型进行修正。

4　修正数学模型

从表 1 可知汽车台架滑行距离比道路滑行距离短,故以汽车台架滑行距离为基本量,考虑汽车质量、测功机转动惯量及滑行初速度等影响因素,道路与台架的滑行距离存在以下关系:

$$S=S_0+kmv^2/m_t \tag{18}$$

式中:S——汽车道路滑行距离计算值,m;

S_0——为汽车台架滑行距离,m;

k——修正系数;

m_t——滚筒和飞轮模拟平移质量之和,kg。

式 18 的物理意义是 S 值由两部分组成:一是汽车台架滑行距离;另一是由汽车质量和测功机模拟平移质量之比及车速的二次函数组成。显然,汽车质量和测功机的惯性质量(模拟平移质量)之比越大,需要修正的参数就越大,这与试验结果一致。由此,计算得 XML6402 汽车在 KDCG—10G 台架上的修正参数 k 为 0.053,即在 KDCG—10G 台架上的滑行距离与道路滑行距离关系为:

$$S=S_0+0.053mv^2/m_t \tag{19}$$

5　结论

汽车在台架和道路的滑行距离存在差异,其主要原因是汽车在台架和道路受到的阻力不同。在台架滑行距离的大小虽然受台架阻力和行驶阻力的影响,但主要取决于滑行时惯性阻力释放能量的大小。惯性阻力大,释放能量就大。而惯性阻力的大小,取决于飞轮系统、滚筒及台架旋转部件的转动惯量是否与路试时汽车在相应车速下的转动惯量一致。因此,为了使使台架滑行距离检测结果更接近实际,建立数学模型进行修正。

参　考　文　献

[1] 马强骏. 汽车底盘测功机关键技术研究 [J]. 中国测试, 2009, 35(3): 93~96.

[2] 邱宗敏. 汽车动力性台架检测与评定方法的研究 [D] . 西安: 长安大学, 2006.

[3] 王建强. 台试轮胎滚动阻力特性研究 [D]. 长春: 吉林大学, 2001.

[4] 余志生. 汽车理论[M]. 北京: 机械工业出版社, 2000.

[5] 戴建国, 王建强, 张忠辉, 等. 轮胎滚动阻力试验系统研究[J]. 汽车技术, 2003, (4): 23~27.

[6] 闵永军, 张为公, 等. 基于车轮扭矩传感器的轮胎滚动阻力测试系统开发[J]. 汽车技术, 2006, (7): 28~31.

[7] 刘浩学, 林彩霞, 马强骏. 基于台架检测汽车滑行距离的修正模型[J]. 长安大学学报(自然科学版), 2006, 26(2): 88~90.

Research of the Difference in Automobile Coast-down Test between Bench and Road

LIN Cai-xia

(*School of Engineering, South China Agricultural University, Guangzhou*, 510640, *China*)

Abstract: Analysis the difference between the bench and the road, taking King-long as testing vehicle, some comparing experiment been done. The main difference are the resistance, such as bench resistance, roil resistance and coast-down inertia. Base on the analysis, the coast-down distance revising model is supposed to set up to improve its accurate on bench test.

Keywords: automobile; coast-down distance; road and bench; difference

国际标准刊号：ISSN 1006-7205　国内统一刊号：CN32-1166/G　邮发代号：28-116　广告许可证号：3201004950023

电话：025-84346296(社长室)　025-84346205(主编室)　025-84346270(编辑部)　cnnnhgxx@public1.ptt.js.cn(编辑地址)　定价：12.00元

agriculture

MDPI

Article

Nondestructive Identification of Litchi Downy Blight at Different Stages Based on Spectroscopy Analysis

Jun Li [1,2], Junpeng Wu [1], Jiaquan Lin [1], Can Li [1], Huazhong Lu [3] and Caixia Lin [1,*]

[1] College of Engineering, South China Agricultural University, Guangzhou 510642, China; autojunli@scau.edu.cn (J.L.); andywjp@stu.scau.edu.cn (J.W.); m15813345752@stu.scau.edu.cn (J.L.); lc0714@stu.scau.edu.cn (C.L.)
[2] Guangdong Laboratory for Lingnan Modern Agriculture, Guangzhou 510640, China
[3] Guangdong Academy of Agricultural Sciences, Guangzhou 510640, China; huazlu@scau.edu.cn
* Correspondence: cxllin@scau.edu.cn; Tel.: +86-020-8528-0868

Abstract: Litchi downy blight caused by *Peronophythora litchii* is the most serious disease in litchi production, storage and transportation. Existing disease identification technology has difficulty identifying litchi downy blight sufficiently early, resulting in economic losses. Thus, the use of diffuse reflectance spectroscopy to identify litchi downy blight at different stages of disease, particularly to achieve the early identification of downy blight, is very important. The diffuse reflectance spectral data of litchi fruits inoculated with *P. litchii* were collected in the wavelength range of 350–1350 nm. According to the duration of inoculation and expert evaluation, they were divided into four categories: healthy, latent, mild and severe. First, the SG smoothing method and derivation method were used to denoise the spectral curves. Then, the wavelength screening methods competitive adaptive reweighted sampling (CARS) and successive projections algorithm (SPA) were compared to verify that the SPA method was more effective. Eleven characteristic wavelengths were selected, accounting for only 1.1% of the original data. Finally, the characteristic wavelengths were tested by six different classification models, and their accuracy was calculated. Among them, the ANN model performed best, with an accuracy of 90.7%. The results showed that diffuse reflectance spectroscopic technology has potential for identifying litchi downy blight at different stages, providing technical support for the subsequent development of related automatic detection devices.

Keywords: litchi downy blight; spectroscopy analysis; SG smoothing; CARS; SPA; classification models

Citation: Li, J.; Wu, J.; Lin, J.; Li, C.; Lu, H.; Lin, C. Nondestructive Identification of Litchi Downy Blight at Different Stages Based on Spectroscopy Analysis. *Agriculture* **2022**, *12*, 402. https://doi.org/10.3390/agriculture12030402

Academic Editor: Maciej Zaborowicz

Received: 5 February 2022
Accepted: 10 March 2022
Published: 14 March 2022

1. Introduction

Litchi (*Litchi chinensis* Sonn.) is a subtropical evergreen fruit tree. Because of its high nutrition and delicious taste, this fruit tree has been planted in many places worldwide and is deeply loved by consumers. In addition, litchi has high economic value and is an important commercial crop. The annual output value of China's litchi industry exceeds four billion US dollars [1]. However, litchi downy blight caused by *Peronophythora litchii* seriously threatens the development of the litchi industry and is one of the most serious and widespread diseases in litchi production, storage and transportation [2]. Litchi downy blight mainly affects mature or nearly mature litchi fruits. The onset of this disease mostly starts from the fruit pedicle [3]. At the beginning, irregular brown spots appear on the fruit surface, and then the spots spread rapidly, causing the whole fruit to turn black and brown within 2–3 days. As the flesh decays and falls off, the tawny juices flow out, giving off a sour wine taste. In the middle and late stages of the disease, especially under humid conditions, white downy mildew is produced on the surface of fruits [4]. Litchi downy blight is highly infectious and occurs quickly. If prevention and control measures are not taken in time, this disease can generally cause a 10–30% yield loss or an 80% yield loss in epidemic years.

Currently, the identification of litchi downy blight mainly relies on a visual screen by agricultural experts to manually identify this blight in orchards, or fruit samples are sent to laboratories for testing using biochemical or molecular methods [5]. The former method is quite subjective, laborious and inefficient. The latter method is destructive and highly expensive. In view of the high infectivity and rapid onset of litchi downy blight, these methods have difficulty identifying an epidemic in actual production, resulting in further loss. Therefore, advanced sensors combined with computer technology have the potential to realize the nondestructive, rapid and accurate automatic identification of litchi downy blight, which can identify an epidemic in orchards and help farmers take measures to prevent the spread of the epidemic so that the yield loss of litchi is markedly reduced [6]. In addition, reducing pesticide use is vigorously promoted. Automatic identification is of great significance for the accurate prevention and control of litchi downy blight.

Regarding the identification of crop diseases, many experts and scholars have performed extensive research, including on cucumber downy mildew [7], leek white tip disease [8], leek white tip disease [9], fusarium head blight of wheat grain [10] and other typical crop diseases. However, there are few studies on litchi disease identification. In addition, as leaves are the main organs of plants and are one of the main areas of infectious diseases [11], most studies have focused on leaf diseases but not fruit diseases. For litchi, the fruit is the most economically valuable part and the main area on which litchi downy blight occurs. This paper focused on this fruit disease and explored the identification of litchi downy blight.

Spectral technology has been proven to be effective in crop disease identification [12]. A large number of studies have shown that when crops are affected by plant diseases, along with the changes in their external morphology, their spectral characteristics usually change, which can be monitored by spectral data acquisition [13]. Therefore, crop disease identification is possible through spectral data analysis. Compared with traditional identification methods based on visible light images, spectral methods have higher sensitivity. The visible light imaging method only shows good recognition of the late stage of obvious disease onset; moreover, it is easily interfered with by light conditions and other factors when applied under natural conditions [14]. Spectral methods enable the identification of the early stage of crop disease and classification of different disease stages.

However, spectral data contain a large amount of redundant information, which may affect the efficiency of the modelling analysis [15]. Therefore, to reduce the interference of useless information, it is necessary to execute characteristic wavelength screening. This screening method not only increases the accuracy and stability of the identification model but is also valuable for practical production applications by reducing costs. Currently, the common characteristic wavelength screening methods mainly include the competitive adaptive reweighted sampling (CARS) method and successive projections algorithm (SPA) method [16]. In this paper, these two screening methods were compared and analysed using different parameters to determine the optimal screening conditions and methods.

In the application of spectral data to solve practical problems, such as crop disease identification, classification models are important analytical and processing methods [17]. The processed spectral data corresponding to litchi fruits infected with downy blight of different severities must be correctly classified to identify litchi downy blight. Therefore, this paper compared different typical classification models, including decision tree, linear discriminant analysis (LDA), naive Bayesian classifier, K-nearest neighbor (KNN), support vector machines (SVMs) and artificial neural networks (ANNs).

In summary, the purpose of this study is to provide a nondestructive litchi downy blight identification method based on spectral data analysis, which can classify litchi fruits infected with downy blight at different severities, including healthy, latent, mild and severe infections. The methodology of this study is as follows (Figure 1):

(1) Through scientific and reliable experiments, the diffuse reflectance spectral dataset of litchi fruits with different stages of downy blight infection was collected as the basis for the following research and analysis.

(2) To simplify the spectral data and make the model more efficient, two different methods of characteristic wavelength screening, CARS and SPA, were evaluated using different preprocessing parameters.
(3) Six different classification models were evaluated and tested to realize nondestructive identification of litchi downy blight at different stages. Then, the model that performed best was identified through comparisons.

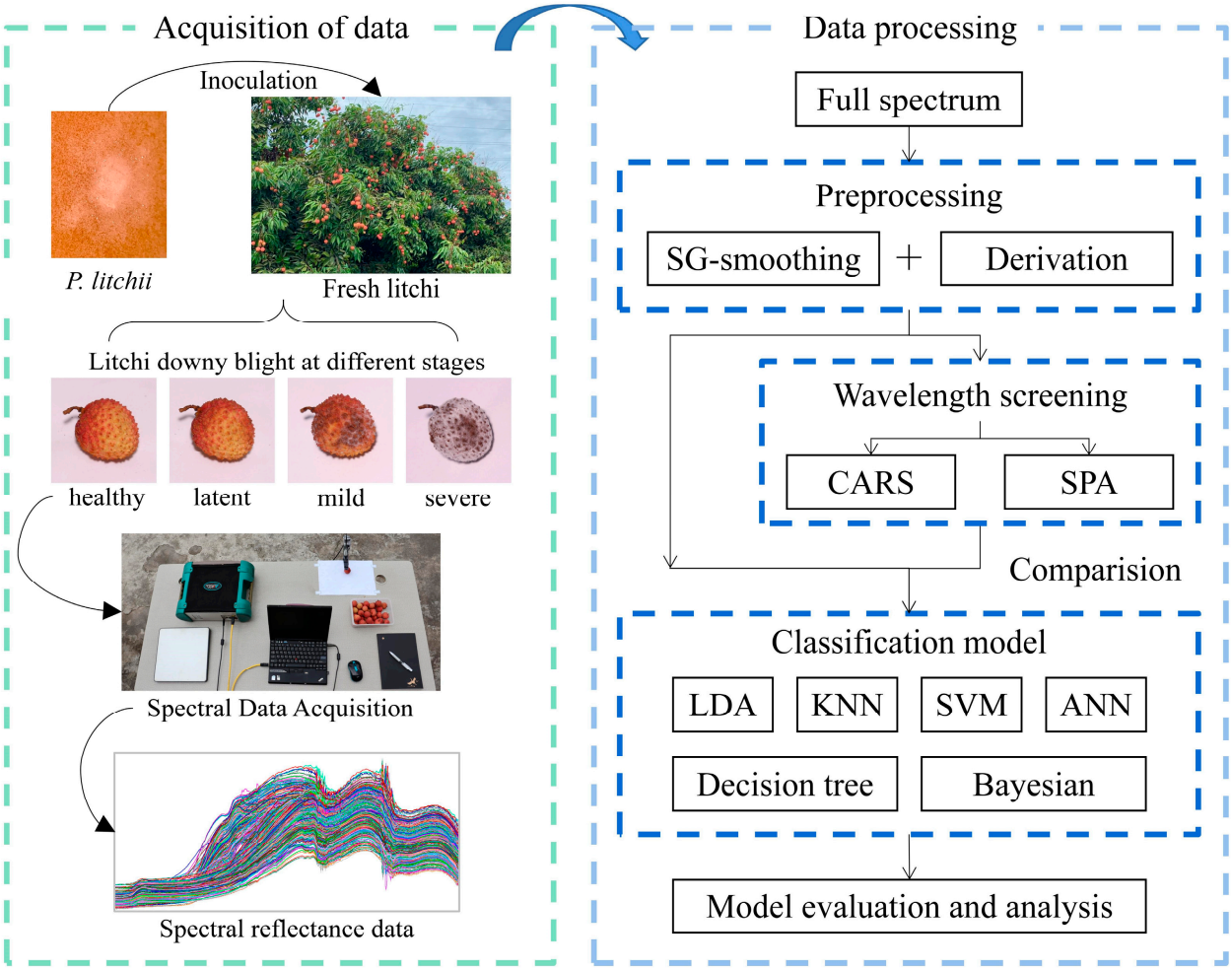

Figure 1. Overall flow chart.

2. Materials and Methods

2.1. Inoculation and Cultivation of Litchi Downy Blight

The inoculation and cultivation experiment of litchi downy blight was carried out in the China Litchi and Longan Industry Technology Research System Integrated Laboratory, College of Engineering, South China Agricultural University, in July 2021. The tested strain of *P. litchii* was SHS3, which was stored in the College of Natural Resources and Environment, South China Agricultural University. The tested litchi fruits were harvested from the litchi orchard at the Institute of Fruit Tree Research, Guangdong Academy of Agricultural Science. Before inoculation, the strain was activated in fresh carrot agar medium, and then, after 5 days of cultivation, a fresh colony of *P. litchii* was obtained. Sterilized water (5 mL) was added to the colony and shaken gently to obtain a sporangial suspension. Meanwhile, the litchi fruits were incubated in the sterile environment of the lab for over 48 h before the experiment to confirm that they were heathy. Afterwards, healthy litchi fruits of moderate size were selected, ensuring that their surface was clean and dry, and placed in a crisper box. Then, 0.05 mL of sporangium suspension was drip-inoculated

using a pipettor onto the epidermal centre of each litchi fruit. The inoculated fruits were placed in an incubator at 25 °C for moisturizing cultivation. The specific processes of the inoculation and cultivation experiment are shown in Figure 2.

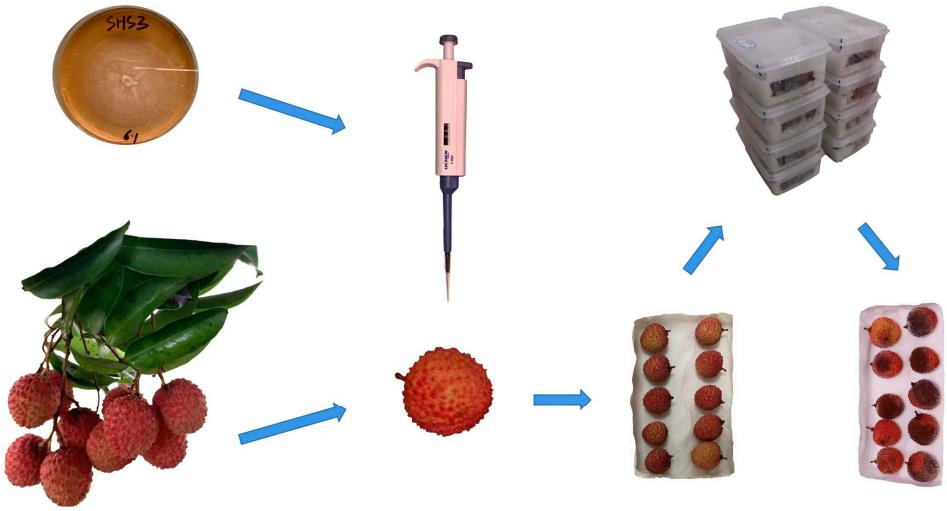

Figure 2. The process of the inoculation and cultivation experiment.

All litchi samples were ensured to be healthy before inoculation, and litchi downy blight was inoculated and cultivated using scientific procedures. Thus, all subsequent changes in litchi samples were due to litchi downy blight, including color changes, disease spots, white downy mildew and some other surface properties.

2.2. Spectral Data Acquisition

Spectral data acquisition of litchi downy blight was conducted in July 2021 in the outdoor space of South China Agricultural University. Spectral data, ranging from 350–1350 nm, of litchi fruits inoculated with *P. litchii* were collected by an ASD Field Spec 3 Portable Spectroradiometer (Analytical Spectral Devices, Inc., Boulder, CO, USA). The instrument is sensitive to visible and near-infrared light, has a spectral sampling interval of 1.377 nm and has a spectral resolution of 3 nm at 700 nm [18]. During data acquisition, an optical fibre probe with a 25° field of view was equipped and placed 2 cm vertically above the litchi sample to be measured. In particular, we ensured that there were no other miscellaneous objects in the field of view of the probe and that the amount of sunlight was sufficient. Three spectral data curves were collected for each litchi sample. The process of spectral data acquisition is shown in Figure 3. The first spectral data acquisition was carried out before inoculation; thereafter, spectral data were acquired every 24 h. Moreover, litchi samples were continuously observed, especially the progression of symptoms and growth of white downy mildew, until the litchi samples were severely infected, at which time the last spectral data were acquired. Finally, a total of 7 spectral data acquisitions were accomplished.

2.3. Disease Stages of Downy Blight

The disease stages of litchi downy blight were divided into 4 categories: healthy, latent, mild and severe. Before the experiment, all litchi samples were observed for 36 h to ensure healthy conditions. The latent category was defined as the period between inoculation with *P. litchii* and the first appearance of prominent lesion spots. As shown in Figure 4, the mild category refers to visible brown lesion spots on the surface of litchi fruit accounting for 10–30% of the surface area. The severe category refers to the surface of litchi fruit being totally browned and covered with white downy mildew.

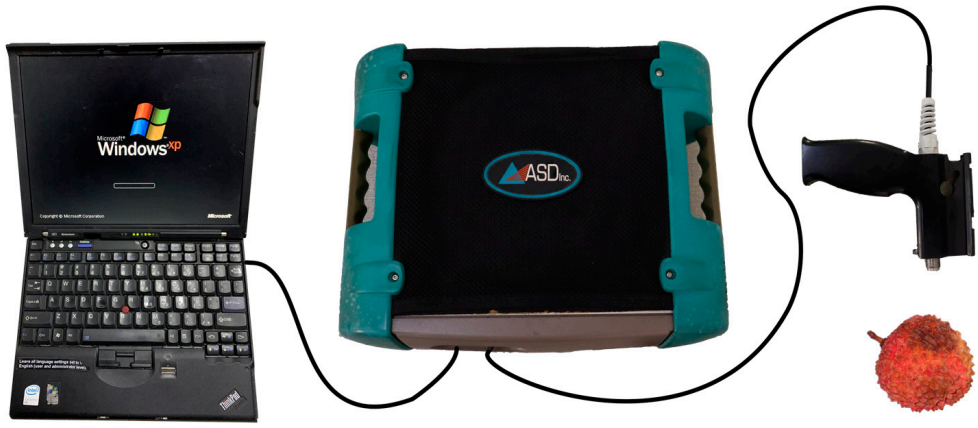

Figure 3. The process of spectral data acquisition.

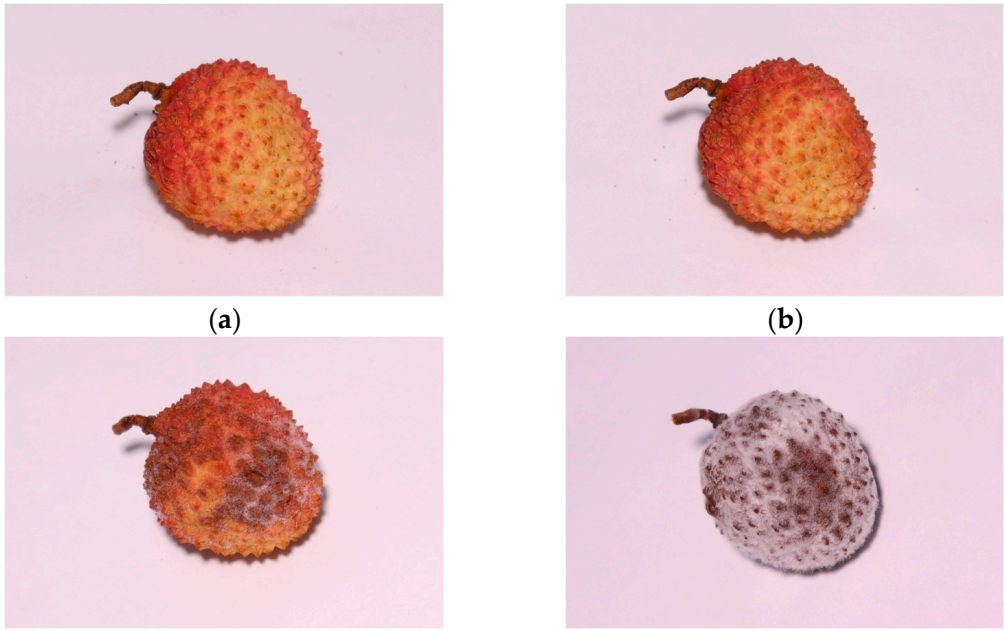

Figure 4. Images of litchi fruit at different disease stages: (**a**) healthy, (**b**) latent, (**c**) mild and (**d**) severe.

Principally, the division of different disease stages was based on the duration of inoculation of *P. litchii*; however, due to experimental error and individual differences between litchi fruit samples, the actual disease progression of each sample was slightly different. Therefore, to improve the quality of the data, agricultural experts were also invited to evaluate the stages of individual litchi samples through images to calibrate the division results. Samples whose disease stage was difficult to accurately define were discarded. Finally, a total of 609 data points were obtained and are shown in Table 1.

Table 1. Distribution of the dataset.

Healthy	Latent	Mild	Severe	Total
121	186	109	193	609

2.4. Spectral Data Preprocessing

The original spectral data not only contained the characteristic spectrum of the tested litchi sample but also contained noise data such as high-frequency random noise and

baseline drift. Moreover, they are also affected by the physical properties of the samples, such as viscosity, particle size, surface texture and density. Therefore, before using spectral data for sample attribute analysis, pretreatment should be carried out first to achieve noise reduction and reduce the interference of other influencing factors.

2.4.1. Savitzky–Golay Smoothing

The Savitzky–Golay (SG) smoothing method is a widely used spectral denoising method. Compared with traditional methods, such as moving average smoothing, this method emphasizes the central role of the centre point. The principle of SG smoothing is to set a smoothing frame in advance, use the weighted average method to carry out polynomial least square fitting to the data in the moving frame, and then use the convolution calculation method to move the frame backwards to complete the smoothing processing of all data [19].

The smoothing effect varies with the size of the smoothing frame. The larger the frame size is, the more significant the smoothing effect but the greater the possibility of losing useful information. In this study, different smoothing frame sizes ranging from 31–51 and different polynomial orders ranging from 2–4 were tested.

2.4.2. Derivation

The derivative method can be used to eliminate the influence of baseline drift or gentle background, which is beneficial to improve the resolution and sensitivity of spectral data. However, if the signal-to-noise ratio (SNR) of the original spectral data is not high enough, the derivation will further amplify the noise signal and adversely affect the analysis. Therefore, the derivative method was combined with the SG smoothing method. The SG smoothing method is a polynomial fitting, and the weighted average expression of the frame centre required by the derivation of the polynomial can be obtained. The derivative coefficient can be obtained by least square calculation. The specific calculation method is as follows

$$x_i' = \frac{1}{A}\sum_{j=-m}^{m} w_j x_{i+j}, \qquad i = 1, \ldots, n-2m \tag{1}$$

where the smoothing frame size is $2m+1$, A is the normalization constant, x_i' is the smoothing data of spectral data x_i, w_j is the corresponding derivative coefficient, and w_j is determined after the frame size is determined. The purpose of multiplying each measured value by the derivative coefficient w_j is to minimize the effect of smoothing on the useful information, and w_j is obtained by polynomial fitting based on the least square principle. The smoothing effect varies with the differentiation order. In this study, different differentiation orders ranging from 0–2 were tested. After smoothing, the spectral data will lose m wavelengths at both ends, and the remaining wavelengths correspond to each original data point. Therefore, smoothing will not affect the feasibility of the following further analysis in practical applications.

2.5. Characteristic Wavelength Screening

2.5.1. Competitive Adaptive Reweighted Sampling

CARS is a characteristic wavelength screening method combining Monte Carlo sampling and the regression coefficient of the PLS model, imitating the principle of "survival of the fittest" in Darwinian evolution theory [20]. In the CARS algorithm, points with a large absolute weight of the regression coefficient in the PLS model were reserved as new subsets through adaptive weighted sampling (ARS) each time, and points with small weights were removed. Then, the PLS model was established based on the new subsets. After several calculations, the wavelengths in the subset of the minimum root mean square error (RMSECV) of the PLS model were selected as the characteristic wavelengths.

2.5.2. Successive Projections Algorithm

SPA is a forward selection variable method of characteristic wavelength screening. By using projection analysis of vectors, the wavelength is projected onto other wavelengths, and the size of the projections is compared [21]. The wavelength with the largest projection vector is selected as the wavelength to be selected, and then the final characteristic wavelengths are selected based on the correction model. SPA selects the combination of variables with the least redundant information and the least collinearity. The main steps of the algorithm are as follows.

The initial iteration vector is denoted as $x_{k(0)}$, the number of variables to be extracted is N and the number of columns of the spectral matrix is J. Any one column in the optional spectral matrix is denoted as column j, and we assign column j of the modelling set to x_j, denoted as $x_{k(0)}$.

The set of unselected column vector positions was denoted as s

$$s = \{j, 1 \le j \le J, j \notin \{k(0), ..., k(n-1)\}\} \quad (2)$$

The projection of x_j to the remaining column vectors was calculated separately P_{x_j}

$$P_{x_j} = x_j - \left(x_j^T x_{k(n-1)}\right) x_{k(n-1)} \left(x_{k(n-1)}^T x_{k(n-1)}\right)^{-1}, j \in s \quad (3)$$

The spectral wavelength of the largest projected vector was extracted

$$k(n) = \arg\left(\max\left(\|P_{x_j}\|\right), j \in s\right) \quad (4)$$

To make $x_j = P_{x_j}$, $j \in s$, when $n \le N$, the rule $n = n + 1$ was applied, and then loop calculations were performed.

Finally, the extracted variables were $\left\{x_{k(n)} = 0, ..., N-1\right\}$, corresponding to $k(0)$ and N in each cycle. Multivariable linear regression (MLR) models were built separately, and the root mean squared error (RMSE) for the interactive validation of the model was obtained. For different candidate characteristic subsets, the values of $k(0)$ and N corresponding to the smallest RMSE value were the optimal values.

2.6. Classification Models

To correctly evaluate the spectral data corresponding to different disease stages of litchi downy blight, the problem was approached as a classification problem. When a group of litchi spectral data is obtained, the model can automatically determine which data point is healthy, latent, mild or severe to complete the identification of the disease stages of litchi downy blight. There are many classification models that can achieve such tasks, such as decision trees, LDA, naive Bayesian classifiers, KNN, SVMs and ANNs.

The decision tree algorithm [22] uses a tree structure and layer reasoning to achieve the final classification. The amount of calculation is relatively small, and it is easy to convert into classification rules. In this study, the split criterion was set as gin's diversity index, and the maximum number of splits was 20.

LDA [23] finds the optimal projection direction, projects the points in the high-dimensional space to the low-dimensional space, and then reclassifies the low-dimensional space. Generally, for linearly separable samples, LDA makes the samples remain linearly separable after dimensionality reduction through a projection direction, the distance between samples of different categories is as far as possible, and the same sample is as concentrated as possible.

The idea of the naive Bayesian classifier [24] is to treat the spectral characteristic vector of the classified sample, calculate the probability of each category under the condition of the spectral characteristic vector, and consider the sample to be classified as the category with the highest probability. In this study, the numeric predictors are set as the kernel, and the kernel type is set as Gaussian.

KNN [25] is a nonparametric method, the idea of which is that if most of the samples have similar K values in the feature space (that is, the closest neighbors in the feature space) belong to a certain category, the sample also belongs to this category. In this study, the distance metric was set as a cosine, and the number of neighbors was 10.

The basic idea of SVMs [26] is to construct an optimal decision hyperplane in the feature space, which maximizes the distance between the hyperplane and the nearest samples of different classes. SVMs are suitable for solving the problem of high-dimensional classification of small samples. In this study, the kernel function of the SVM was set as quadratic.

ANNs are designed based on the research results of biological neural networks and are systems composed of many simple processing units working in parallel. The ANN function depends on the structure of the network, the connection strength and the processing mode of each unit. ANNs have great potential in information processing. In this study, the type of ANN was a wide neural network, and the number of fully connected layers was one, with a layer size of 100. The activation function was ReLU, the iteration limit was 1000, and the regularization strength (lambda) was 0.

In summary, the classification models were used to identify the spectral data of litchi downy blight at different disease stages. In this study, both the original full-band spectral data and the selected characteristic wavelength data were tested, and their accuracy calculated and compared.

All of the analytical procedures used in this study were performed with algorithms developed in MATLAB vR2021a software; specifically, the classification models were analysed using the Statistics and Machine Learning Toolbox (Version 12.1).

3. Results

3.1. Spectral Data Characteristics of Litchi Downy Blight

The pathogenic process of litchi downy blight developed rapidly after inoculation with *P. litchii*, and it only took 5 days to achieve the severe stage. The figures show the original spectral data corresponding to samples at different disease stages of litchi downy blight. Overall, the trend of the spectral curves was basically consistent, indicating that the experiment is reliable. The characteristics of spectral curves corresponding to different disease stages were significantly different, especially in the range of 400–950 nm, which covers visible and near-infrared light (Figure 5). Therefore, it is feasible to distinguish different disease stages of litchi downy blight through spectral data.

Litchi fruits of the healthy category of downy blight had abundant spectral reflection in the visible light range, showing a reflection peak at approximately 660 nm, reflecting the red color characteristic of litchi fruits and forming a platform characteristic at 750–930 nm (Figure 5a).

During the latent category of downy blight, the litchi fruit surface began to show slight browning, which was difficult to detect by visual observation. The spectral curve of litchi fruit in the range of 600–930 nm was smoother than that of healthy fruit, showing an upwards convex curve in general, especially the small wave valley at 685 nm, which decreased or even disappeared (Figure 5b).

When the mild category of downy blight was present, there were obvious dark brown spots on the surface of litchi fruits, with white downy mildew present around the spot area. The reflectance of the spectral curve in the range of 600–930 nm was lower than that of the latent category, and the slope was close to 1 (Figure 5c).

The surface of litchi fruit of the severe category of downy blight was completely brown and covered with a thick layer of white downy mildew. The reflectance of the spectral curve decreased further in the range of 700–930 nm but increased in the range of visible light, which was inferred to be related to the significant change in the surface color characteristics of litchi fruit (Figure 5d).

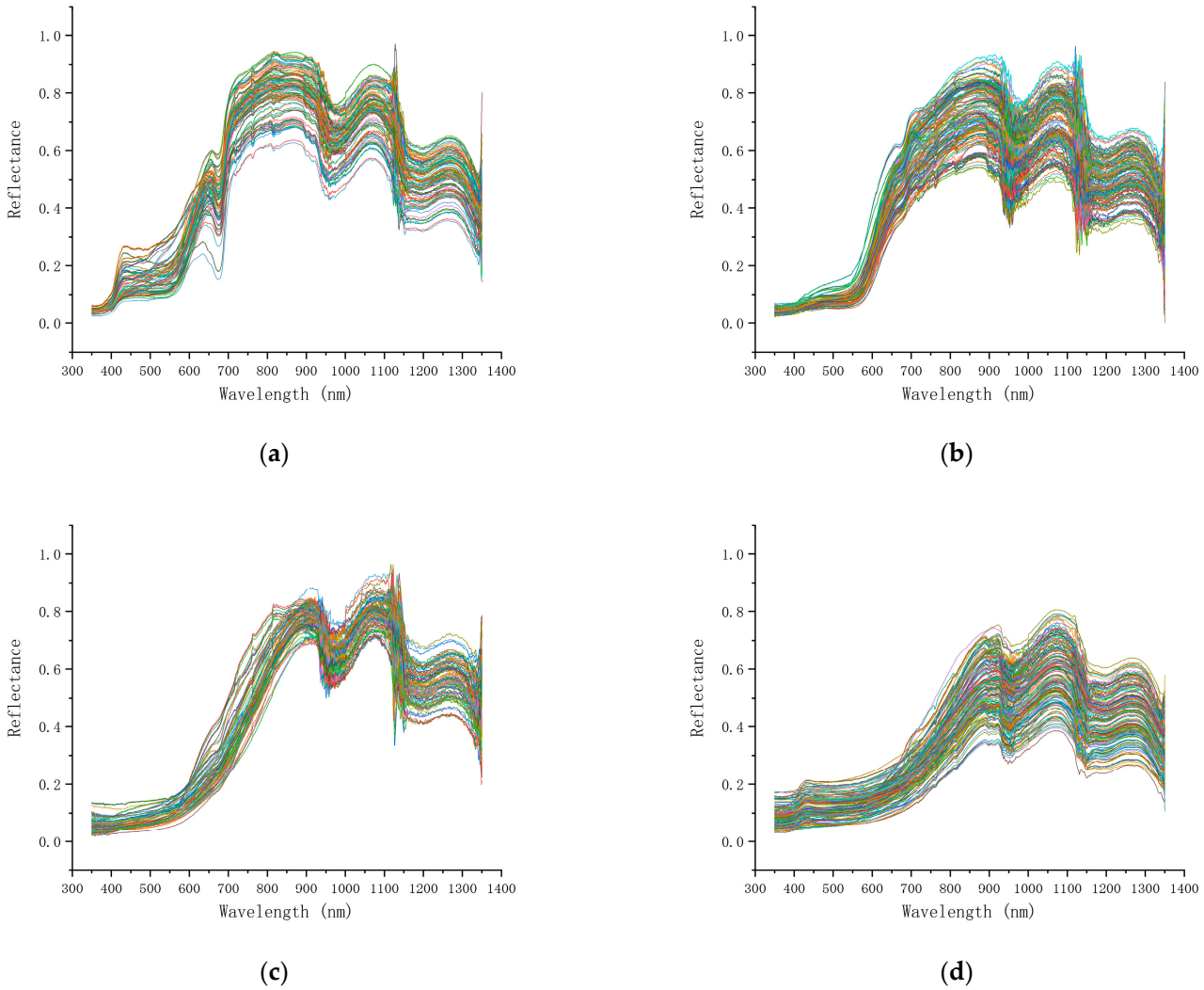

Figure 5. Spectral curves recorded at different disease stages: (**a**) healthy, (**b**) latent, (**c**) mild and (**d**) severe.

In addition, in the near-infrared spectrum range of 950–1350 nm, the spectral data corresponding to different disease stages of downy blight showed little difference. At approximately 1150 nm, relatively obvious noise was observed. This noise existed in the spectral data of all samples and was relatively uniform. Therefore, noise was not considered to affect the subsequent experimental analysis.

3.2. Result of Spectral Data Preprocessing

The original spectral data without processing have a large number of fluctuations caused by high-frequency noise, showing a jagged shape on the spectral curve. In addition, due to the difference in ambient light in different samples and the scattering influence brought by sample surface granularity, although the equipment was calibrated in time during the experiment, there was still a certain difference in the amplitude of the spectral curve (Figure 6a).

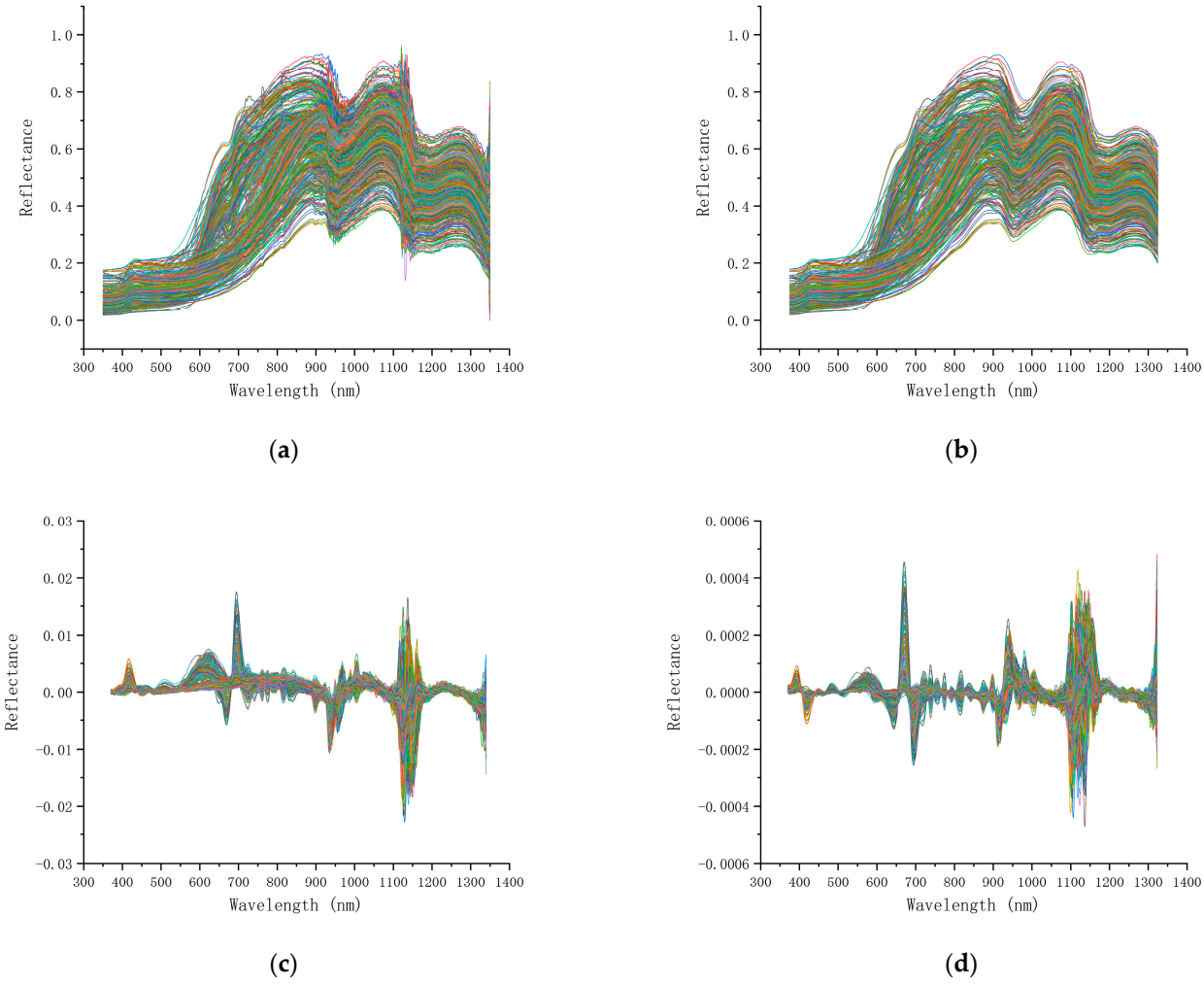

Figure 6. Spectral curves obtained using different preprocesses of derivation and SG smoothing: (**a**) original data; (**b**) frame size: 51, polynomial order: 3, differentiation order: 0; (**c**) frame size: 31, polynomial order: 4, differentiation order: 1; (**d**) frame size: 41, polynomial order: 2, differentiation order: 2.

The original spectral data were processed by SG smoothing, the sawtooth on the spectral curve was reduced, the curve became smoother, and the noise was reduced. Moreover, the original trend and characteristics of the spectral curves were preserved. In particular, the noise near 1150 nm was substantially reduced, which sufficiently reflected the effect of smoothing (Figure 6b).

Additionally, the original spectral data were processed by first and second derivatives with the SG smoothing method, which greatly reduced the difference in the amplitude of the spectral curve and made all curves more concentrated. The smoothing process of spectral data also plays a role in normalization, and the absolute value difference between different spectral curves can be weakened, while the relative value difference can be prominent. Among them, the normalization effect of data smoothed by the second derivative was better than that achieved by the first derivative, and all curves were clustered near each other, which simplified and stabilized subsequent operations. The positions with large curve fluctuations reflect the differences of different curves, and these positions are also more likely to have characteristic wavelengths (Figure 6c,d).

In conclusion, smoothing processing can effectively reduce the impact of noise on spectral data and helps the subsequent selection of characteristic wavelengths and the establishment of an analysis model [27]. However, in the process of smoothing, the selection

of key parameters is also very important, and parameter selection will be further discussed in the following paragraphs.

3.3. Characteristic Wavelength Sensing Results

3.3.1. Result of Key Parameter Selection

In the experimental process, it was found that when derivations with the SG smoothing method were used to preprocess spectral data, different key parameters not only had a direct impact on the shape of the spectral curve but also had a significant impact on the subsequent results of characteristic wavelength screening. Among them, different frame sizes, polynomial orders and differentiation orders had a decisive influence on data smoothing and subsequent characteristic wavelength screening. Thus, orthogonal experiments were designed for these parameters to optimize the combinations. Through a certain pretest, three levels of smoothing frame size were selected, 31, 41 and 51; three levels of polynomial order were selected, 2, 3 and 4; three levels of differentiation order were selected, 0, 1 and 2. In summary, an orthogonal experiment with three factors and three levels was designed, with a total of nine groups of experiments. Then, on the basis of the results of each group of experiments, CARS and SPA were used to select characteristic wavelengths, and the corresponding number of characteristic wavelengths was obtained, as shown in Table 2.

Table 2. Orthogonal experiments of parameter combinations in preprocessing and the corresponding number of characteristic wavelengths obtained using CARS and SPA.

	Frame Size	Polynomial Order	Differentiation Order	CARS	SPA
①	31	2	0	146	37
②	31	3	2	41	21
③	31	4	1	60	22
④	41	2	2	36	11
⑤	41	3	1	99	26
⑥	41	4	0	113	44
⑦	51	2	1	68	32
⑧	51	3	0	77	25
⑨	51	4	2	87	26

It can be seen from the experimental results that the influence of different parameter combinations on the selection of characteristic wavelengths was significant. Overall, the results of CARS and SPA showed the same variation trend under different parameter combinations, but the result of SPA was better than that of CARS in each group. Among them, the best results all appeared in group ④, where the smoothing frame size was 41, the polynomial order was 2, and the differentiation order was 2. CARS selected 36 wavelengths, and SPA selected 11 wavelengths.

3.3.2. Result of Competitive Adaptive Reweighted Sampling

The process of CARS characteristic wavelength screening was as follows. After repeated comparison, Monte Carlo sampling times were set to 50 in this study [28]. As shown in Figure 7a, with increasing sampling times, the number of selected wavelengths gradually decreased. As shown in Figure 7b, RMSECV gradually decreased and then gradually increased after reaching the lowest point. It is generally believed that the decline in RMSECV reflects the removal of invalid information in spectral data, while the rise in RMSECV reflects the removal of effective information in spectral data. Therefore, the lowest RMSECV was selected as the result. The positions marked by solid vertical lines in Figure 7c represent the regression coefficients of each variable when RMSECV reached the minimum value. At this time, the sampling ran 27 times, and the number of characteristic wavelengths selected by CARS was 36.

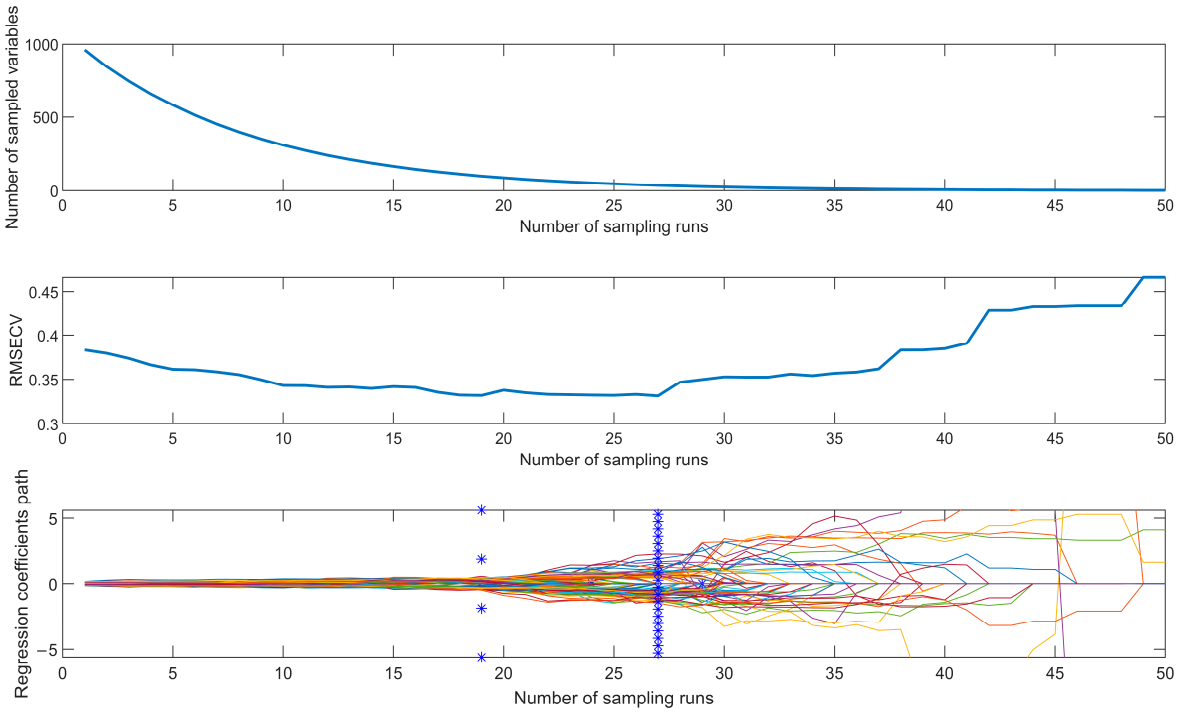

Figure 7. The CARS process. Numbers of selected wavelengths (**a**), RMSECV (**b**) and regression coefficient paths (**c**).

3.3.3. Result of Successive Projections Algorithm

The process of applying SPA to characteristic wavelength screening was as follows. SPA determined the number of characteristic wavelengths based on RMSE. As shown in Figure 8a, when the number of wavelengths increased from 1 to 11, the RMSE decreased rapidly and then plateaued after a slight fluctuation. Through experiments, it was found that RMSE tended to flatten after a rapid decline, and the RMSE changed very little at this time. If the minimum RMSE point was pursued, the number of characteristic wavelengths increased to varying degrees. Therefore, a point that was not significantly greater than the minimum RMSE was selected as the result according to the F test in this study to optimize the characteristic wavelength screening process [29]. Finally, 11 wavelengths were selected as characteristic wavelengths, and the specific distribution is shown in Figure 8b. The characteristic wavelengths were mainly distributed in the visible spectral range of 550–760 nm and the near-infrared spectral range of 1100–1150 nm.

3.3.4. Result of Characteristic Wavelengths

By observing the characteristic wavelength distribution corresponding to the characteristic wavelength selection test results, it was found that the characteristic wavelengths selected by CARS were relatively scattered, with many consecutive adjacent wavelengths and more redundancy, which had a relatively poor performance.

The characteristic wavelengths selected by SPA were mainly distributed in the visible spectral range of 560–760 nm and the near-infrared spectral range of 1100–1150 nm, which corresponded to the regions with large fluctuations, as shown in Figure 6d, with fewer numbers and better effects. Therefore, 11 wavelengths selected by SPA in group ④ of the experiment shown in Table 2 were finally confirmed as characteristic wavelengths for subsequent analysis [30]. The selected characteristic wavelengths are shown in Table 3.

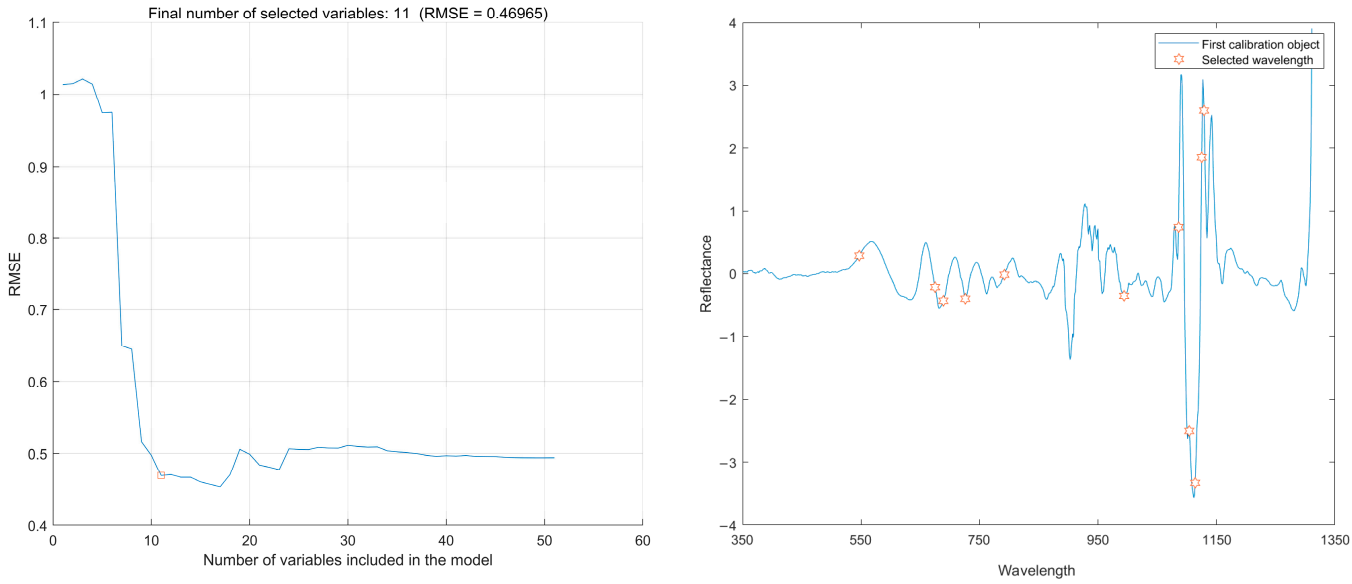

(**a**) (**b**)

Figure 8. The process and result of SPA. Number of selected wavelengths (**a**) and distribution of selected wavelengths (**b**).

Table 3. Characteristic wavelengths.

Method	Selected Wavelength (nm)
CARS	426, 549, 550, 637, 638, 639, 689, 707, 708, 727, 728, 739, 740, 746, 806, 811, 812, 817, 831, 832, 833, 834, 902, 903, 984, 997, 1011, 1026, 1075, 1192, 1208, 1224, 1275, 1284, 1292, 1295
SPA	567, 695, 709, 746, 812, 1014, 1106, 1124, 1134, 1145, 1149

3.4. Result of Classification Models

In this study, full-band spectral data and 11 characteristic wavelengths selected by SPA were tested to compare the effects of different classification models. As shown in Table 4, 70% of all 609 data points were used as training data, and 30% were used as test data. Considering the small training set, cross-validation was adopted in the training process, and the number of cross-folds was 15.

Table 4. Partitioning of the training set and test set.

	Quantity	Percentage
train	426	70%
test	183	30%
total	609	100%

The data of the training set were imported into a decision tree, LDA, a naive Bayesian classifier, KNN, an SVM and an ANN. After the training, the model was tested with the test set, and the accuracy of different classification models was calculated. Accuracy P was calculated as follows, where T represents the total number of samples in the test set and C represents the number of correctly classified samples in the test set.

$$P = \frac{C}{T} \times 100\% \quad (5)$$

Finally, the accuracy of each classification model is shown in Table 5. In general, the accuracy of the test set reached a good level, which had reference significance for practical

production practice. Among them, the average accuracy of the test set of full-band spectral data was 92.1%, and the average accuracy of the test set of 11 characteristic wavelengths selected by SPA was 85.6%. By selecting characteristic wavelengths, 1001 wavelengths were replaced by 11 wavelengths, and the number of wavelengths was only 1.1% of the original. Even if the number of wavelengths was greatly reduced, the accuracy of the classification model was only reduced by 6.5 percentage points, and the performance of classification was basically not reduced, which fully embodied the value of preprocessing with SG smoothing and the SPA algorithm.

Table 5. The accuracy of each classification model.

Model	Full Wavelengths		11 Selected Wavelengths	
	Validation	Test	Validation	Test
Decision Tree	91.5%	87.4%	92.0%	82.5%
LDA	89.9%	94.5%	88.5%	80.3%
Naive Bayes	90.1%	83.6%	93.0%	86.3%
KNN	91.5%	93.4%	91.8%	84.2%
SVM	99.5%	96.2%	94.8%	89.6%
ANN	99.5%	97.3%	91.8%	90.7%

Specifically, the best classification models were the SVM and ANN. The accuracy of the test set of the full-band spectral data reached 96.2% and 97.3%, and the accuracy of the test set of the 11 characteristic wavelengths reached 89.6% and 90.7% for the SVM and ANN, respectively.

For further analysis of the ANN model, with the highest accuracy of 90.7% in the test set, 11 characteristic wavelengths were used. Through a confounding matrix, the accuracy of categories of health, latent, mild and severe were 100%, 85.7%, 72.7% and 100%, respectively (Figure 9).

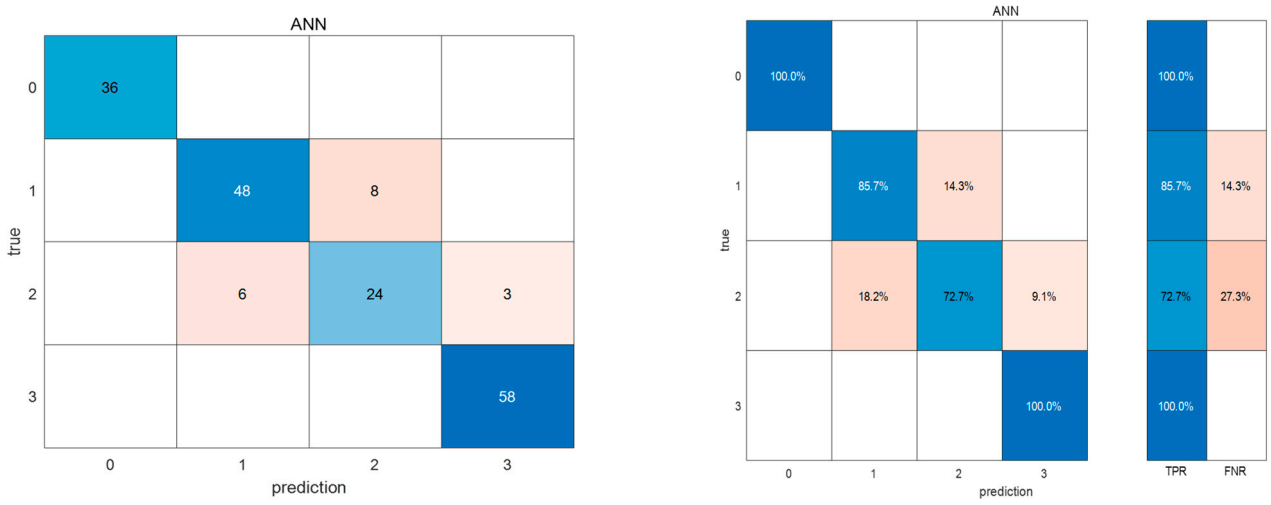

(**a**) (**b**)

Figure 9. The confounding matrix of the ANN model. Confounding matrix of quantity (**a**) and confounding matrix of percentage (**b**).

In the classification and recognition of litchi downy blight, the classification model can recognize and classify health and severe categories well, but it may misidentify the latent and mild categories to some extent. This result is because both the healthy and severe categories have distinct and definite characteristics that are relatively easy to accurately evaluate. However, the latent and mild categories were the transition state in the process

of change, and the characteristics were relatively obscure, so they were more difficult to classify.

4. Discussion

According to the results shown above, the nondestructive testing method based on the spectral analysis proposed in this paper has unique advantages in the detection of litchi downy blight. On the one hand, compared with the image recognition method based on visible light images, the spectral method has higher sensitivity and accuracy, enabling the identification of the early stage of litchi downy blight and classification of different disease stages. Imaging methods are unable to easily perform this identification and classification. On the other hand, compared with traditional biochemical or molecular detection methods, the spectral method is more intelligent and shows potential to achieve the nondestructive identification of litchi downy blight at different stages.

In the analysis of spectral data in this paper, the SG smoothing method was used for pretreatment and was found to be effective. Additionally, the noise caused by the environment, equipment and other factors in the original spectral data can be effectively reduced. Smoothing and denoising were essential in the processing of spectral data analysis. Notably, several parameters, such as frame size, polynomial order and differentiation order, affected the smoothing results. In general, excessive smoothing resulted in the loss of some information. Therefore, there was a balance to be achieved.

The original spectral data of litchi downy blight collected in this paper cover a wide range of wavelengths from 350–1350 nm; however, the large amount of spectral data is unacceptable in practical applications due to the associated cost. Thus, the selection of characteristic wavelengths is very constructive. CARS and SPA are typical characteristic wavelength screening methods. In this paper, SPA performed better, as also reported in other studies [31]. Moreover, our results confirmed that characteristic wavelength screening can improve the efficiency of the applied model because the quantity of spectral data significantly reduced.

Of the 11 characteristic wavelengths selected, four belonged to the visible band, which was distributed in the region of red and yellow light. Visible light is often used for color evaluation and pigment analysis. With the infection of downy blight, the surface of litchi gradually changed from red to brown and white, indicating that the spectroscopy analysis could be used to identify downy blight by obtaining the color and pigment information [32]. The other seven characteristic wavelengths belonged to near-infrared bands, and the correlation between these wavelengths and litchi downy blight was difficult to determine, but it was inferred to be related to the following factors. When infected with downy blight, the epidermis of litchi became softer, stickier, smoother and moister. Furthermore, the inside of litchi fruit began to rot when severely infected. Theoretically, the NIR spectrum is sensitive to these changes, which can be beneficial for identifying litchi downy blight.

In this paper, the last and most important step of spectral data analysis was to classify spectral data with classification models. Studies in many other fields have verified that classification models have strong analytical ability. In our identification of litchi downy blight based on spectral data, it was also verified that classification models perform well. The excellent performance of ANNs, as advanced deep learning tools, was expected.

5. Conclusions

This study was the first to complete the exploration of applying the diffuse reflectance spectrum data analysis method to the intelligent identification of litchi downy blight and confirmed that the classification and judgement of different disease stages of litchi downy blight can be realized by analyzing diffuse reflectance spectrum data with certain methods. By preparing experimental materials and collecting experimental data, a controlled and scientific dataset of litchi downy blight was obtained, including the spectral data of different categories of healthy and latent, mild and severe infection. In data analysis, SG smoothing and the derivation method were combined to preprocess the original data, and then CARS

and SPA characteristic wavelength screening methods were compared. The experiment showed that the SPA method had better performance after optimizing the parameters. Afterwards, 11 characteristic wavelengths were selected, accounting for only 1.1% of the original data. Finally, the characteristic wavelengths were imported into different classification models for training, and their accuracy was tested. Decision tree, LDA, naive Bayesian classifier, KNN, SVM and ANN methods were compared, and the ANN model was the best, with an accuracy of 90.7%. The above work laid a theoretical foundation for diffuse reflectance spectroscopy in the identification of litchi downy blight and provided a reference for its application in practical production. An improvement in the precise control of litchi downy blight is beneficial to promote a reduction in chemical use and improvements in the yield and quality of litchi. Litchi producers obtain greater economic benefits, litchi consumers obtain more delicious high-quality litchi, and the litchi industry continues to develop well.

Author Contributions: Conceptualization, J.L. (Jun Li) and C.L. (Caixia Lin); methodology, J.L. (Jun Li) and H.L.; software, J.W.; validation, J.W., J.L. (Jiaquan Lin) and C.L. (Can Li); writing—original draft preparation, J.W.; writing—review and editing, J.L. (Jun Li); supervision, C.L. (Caixia Lin). All authors have read and agreed to the published version of the manuscript.

Funding: This research was funded by earmarked funds for the Laboratory of Lingnan Modern Agriculture Project (No. NZ2021009), the Guangdong Provincial Modern Agricultural Industry Technology System (No. 2019KJ123) and the Special Project of Rural Vitalization Strategy of Guangdong Academy of Agricultural Sciences (No. TS-1–4).

Institutional Review Board Statement: Not applicable.

Informed Consent Statement: Not applicable.

Data Availability Statement: Not applicable.

Conflicts of Interest: The authors declare no conflict of interest.

References

1. Qi, W.; Chen, H.; Luo, T.; Song, F. Development Status, Trend and suggestion of litchi industry in mainland China. *Guangdong Agric. Sci.* **2019**, *46*, 132–139. [CrossRef]
2. Zhang, J.; Zhu, F.; Gu, M.; Ye, H.; Gu, L.; Zhan, L.; Liu, C.; Yan, C.; Feng, G. Inhibitory activity and action mechanism of coumoxystrobin against Phytophthora litchii, which causes litchi fruit downy blight. *Postharvest Biol. Technol.* **2021**, *181*, 111675. [CrossRef]
3. Ye, W.; Wang, Y.; Shen, D.; Li, D.; Pu, T.; Jiang, Z.; Zhang, Z.; Zheng, X.; Tyler, B.M.; Wang, Y. Sequencing of the Litchi Downy Blight Pathogen Reveals It Is a Phytophthora Species with Downy Mildew-Like Characteristics. *Mol. Plant Microbe Interact.* **2016**, *29*, 573–583. [CrossRef]
4. Kong, G.; Feng, D.; Li, W.; Lian, S.; Xi, P.; Jiang, Z. Research progress in studies on the downy blight disease in litchi. *J. Fruit Sci.* **2021**, *38*, 603–612. [CrossRef]
5. Zhang, D.; Fang, H.; He, Y. Research of crop disease based on visible/near infrared specttral image technology: A Review. *Spectrosc. Spect. Anal.* **2019**, *39*, 1748–1756. [CrossRef]
6. Bai, B.; Yu, J.; Fu, Z.; Zhang, L.; Li, X. Application of spectral imaging technology for detecting crop disease information: A review. *Spectrosc. Spect. Anal.* **2020**, *40*, 350–355. [CrossRef]
7. Kai, L.; Zhang, X.; Zhang, X. Early Detection of Cucumber Downy Mildew in Greenhouse by Hyperspectral Disease Differential Feature Extraction. *Trans. Chin. Soc. Agric. Mach.* **2020**, *50*, 212–220. [CrossRef]
8. Appeltans, S.; Pieters, J.G.; Mouazen, A.M. Detection of leek white tip disease under field conditions using hyperspectral proximal sensing and supervised machine learning. *Comput. Electron. Agric.* **2021**, *190*, 106453. [CrossRef]
9. Appeltans, S.; Pieters, J.G.; Mouazen, A.M. Detection of Leek Rust Disease under Field Conditions Using Hyperspectral Proximal Sensing and Machine Learning. *Remote Sens.* **2021**, *13*, 1341. [CrossRef]
10. Liu, S.; Tan, X.; Liu, C.; Zhu, C.; Li, W.; Cui, S.; Du, Y.; Huang, D.; Xie, F. Recognition of fusarium head blight wheat grain based on hyperspectral data processing algorithm. *Spectrosc. Spect. Anal.* **2019**, *39*, 3540–3546. [CrossRef]
11. Lucas Domingos da Silva, A.; Alves Filho, E.G.; Silva, L.M.A.; Carlos Huertas Tavares, O.; Gervasio Pereira, M.; de Campos, T.; Manoel da Silva, L. Near infrared spectroscopy to rapid assess the rubber tree clone and the influence of maturation and disease at the leaves. *Microchem. J.* **2021**, *168*, 106478. [CrossRef]
12. Ali, M.M.; Bachik, N.A.; Muhadi, N.A.; Tuan Yusof, T.N.; Gomes, C. Nondestructive techniques of detecting plant diseases: A review. *Physiol. Mol. Plant Pathol.* **2019**, *108*, 101426. [CrossRef]

13. Zhao, X.; Zhang, J.; Huang, Y.; Tian, Y.; Yuan, L. Detection and discrimination of disease and insect stress of tea plants using hyperspectral imaging combined with wavelet analysis. *Comput. Electron. Agric.* **2022**, *193*, 106717. [CrossRef]
14. Indrakumari, R.; Poongodi, T.; Khaitan, S.; Sagar, S.; Balamurugan, B. A review on plant diseases recognition through deep learning. In *Handbook of Deep Learning in Biomedical Engineering*; Academic Press: Cambridge, MA, USA, 2021; pp. 219–244. [CrossRef]
15. Mahlein, A.K.; Rumpf, T.; Welke, P.; Dehne, H.W.; Plümer, L.; Steiner, U.; Oerke, E.C. Development of spectral indices for detecting and identifying plant diseases. *Remote Sens. Environ.* **2013**, *128*, 21–30. [CrossRef]
16. Song, X.; Huang, Y.; Yan, H.; Xiong, Y.; Min, S. A novel algorithm for spectral interval combination optimization. *Anal. Chim. Acta* **2016**, *948*, 19–29. [CrossRef]
17. Shang, X.; Chisholm, L.A. Classification of australian native forest species using hyperspectral remote sensing and machine-learning classification algorithms. *IEEE J. Select. Top. Appl. Earth Obs. Remote Sens.* **2014**, *7*, 2481–2489. [CrossRef]
18. Wang, P.; Zhang, J.; Lan, Y.; Zhou, Z.; Luo, X. Radiometric calibration of low altitude multispectral remote sensing images. *Trans. CSAE* **2014**, *30*, 199–206. [CrossRef]
19. Chen, H.; Pan, T.; Chen, J.; Lu, Q. Waveband selection for NIR spectroscopy analysis of soil organic matter based on SG smoothing and MWPLS methods. *Chemom. Intell. Lab.* **2011**, *107*, 139–146. [CrossRef]
20. Li, H.; Liang, Y.; Xu, Q.; Cao, D. Key wavelengths screening using competitive adaptive reweighted sampling method for multivariate calibration. *Anal. Chim. Acta* **2009**, *648*, 77–84. [CrossRef]
21. Araújo, M.C.U.; Saldanha, T.; Galvo, R.K.H.; Yoneyama, T.; Visani, V. The successive projections algorithm for variable selection in spectroscopic multicomponent analysis. *Chemom. Intell. Lab.* **2001**, *57*, 65–73. [CrossRef]
22. Safavian, S.R.; Landgrebe, D. A survey of decision tree classifier methodology. *IEEE Trans. Syst. Man Cybern.* **1991**, *21*, 660–674. [CrossRef]
23. Altman, E.I.; Marco, G.; Varetto, F. Corporate distress diagnosis: Comparisons using linear discriminant analysis and neural networks (the Italian experience). *J. Bank. Financ.* **1994**, *18*, 505–529. [CrossRef]
24. Yager, R.R. An extension of the naive bayesian classifier. *Inform. Sci.* **2006**, *176*, 577–588. [CrossRef]
25. Keller, J.M.; Grey, M.R.; Givens, J.A. A fuzzy k-nearest neighbour algorithm. *IEEE Trans. Syst. Man Cybern.* **1985**, *SMC-15*, 580–585. [CrossRef]
26. Hearst, M.A.; Dumais, S.T.; Osman, E.; Platt, J.; Scholkopf, B. Support vector machines. *IEEE Intell. Syst.* **1998**, *13*, 18–28. [CrossRef]
27. Li, L.; Jang, X.; Li, B.; Liu, Y. Wavelength selection method for near-infrared spectroscopy based on standard-sample calibration transfer of mango and apple. *Comput. Electron. Agric.* **2021**, *190*, 106448. [CrossRef]
28. Guo, P.; Li, M.; Luo, W.; Cha, Z. Estimation of foliar nitrogen of rubber trees using hyperspectral reflectance with feature bands. *Infrared Phys. Technol.* **2019**, *102*, 103021. [CrossRef]
29. Wang, Z.; Fan, S.; Wu, J.; Zhang, C.; Xu, F.; Yang, X.; Li, J. Application of longwave near infrared hyperspectral imaging for determination of moisture content of single maize seed. *Spectrochim. Acta* **2021**, *254*, 119666. [CrossRef]
30. Lee, A.; Shim, J.; Kim, B.; Lee, H.; Lim, J. Nondestructive prediction of soluble solid contents in Fuji apples using visible near-infrared spectroscopy and various statistical methods. *J. Food Eng.* **2022**, *321*, 110945. [CrossRef]
31. Xu, L.; Chen, M.; Wang, Y.; Chen., X.; Lei., X. Study on Non-Destructive Detection Method of Kiwifruit Sugar Content Based on Hyperspectral Image Technology. *Spectrosc. Spect. Anal.* **2021**, *40*, 2188–2195. [CrossRef]
32. Walsh, K.B.; Blasco, J.; Zude-Sasse, M.; Sun, X. Visible-NIR 'point' spectroscopy in postharvest fruit and vegetable assessment: The science behind three decades of commercial use. *Postharvest Biol. Technol.* **2020**, *168*, 111246. [CrossRef]

Computers and Electronics in Agriculture 229 (2025) 109789

Contents lists available at ScienceDirect

Computers and Electronics in Agriculture

journal homepage: www.elsevier.com/locate/compag

A novel method for detecting missing seedlings based on UAV images and rice transplanter operation information

Shuanglong Wu [a], Xingang Ma [a], Yuxuan Jin [a], Junda Yang [a], Wenhao Zhang [a], Hongming Zhang [a], Hailin Wang [e], Ying Chen [d,***], Caixia Lin [a,**], Long Qi [b,c,d,*]

[a] College of Engineering, South China Agricultural University, Guangzhou, Guangdong Province, 510642, China
[b] College of Water Conservancy and Civil Engineering, South China Agricultural University, Guangzhou, Guangdong Province, 510642, China
[c] State Key Laboratory of Agricultural Equipment Technology, Guangzhou, Guangdong Province, 510642, China
[d] Department of Biosystems Engineering, University of Manitoba, Winnipeg, MB, R3T 5V6, Canada
[e] Guangdong Polytechnic of Science and Trade, Guangzhou, Guangdong Province, 510640, China

ARTICLE INFO

Keywords:
UAV images
Seedling information
Transplanting trajectory
Missing seedlings
Target detection

ABSTRACT

In mechanized rice planting, missing seedlings can result from several factors, such as missed transplanting by transplanters, missed sowing by seed sowing machines, and floating or dead seedlings after transplanting, ultimately decreasing land utilization and rice yield. Timely detection of missing seedlings and targeted replanting are essential for minimizing wastage of land, water, and fertilizer resources, while also enhancing yield. Traditional detection methods, including photoelectric sensors and machine vision, suffer from limitations like complex structures and difficulty in rapidly and accurately obtaining geographical coordinates of missing seedlings. To address these limitations, this paper proposes a novel missing seedling detection method based on UAV (unmanned aerial vehicle) imagery combined with rice transplanter operation information. Initially, UAVs captured images of rice seedlings to construct a comprehensive dataset, from which a rice seedling detection model meeting accuracy requirement was developed. Subsequently, the transplanting trajectory of the transplanter was derived based on the navigation data, and combined with parameters such as transplanting and row spacing, the "theoretical" position points of each seedling in the paddy field were determined. A rectangular area with a defined threshold range centered on each "theoretical" position point was constructed as the missing seedling detection region. The developed detection model was then applied to detect the presence of actual seedlings within these regions, identifying missing seedling areas. Additionally, a coordinate transformation algorithm was implemented to derive precise geographical coordinates for each missing seedling location. Experimental results indicated that, in randomly selected plots, the proposed method achieved a recall rate exceeding 80% and a precision rate over 75%. By leveraging UAV imagery and transplanter operation data, this method minimizes dependency on complex detection algorithms, enhances detection accuracy, and enables acquisition of precise geographical coordinates for missing seedlings, supporting subsequent unmanned replanting efforts

1. Introduction

Rice is one of the three major food crops in the world, with over 50 % of the global population relying on rice as their staple food (Singh et al., 2023). At present, the mechanized planting of rice mainly includes two methods: seedling raising and transplanting, and direct sowing (Hou et al., 2019). The seedling raising and transplanting method mainly involves the processes of selecting seeds, sun drying seeds, soaking seeds, and promoting germination to first raise rice seedlings, and then transplanted the raised seedlings to the paddy field. In contrast, the

* Corresponding author.
** Corresponding author.
*** Corresponding author.
E-mail addresses: wushuanglong@scau.edu.cn, zymwgl@foxmail.com (S. Wu), 1013453551@qq.com (X. Ma), 1290556223@qq.com (Y. Jin), 2856966590@qq.com (J. Yang), 2065551820@qq.com (W. Zhang), 243150122@qq.com (H. Zhang), hlwang@scau.edu.cn (H. Wang), Ying.Chen@umanitoba.ca (Y. Chen), cxllin@scau.edu.cn (C. Lin), qilong@scau.edu.cn (L. Qi).

https://doi.org/10.1016/j.compag.2024.109789
Received 28 September 2024; Received in revised form 1 December 2024; Accepted 4 December 2024

direct sowing method simplifies this process by allowing seeds to be sown directly onto the ridges of the paddy field using a sowing machine. When the seedling picking or feeding mechanism of the rice transplanter malfunctions or the seedlings are raised unevenly, or when the metering device of the seed sowing machines malfunctions, it can lead to missing seedlings (Deng et al., 2023). In addition, after transplanting (or direct sowing), seedlings (or seeds) are susceptible to temperature, soil quality, light, diseases, insects and other factors. These can prevent some seedlings (seeds) from surviving and growing healthily and normally, leading to seedlings missing in the field. Therefore, missed planting by transplanters, missed sowing by seed sowing machines, as well as floating and dead seedlings after transplanting can all contribute to seedling missing, thereby reducing land utilization and rice yield.

For the problem of missing seedlings, the most used solution is "planting first and filling later", which means transplanting or sowing first, and then replanting the seedlings in positions of missing seedlings (Cui et al., 2023). Currently, the main method for replacing missing seedlings is manual labor, which involves manually traversing and inspecting farmland, searching for the location of the missing seedlings, and then manually replanting. However, this method is inefficient, time-consuming, and labor-intensive, which is not suitable for large-scale agricultural productions (Vong et al., 2021). If missing seedlings can be detected first after transplanting or sowing, allowing for the precise identification of their locations, it would significantly reduce the time and labor required for replanting. It can also provide accurate missing seedling location coordinates for future unmanned automatic replanting, facilitating precise interventions. Therefore, conducting research on missing seedlings detection will help improve the efficiency of seedling replanting and achieve unmanned and precise replanting, which is of great significance for reducing waste of land, water and fertilizer resources, and increasing rice yield.

Regarding seedlings detection, researchers have conducted extensive studies and achieved significant results. Technically, there are mainly two detection methods: photoelectric sensor detection (Maldaner et al., 2021; Abbas et al., 2020) and machine vision detection (Varela et al.,2018; Wu et al., 2019).

The photoelectric sensor detection method is primarily used during the seedling stage or the transplanting process. It involves positioning photoelectric sensors, such as lasers and optical fibers, at specific points to monitor seedling trays, stems, and tubes (Yao et al., 2024). By analyzing variations in photoelectric signals with and without seedlings, it allows for the identification of missing seedlings. Jin et al. (2018) developed an intelligent transplanting system that utilizes photoelectric sensors to bypass empty soil bases in potted pepper seedlings, effectively addressing yield loss due to high rates of missed transplants. Yao et al. (2024) created a transverse conveying device for cabbage seedling trays and a longitudinal seedling picking device, incorporating photoelectric sensors to ensure precise positioning during conveyance and picking, thus minimizing damage to remaining seedlings. Sharma et al. (2022) introduced an intelligent transplanting method for Mexican pepper seedlings that accurately identified healthy, sub-healthy, low-quality, and empty tray units using photoelectric sensors, achieving a 12 % reduction in the annual missed transplanting rate compared to traditional methods. However, the effectiveness of the photoelectric sensor detection method is significantly influenced by lighting conditions and the farmland background, and some sensors can be prohibitively expensive, limiting their application for missing seedling detection in large-scale rice fields after transplanting.

With the rapid development of algorithms and the continuous improvement of computer hardware performance, machine vision detection methods have gained significant popularity in crop seedling detection (Oh et al., 2020). Researchers have employed these methods to assess the growth conditions of various crops, including rice (Cui et al., 2023), corn (Osco et al., 2021), citrus trees (Osco et al., 2020), and cotton (Feng et al., 2020). Machine vision detection methods can be broadly classified into two main categories: traditional machine learning and deep learning. Traditional machine learning methods primarily rely on manually defined rules and features for object recognition, making it difficult to handle complex and dynamic environments and resulting in poor performance when recognizing newly emerging objects (Banerjee et al., 2021; Shirzadifar et al., 2020). In contrast, deep learning methods use neural networks to automatically learn the features of objects, eliminating the need for manually defined rules. These models are capable of automatically extracting high-level features from images, making them particularly well-suited for complex and dynamic environments. As a result, deep learning has become the dominant approach in visual detection. Cui et al. (2023) introduced a deep learning-based approach to estimate the number of missing rice seedlings using low-altitude UAV video. This method integrates the Paddy-YOLOv5s-Prune model, the ByteTrack tracking algorithm, and a Python program for counting the missing seedlings. Barreto et al. (2021) developed a sugar-beet seedling counting model based on drones (UAV) and deep learning, which can accurately determine the exact stem positions of crop and weed plants and perform pixel-wise plant classification, taking into account crops, weeds, and soil. Additionally, machine vision method can also be applied to detect plug seedlings (Li et al., 2024; Fu et al., 2022). Liu et al. (2023) developed an algorithm to determine the optimal gripping angle for seedling insertion based on machine vision, which minimizes mechanical damage during seedling pickup and enhances the transplanting quality of plug seedlings. Yan et al. (2023) proposed a detection method for missed tomato plug tray seedings using machine vision, allowing for precise identification of tomato seeds and plug trays against complex backgrounds, locating the corresponding holes, and providing coordinates for missed holes to control replanting devices for cell replenishment. However, the machine vision detection method has high requirements for image quality, and it cannot directly and accurately obtain the geographical coordinates of the missing seedling locations, which is not conducive to subsequent unmanned precise replanting.

In response to the limitations of the commonly used photoelectric sensor detection and machine vision inspection methods mentioned above, this paper proposed a novel missing seedling detection method based on UAV images and rice transplanter operation information. Through image recognition and combined with rice transplanter operation information, the proposed method can quickly detect the location of missing seedlings and accurately obtain their coordinates.

The detection process for the method proposed in this paper is as follows: first, rice seedling images were captured by UAVs, and a rice seedling dataset was established. After training, a rice seedling detection model that met accuracy requirements was developed. Next, the transplanting trajectory of the transplanter was acquired, which, combined with parameters such as plant spacing and row spacing, allowed for determining the "theoretical" position of each seedling in the paddy field. Then, a rectangular area centered around each "theoretical" seedling position with a specific threshold range was created as the missing seedling detection region. The trained rice seedling detection model was subsequently used to determine the presence of actual seedlings within this constructed region, thereby identifying any missing seedlings. Additionally, a coordinate transformation algorithm was applied to retrieve the geographical coordinates corresponding to the locations of missing seedlings.

2. Materials and methods

2.1. Seedling images acquisition and recognition

2.1.1. Rice field images acquisition, synthesis, and segmentation

The rice field images used in this paper were collected by using a DJI Phantom 4 RTK aerial survey drone at Shapu Farm in Dinghu District, Zhaoqing City, Guangdong Province, China. The left side of Fig. 1 highlights the specific area where the UAV image acquisition took place in the Shapu Farm. The first round of image acquisition occurred on the

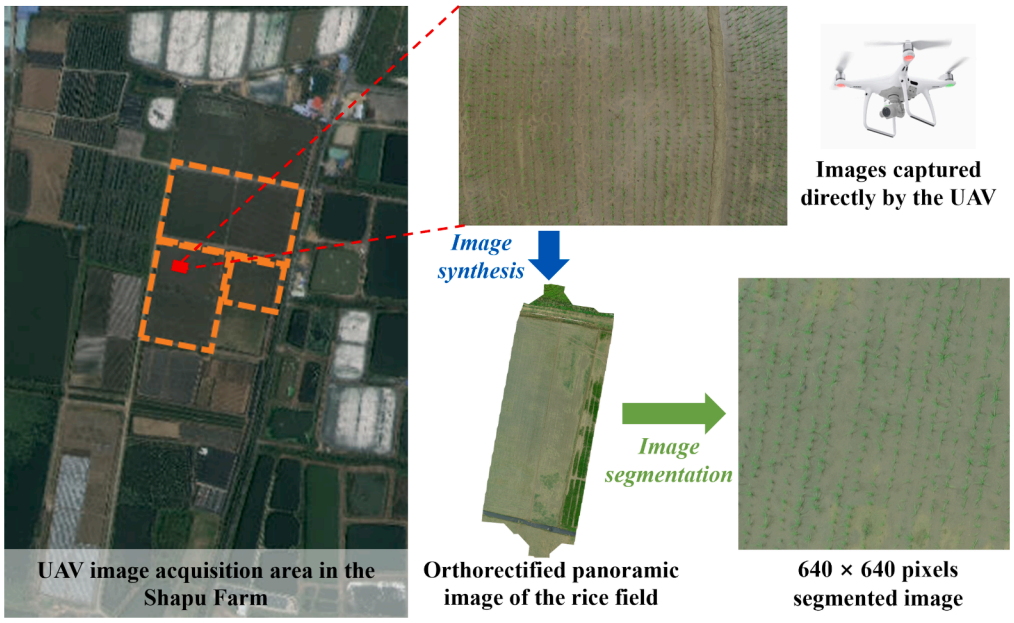

Fig. 1. Rice field image acquisition, synthesis, and segmentation.

day of rice transplanting, followed by two additional rounds within a month after the transplanting operation. These acquisitions took place on March 29, 2023, at 11:00 AM; April 11, 2023, at 11:00 AM; and April 21, 2023, at 11:00 AM, respectively. At these times, the sunlight conditions were optimal, with minimal water reflection in the rice fields, aligning with the experimental requirements. The three image acquisitions resulted in 1242, 1063, and 2019 images, respectively, totaling 4324 images. The upper part of Fig. 1 shows a typical low-altitude high-definition remote sensing image of the rice fields, highlighting the distortions present in the image captured directly by the UAV.

Since it is impossible to directly obtain the overall coordinate information of the rice field from the local images collected by the UAV, it is necessary to synthesize the local images to obtain the panoramic image of the rice field (Wu et al., 2023). In this paper, DJI TERRA software was used to synthesize the panoramic image of rice field. DJI TERRA is a 3D (three dimensional) model reconstruction software that has photogrammetry as its core technology. Utilizing Structure from Motion (SFM) and Multi-View Stereo (MVS) techniques, it stitches segmented images into a high-definition 2D (two dimensional) panoramic image of the entire rice field, based on parameters such as shooting height, geographical position, pan-tilt angle, and the overlap rate between adjacent images. The middle section of Fig. 1 displays the synthesized 2D orthorectified panoramic image of the rice field. While this image provides overall coordinate information, it cannot be directly applied to deep learning models due to the detection principles of object detection frameworks. Therefore, it is essential to crop the panoramic image into a series of 640 × 640 pixel segments. The lower right part of Fig. 1 shows one of these segmented images, which will serve as the dataset for subsequent model training and missing seedling detection.

2.1.2. Rice seedlings recognition

To achieve rapid and accurate detection of seedlings in images, we employed the YOLOv5 7.0 algorithm to develop a seedling detection model, leveraging its strong generalization capabilities and fast detection speed. Initially, the image annotation tool LabelImg was used to annotate the rice seedlings in the images (640 × 640 pixel segmented images) collected in Section 2.1.1. A total of 6407 images were annotated, and the dataset was randomly divided into a training set and a validation set in a 4:1 ratio. Through training, the optimal weight value was obtained. The training environment consisted of Ubuntu 18.04, an RTX A4000 (16 GB) GPU, an i7-12700 K CPU, 64 GB of RAM, and the PyTorch framework. Ultimately, a seedling detection model was constructed using the optimal weights obtained from the training process.

To enhance the training speed of the seedling detection model, improve its recognition capability, and reduce the risk of overfitting, incremental training method was employed to train the rice seedling detection model. This approach consists of two training sessions: pre-training and final training. Initially, the rice seedling detection model was pre-trained using the initial weights of YOLOv5, with 1397 randomly selected images as input for 100 training rounds. Upon completing the pre-training, the optimal weights obtained were then utilized for the final training phase. In this stage, 5103 randomly selected images were inputted for an additional 300 training rounds. However, as the number of training rounds increased during the final phase, the model's performance improvements became marginal. To avoid the risk of overfitting, training was halted at the 185th round. Fig. 2 shows the flowchart of the training process for the rice seedling detection model. Through this incremental training method, a total of 285 rounds of pre-training and final training were conducted, resulting in the seedling detection model achieving an accuracy of 87 % in identifying rice seedlings. This demonstrates good detection performance and meets the detection requirements outlined in this paper.

2.2. Theoretical position determination of rice seedlings based on transplanter operation information

2.2.1. Construction of operation trajectory of rice transplanter

To determine the theoretical position of rice seedlings in the paddy field, it is essential to first obtain the trajectory of the rice transplanter during the transplanting process. Due to the difficulty of directly capturing the transplanting trajectory from UAV images of the rice field, the navigation data stored in the transplanter's navigation system would be utilized to reconstruct the transplanting trajectory.

The rice transplanter used in this paper is the ISEKI PZ60, equipped with a Beidou navigation system. It features a six-row synchronous transplanting mechanism, allowing for the simultaneous transplanting of six rows of rice seedlings, as illustrated in Fig. 3. The transplanter has a wheelbase of 1000 mm and a track width of 1200 mm. During operation, the theoretical distance between adjacent seedlings in the same row is 18 cm, while the distance between rows is 30 cm, with all rows

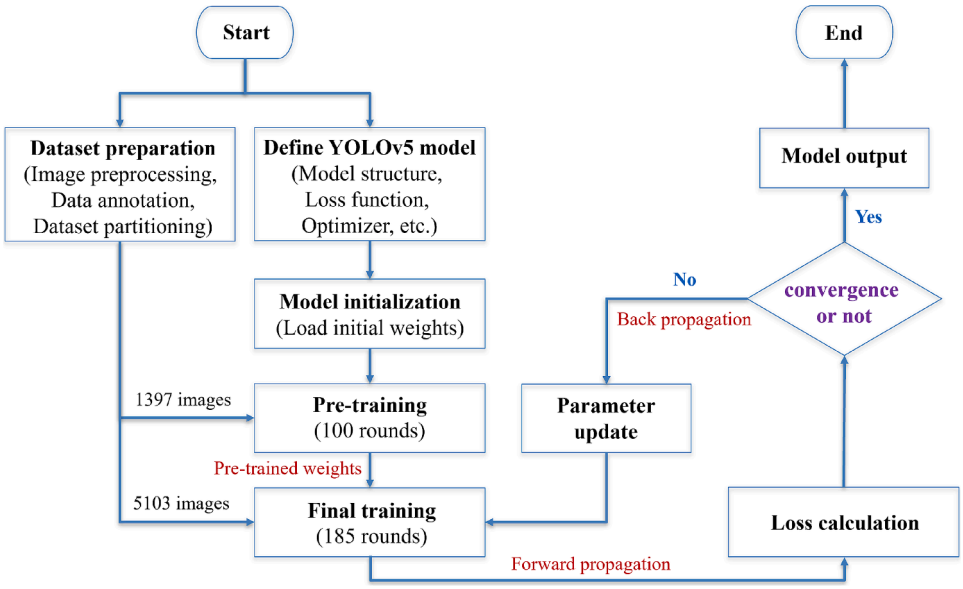

Fig. 2. Flowchart of the training process for rice seedling detection model.

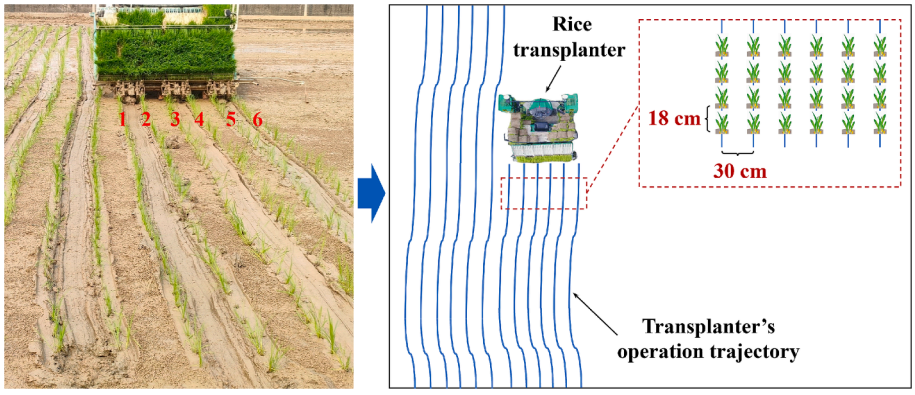

Fig. 3. Operation scenario and schematic diagram of the transplanting process.

running parallel. Using the orientation of the transplanter head as a reference, the transplanter receives and records the position information of the rightmost transplanting trajectory (among the 6 transplanting trajectories) via a satellite signal receiver. During transplanting operations, the transplanting mechanism attached to the tail of the transplanter synchronously transplants six rows of rice seedlings. The trajectory of the transplanter is consistent with the rice seedling row. A schematic diagram of the transplanting process is shown in Fig. 3.

To generate the transplanting trajectory of the rice transplanter and facilitate subsequent detection of missing seedlings, a blank image matching the dimensions of the 2D orthorectified panoramic image of the entire rice field (shown in Fig. 1) is first created. Considering that

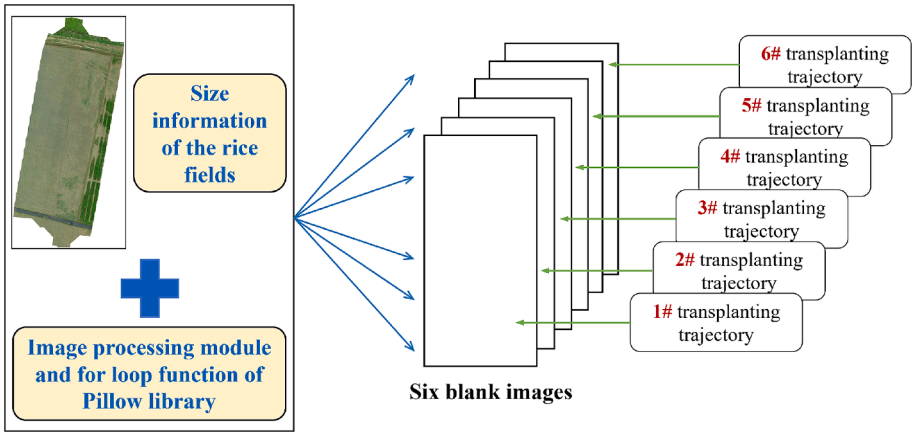

Fig. 4. Schematic diagram for creating blank images of rice field.

each transplanting operation consists of six seedling rows, drawing all six rows simultaneously on a single blank image complicates the recognition process. It also makes it more difficult to derive the theoretical positions of the rice seedlings. Therefore, six identical blank images will be created in this paper (as shown in Fig. 4), and the six seedling rows will be drawn on the six blank images respectively.

The autonomous rice transplanter utilizes longitude and latitude information for localization and path planning. During the transplanting operation, the satellite signal receiver mounted on the right side of the transplanter only receives and records the position information of the rightmost transplanting trajectory among the six transplanting trajectories. Consequently, it is essential to deduce the positions of the other five transplanting trajectories to form a complete set. The rightmost transplanting trajectory can be obtained by sequentially connecting actual satellite navigation recording points. To obtain the other five simultaneous transplanting trajectories, we first need to derive the virtual navigation recording points for these five trajectories. Considering that in each transplanting operation, the six simultaneous transplanting trajectories are parallel to each other and the distance between any two adjacent trajectories is equal, the virtual navigation recording points on the other five simultaneous transplanting trajectories can be deduced from the actual navigation recording point on the rightmost trajectory, as illustrated in Fig. 5.

As shown in Fig. 5, the geographical distance between the virtual navigation recording point T on the adjacent transplanting trajectory to be derived and the actual navigation recording point D on the rightmost transplanting trajectory is 30 cm. This means that the distance between the two points in the geographical coordinate system is 30 cm. Since the pixel coordinate and geographical coordinate of point D are known, along with the angle between the rightmost transplanting trajectory X and the Earth's true north direction, the latitude and longitude values of the virtual navigation recording point T on the adjacent transplanting trajectory can be calculated using formulas (1) to (5). Subsequently, the corresponding pixel coordinates can be obtained through coordinate transformation. Fig. 6 illustrates the schematic of spherical coordinate points on Earth, where points A and B represent two locations on the Earth's spherical surface. The angle a is defined as the angle between the line connecting point A and the center of the Earth and the line connecting the North Pole to the Earth's center. Similarly, angle b represents the angle for point B, and angle c is the angle between the lines connecting points A and B to the center of the Earth. Since the Earth can be approximated as a sphere, the distance between two points on its surface can be calculated using the spherical cosine formula (Tian et al., 2023). While the Earth is, in fact, an imperfect sphere, applying the spherical cosine formula may introduce some error. However, because the Earth's radius is significantly larger than the distance between the two points being measured, this error can be considered negligible.

Since the spherical distance L_{AB} between points A and B is known,

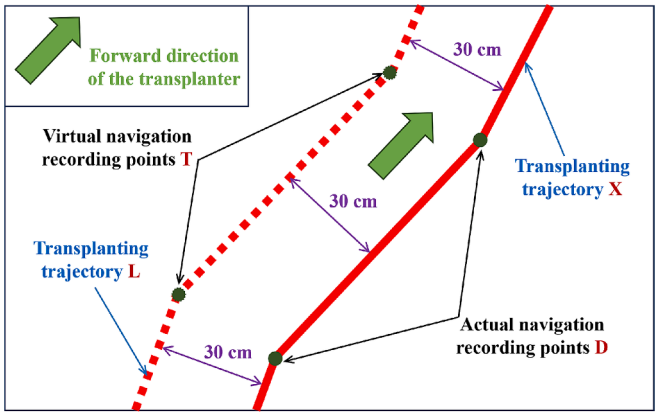

Fig. 5. Schematic diagram for deriving the transplanting trajectory.

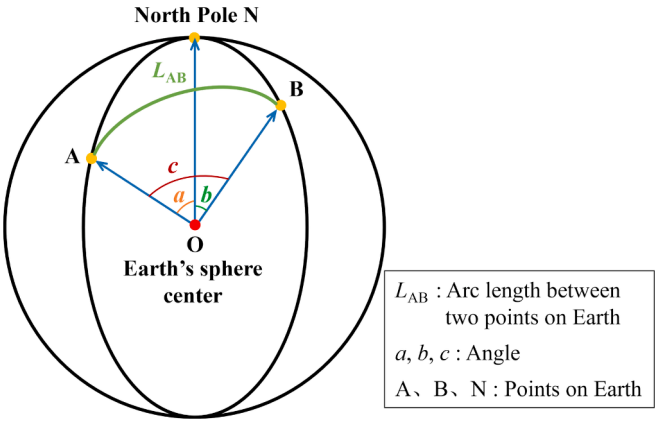

Fig. 6. Schematic diagram of spherical coordinate points on Earth.

combined with the Earth's mean radius R, the curvature value c' of angle c can be derived using formula (1)

$$c' = \frac{L_{AB}}{R} \tag{1}$$

Radians can be converted into angular values by using formula (2)

$$c = 180 \cdot \frac{c'}{\pi} \tag{2}$$

Since the longitude and latitude coordinates (A_j, A_w) of point A are known, the magnitude of angle a is $a = 90\text{-}A_w$. By applying the spherical cosine formula (3) in conjunction with the trigonometric identity formula (4), the magnitude of angle b can be determined. Consequently, the latitude of point B is $B_w = 90\text{-}b$.

$$\cos c = \sin a \cdot \sin b \cdot \cos c + \cos a \cdot \cos b \tag{3}$$

$$(\sin a)^2 + (\cos a)^2 = 1 \tag{4}$$

Then, according to the spherical distance formula (5), the longitude value B_j of point B can be obtained.

$$L_{AB} = R \cdot \arccos\left[\cos A_w \cos A_w \cos(A_j - B_j) + \sin B_w \sin B_w\right] \tag{5}$$

It is important to note that the B_j obtained from formula (5) yields two possible values. Therefore, the longitude of point B must be determined based on the relative positions of points A and B.

Since any two transplanting trajectories are parallel to each other and the distance between adjacent trajectories is fixed, the pixel coordinate value of each virtual navigation recording point on any transplanting trajectory can be sequentially derived based on the calculation principle of distance between spherical coordinate points discussed above. These derived pixel coordinates can then be connected in sequence to create six sets of simultaneous transplanting trajectories, which can be plotted onto the six blank images shown in Fig. 4 to produce six transplanting trajectory maps. As described in section 2.1.1, the 2D orthorectified panoramic image of the entire rice field (illustrated in Fig. 1) has been segmented to generate images of uniform size (640 × 640 pixel). To ensure that the transplanting trajectories in the maps align with the actual transplanting paths in the segmented images, it is necessary to apply the same segmentation process to the six transplanting trajectory maps, yielding segmented images of 640 × 640 pixel. Fig. 7 presents a schematic diagram of the segmentation process for the six transplanting trajectory maps.

2.2.2. *Determination of the theoretical position of rice seedlings*

There is a one-to-one correspondence between the transplanting trajectory in the segmented image of the transplanting trajectory map and the transplanting trajectory in the segmented image of the rice field. Therefore, recognizing the transplanting trajectory in the rice field

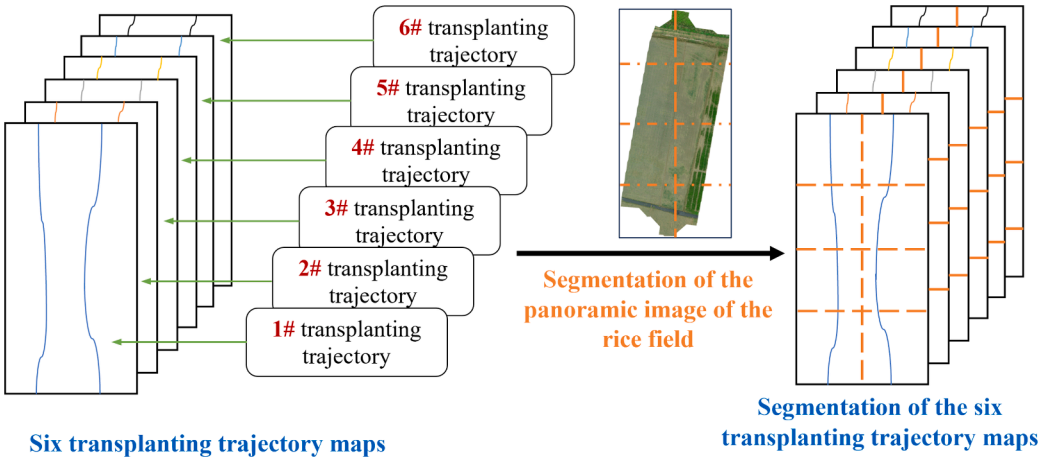

Fig. 7. Schematic diagram of the segmentation process for the six transplanting trajectory maps.

image can be transformed into identifying the transplanting trajectory in the segmented image of the transplanting trajectory map. In the transplanting trajectory map, aside from the transplanting trajectory and navigation recording points, all other areas feature a pure white background, eliminating interference from the colors of rice seedlings, paddy fields, water reflections, weeds, and other elements. Consequently, color information recognition technology will be employed to identify the rice seedling transplanting trajectory within the transplanting trajectory map.

The transplanting trajectory can be obtained by sequentially connecting satellite navigation recording points. Since the navigation controller of the rice transplanter records a navigation position point every 6 s and the transplanter operates at a forward speed of approximately 0.7 m/s, a segmented image with dimensions of 640 × 640 pixel corresponds to an actual area of 5.2 × 5.2 m. Consequently, the segmented image may not always include satellite navigation recording points, leading to the following two possible scenarios.

(1) There is no satellite navigation recording point in the segmented image of the transplanting trajectory maps, meaning the transplanting trajectory appears as a straight line without any "breakpoints" that would alter its slope, as illustrated in Fig. 8.
(2) There is a satellite navigation recording point in the segmented image of the transplanting trajectory maps, indicating that the transplanting trajectory appears as a broken line with "breakpoints" that alter its slope, as shown in Fig. 9.

As shown in Fig. 9, when there is a satellite navigation recording point in the segmented image of the transplanting trajectory maps, the transplanting trajectory may be divided into two sections with different slopes. To enhance the accuracy of identifying the transplanting trajectory, it is essential to first identify the navigation recording point in the segmented image of the transplanting trajectory map. Using the same method applied to identify the starting and ending points of the transplanting trajectory, the RGB value comparison method will be employed to locate the navigation recording point. Each pixel in the image will be traversed using a vertical traversal method, with the identified navigation recording points sequentially stored.

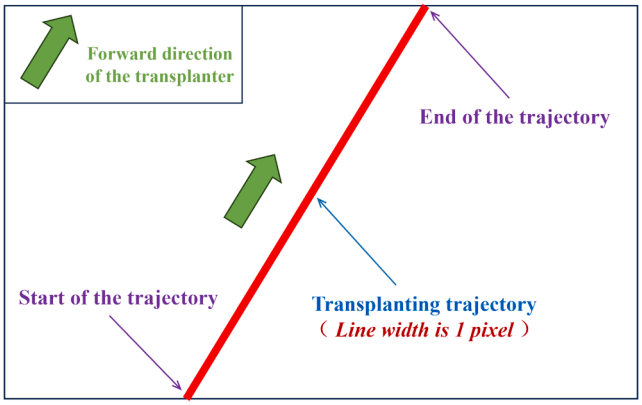

Fig. 8. Schematic diagram of transplanting trajectory with no "breakpoint".

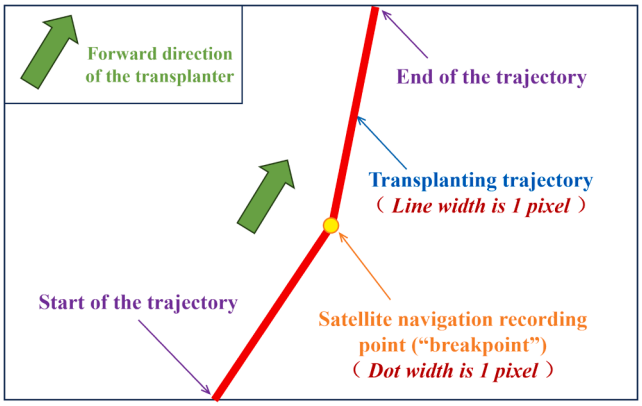

Fig. 9. Schematic diagram of transplanting trajectory with "breakpoint".

Based on the starting and ending points of the transplanting trajectory, as well as the satellite navigation recording points, the transplanting trajectory of the rice transplanter can be derived. This derived trajectory serves as the seedling line, allowing the determination of the theoretical position point for each rice seedling when combined with information such as seedling spacing. Since the identification task of the navigation recording points distinguishes different transplanting trajectories based on the presence or absence of these points in the segmented images of the transplanting trajectory map, the derivation of the theoretical position points for rice seedlings must be divided into the following two situations.

(1) If the segmented image of the transplanting trajectory map does not contain any navigation recording points of the transplanter, there will be no "breakpoints" that cause changes in the slope of the transplanting trajectory. In this case, the transplanting trajectory is a straight line and can be directly determined from the pixel coordinates of the start and end points. Once the transplanting trajectory is established, the theoretical seedling coordinates can be directly deduced using the theoretical seedling spacing information. The principle for deducing

theoretical seedling coordinates in a segmented image of the transplanting trajectory map without navigation recording points is illustrated in Fig. 10. Since the seedling spacing is a fixed value of 18 cm, and the pixel and geographic coordinates of the starting point of the transplanting trajectory are known, the geographic coordinates of all theoretical seedling points in the segmented image can be successively derived using formulas (1) to (5) provided in section 2.2.1. The corresponding pixel coordinates of these points can then be obtained through coordinate transformation.

(2) If the segmented image of the transplanting trajectory map contains navigation recording points of the transplanter, there will be "breakpoints" that cause changes in the slope of the transplanting trajectory. In this case, the transplanting trajectory appears as a broken line and should be determined based on the pixel coordinates of the start point, end point, and the navigation recording points. The process for deriving the theoretical seedling coordinates is similar to that in situation (1), with slight variations near the "breakpoints". To simplify processing, the line segments before and after the "breakpoints" are directly accumulated. As shown in Fig. 11, the geographical coordinates of the theoretical seedling point Q can be directly calculated using formulas (1) to (5) based on the geographical coordinates of theoretical seedling point P. However, the geographical coordinates of theoretical seedling point S cannot be derived using the method as for point Q due to the "breakpoint" between points S and Q. In this case, the distance m between theoretical seedling point Q and navigation recording point J must first be calculated using the geographical coordinates of points Q and J. The distance n between the navigation recording point J and the theoretical seedling point S can then be determined, as $m + n = 18$ cm. Finally, the geographical coordinates of theoretical seedling point S can be obtained using formulas (1) to (5) based on the geographical coordinates of navigation recording point J.

Based on the aforementioned technical principles, traversing all transplanting trajectories allows for the derivation of the geographical and pixel coordinates of all theoretical seedlings.

2.2.3. Determination of seedling detection region

The previous section established the theoretical seedling coordinates. However, during the actual rice transplanting process, factors such as uneven paddy field surfaces or side-slipping of the transplanter can lead to deviations between actual and theoretical seedling positions. To accurately detect missing seedlings and minimize false detections, it is essential to conduct missing seedling detection within a defined threshold range around each theoretical seedling position. If a real seedling is detected within this threshold, the area is deemed free of missing seedlings; otherwise, it is considered to have a missing seedling. The principle for detecting missing seedlings is illustrated in Fig. 12. Considering that the distance between two adjacent seedlings in the same row is 18 cm and the row spacing is 30 cm, with the rows of seedlings parallel to each other, a rectangular area centered on the theoretical seedling coordinates is selected as the detection region for missing seedlings. The parameters of this rectangular detection region are depicted in Fig. 13.

As shown in Fig. 13, the theoretical seedling point G serves as the center of the rectangular seedling detection region. The width of this region corresponds to the seedling spacing of 18 cm, while the length matches the row spacing of 30 cm. The transplanting trajectory, formed

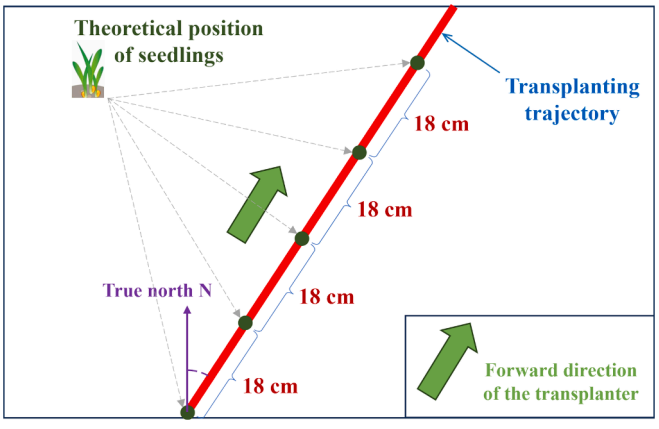

Fig. 10. Diagram of the principle for deducing theoretical seedling coordinates with no "breakpoint".

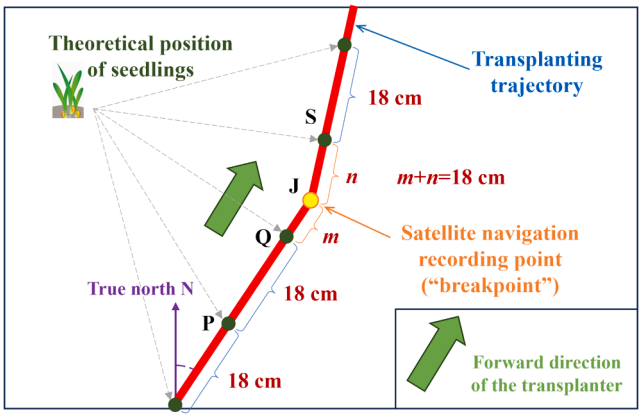

Fig. 11. Diagram of the principle for deducing theoretical seedling coordinates with "breakpoint".

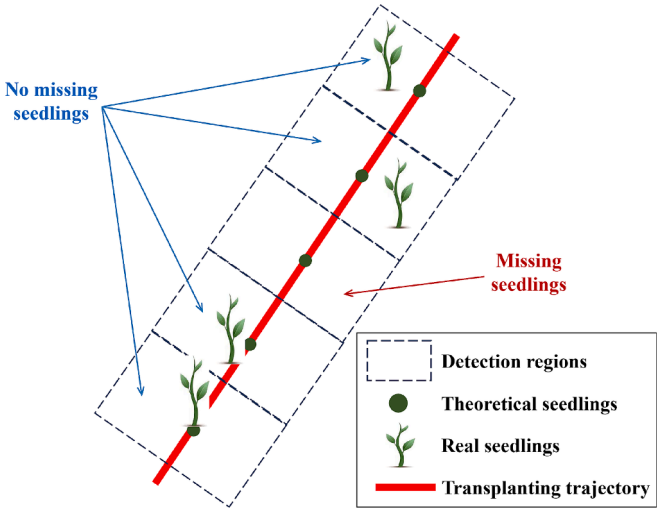

Fig. 12. Diagram of the missing seedling detection principle.

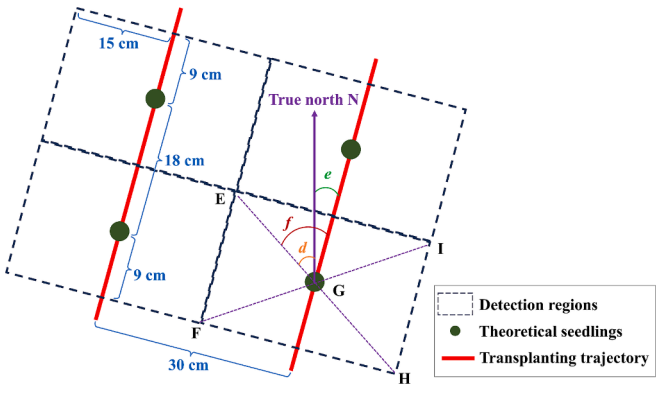

Fig. 13. Diagram of the parameters for the rectangular detection region.

by sequentially connecting the navigation recording points of the transplanter, allows for the calculation of angle *e*, which represents the angle between the transplanting trajectory and true north. With the known dimensions of the detection region, angles *f* and the length of *EG* can also be determined. By subtracting angle *e* from angle *f*, angle *d* can be obtained. Utilizing formulas (1) to (5) from Section 2.2.1, the geographical coordinates of point E can be derived and subsequently converted into pixel coordinates.

The pixel coordinates of the remaining three vertices (F, H, I) of the rectangular seedling detection region can be calculated using the same method. Therefore, based on the theoretical seedling coordinates established in Section 2.2.2, the positions of all rectangular seedling detection regions can be determined.

3. 3.Results and discussion

3.1. Sequential detection of each seedling

The images of rice seedlings were collected in Section 2.1, and a deep learning-based seedling detection model was established. In Section 2.2, the theoretical positions of the seedlings were derived from the transplanting trajectory of the rice transplanter, leading to the creation of rectangular detection regions for each theoretical seedling. In this section, the established detection model will be used to detect seedlings within these rectangular detection regions. Since the missing seedling detection method proposed in this paper requires sequential detection of each rectangular detection region in the image, directly inputting the image into the YOLO object detection convolutional neural network would lead to the detection of all seedlings across the image, hindering the ability to focus on individual rectangular detection areas. Therefore, image processing technology is necessary to ensure that detection is confined to the specified regions. In this paper, mask technology will be employed, as illustrated in Fig. 14. Masking is a fundamental technique in image processing that use binary 0 s and 1 s to select, filter, or hide specific image areas. Masks control which regions of an image are processed by blocking out certain parts, thus allowing focus on the areas of interest. In practice, binary 1 represents areas to be processed, while binary 0 indicates areas to be ignored, enabling targeted detection of specific regions. Since the use of the mask technology only limits the area being detected at each step, without altering the image features, it would not affect the detection accuracy of the seedling recognition model. In contrast to directly detecting all areas of the entire image, the proposed method focuses on specific regions at a time, which reduces interference from environmental factors such as water reflections and weeds. Furthermore, by concentrating on particular parts of the image, this method enhances detection accuracy for weak targets like seedlings, thereby decreasing reliance on the algorithm. Of course, the essence of the proposed method is still image detection, making image quality crucial. Therefore, it is necessary to ensure good weather conditions and stable UAV flight during the image acquisition process. Under the hardware conditions mentioned in Section 2.1.2, the proposed method takes approximately 7 s to detect a single image. Of course, upgrading the hardware can further reduce the detection time.

To sequentially detect all rectangular detection regions in the image, it is essential to identify the detection region for each step. The pixel coordinates of all vertices of the rectangular seedling detection regions are established in Section 2.2.3, allowing each rectangular detection region to serve as the basis for each detection step. For the rectangular seedling detection regions discussed in this paper, it suffices to calculate the proportion of the coordinates of the four vertices relative to the horizontal and vertical axes of the image. Based on these calculations, the detection model algorithm can be adjusted to enable the sequential detection of all rectangular seedling regions. If a seedling is detected within a rectangular detection region, it indicates that no seedling is missing at that position, and the detection will proceed to the next region (as illustrated in Fig. 15(a)). Conversely, if no seedling is detected, it confirms the presence of a missing seedling, which will be marked and its coordinates recorded (as shown in Fig. 15(b)).

3.2. Missing seedling detection tests and result evaluation

Since each image has been numbered, experimental plots for missing seedling detection can be randomly selected by randomly choosing image numbers. Once the detection is completed, the algorithm will visually mark the locations of detected missing seedling (represented by yellow dots in Fig. 16). Additionally, the pixel coordinates of these missing seedling locations will be recorded and converted into geographic coordinates simultaneously. Table 1 presents the pixel coordinates and corresponding geographic coordinates of the missing seedling positions numbered 1–6 detected in Fig. 16.

To verify the accuracy of the missing seedling detection method proposed in this paper, two metrics, “recall rate” and “precision rate” (Guo et al., 2024), were introduced to evaluate the detection results. The recall rate refers to the ability of the method to identify all actual missing seedling locations in the rice field, while the precision rate refers to the ability of the method to detect missing seedling locations and ensure that the detected locations are indeed genuine missing seedling spots. The calculation formulas for the recall rate and precision rate are presented in formulas (6) and (7), respectively.

$$FA = \frac{FT}{FT + NT} \tag{6}$$

$$FC = \frac{FT}{FT + FF} \tag{7}$$

where *FA* represents the recall rate, *FT* denotes the number of detected missing seedling locations that are indeed actual missing

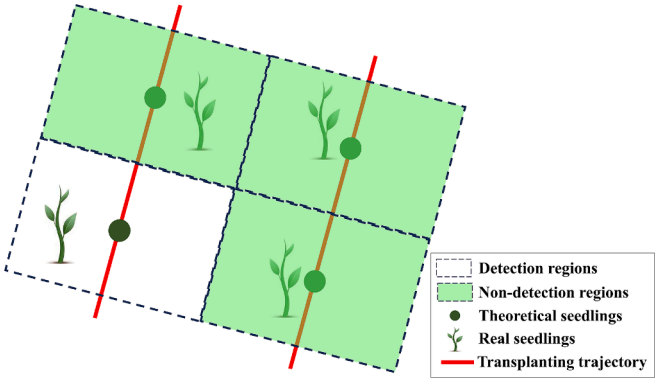

Fig. 14. Schematic diagram of the masking technology.

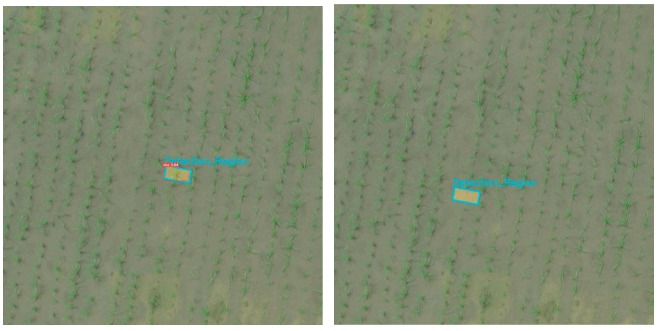

(a) (b)

Fig. 15. Seedling detection in an actual seedling image: (a) Rectangular detection region with seedling; (b) Rectangular detection region without seedling.

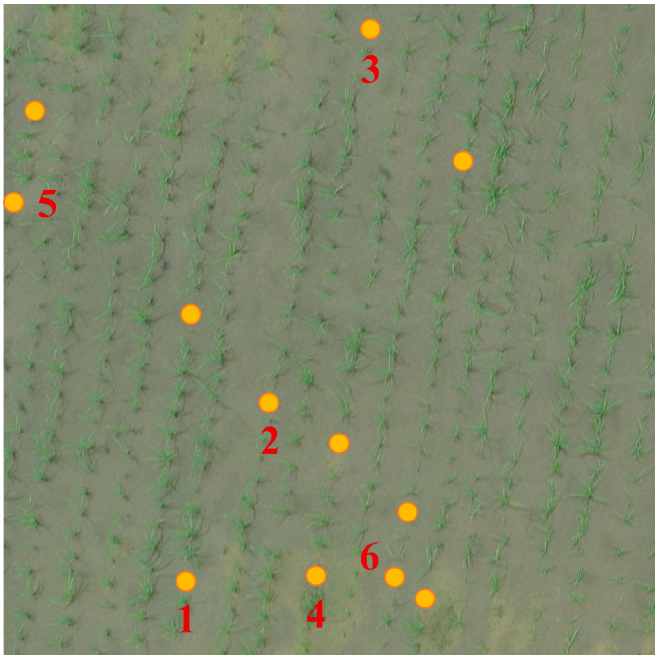

Fig. 16. Map of missing seedling locations in the experimental plot.

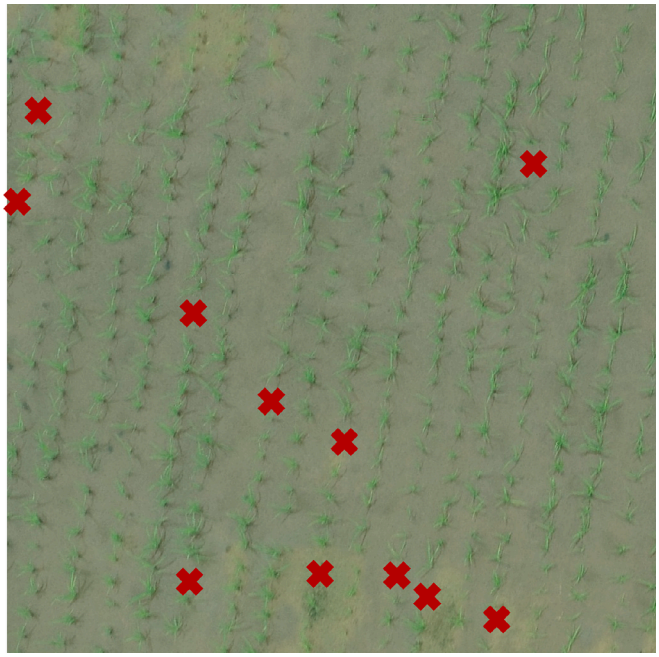

Fig. 17. Actual missing seedling location points.

Table 1
Pixel coordinates and geographic coordinates of partial missing seedling positions.

Missing seedling position number	Pixel coordinates	Geographic coordinates
1	(280, 901)	(23.1564558814, 112.6581241821)
2	(405, 612)	(23.1564686552, 112.6581301571)
3	(581, 36)	(23.1564941144, 112.6581385699)
4	(481, 900)	(23.1564559256, 112.6581337899)
5	(3, 360)	(23.1564797936, 112.6581109415)
6	(604, 900)	(23.1564559256, 112.6755490029)

seedling spots, and *NT* indicates the number of actual missing seedling locations that were not detected. *FC* represents the precision, while *FF* is the number of detected missing seedling locations that are not actual missing seedling spots.

In this missing seedling detection experiment, there were 11 actual missing seedling locations (as shown in Fig. 17), indicating that the sum of *FT* and *NT* is 11. Using the missing seedling detection method proposed in this paper, 12 missing seedling locations were identified (as shown in Fig. 16), meaning the sum of *FT* and *FF* is 12. Among the detected locations, 9 were actual missing seedling spots, and thus, *FT* is 9. The number of actual missing seedling locations that were not detected is 2, giving *NT* a value of 2. Additionally, 3 detected locations were not actual missing seedling spots, resulting in *FF* being 3. Based on formulas (6) and (7), the recall rate for the proposed missing seedling detection method was 81.8 %, while the precision rate was 75.0 %.

The analysis reveals that the missing seedling detection method proposed in this paper effectively identifies actual missing seedling locations, but it also generates false detections in areas where no seedlings are absent. Upon examining these false detection sites, it was noted that while seedlings are present, they are smaller and less robust compared to healthy seedlings of the same age (as illustrated in Fig. 18). This discrepancy led to the detection algorithm's misjudgment. In agricultural practice, however, seedlings that are too small are deemed low-quality. In contrast to high-quality seedlings, they often exhibit unstable metabolism, weaker morphology, and lower productivity, and may pose a higher disease risk, potentially impacting the final rice yield. Consequently, when conducting seedling replacement in the field, it is beneficial to selectively replace these smaller seedlings, thereby enhancing the overall quality of the rice seedlings and increasing the final yield.

To thoroughly assess the practicality of the missing seedling detection method proposed in this paper, four additional rice field plots were randomly selected for testing. The recall and precision rates of each detection were calculated, with the results presented in Table 2. As shown in the table, the proposed method achieved a recall rate of up to 80 % and a precision rate of up to 75 %. These results indicate that the method effectively meets the requirements for missing seedling detection. Furthermore, it provides precise location coordinates for the missing seedlings, facilitating accurate replanting efforts. It is important to note that the test results vary across different field plots. For instance, the recall and precision rates for field plot 5 are both higher than those for field plot 1. This variation is attributed to the random selection of detection plots, as the growth conditions and missing seedling situations can differ significantly among them. Actually, many factors can influence the recall and precision rates of detection results, including the quality of the captured images, the growth status of the seedlings, and the growth stage of the seedlings. Under the same conditions for the algorithm and other factors, higher-quality images, better-growing seedlings, and seedlings that have been growing longer will lead to better detection results. However, considering that earlier replanting is preferable (typically within one month after transplanting), image capture for this study was completed within one month after transplanting.

4. Conclusions

In this study, we developed a novel method for detecting missing rice seedlings by integrating UAV imagery with operational data from rice transplanters, effectively addressing the limitations of existing detection methods, such as photoelectric sensors and machine vision. The proposed method involved synthesizing a panoramic image of the rice field,

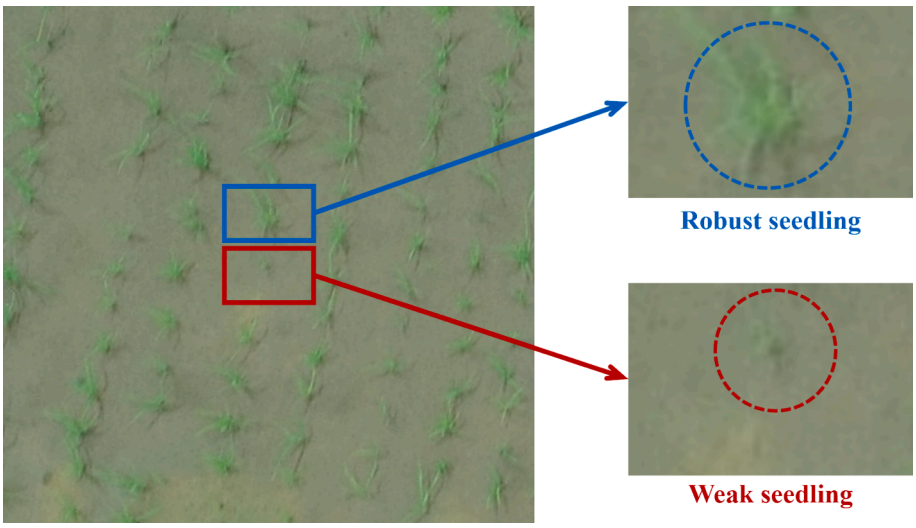

Fig. 18. Comparison of images of rice seedlings with different growth vigor.

Table 2
Results of the missing seedling detection tests.

Field plot number	*FT*	*NT*	*FF*	*FA*	*FC*
1	9	2	3	81.8 %	75.0 %
2	7	1	2	87.5 %	77.8 %
3	13	3	3	81.3 %	81.3 %
4	11	2	3	84.6 %	78.5 %
5	9	1	2	90.0 %	81.8 %

which is essential since UAV images alone do not provide comprehensive field coordinates. The panoramic image was then cropped into 640 × 640 pixel segments to create datasets for training and detection. Subsequently, an accurate seedling detection model was developed using the YOLOv5 7.0 algorithm combined with incremental training techniques, achieving an accuracy of 87 %. Furthermore, we utilized navigation data from the rice transplanter to reconstruct its transplanting trajectory, enabling the calculation of theoretical seedling positions based on parameters such as seedling spacing. This process involved establishing rectangular detection regions around each theoretical seedling position within a defined threshold range. By applying mask technology for sequential detection and evaluating our method through recall and precision metrics, we achieved a recall rate of 80 % and a precision rate of 75 %. These results demonstrate strong detection performance, and upon completion of the detection process, we can output the pixel and geographic coordinates of missing seedlings, facilitating precise unmanned replanting. This methodology not only enhances seedling monitoring but also significantly contributes to the advancement of precision agriculture.

The missing seedling detection method proposed in this paper relies on navigation data from the rice transplanter to reconstruct the seedling row lines. Therefore, in scenarios where navigation data is unavailable, such as with manually operated transplanters, the method is not applicable.

CRediT authorship contribution statement

Shuanglong Wu: Writing – original draft, Methodology, Conceptualization. **Xingang Ma:** Writing – original draft, Methodology, Conceptualization. **Yuxuan Jin:** Writing – review & editing, Validation, Software. **Junda Yang:** Writing – review & editing, Validation, Software. **Wenhao Zhang:** Visualization, Investigation. **Hongming Zhang:** Visualization, Investigation. **Hailin Wang:** Supervision, Project administration. **Ying Chen:** Writing – review & editing. **Caixia Lin:** Supervision, Project administration. **Long Qi:** Project administration, Funding acquisition.

Funding

This research was funded by the National Natural Science Foundation of China (U23A20174), the Key-area Research and Development Program of Guangdong Province (2023B0202130001), the Earmarked Fund for Modern Agro-industry Technology Research System in China (CARS-01), the Laboratory of Lingnan Modern Agriculture Project (NT2021009), the National Key Research and Development Program of China (2023YFD1401100), and the Specific University Discipline Construction Project (2023B10564002).

Declaration of competing interest

The authors declare that they have no known competing financial interests or personal relationships that could have appeared to influence the work reported in this paper.

Data availability

Data will be made available on request.

References

Abbas, I., Liu, J., Faheem, M., Noor, R.S., Shaikh, S.A., Solangi, K., Raza, S.M., 2020. Different sensor based intelligent spraying systems in Agriculture. Sens. Actuators A Phys. 316, 112265. https://doi.org/10.1016/j.sna.2020.112265.

Banerjee, B.P., Sharma, V., Spangenberg, G., Kant, S., 2021. Machine learning regression analysis for estimation of crop emergence using multispectral UAV imagery. Remote Sens. 13 (15), 2918. https://doi.org/10.3390/rs13152918.

Barreto, A., Lottes, P., Yamati, F.R.I., Baumgarten, S., Wolf, N.A., Stachniss, C., Mahlein, A.K., Paulus, S., 2021. Automatic UAV-based counting of seedlings in sugar-beet field and extension to maize and strawberry. Comput. Electron. Agric. 191, 106493. https://doi.org/10.1016/j.compag.2021.106493.

Cui, J., Zheng, H., Zeng, Z., Yang, Y., Ma, R., Tian, Y., Tan, J., Feng, X., Qi, L., 2023. Real-time missing seedling counting in paddy fields based on lightweight network and tracking-by-detection algorithm. Comput. Electron. Agric. 212, 108045. https://doi.org/10.1016/j.compag.2023.108045.

Deng, S., Gao, P., Wang, H., Chen, Y., Wei, H., Dai, Q., 2023. Effects of mixed planting on machine transplanting adaptability and grain yield of hybrid rice. Agric. 13 (2), 384. https://doi.org/10.3390/agriculture13020384.

Feng, A.J., Zhou, J.F., Vories, E., Sudduth, K.A., 2020. Evaluation of cotton emergence using UAV-based imagery and deep learning. Comput. Electron. Agric. 177, 105711. https://doi.org/10.1016/j.compag.2020.105711.

Fu, W., Gao, J., Zhao, C., Jiang, K., Zheng, W., Tian, Y., 2022. Detection method and experimental research of leafy vegetable seedlings transplanting based on a machine vision. Agronomy 12 (11), 2899. https://doi.org/10.3390/agronomy12112899.

Guo, Z., Cai, D., Bai, J., Xu, T., Yu, F., 2024. Intelligent rice field weed control in precision agriculture: from weed recognition to variable rate spraying. Agronomy 14 (8), 1702. https://doi.org/10.3390/agronomy14081702.

Hou, P., Xue, L., Zhou, Y., Li, G., Yang, L., Xue, L., 2019. Yield and N utilization of transplanted and direct-seeded rice with controlled or slow-release fertilizer. Agron. J. 111 (3), 1208–1217. https://doi.org/10.2134/agronj2018.03.0192.

Jin, X., Zhao, K., Ji, J., Du, X., Ma, H., Qiu, Z., 2018. Design and implementation of Intelligent transplanting system based on photoelectric sensor and PLC. Futur. Gener. Comput. Syst. 88, 127–139. https://doi.org/10.1016/j. future.2018.05.034.

Li, Y., Wei, H., Tong, J., Qiu, Z., Wu, C., 2024. Evaluation of health identification method for plug seedling transplantation robots in greenhouse environment. Biosyst. Eng. 240, 33–45. https://doi.org/10.1016/j.biosystemseng.2024.02.014.

Liu, J., Xiao, Z., Tan, Y., Sun, E., He, B., Ma, G., 2023. A study on the optimal grasping angle algorithm for plug seedlings based on machine vision. Agronomy 13 (9), 2255. https://doi.org/10.3390/agronomy13092253.

Maldaner, L.F., Molin, J.P., Canata, T.F., Martello, M., 2021. A system for plant detection using sensor fusion approach based on machine learning model. Comput. Electron. Agric. 189, 106382. https://doi.org/10.1016/j.compag.2021.106382.

Oh, S., Chang, A.J., Ashapure, A., Jung, J.H., Dube, N., Maeda, M., Gonzalez, D., Landivar, J., 2020. Plant counting of cotton from UAS imagery using deep learning-based object detection framework. Remote Sens. 12 (18), 2981. https://doi.org/10.3390/rs12182981.

Osco, L.P., De Arruda, M.D., Marcato, J., Da Silva, N.B., Ramos, A.P.M., Moryia, E.A.S., Imai, N.N., Pereira, D.R., Creste, J.E., Matsubara, E.T., Li, J., Goncalves, W.N., 2020. A convolutional neural network approach for counting and geolocating citrus-trees in UAV multispectral imagery. ISPRS J. Photogramm. Remote Sens. 160, 97–106. https://doi.org/10.1016/j.isprsjprs.2019.12.010.

Osco, L.P., De Arruda, M.D., Goncalves, D.N., Dias, A., Batistoti, J., De Souza, M., Gomes, F.D.G., Ramos, A.P.M., Jorge, L.A.D., Liesenberg, V., Li, J., Ma, L.F., Marcato, J., Goncalves, W.N., 2021. A CNN approach to simultaneously count plants and detect plantation-rows from UAV imagery. ISPRS J. Photogramm. Remote Sens. 174, 1–17. https://doi.org/10.1016/j.isprsjprs.2021.01.024.

Sharma, B.B., Raffik, R., Chaturvedi, A., Geeitha, S., Akram, P.S., Natrayan, L., Mohanavel, V., Sudhakar, M., Sathyamurthy, R., 2022. Designing and implementing a smart transplanting framework using programmable logic controller and photoelectric sensor. Energy Rep. 8, 430–444. https://doi.org/10.1016/j.egyr.2022.07.019.

Shirzadifar, A., Maharlooei, M., Bajwa, S.G., Oduor, P.G., Nowatzki, J.F., 2020. Mapping crop stand count and planting uniformity using high resolution imagery in a maize crop. Biosyst. Eng. 200, 377–390. https://doi.org/10.1016/j.biosystemseng.2020.10.013.

Singh, N.K., Narang, M.K., Thakur, S.S., Singh, M., Singh, S.K., Prakash, A., 2023. Influence of transplanting techniques and age of wash root type seedlings on planting attributes of paddy rice. Cogent Food Agric. 9 (1), 2176978. https://doi.org/10.1080/23311932.2023.2176978.

Tian, Y., Mai, Z., Zeng, Z., Cai, Y., Yang, J., Zhao, B., Zhu, X., Qi, L., 2023. Design and experiment of an integrated navigation system for a paddy field scouting robot. Comput. Electron. Agric. 214, 108336. https://doi.org/10.1016/j.compag.2023.108336.

Varela, S., Dhodda, P.R., Hsu, W.H., Prasad, P.V.V., Assefa, Y., Peralta, N.R., Griffin, T., Sharda, A., Ferguson, A., Ciampitti, I.A., 2018. Early-season stand count determination in corn via integration of imagery from unmanned aerial systems (UAS) and supervised learning techniques. Remote Sens. 10 (2), 343. https://doi.org/10.3390/rs10020343.

Vong, C.N., Conway, L.S., Zhou, J., Kitchen, N.R., Sudduth, K.A., 2021. Early corn stand count of different cropping systems using UAV-imagery and deep learning. Comput. Electron. Agric. 186, 106214. https://doi.org/10.1016/j.compag.2021.106214.

Wu, S., Chen, Z., Bangura, K., Jiang, J., Ma, X., Li, J., Peng, B., Meng, X., Qi, L., 2023. A navigation method for paddy field management based on seedlings coordinate information. Comput. Electron. Agric. 215, 108436. https://doi.org/10.1016/j.compag.2023.108436.

Wu, J., Yang, G., Yang, X., Xu, B., Han, L., Zhu, Y., 2019. Automatic counting of in situ rice seedlings from UAV images based on a deep fully convolutional neural network. Remote Sens. 11 (6), 691. https://doi.org/10.3390/rs11060691.

Yan, Z., Zhao, Y., Luo, W., Ding, X., Li, K., He, Z., Shi, Y., Cui, Y., 2023. Machine vision-based tomato plug tray missed seeding detection and empty cell replanting. Comput. Electron. Agric. 208, 107800. https://doi.org/10.1016/j.compag.2023.107800.

Yao, M., Lv, J., Wang, L., Yue, R., Hu, J., 2024. Cooperative operation method of seedling conveying and picking by full-automatic transplanter based on multi-sensor combination. Comput. Electron. Agric. 225, 109311. https://doi.org/10.1016/j.compag.2024.109311.

Journal of Electrical Engineering & Technology (2025) 20:5199–5214
https://doi.org/10.1007/s42835-025-02401-4

ORIGINAL ARTICLE

Analysis of Radial Electromagnetic Force in Claw Pole Alternator Considering Excitation Current Harmonics

Shuanglong Wu[1] · Xiangyu Yan[1] · Junda Yang[1] · Hailin Wang[2] · Hongmin Zhong[3] · Caixia Lin[1]

Received: 28 November 2023 / Revised: 29 July 2025 / Accepted: 7 August 2025 / Published online: 25 August 2025

Abstract

This paper presents a novel investigation into the impact of excitation current harmonics on the radial electromagnetic forces in electric excitation claw-pole alternators. First, the frequency and spatial order of the radial electromagnetic forces, considering excitation current harmonics, are analytically derived. To accurately determine the amplitudes of these forces, a three-dimensional finite element model is developed and validated through an indirect comparison with back-electromotive force (back-EMF) bench test. The study then simulates the radial electromagnetic forces, focusing particularly on the zero-order spatial components, which have the greatest influence on acoustic noise. Various excitation current harmonics, including different phase sequences, frequencies, and amplitudes, are incorporated into these simulations. The results show that even-order harmonics affect only the amplitude without introducing new major vibration sources, whereas odd-order harmonics can generate additional significant vibration sources. For a three-phase, 12-pole/36-slot claw-pole alternator, the 2nd, 3rd, and 6th current harmonics were found to have a significant impact on the amplitude of the radial electromagnetic forces. The 2nd harmonic with a negative phase sequence and the 3rd harmonic with a positive phase sequence effectively reduce the radial electromagnetic force, while the 6th harmonic (in both positive and negative phase sequences) increases it. The simulation analysis results were validated through vibration bench test. These findings provide crucial insights into the effects of excitation current harmonics on claw-pole alternators, offering a foundation for optimizing excitation current design to minimize unwanted vibrations and enhance performance. This study introduces a novel analytical framework and simulation methodology that could be applied to future advancements in motor and alternator design.

Keywords Claw-pole alternator · Excitation current · Current harmonic · Radial electromagnetic force

✉ Caixia Lin
cxllin@scau.edu.cn

Shuanglong Wu
zymwgl@foxmail.com

Xiangyu Yan
2021@stu.scau.edu.cn

Junda Yang
2856966590@qq.com

Hailin Wang
hlwang@scau.edu.cn

Hongmin Zhong
zhong_hongmin@foxmail.com

[1] College of Engineering, South China Agricultural University, Guangzhou, China

[2] Guangdong Polytechnic of Science and Trade, Guangzhou, China

[3] School of Automotive Studies, Tongji University, Shanghai, China

1 Introduction

Claw pole alternators are widely used in the modern automotive industry due to their simple manufacturing process, reliable construction, and low cost [1–3]. To fulfill the increasing power demands of onboard equipment, electric excitation claw-pole alternators are often designed with high electromagnetic loads, which cause annoying noise problems [4, 5]. The air-gap magnetic field in claw-pole alternators is generated by the excitation current in the rotor field winding. Consequently, harmonics in the excitation current influence the air-gap magnetic field and electromagnetic force, which ultimately affect the vibration and noise of the claw-pole alternators. Therefore, it is necessary to investigate the influence of excitation current harmonics on the radial electromagnetic force of the claw-pole alternator.

Until now, there is relatively little literature on the generation mechanisms of radial electromagnetic force in the claw-pole alternator. In [6], the characteristics of radial electromagnetic force generated by claw-pole alternators with different pole-slot combinations and phase numbers were analytically derived. In [7], a three-dimensional multiphysics finite element model incorporating electromagnetic, mechanical, and acoustic fields has been established and experimentally validated to predict the spatial order of the major radial force of a claw-pole alternator. In addition, factors such as temperature, assembly method, and stator winding faults can also affect the electromagnetic force and vibration of the claw-pole alternator [8–11]. The most notable of these papers is [11], which states that a short-circuit fault between turns in the stator winding changes the amplitude and phase of the stator current. As a result, the spatial order of the primary radial force of the claw-pole alternator is altered. Since the stator current is ultimately induced by the excitation current, it can be deduced that the amplitude and phase of the excitation current harmonics will have a corresponding influence on the radial electromagnetic force. However, all of the literature mentioned above assumed that the excitation current is the ideal direct current (DC), which ignored the potential influence of excitation current harmonics. This leads to a lack of robust theoretical support for methods of vibration damping by injecting current harmonics into the claw-pole alternators.

Meanwhile, extensive research has been carried out on the influence of different current harmonics on the radial electromagnetic force of motors. Liang et al. [12] pointed out that the air-gap magnetic field caused by the rotor current harmonics would excite additional radial force on the inner surface of the induction motor stator. Zhu et al. [13] investigated the distribution of electromagnetic force in switched reluctance motors (SRM) when excited by several current waveforms, pointing out that the electromagnetic vibrations are strongly related to stator current harmonics. Current harmonics have also been well-studied in permanent magnet synchronous motors (PMSM). By a combination of analytical and finite element methods, the influences of phase sequence, frequency, and stator winding arrangement on radial forces and vibrations are discussed in the paper [14–16]. In addition, the enhancement of the radial electromagnetic force by the combined effect of the current harmonics from the stator winding, the permanent magnets, and the slotting effect should also be carefully considered during the design of a permanent magnet synchronous auxiliary motor [17]. Once the mechanism of the influence of current harmonics on the radial electromagnetic force has been fully investigated, it is possible to suppress the target radial electromagnetic force by injecting harmonic currents of a specific phase and frequency. The method is widely used in the noise reduction of PMSM [18–21] and SRM [22–24]. Apparently, the topology of the motor has an impact on the category of current harmonics. The PMSM structure is isotropically symmetric, generating radial electromagnetic forces of even order, and only odd harmonics can be injected to reduce vibration. For example, the injection of the 7th current harmonic effectively reduced the amplitude of the 6th major radial force harmonic for an IPMSM under FOC control [18]. By contrast, the SRM has a relatively complex cogging structure, which generates a more varied distribution of radial electromagnetic forces on the frequency spectrum. To improve its noise performance, injection of integer-order current harmonics is then required. As in [23] and [24], different optimized current waveforms are proposed by injecting 1st-4th order current harmonics into the excitation DC, effectively weakening or even eliminating some of the lowest-order radial forces. Similarly, the claw-pole structure is asymmetrical in the axial direction, which induces complex radial electromagnetic force harmonics. Therefore, a detailed investigation of the harmonic order of the injected current is required. From the literature above, it can be noted that research on the influence of current harmonics on the radial electromagnetic force in motors is focused on: (a) investigating the influences of different current harmonics on radial forces by analytical or finite element methods, (b) reduction of radial electromagnetic force by injecting current harmonics of specific order and frequency. However, there is little literature available in the present study of radial electromagnetic forces in claw-pole alternators regarding the research points mentioned above. Therefore, the influence of the excitation current harmonics on the radial electromagnetic force of the electric excitation claw-pole alternator will be investigated. Compared to prior work that assumed ideal DC excitation, modeling radial forces in claw pole alternators considering non-ideal excitation with harmonics is novel and meaningful.

The content of this article is arranged as follows: in Sect. 2, the sources of excitation current harmonics are analyzed from the perspective of the claw-pole alternator operation process. In Sect. 3, an analytical derivation of the no-load radial electromagnetic force of the claw-pole alternator considering the excitation current harmonics is presented. For precisely calculating the radial electromagnetic force, a finite element model of the test prototype is developed in Sect. 4, the accuracy of which is verified by back-EMF bench test. In Sect. 5, the influence of the excitation current harmonics with different phase sequences, frequency, and amplitude on the radial electromagnetic force is investigated. Section 6 summarizes the conclusions of this paper.

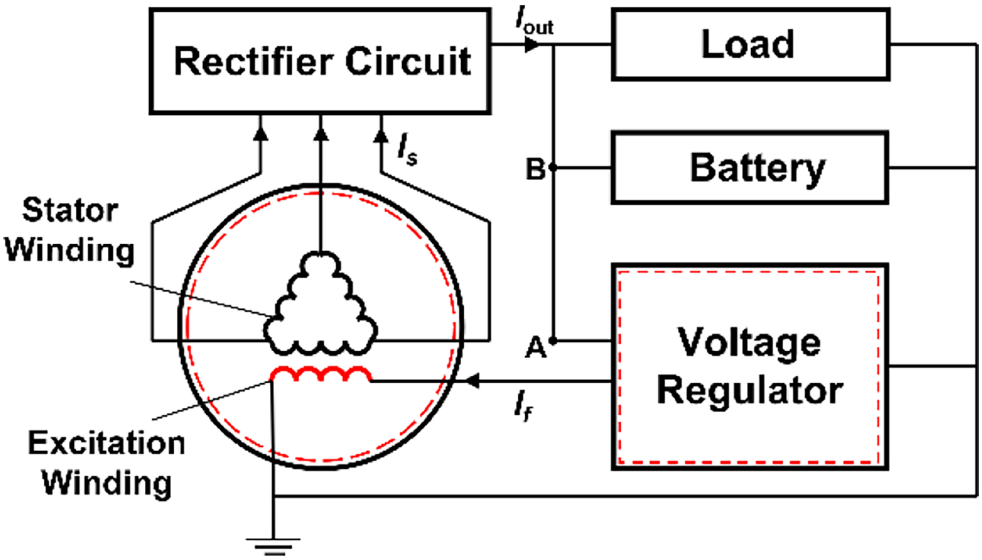

Fig. 1 Operating circuit of the electric excitation claw-pole alternators

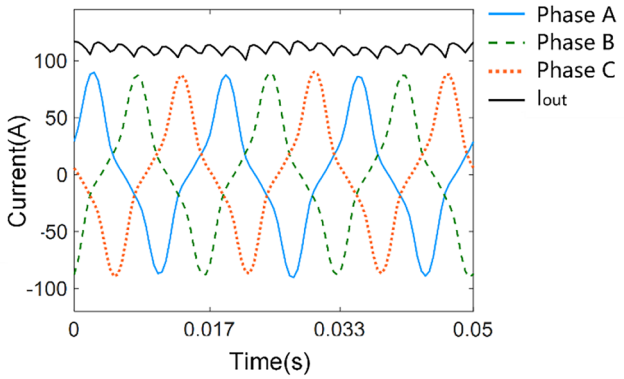

Fig. 2 Phase current and output current in self-excitation state

2 Sources of Excitation Current Harmonics

The three-phase 12-pole 36-slot electric excitation claw-pole alternator is a type of synchronous generator commonly used in vehicles, and its operating circuit is shown in Fig. 1. When the excitation current flows through the rotor field winding, a three-phase alternating current I_s (AC) is induced in the stator winding. The AC is rectified into DC. Then it supplies power to the onboard equipment and charges the battery.

The claw-pole alternator is separately excited (i.e., the excitation current I_f is mainly supplied by the battery) at the beginning of the vehicle start. As the motor speed increases, the output current I_{out} increases as well. When the voltage of point A exceeds the voltage of the battery, the battery stops supplying power and the claw-pole alternator enters a self-excited state. In such situations, the output current of the alternator is then controlled by the voltage regulator and becomes the sole source of excitation current.

The main component of the excitation current I_f is DC, but fluctuations and harmonics are inevitable. The primary reason for this phenomenon is the presence of non-ideal rectifier harmonics. Firstly, the excitation current directly derives from I_{out}. The rectifier utilizes the unidirectional conductivity of the switching device to achieve AC-DC conversion, which is essentially an approximate synthesis of DC waveforms with multiple sine wave harmonics. Secondly, the actual generator output current is not the ideal three-phase sinusoidal AC. This introduces an additional non-0sinusoidal component to the input of the rectifier, which ultimately acts on I_{out}. Figure 2 shows the output total current and phase current of a claw-pole alternator in the self-excitation state at a rotational speed of 2000 r/min. It can be seen that the output current fluctuates slightly around 110 A.

On the other hand, the voltage regulator also causes fluctuations in the claw-pole alternator output current. Since the onboard battery voltage is about 14 V, the relative stability of the generator output voltage at different rotor speeds needs to be guaranteed. The output voltage amplitude is proportional to the product of rotor speed and excitation current so the voltage regulators are installed to change the excitation current in real-time according to the rotational speed. The effect of speed variation is offset by changing the magnitude of the excitation flux. Figure 3 illustrates the dynamic regulation of the excitation current by the voltage regulators. When the rotational speed increases, the regulator will reduce its excitation. This in turn reduces the air-gap flux of the generator and vice versa.

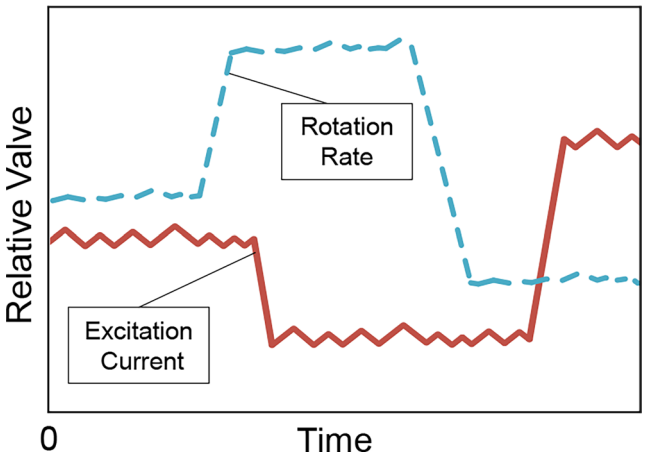

Fig. 3 Dynamic regulation of excitation current by the voltage regulator

3 Characteristics Analysis of Radial Electromagnetic Force Considering Excitation Current Harmonics

As it is mentioned earlier, the non-ideal characteristics of the rectifier circuit and the regulation of the excitation current by the voltage regulator will generate abundant current harmonics. The current harmonics distort the air-gap magnetic field, which consequently affects the radial electromagnetic force.

According to Maxwell's tensor method, the radial electromagnetic force (Maxwell tensor, not lumped forces) causing motor vibration can be expressed as Eq. (1) while ignoring tangential field, where μ_0 is the vacuum permeability and B_r is the radial air-gap flux density [25].

$$P_r \approx \frac{{B_r}^2}{2\mu_0} \tag{1}$$

Assuming that the influence of magnetic saturation and flux leakage on the amplitude of the air-gap magnetic field can be neglected. The B_r at no-load is obtained by multiplying the rotor magnet-motive force (MMF) by the air-gap permeability Λ [25], as shown in Eq. (2).

$$B_r = F_f \times \Lambda \tag{2}$$

Λ was introduced to indicate the influence of slotting on the air-gap magnetic field, which can be expressed by the Fourier series as Eq. (3) [25]. Q_s is the number of stator slots. Λ_0 represents the average value of air-gap permeability and Λ_k is the kth (k=1,2,3, …) air-gap permeability harmonic.

$$\Lambda = \Lambda_0 + \sum_k \Lambda_k \cos(kQ_s\theta) \tag{3}$$

Meanwhile, F_f is a function of the axial position z, as shown in Eq. (4):

$$F_f(\theta, z, t) = F_0 + \sum_{\mu=1} c_\mu \cos\left(\mu p\theta - \mu\omega_e t\right) \tag{4}$$

Where $\omega_e = p\omega_r$ is the angular frequency of the fundamental current. The mean value of the MMF F_0 and the μth harmonic scale factor of the MMF when the excitation current is DC can be expressed as Eqs. (5)-(6) [6]:

$$F_0 = \frac{N_f I_f}{4\tau_p}(b_{\mathcal{N}} - b_{\mathcal{S}}) \tag{5}$$

$$c_\mu = \frac{N_f I_f}{\mu\pi}[\sin(\mu\beta_{\mathcal{N}}\pi) + \varepsilon\sin(\mu\beta_{\mathcal{S}}\pi)] \tag{6}$$

In the equations, N_f is the number of turns of the rotor field winding, I_f represents the amplitude of the excitation current and τ_p is the pole pitch of the claw-pole alternator. b_{N} and b_{S} are equivalent pole-arc widths, β_{N}, and β_{S} are equivalent pole-arc coefficients, all four related to the axial position z. The constant factor ε is taken as 1 when μ is odd, otherwise, ε is taken as −1. Unlike the PMSM, the claw-pole alternator is axially asymmetric, so the F_0 is not zero; meanwhile, μ is an integer (the MMF of PMSM contains only odd harmonics), so the characteristics of air-gap magnetic field and radial electromagnetic force in the claw-pole alternator are more complex.

Substituting Eqs. (3)-(6) into Eq. (2), the no-load air-gap magnetic density $B_{I_{f,0}}$ at DC excitation is obtained, as shown in Eq. (7):

$$\begin{aligned} B_{I_{f,0}} = & B_0 + \sum_\mu B_\mu \cos(\mu p\theta - \mu\omega_e t) + \\ & \sum_\mu \sum_k B_{\mu,k} \cos[(\mu p \pm kQ_s)\theta - \mu\omega_e t] \end{aligned} \tag{7}$$

Where B_0 is the amplitude of the time-invariant magnetic field calculated by multiplying the mean value of the MMF with the Λ_0. For convenience, this magnetic field is designated as the fundamental magnetic field. B_μ denotes the amplitude of the magnetic field caused by the MMF harmonics, while $B_{\mu,k}$ represents the amplitude of the magnetic field due to the slotting effect.

$$
\begin{aligned}
P_r &\approx \frac{1}{2\mu_0}(B_{I_{f,0}})^2 \\
&= \frac{1}{2\mu_0}\left\{\begin{array}{l} B_0 + \sum_{\mu} B_{\mu} \\ \cos(\mu p\theta - \mu\omega_e t) \\ + \sum_{\mu}\sum_{k} B_{\mu,k} \\ \cos[(\mu p \pm kQ_s)\theta - \mu\omega_e t] \end{array}\right\}^2 \\
&= \frac{1}{2\mu_0}\left\{\begin{array}{l} {B_0}^2 + 2B_0 \sum_{\mu} B_{\mu}\cos(\mu p\theta - \mu\omega_e t) \\ + \sum_{\mu} B_{\mu_1}B_{\mu_2} \\ \cos[(\mu_1 \pm \mu_2)p\theta - (\mu_1 \pm \mu_2)\omega_e t] \\ + 2B_0 \sum_{\mu}\sum_{k} B_{\mu,k} \\ \cos[(\mu p \pm kQ_s)\theta - \mu\omega_e t] \\ + 2\sum_{\mu}\sum_{k} B_{\mu_1,k}B_{\mu_2} \\ \cos\left\{\begin{array}{l}[(\mu_1 \pm \mu_2)p \pm \\ kQ_s]\theta - (\mu_1 \pm \mu_2)\omega_e t\end{array}\right\} \\ + \sum_{\mu}\sum_{k} B_{\mu_1,k_1}B_{\mu_2,k_2} \\ \cos\left\{\begin{array}{l}[(\mu_1 \pm \mu_2)p \pm (k_1 \pm k_2)Q_s]\theta \\ -(\mu_1 \pm \mu_2)\omega_e t]\end{array}\right\} \end{array}\right\}
\end{aligned} \tag{8}
$$

As a control, in the next step, substitute Eq. (7) into Eq. (1) to calculate the radial electromagnetic force caused by the DC excitation, as shown in Eq. (8). To indicate the frequency and spatial order of the radial force, define the array as (*f*, *m*), where *f* is the frequency order of the radial force and *m* is the spatial order. The magnitude of the radial forces at higher orders can be ignored. Therefore, the main focus is on the radial electromagnetic forces with the spatial order of zero and the smallest non-zero order. The source, frequency, and spatial order statistics of the forces are shown in Table 1, where$\mu_1, \mu_2, k_1, k_2 \in N$. Each electromagnetic force source (each row) in Table 1 corresponds to one term in Eq. (8).

As shown in Table 1, there are two types of radial electromagnetic forces: $\left\{\begin{array}{c}(Kp, Kp) \\ (Mp, Mp \pm NQ_s)\end{array}\right.$ at DC excitation, where *K*, *M*, and *N* are non-zero integers.

For a three-phase 12-pole/36-slot claw-pole alternator, since $K \neq 0$, only (Mp, $Mp \pm NQ_s$) maybe a radial force with the spatial order of zero, which has a frequency of $\pm 36N$.

On the other hand, the lowest non-zero spatial order is noted as *T*. For (*Kp*, *Kp*), $T = 6$, the frequency is six times the rotational frequency. However, this frequency is much lower than the stator mode frequency under the low and middle rotation speeds. Let $Mp \pm NQ_s = T$, then $M = (T/6) \pm 6N$. As *M*, *N*, and *T* are all non-zero integers, $|T|$ has a minimum of six, corresponding to a radial electromagnetic force frequency of $36N \pm 6$. Therefore, the major radial forces under DC excitation of the three-phase 12-pole/36-slot claw-pole alternator are ($\pm 36N$, 0) as well as ($36N \pm 6$, 6). (6, 6) is less likely to cause resonance, although the amplitude is large.

When the excitation current harmonics are considered, the amplitude of the excitation current I_f in Eq. (5) and Eq. (6) will vary with time. Supposing that I_f consists of DC and the *v*th current harmonic (a similar approach can be extended to any number of current harmonics), then the excitation current becomes Eq. (9):

$$
I_f(t) = I_{f,0} + I_{f,\nu}\cos(\nu\omega_e t) \tag{9}
$$

Where $I_{f,0}$ is the DC amplitude and $I_{f,v}$ indicates the *v*th current harmonic amplitude.

By substituting Eq. (9) into Eqs. (7)-(6), the rotor MMF under the influence of current harmonics is calculated, which is noted as $F_f(\theta,z,t)$. The air-gap magnetic density caused by the *v*th current harmonic ($B_{I_{f,\nu}}$) is calculated by multiplying $F_f(\theta,z,t)$ with Eq. (3), as shown in Eq. (10). B_1-B_4 are the amplitudes of the different magnetic harmonics caused by the *v*th current harmonics. The source, frequency, and spatial order statistics of the radial electromagnetic force are shown in Table 2.

$$
\begin{aligned}
B_{I_{f,\nu}} = B_1\cos(\nu\omega_e t) + \sum_{k} B_2\cos(kQ_s\theta \pm \nu\omega_e t) + \\
\sum_{\mu} B_3\cos[\mu p\theta - (\mu \pm \nu)\omega_e t] + \\
\sum_{\mu}\sum_{k} B_4\cos[(kQ_s \pm \mu p)\theta - (\mu \pm \nu)\omega_e t]
\end{aligned} \tag{10}
$$

The total radial magnetic density is the sum of $B_{I_{f,0}}$ and $B_{I_{f,\nu}}$, as in Eq. (11).

Table 1 Radial electromagnetic force with DC excitation

Sources of force	Frequency	Spatial order
Fundamental magnetic field + MMF harmonic	μp	μp
Fundamental magnetic field + MMF harmonic + Slotting effect	μp	$\mu p \pm kQ_s$
MMF harmonic	$(\mu_1 \pm \mu_2)p$	$(\mu_1 \pm \mu_2)p$
MMF harmonic + Slotting effect	$(\mu_1 \pm \mu_2)p$	$(\mu_1 \pm \mu_2)p \pm (k_1 \pm k_2)Q_s$

Table 2 Main radial electromagnetic forces caused by the νth current harmonic

Source	Frequency	Spatial order
Fundamental magnetic field + Current harmonic	νp	0
Fundamental magnetic field + Current harmonic + MMF harmonic	$(\mu \pm \nu)p$	μp
Current harmonic + MMF harmonic	$(\mu_1 \pm \mu_2 \pm \nu)p$	$(\mu_1 \pm \mu_2)p$
Fundamental magnetic field + current harmonic +MMF harmonic+ Slotting effect	$(\mu \pm \nu)p$	$\mu p \pm kQ_s$
Current harmonic+ MMF harmonic +Slotting effect	$(\mu_1 \pm \mu_2 \pm \nu)p$	$(\mu_1 \pm \mu_2)p \pm (k_1 \pm k_2)Q_s$

$$B_r(\theta, z, t) = B_{I_{f,0}} + B_{I_{f,\nu}} \tag{11}$$

Finally, Eq. (7), Eq. (10), and Eq. (11) are substituted into Eq. (1) to calculate the radial electromagnetic force considering the excitation current harmonics. In the no-load case, $B_{I_{f,0}}$ is the dominant component of air-gap magnetic density for an electro-excited claw-pole alternator. Hence, the radial electromagnetic force generated by the νth current harmonic is derived mainly from the interaction between $B_{I_{f,\nu}}$ and $B_{I_{f,0}}$ (i.e. $B_{I_{f,0}} \times B_{I_{f,\nu}}$). The source, frequency, and spatial order of the newly generated electromagnetic force are summarized in Table 2.

Table 2 illustrates the influence of the νth current harmonic on the radial electromagnetic force harmonics. Firstly, an additional radial force harmonic with the spatial order of zero is generated. Secondly, the original radial electromagnetic force $\begin{cases} (Kp, Kp) \\ (Mp, Mp \pm NQ_s) \end{cases}$ is shifted $\pm\nu p$ in the frequency spectrum, which can be described as $\begin{cases} (Kp \pm \nu p, Kp) \\ (Mp \pm \nu p, Mp \pm NQ_s) \end{cases}$. For the three-phase, 12-pole/36-slot claw-pole alternator, new radial forces (36N, 6) and (36N ±6, 0) will appear while ν=6N ±1, and the original radial force (36N, 0) is enhanced while ν=6N. When ν=1, (36N ±6, 6) is enhanced. These new radial electromagnetic force harmonics with low spatial order will have a significant effect on vibration.

4 Computation Model of Radial Electromagnetic Force Considering Excitation Current Harmonics

The spatial order and frequency of the radial electromagnetic force generated by the current harmonics at no-load have been analyzed in Sect. 3. However, the amplitude of the radial electromagnetic force cannot be accurately calculated by the analytical method due to the flux leakage and magnetic saturation effects. Meanwhile, additional stator currents are induced by the excitation current harmonics under load conditions. These stator current harmonics are difficult to model mathematically. Hence, the magnitude of the electromagnetic force at load can hardly be calculated precisely using the analytical method described above. Therefore, a 3-D finite element model is established in this paper. The current harmonics of specific order are injected by defining the excitation current for the rotor in the simulation software. Then the radial electromagnetic force amplitude changes caused by the current harmonics are calculated and analyzed. To simplify the modeling process, the 3-D finite element simulation is performed in current driven mode rather than in circuit coupling mode. In current driven mode, the excitation current is completely equal to the given current, without considering the influence of the physical characteristics of the voltage regulator itself and the influence of different battery voltages, nor the influence of current harmonics on itself through circuit coupling.

Figure 4 shows the stator and rotor structure of the electromagnetic simulation model of a three-phase 12-pole/36-slot electric excitation claw-pole alternator. The relevant parameters are shown in Table 3. During the operation of the claw-pole alternator, the voltage regulator applies a DC field current (containing current harmonics) to the field winding through carbon brushes and slip rings. When the field current flows through the ring-shaped field winding, the magnetic flux in the air gap is produced. As the rotor is turned by the belt, the rotor magnetic field cuts the stator winding, and a three-phase alternating current is generated in the stator windings. Considering the circumferential symmetry of the claw-pole alternator, a 1/6 3-D finite element model is employed as an example of the calculation [26], as shown in Fig. 5. In the finite element model, only four components need to be defined their materials, in which the stator winding and the rotor field winding are copper, the stator core and rotor claw-poles are silicon steel.

It is difficult to measure tmodel unchanged, the excitation current distribution on the inner surface of the claw-pole alternator stator. Therefore, the accuracy of the current and electromagnetic force simulations is verified by measuring the back-EMF. The reverse driving method was used to measure the back-EMF of the test prototype at an excitation current of 3 A and a rotation speed of 1500 r/min. The layout of the test system is illustrated in Fig. 6. In the experiment, the claw-pole

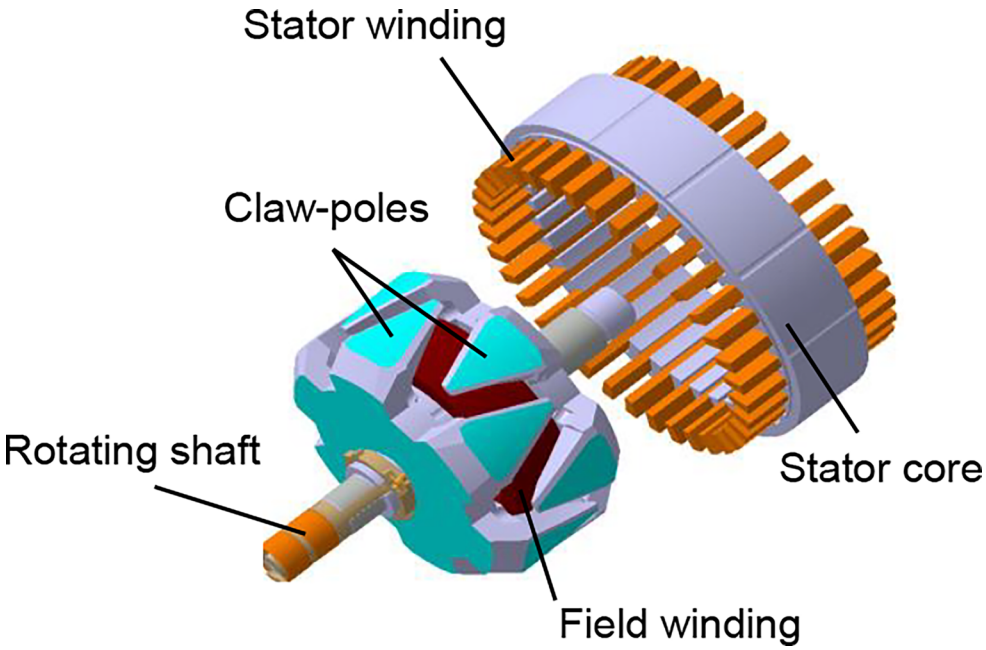

Fig. 4 Claw-pole alternator structural model

Table 3 Main parameters of the claw-pole alternator

Parameter	Value
Number of rotor pole pairs p	6
Number of stator slots Q_s	36
Stator inner diameter R (mm)	49.5
Rotor outer diameter r (mm)	49.175
Slot width b_0 (mm)	3.07
Air-gap length g (mm)	0.325
Air-gap at chamfer g' (mm)	0.929
Circumferential angle corresponding to the chamfer δ (rad)	0.0313
Rotor pole jaw length L (mm)	23.65
Rotor pole jaw tip width b_1 (mm)	6
Rotor pole jaw root width b_2 (mm)	26.1
Number of turns of rotor excitation windings N_r	355
Number of turns per slot of stator winding N_s	9
DC component of the excitation current $I_{f,0}$ (A)	4
Rated rotor speed (r/min)	6000
Rated power (kw)	1.54
Rated output current (A)	110

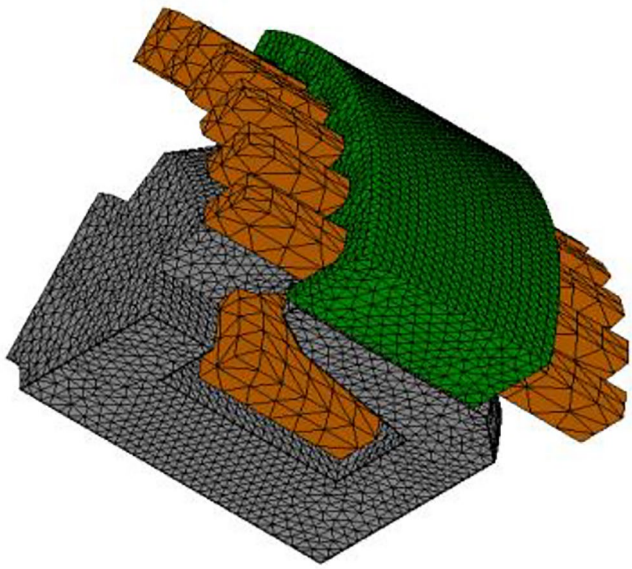

Fig. 5 1/6 3-D finite element model of claw-pole alternator

Fig. 6 Experimental system to measure the back-EMF

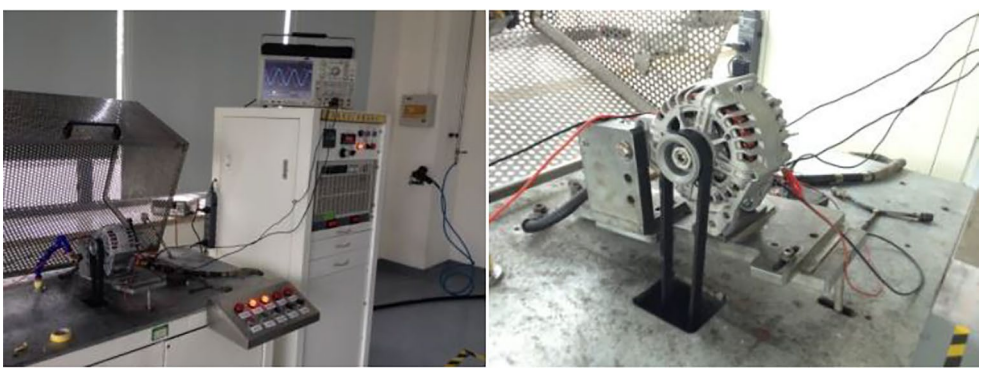

alternator is fixed on a bench. After disconnecting its rectifier circuit, an external power supply is employed to provide 3 A DC power to the rotor field winding. An induction motor drags the rotor of the alternator to provide a fixed speed of 1500 r/min. The speed of the claw-pole alternator is measured by a photoelectric speed sensor, and the induced EMF at the ends of the phase windings is measured by an oscilloscope. The test results obtained and the calculations of the finite element model, as shown in Fig. 7, generally coincide, which indirectly indicates that the model can precisely calculate the current amplitude and radial electromagnetic forces.

Keeping the structural parameters of the finite element model unchanged, the excitation current with the νth current harmonic is artificially defined as in Eq. (12):

$$If(t) = If,\ 0 + \delta If,\ \nu \cos(\nu p\omega rt)\ (\delta = \pm 1) \tag{12}$$

The coefficient δ reflects the phase sequence of the harmonics: when δ=1, it means the harmonics are in a positive phase sequence, otherwise they are in a negative phase sequence. Current harmonics with a frequency of 1p to 6p times the rotational speed are injected into the excitation DC. This is because the amplitude of the current harmonics at higher frequencies is so small that the influence on the electromagnetic force is almost negligible.

Since the air-gap magnetic density and radial force of the claw-pole alternator are related to the axial offset z. Therefore, the axial order is introduced when the Fourier decomposition of the results obtained from the simulation is performed.

5 Influence of Excitation Current Harmonics on Radial Electromagnetic Force of Claw-Pole Alternator

From the analysis in Sect. 3, it is known that the main radial electromagnetic forces of the three-phase 12-pole/36-slot claw-pole alternator under DC excitation are (f=36N, m=0) and (f=36N±6, m=6) at no-load. Meanwhile, the current harmonics induced (f=36N, m=6) and (f=36N±6, m=0) additionally. Considering that only radial forces with low axial spatial order cause significant vibration, the effect of current harmonics on the electromagnetic force of (f=30,36,42, m=0,6, n=0,1) is investigated.

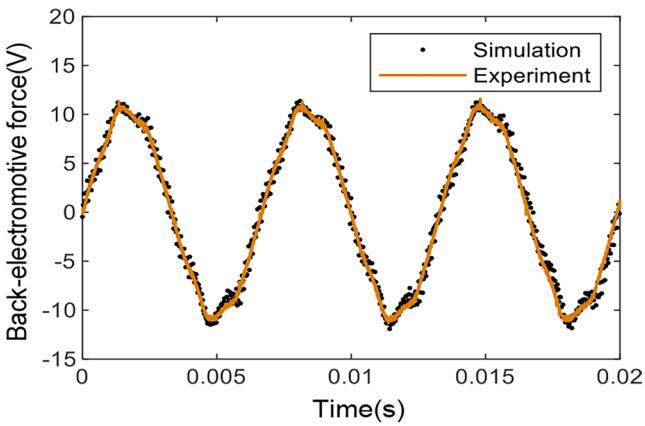

Fig. 7 Back-EMF at no-load

When the excitation current is DC, the Fourier transform is done in circumferential and axial directions for the radial electromagnetic force of f=30,36,42. As is shown in Fig. 8, the f=36 radial force at DC excitation is dominated by the electromagnetic force with the circumferential spatial order of zero (m=0); Meanwhile, the electromagnetic force of m=6 dominates the f=36N±6 radial electromagnetic force. This phenomenon coincides with the analysis in Sect. 3: at no load, there is theoretically no radial force of (f=36N, m=6) and (f=36N±6, m=0).

The influence of excitation current harmonics with different phase sequences, frequencies, and amplitudes on the low spatial order radial electromagnetic force is studied below.

Keep the excitation DC at 4 A and inject an even-order current harmonic with an amplitude of 1 A. The effect of even-order harmonic injection on the harmonic amplitude of the low-order radial electromagnetic force is shown in Table 4. The array (f, m, n) is redefined to describe the characteristics of the radial force. Where f is the radial force frequency order, m is the circumferential spatial order, and n is the axial spatial order. For instance, (36,6,1) represents the radial electromagnetic force harmonics with a frequency of 36 times the fundamental frequency, the circumferential spatial order of 6, and the axial spatial order of 1. The first 1–6 rows of Table 4 show the six major radial electromagnetic forces that contribute most to the electromagnetic vibration of the three-phase 12-pole/36-slot claw-pole alternator under DC excitation. ↑↓ represent their amplitude fluctuations of more than 15%. The remaining forces (rows 7–12) have an amplitude of no more than 30% of the main radial electromagnetic force under DC excitation. Hence only in the case of amplitude fluctuations exceeding 50% is it considered that it starts to have a significant impact on the total radial electromagnetic force amplitude.

The most striking aspect of Table 4 is the effect of the 6th (v=6) current harmonic on the amplitude of the electromagnetic force in rows 1–6. These radial forces originally act as the primary source of vibration, so changes in their amplitude can greatly affect the total radial electromagnetic force in the claw-pole alternator. The rate of change of the main radial force amplitude under the influence of the 6th current harmonic is calculated and collated to obtain Fig. 9.

As Fig. 9 illustrates, except for a relatively obvious weakening effect on (42,6,1), the 6th current harmonic with positive phase sequence dramatically strengthens the electromagnetic force of both (f=36, m=0, n=0,1) and (f=30,

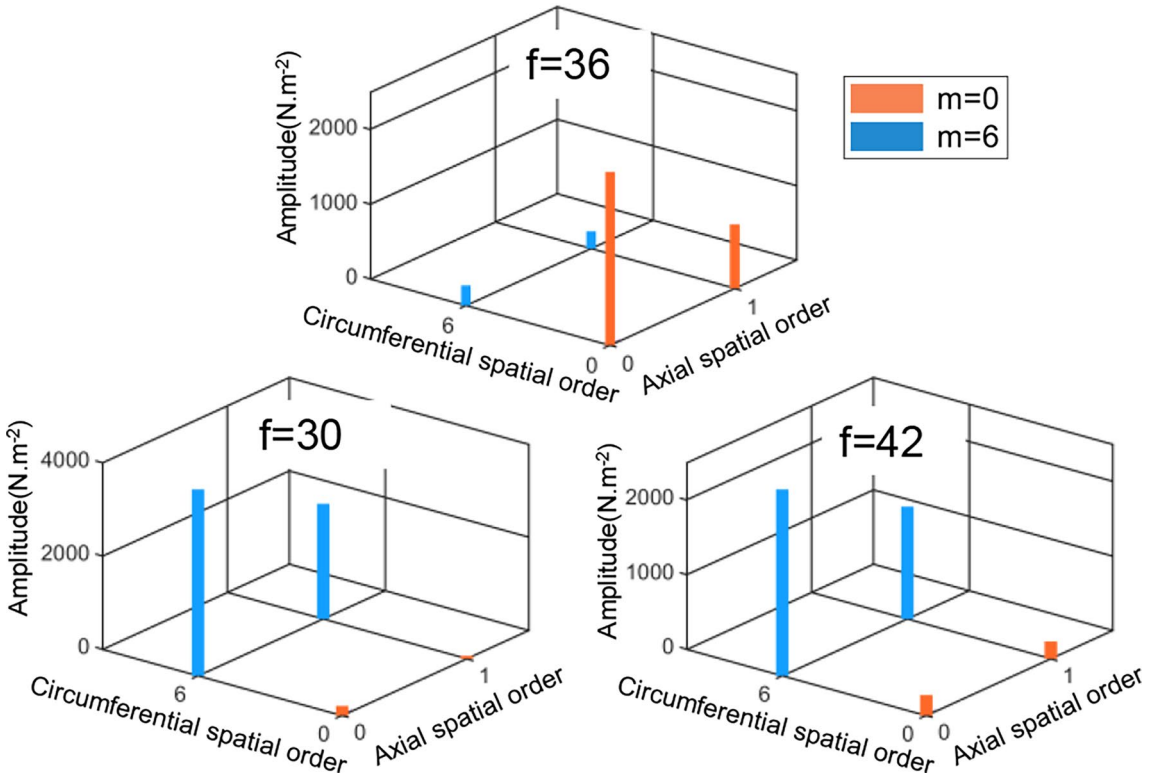

Fig. 8 Radial electromagnetic force under DC excitation

Table 4 Influence of even-order current harmonics on the amplitude of low-order radial electromagnetic force

Force harmonics	Amplitude ($N.m^{-2}$)						
	Initial	2nd	-2nd	4th	-4th	6th	-6th
(30,6,0)	4840	-	-	-	-	5738↑	3599↓
(30,6,1)	2477	2615	2087↓	3030↑	1958↓	2913↑	2184
(36,0,0)	2320	-	-	-	-	3321↑	1733↓
(36,0,1)	857.6	-	-	-	-	2962↑	1519↑
(42,6,0)	2524	-	-	-	-	-	-
(42,6,1)	1508	1896↑	1002↓	-	-	804.2↓	2321↑
(30,0,0)	204.5	-	-	-	-	332.1↑	149.3
(30,0,1)	67.41	-	-	-	-	39.26↓	68.93
(36,6,0)	264.8	-	-	-	-	-	-
(36,6,1)	236.8	-	-	57.71↓	92.83↓	124.8↓	117.2↓
(42,0,0)	277.1	-	-	-	-	-	-
(42,0,1)	233.2	-	-	272.3	80.28↓	226.3	108.5↓

Note: "-" represents the insignificant change in amplitude

$m=6$, $n=0,1$). Among them, the radial force (36,0,1) is enhanced by up to 245%. The 6th current harmonic with a negative phase sequence also causes a sharp increase in (36,0,1) and (42,6,1), although it can weaken some of the harmonics. Combined with the analysis in Sect. 3: the increase in ($f=36$, $m=0$, $n=0,1$) is due to the 6th harmonic interacting with the fundamental magnetic field to produce a new radial force with the spatial order of zero (Table 2, row 1, $v=6$). The rise in ($f=30$, $m=6$, $n=0,1$) is then caused by the 6th current harmonic in combination with the fundamental magnetic field, MMF harmonics, and permeability harmonics (Table 2, row 4, eg. $v=6$ $\mu=11$ $k=2$). Simultaneously, the changes at ($f=42$, $m=6$, $n=0,1$) are explained by the interaction of the 6th current harmonic with the fundamental wave of the MMF shifting the radial force ($f=6$, $m=6$) towards the higher frequency region (Table 2, row 3, $v=6$ $\mu=1$). Therefore, the 6th current harmonic, regardless of positive or negative phase sequence, trigger a significant increase in the original major radial electromagnetic forces and is a hazardous harmonic.

Notice that, in Fig. 9, the radial electromagnetic force amplitude changes in the opposite direction for all five

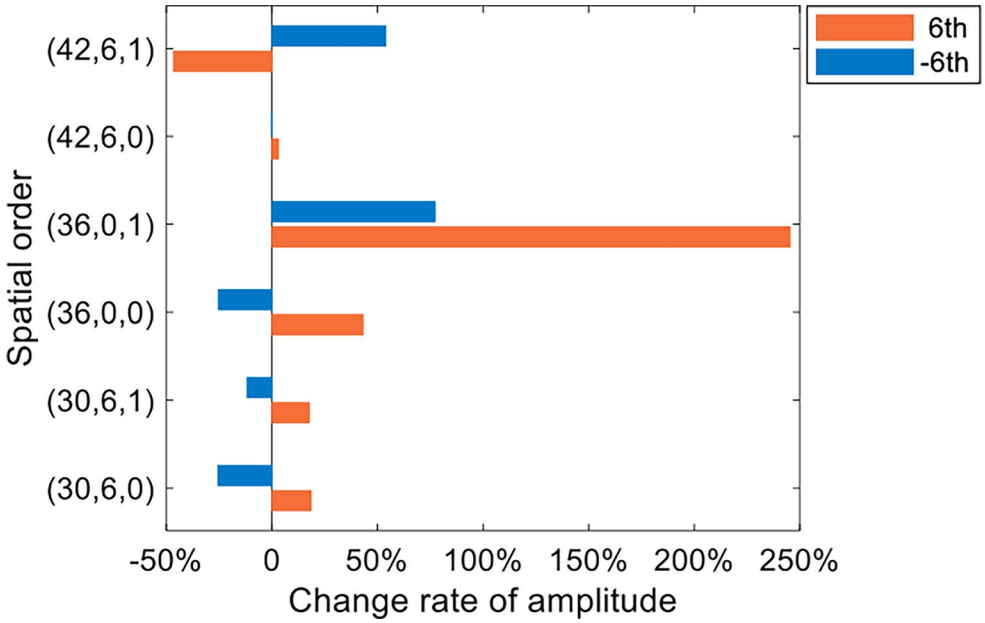

Fig. 9 Influence of the 6th harmonic on the main radial electromagnetic force of the prototype

Table 5 Influence of even-order current harmonics on the amplitude of low-order radial electromagnetic force

Force harmonics	Amplitude ($N.m^{-2}$)						
	Initial	1st	-1st	3rd	-3rd	5th	-5th
(30,6,0)	4840	-	-	-	-	-	-
(30,6,1)	2477	-	-	-	-	-	-
(36,0,0)	2320	-	-	-	-	-	-
(36,0,1)	857.6			613.4↓	598.9↓	718.5↓	926.9
(42,6,0)	2524	-	-	-	-	-	-
(42,6,1)	1508	-	-	-	-	-	-
(30,0,0)	204.5	293.4↑	187	-	-	2708↑	2514↑
(30,0,1)	67.41	12.19↓	72.64	-	-	1063↑	1132↑
(36,6,0)	264.8	703.1↑	568.9↑	-	-	1142↑	1213↑
(36,6,1)	236.8	425.7↑	465.8↑	132.4↓	136.5↓	344.8↑	1058↑
(42,0,0)	277.1	83.3↓	377.9				
(42,0,1)	233.2	71.56↓	207.1	51.47↓	149.2	153.9	135.9↓

groups except for (36,0,1), after the 6th harmonic of the injected current is inverted. Recalling Table 4, the 4th current harmonic with positive phase sequence enhances (30,6,1) by 18.3%, and the 4th current harmonic with negative phase sequence will weaken the (30,6,1) amplitude by 30.0%; a similar effect is observed for the 2nd current harmonic on (30,6,1) and (42,6,1). Hence, it can be deduced that the influence of the even-order current harmonics on the main radial electromagnetic force (Table 4, rows 1–6) is phase sequence-related. In particular, if an even-order current harmonic with a positive phase sequence boosts a radial electromagnetic force, injecting it in reverse will significantly reduce its enhancement of that force, or even weaken it, and vice versa.

Finally, rows 7–12 in Table 4 illustrate that the radial electromagnetic force does not change significantly after the injection of even-order harmonics (In addition to the slight enhancement of the positive-phase 6th current harmonic to (30,0,0). (36,6,1) is extensively suppressed by the even-order current harmonics (Table 4, row 10), where the positive-phase 4th current harmonic weakens this electromagnetic force by up to 310%. This indicates that the even-order current harmonics do not generate the new major source of vibration.

Similarly, the effect of odd-order current harmonics on the lower spatial order radial electromagnetic force amplitudes is shown in Table 5, which shares the format of Table 4.

From Table 5, the influence of the odd-order current harmonics on the radial electromagnetic force is concentrated in rows 7–12. The contribution of these forces to the vibration is relatively small when the DC excitation is applied. The 5th and 1st current harmonics have the most noticeable effect on the enhancement of radial forces.

Figure 10 illustrates the effect of the 5th current harmonic on the radial electromagnetic force of $f=30$. It is clear that

the radial forces (30,0,0) and (30,0,1), respectively, are only 8.2% and 2.72% of the magnitude of the main radial force (30,6,1) with DC excitation. However, after the 5th current harmonic with positive phase sequence was injected, the amplitudes of (30,0,0) and (30,0,1) increased by 1224 and 1477%, respectively. At this point, the amplitude of (30,0,0) exceeds that of (30,6,1) and the amplitude of (30,0,1) reaches 50% of that of (30,6,1), which means that their effect on vibration is no longer negligible. This suggests that certain odd-order current harmonics will cause a new major source of vibration.

The phenomena identified above can also be explained by the analysis in Sect. 3. The increase in (f=30, m=0, n=0,1) is a result of the newly induced radial force whose spatial order is zero, which is generated by the interaction of the injected 5th current harmonic with the fundamental magnetic field (Table 2, row 1, v=5). Similarly, the enhancement of the amplitude of (f=36, m=6, n=0,1) (Table 5, rows 9–10) by the 5th and 1st current harmonics is attributed, respectively, to (a) The 5th current harmonic reacts with two MMF harmonics of (μ_1-μ_2=1), causing a frequency shift in the radial force (f=6, m=6) (Table 2, row 3, v=5 μ_1=2 μ_2=1); (b) The combined interaction of the 1st current harmonic with the fundamental magnetic field, the MMF harmonic and the slotting effect cause a frequency shift in the radial force (f=30, m=6) (Table 2, row4, v=1 μ=5 k=1).

In addition, as shown in Fig. 10, the 5th harmonics with both the positive and negative phase sequence induce an increase in (f=36, m=6, n=0,1). Many more similar cases can be observed in Table 4. For example, the 3rd current harmonics with positive phase sequence weaken (36,0,1) and (36,6,1) (Table 5, rows 4,10) by 28.5% and 44.1% respectively, while the 3rd order harmonic with negative phase sequence also reduces both radial electromagnetic forces by 30.2% and 42.4% individually, with no significant change in trend or magnitude. Hence, it can be deduced that the influence of the odd-order current harmonics on electromagnetic force is phase sequence-free. Specifically, if an odd-order excitation current harmonic diminishes a radial electromagnetic force, then its inversion will still have a weakening effect on that force, and vice versa.

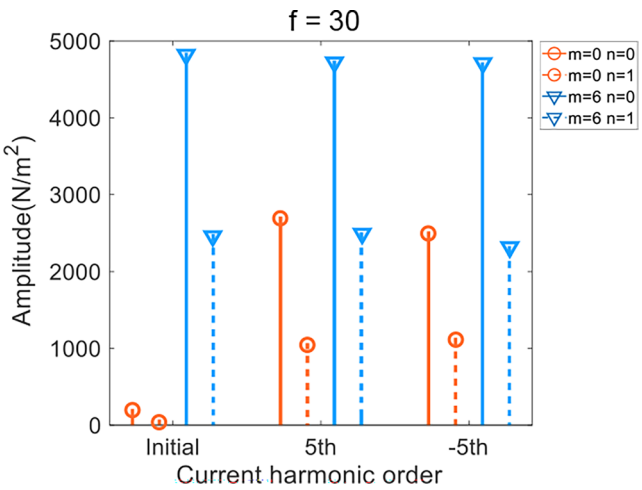

Fig. 10 Variation of radial electromagnetic force (f=30) amplitude before and after 5th harmonic injection

From Tables 4 and 5, it can be observed that: the 3rd current harmonic with positive phase sequence and the 2nd current harmonics with negative phase sequence reduce one of the main low spatial order electromagnetic forces (Table 4, Table 5, rows 1–6) by more than 25% and suppress other electromagnetic forces, which are beneficial harmonics. The 6th harmonic will, on the other hand, increase the amplitude of at least two of the main radial electromagnetic force and is therefore a hazardous harmonic. Hence, the three current harmonics mentioned above are used as examples to investigate the influence of the harmonic amplitude on the radial electromagnetic force.

Set the DC component of the excitation current to 4 A. For the 2nd current harmonic with negative phase sequence and the 3rd current harmonic with positive phase sequence, their amplitudes range are set to 0–4 A. Considering that the 6th current harmonic with an amplitude of 1 A would then drastically increase the amplitude of the main electromagnetic force, such as (36,0,1), the amplitude of such harmonics is limited to 0–1 A.

Figure 11 illustrates that, as the amplitude of the 2nd current harmonic with negative phase sequence increases, the electromagnetic force harmonics (30,6,0), (30,6,1), and (42,6,1) are approximately linearly decreased. For each 1A increase in harmonic amplitude, the corresponding electromagnetic force is diminished by 20% to 33%. Meanwhile, the electromagnetic force harmonics (36,0,0) and (36,6,0) are also weakened as the amplitude of the 2nd harmonic increases, with no appreciable change in the remaining electromagnetic force. Consequently, the ability of the inverse 2nd harmonic to weaken the radial electromagnetic force is positively related to its amplitude.

From Fig. 12, it can be seen that the sum of f=36 electromagnetic force is lowest when the amplitude of the 3rd current harmonic is injected up to half of the DC amplitude, which is only 58% of that before injection. However, when the current harmonic amplitude reaches 75% of the DC (3A), the total electromagnetic force for f=36 increases instead. The f=36±6 electromagnetic force is affected similarly, only if the harmonic amplitude is less than 25% of the DC will it ensure that the total radial forces do not rise after injection. Therefore, there exists an optimum amplitude of the 3rd current harmonics to weaken the radial electromagnetic force. In actual excitation currents, the harmonic amplitude generally does not exceed 15% of the DC. Within

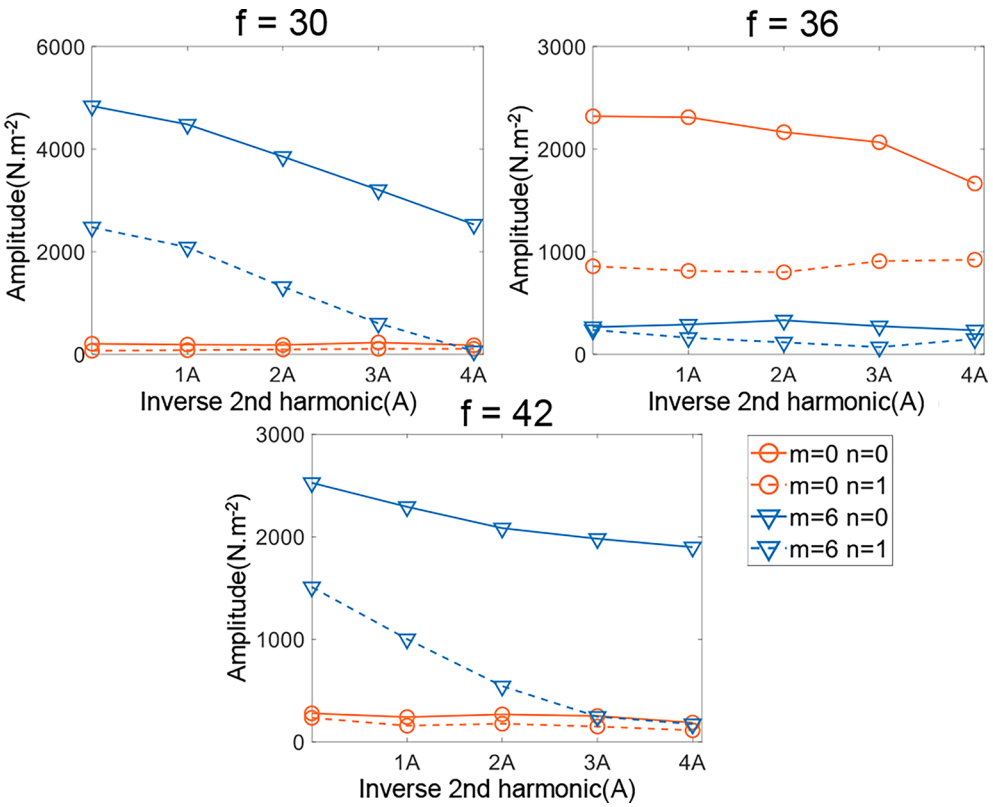

Fig. 11 Influence of the 2nd current harmonic with negative phase sequence on radial electromagnetic forces

this range, the 3rd current exhibits an overall suppression effect on electromagnetic force.

Notice that the 3rd harmonic is an odd-order harmonic. As the harmonic amplitude increases, the radial electromagnetic force (36,6,0) continues to increase and eventually replaces the original (36,0,1) as the new dominant vibration source. This is consistent with the conclusions drawn above.

As shown in Fig. 13, the amplitudes of both force harmonics (f=30, m=6, n=0,1) and (f=36, m=6, n=0,1) increase approximately linearly with the 6th current harmonic amplitude, except for (42,6,1) which is weakened. The (36,0,1) increases most dramatically, with each 0.25A rise in harmonic amplitude causing a 60% increase in radial force amplitude over that before injection. Thus, increases in the amplitude of the 6th current harmonic show an overall enhancement of the electromagnetic force.

To verify the accuracy of the simulation analysis results, vibration testing of the claw-pole alternator was conducted under varying excitation current conditions. The alternator was first secured to the test bench, with an asynchronous motor driving the rotor via a belt. A DC power supply was connected to the rotor's excitation windings to provide power, allowing for adjustments to the excitation current. To match the simulation setup, the DC component of the excitation current was set to 4A, and the amplitude of the harmonic current was set to 1A. A vibration accelerometer was then attached to the surface of the claw-pole alternator housing, as shown in Fig. 14(a). Figure 14(b) presents the vibration acceleration spectrum at a rotor speed of 6000 r/min under different excitation currents. As illustrated, the introduction of the 2nd harmonic current with a negative phase sequence significantly reduces the vibration amplitude at 3000 Hz, 4200 Hz, 6600 Hz, and 7800 Hz, while also attenuating vibrations at 3600 Hz and 7200 Hz to some extent. Conversely, the introduction of the 6th harmonic current with a positive phase sequence increases the vibration amplitude at these frequencies, particularly at 3600 Hz and 7200 Hz, which aligns with the simulation analysis results.

From the analysis above, it is clear that specific current injection can suppress radial electromagnetic force. The influence of the current harmonics on the output current of the claw-pole alternator is then studied below. To prevent overloading of the circuit, the amplitudes of the injected harmonics are generally low. Hence, the DC component of the excitation current is set to 4 A and the current harmonic amplitude is limited to 1 A. The variation of the output current amplitude with the order and phase sequence of the current harmonics is shown in Fig. 15, where 'Initial' indicates that the excitation current is DC.

From Fig. 15, when the amplitude of the current harmonics reaches 25% of the DC, the 1st current harmonic has the strongest amplitude attenuation effect on the output current

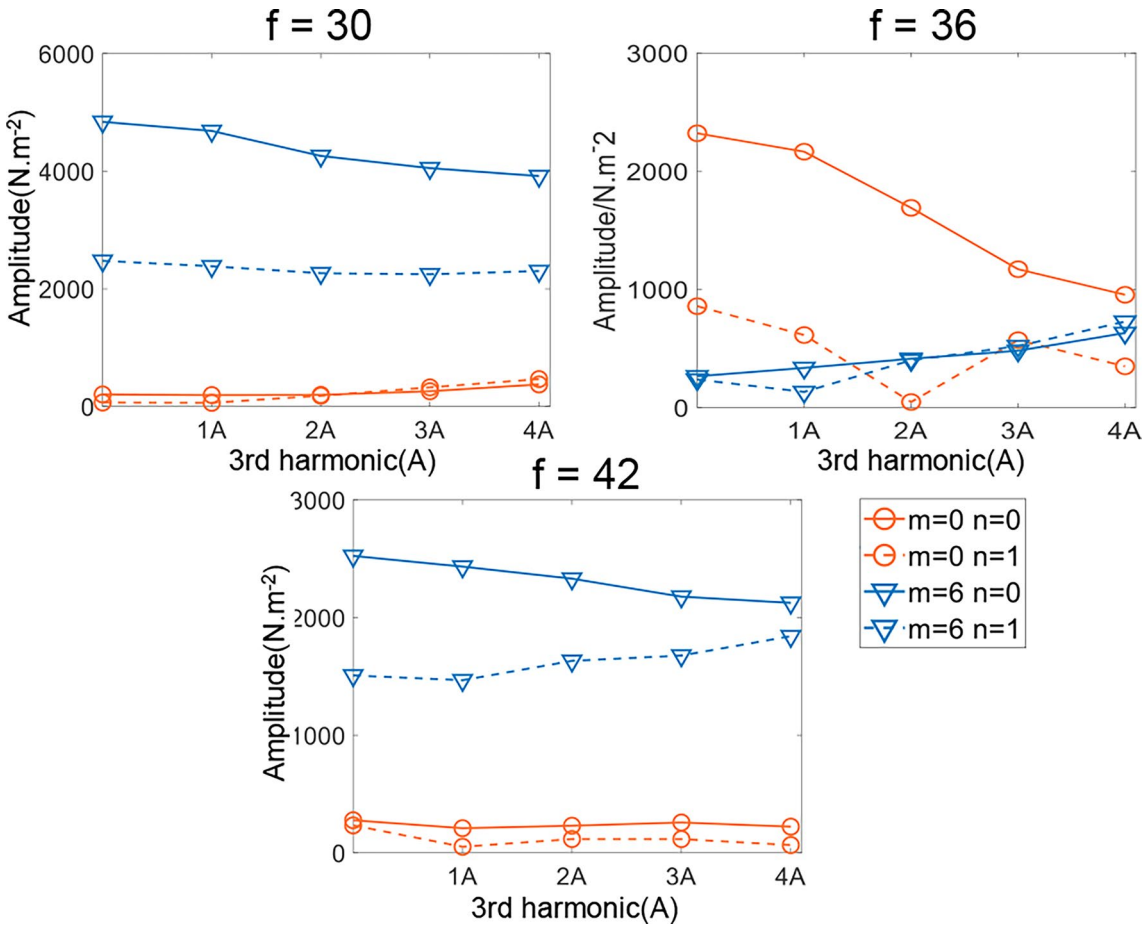

Fig. 12 Influence of the 3rd current harmonic with positive phase sequence on radial electromagnetic forces

(−2.2%), while both the 2nd and the 3rd current injection cut the output current by about 1.5%. Therefore, it can be assumed that the current harmonics with small amplitudes do not cause a significant deterioration in the power generation performance of the claw-pole alternator.

6 Conclusion

In this study, the influence of excitation current harmonics on the radial electromagnetic forces of electric excitation claw-pole alternators was systematically examined. A novel analytical framework was developed to derive the frequency and spatial order of the radial electromagnetic forces considering excitation current harmonics. Additionally, a comprehensive simulation was performed on the zero-order spatial components of the radial electromagnetic forces, taking into account various types of excitation current harmonics with different phase sequences, frequencies, and amplitudes. The underlying influence mechanism of these harmonics on the electromagnetic forces was thoroughly explored. The simulation analysis results were validated through vibration bench test. Based on the results, the following key conclusions are drawn:

(a) The frequency and phase sequence of excitation current harmonics significantly affect the amplitude of the radial electromagnetic force, with distinct impacts observed for different harmonic orders.
(b) Even-order current harmonics do not generate new major sources of vibration but only modulate the amplitude of existing vibrations. In contrast, odd-order current harmonics induce new major sources of vibration, thereby influencing the vibration characteristics more profoundly.
(c) Specifically, the 2nd current harmonic with a negative phase sequence and the 3rd current harmonic with a positive phase sequence can effectively reduce the radial electromagnetic force, whereas the 6th current harmonic, regardless of phase sequence, enhances the electromagnetic force.

These findings present a novel perspective on the interaction between excitation current harmonics and radial

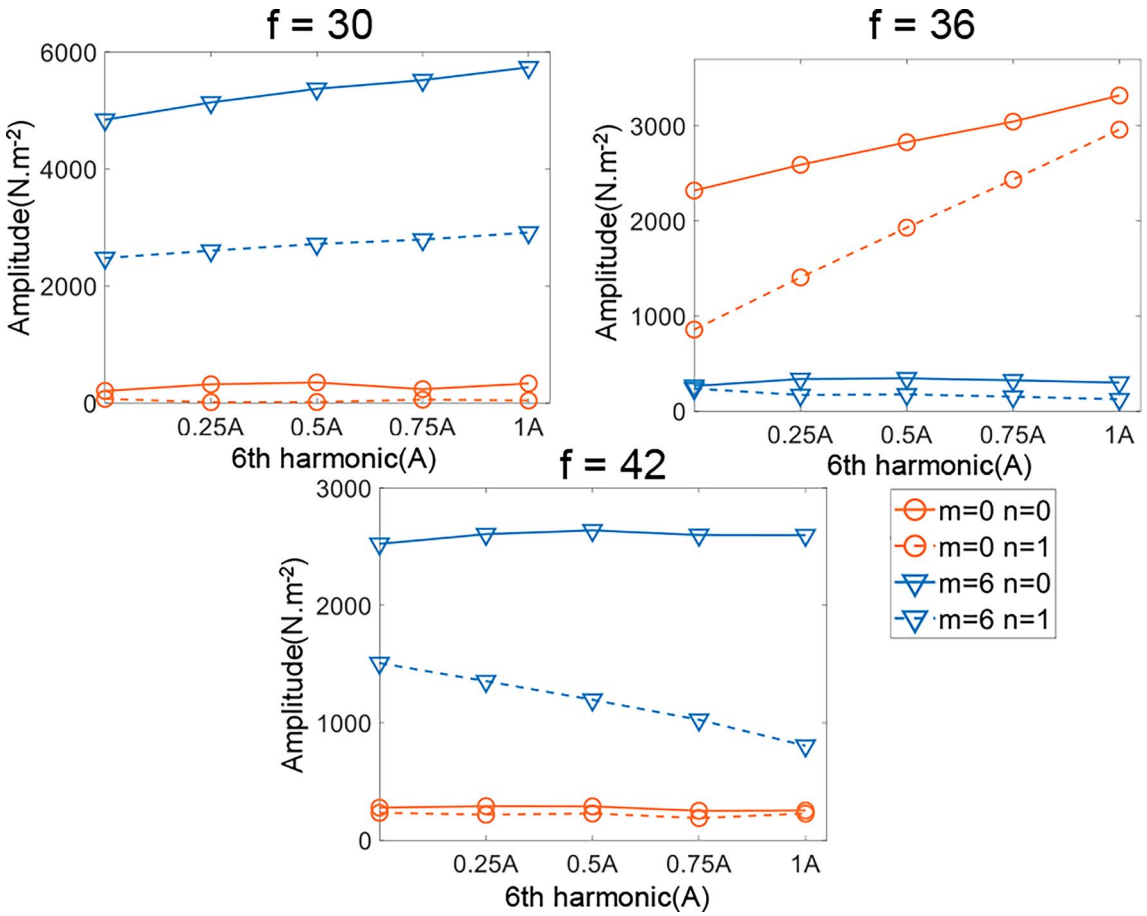

Fig. 13 Influence of the 6th current harmonic with positive phase sequence on radial electromagnetic forces

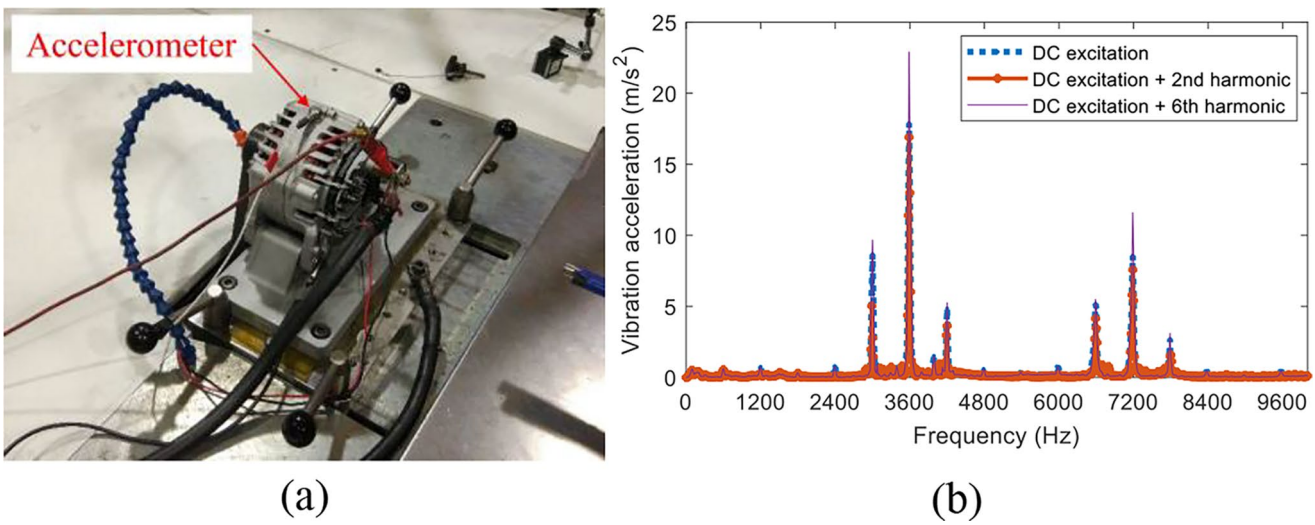

Fig. 14 Vibration testing of claw pole alternator under different excitation currents. (**a**) experimental setup. (**b**) test result

electromagnetic forces in claw-pole alternators, providing valuable insights for optimizing alternator design to mitigate unwanted vibrations. Future work could focus on further investigating the harmonic characteristics of the output current from the voltage regulator at varying battery voltages or rotor speeds, as well as exploring the coupling effects of multiple current harmonics on electromagnetic forces. This study opens new avenues for enhancing the performance and efficiency of claw-pole alternators by addressing the impact of current harmonics on their operational dynamics.

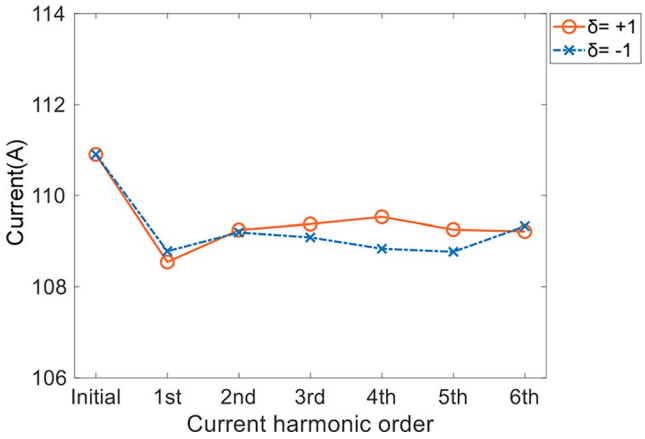

Fig. 15 Influence of different current harmonics on the output current

Acknowledgements This work was supported in part by the National Natural Science Foundation of China (No. 52205102), the Guangdong Basic and Applied Basic Research Foundation (No. 2023A1515011872) and the Science and Technology Program of Guangzhou (No. 2023A04J0958).

Declarations

Competing interests The authors declare that they have no competing financial interests or personal relationships that could have appeared to influence the work reported in this paper.

References

1. Boldea I, Tutelea LN, Parsa L, Dorrell D (2014) Automotive electric propulsion systems with reduced or no permanent magnets: an overview. IEEE Trans Ind Electron 61(10):5696–5711. https://doi.org/10.1109/TIE.2014.2301754.
2. Wu S, Zuo S, Zhang Y (2018) Optimization for electromagnetic noise reduction in claw pole alternator by rotor claw chamfering. IEEE Trans Ind Electron 65(12):9325–9335. https://doi.org/10.1109/TIE.2018.2815946.
3. Boldea I, Tutelea L, Popa A (2021) Claw-pole synchronous motors/generators (CP-SM/G) design and control: recent progress. In IEEE Journal of Emerging and Selected Topics in Power Electronics, pp 1–1. https://doi.org/10.1109/JESTPE.2021.3125044.
4. Cao Y, Zhu S, Yu J, Liu C (2022) Optimization design and performance evaluation of a hybrid excitation claw pole machine. Processes 10(3). https://doi.org/10.3390/pr10030541.
5. Tan-Kim A, Lanfranchi V, Vivier S, Legranger J, Palleschi F (2016) Vibro-acoustic simulation and optimization of a claw-pole alternator. IEEE Trans Ind Appl 52(5):3878–3885. https://doi.org/10.1109/TIA.2016.2582121.
6. Wu S, Zuo S (2018) Characteristics analysis of electromagnetic force and noise of claw pole alternators with different Pole and slot combinations and phase number. IET Electr Power Appl 12(9):1357–1364, 2018/11/01 https://doi.org/10.1049/iet-epa.2018.5127.
7. Wu S, Zuo S, Wu X, Lin F, Zhong H, Zhang Y (2017) Vibro-acoustic prediction and mechanism analysis of claw pole alternators. IEEE Trans Ind Electron 64(6):4463–4473. https://doi.org/10.1109/TIE.2016.2645502.
8. Eversman W, Burns S, Pekarek S, Bai H, Tichenor J (2005) Noise generation mechanisms in claw pole alternators. J Sound Vib 283(1):369–400, 2005/05/06/ https://doi.org/10.1016/j.jsv.2004.04.012.
9. Tan-Kim A, Lanfranchi V, Legranger J, Palleschi F, Redon M (2014, 2014 Sept 2–5) Influence of temperature on the vibro-acoustic behavior of claw-pole alternators. In 2014 International Conference on Electrical Machines (ICEM), pp 1628–1634). https://doi.org/10.1109/ICELMACH.2014.6960400.
10. Tan-Kim A et al. (2017) Influence of the manufacturing process of a claw-pole alternator on its stator shape and acoustic noise. IEEE Trans Ind Appl 53(5):4389–4395. https://doi.org/10.1109/TIA.2017.2708019.
11. Wu S (2021) Research on electromagnetic noise of claw pole alternators under stator winding interturn short circuit faults. IEEE Trans On Energy Convers 36(2):640–648. https://doi.org/10.1109/TEC.2020.2983187.
12. Liang X, Luy Y (2006) Harmonic analysis for induction motors. In 2006 Canadian Conference on Electrical and Computer Engineering, 7–10 May 2006, 172–177. https://doi.org/10.1109/CCECE.2006.277368.
13. Zhu ZQ, Lee B, Huang L, Chu W (2017) Contribution of current harmonics to average torque and torque ripple in switched reluctance machines. IEEE Trans Magn 53(3):1–9. https://doi.org/10.1109/TMAG.2016.2633477.
14. Lin F, Zuo S, Deng W, Wu S (2016) Modeling and analysis of electromagnetic force, vibration, and noise in permanent-magnet synchronous motor considering current harmonics. IEEE Trans Ind Electron 63(12):7455–7466. https://doi.org/10.1109/TIE.2016.2593683.
15. Hara T, Ajima T, Tanabe Y, Watanabe M, Hoshino K, Oyama K (2018) Analysis of vibration and noise in permanent magnet synchronous motors with distributed winding for the PWM method. IEEE Trans Ind Appl 54(6):6042–6049. https://doi.org/10.1109/TIA.2018.2847620.
16. Lu Y, Li J, Yang K (2022) A hybrid calculation method of electromagnetic vibration for electrical machines considering high-frequency current harmonics. IEEE Trans Ind Electron 69(10):10385–10395. https://doi.org/10.1109/TIE.2022.3152021.
17. Lu Y et al. (2018) Electromagnetic force and vibration analysis of permanent-magnet-assisted synchronous reluctance machines. IEEE Trans Ind Appl 54(5):4246–4256. https://doi.org/10.1109/TIA.2018.2837035.
18. Harries M, Hensgens M, Doncker RWD (2018) Noise reduction via harmonic current injection for concentrated-winding permanent magnet synchronous machines. In 2018 21st International Conference on Electrical Machines and Systems , 2018 Oct 7–10. (ICEMS), pp 1157–1162. https://doi.org/10.23919/ICEMS.2018.8549254.
19. Evestedt F, Perez-Loya JJ, Abrahamsson CJD, Lundin U (2021) Controlling airgap magnetic flux density harmonics in synchronous machines using field current injection. Electr Eng 103(1):195–203. https://doi.org/10.1007/s00202-020-01069-5.
20. Hollstegge P, Wanke A, Doncker RWD (2019) Noise mitigation in dual three-phase internal permanent magnet machines by injection of current harmonics. J Eng 2019(17):4273–4277. 2019/06/01 https://doi.org/10.1049/joe.2018.8223.
21. Kang L, Xia J, Su H, Li Z, Liu S (2022) On-line control strategy for radial vibration suppression of PMSM by multi-harmonic current injection method. IEEE Trans Ind Electron 69(9):8692–8704. https://doi.org/10.1109/TIE.2021.3106027.
22. Kurihara N, Chiba A, Yamada K, Souda A (2015) A relationship of radial force sum and current waveforms in switched reluctance motor for noise reduction. In 2015 IEEE Energy Conversion

Congress and Exposition (ECCE), pp 5560–5566. 2015 Sept 20–24. https://doi.org/10.1109/ECCE.2015.7310442.
23. Takiguchi M, Sugimoto H, Kurihara N, Chiba A (2015) Acoustic noise and vibration reduction of SRM by elimination of third harmonic component in sum of radial forces. IEEE Trans On Energy Convers 30(3):883–891. https://doi.org/10.1109/TEC.2015.2401398.
24. Gundogmus O, Sozer Y, Vadamodala L, Kutz J, Tylenda J, Wright RL (2019) Current harmonics injection method for simultaneous torque and radial force ripple mitigation to reduce acoustic noise and vibration in SRMs. In 2019 IEEE Energy Conversion Congress and Exposition (ECCE), 29, pp 7091–7097. Sept-3.Oct. 2019. https://doi.org/10.1109/ECCE.2019.8913056.
25. Gieras JF, Wang C, Lai J C (2006) Noise of polyphase electric motor. CRC Press, Boca Raton
26. Wu S, Chen S, He J, Huang Y, Yan X, Chen Z, Qi L (2023) Influence of stator teeth deformation on the electromagnetic force and acoustic noise of claw pole alternators. Electr Eng 105(5):3399–3410. https://doi.org/10.1007/s00202-023-01919-y.

Shuanglong Wu He was born in Meizhou, Guangdong, China, in 1990. He received the B.S.E. degree from South China University of Technology, Guangzhou, China, in 2013, and the Ph.D. degree from Tongji University, Shanghai, China, in 2018, both in vehicle engineering.In August 2018, he joined the GAC R&D left, Guangzhou Automobile Group Co. Ltd., as a New Energy NVH Engineer. In April 2021, he joined the College of Engineering, South China Agricultural University, Guangzhou, China, where he is currently an Associate Professor. His main research interests are the design and command of multiphysics electrical systems (electromagnetic, mechanical, and acoustic).

Xiangyu Yan He was born in Wuhu city, Anhui, China, in 1998. He received the B.S. degree in microelectronics engineering from University of Electronic Science and Technology, Chengdu, China, in 2020. He is currently working toward the M.S. degree in electronic and information engineering at South China Agricultural University, Guangzhou, China. His research interests include the electromagnetic vibration and noise of electric machines.

Junda Yang He was born in Guangzhou city, Guangdong, China, in 2000. He received the B.S. degree in agricultural mechanization and automation from South China Agricultural University, Guangzhou, China, in 2023. He is currently working toward the M.S. degree in agricultural machinery equipment engineering at South China Agricultural University, Guangzhou, China. His research interests include the analysis and control of electric machines.

Hailin Wang He was born in Zhangjiakou city, Hebei, China, in 1972. He received the B.S. and M.S. degrees in automotive engineering from Chang'an University, Xi'an, China, in 1994 and 1997, respectively, and the Ph.D. degree in mechanical and electronic engineering from Xi'an Jiaotong University, Xi'an, China, in 2000. From 2000 to 2001, He was a lecturer with the School of Mechanical Engineering, Xi'an Jiaotong University, Xi'an, China. He is currently the president of Guangdong Polytechnic of Science and Trade, Guangzhou, China. His research interests include vehicle system dynamics and control, and vibration and noise of electrical machines.

Hongmin Zhong He was born in Anhui, China, in 1992. He received the B.S.E. degree from Jilin University, Changchun, China, in 2014 and the M.S. degree from Tongji University, Shanghai, China, in 2017, both in vehicle engineering. In 2017, he joined the SAIC Motor Passenger Vehicle Co., Ltd., where he is currently an electrical machines engineer. His research interests include vibration and noise of electrical machines.

Caixia Lin She was born in Yangjiang, Guangdong, China, in 1976. She received the B.S. and M.S. degrees in automotive engineering from Chang'an University, Xi'an, China, in 2000 and 2003, respectively, and the Ph.D. degree in agricultural mechanization from South China Agricultural University, Guangzhou, China, in 2012. In July 2003, she joined the College of Engineering, South China Agricultural University, Guangzhou, China, where she is currently a lecturer. Her main research interest is the electric machine control.

证书号第7007294号

北京市海淀区地方税务局 印花税 代扣专用章 国家知识产权局

实用新型专利证书

实用新型名称：一种山地果园运输车可发电式轮边缓速装置

发　明　人：林彩霞；吴伟斌；姬兴；邱小倩；游展辉；张震邦；张成
杨晓彬；李泽艺；黎源鸿

专　利　号：ZL 2017 2 0990120.X

专利申请日：2017年08月09日

专利权人：华南农业大学

授权公告日：2018年02月23日

本实用新型经过本局依照中华人民共和国专利法进行初步审查，决定授予专利权，颁发本证书并在专利登记簿上予以登记。专利权自授权公告之日起生效。

本专利的专利权期限为十年，自申请日起算。专利权人应当依照专利法及其实施细则规定缴纳年费。本专利的年费应当在每年08月09日前缴纳。未按照规定缴纳年费的，专利权自应当缴纳年费期满之日起终止。

专利证书记载专利权登记时的法律状况。专利权的转移、质押、无效、终止、恢复和专利权人的姓名或名称、国籍、地址变更等事项记载在专利登记簿上。

局长
申长雨

中华人民共和国国家知识产权局

2018年02月23日

证书号第22822562号

专利公告信息

实用新型专利证书

实用新型名称：基于舵机驱动的曲柄滑块式末端执行器及茶叶采摘机器

专 利 权 人：华南农业大学

地　　址：510640 广东省广州市天河区五山路483号

发　明　人：林彩霞;叶子康;马登峰;刘梓帆;黄卓为;刘希玮;魏上凯

专　利　号：ZL 2024 2 1786165.1　　授权公告号：CN 222827706 U

专利申请日：2024年07月25日　　授权公告日：2025年05月06日

申请日时申请人：华南农业大学

申请日时发明人：林彩霞;叶子康;马登峰;刘梓帆;黄卓为;刘希玮;魏上凯

国家知识产权局依照中华人民共和国专利法进行审查，决定授予专利权，并予以公告。

专利权自授权公告之日起生效。专利权有效性及专利权人变更等法律信息以专利登记簿记载为准。

局长

申长雨

国家知识产权局

2025年05月06日

证书号第8459597号

专利公告信息

发明专利证书

发明名称：减速器变速工况轴承力预测方法、装置、设备及介质

专利权人：华南农业大学

地　　址：510640 广东省广州市天河区五山路483号

发 明 人：吴双龙;杨沄瑾;齐龙;林彩霞;黄昱燊;陈少涛;何继瀚
杨骏达

专　利　号：ZL 2024 1 0586508.8　　授权公告号：CN 118395597 B

专利申请日：2024年05月13日　　授权公告日：2025年11月11日

申请日时申请人：华南农业大学

申请日时发明人：吴双龙;杨沄瑾;齐龙;林彩霞;黄昱燊;陈少涛;何继瀚
杨骏达

国家知识产权局依照中华人民共和国专利法进行审查，决定授予专利权，并予以公告。

专利权自授权公告之日起生效。专利权有效性及专利权人变更等法律信息以专利登记簿记载为准。

局长
申长雨

国家知识产权局
2025年11月11日

荣誉证书

华南农业大学

卢育强 叶浩亮 杜庆炜 许逸枫 刘子豪 高华东 柯春平 同学：

你（们）的作品《非接触式轮边节能缓速器》在第七届广东大学生科技学术节之节能减排工业设计大赛中获得本科组优胜奖。

指导老师：林彩霞

特发此证，以资鼓励。

共青团广东省委员会　广东省教育厅　广东省科学技术厅　广东省学生联合会

二〇一三年六月

荣誉证书

高旭嵘、黄俊鹏、曾美琪、李晨、何廷凯、吴维浩、张颖同学:

你们队伍的作品《基于太阳追踪的变重心式山地果园运输车》在第十五届全国大学生节能减排社会实践与科技竞赛校内选拔赛中荣获

一等奖

指导老师：朱余清、林彩霞、曾志雄

特发此奖，以资鼓励

共青团华南农业大学委员会　华南农业大学工程学院

2022 年 5 月 25 日

荣誉证书

金宇轩、陈乐禧、温军、陈树斌、何乙杰同学：

你（们）的作品《同轴对转风送喷雾器的设计》在“菱朗杯”第九届广东省汽车与农机电子环保大赛中表现优异，荣获

三等奖

指导老师：林彩霞

特发此证，以资鼓励。

广东省电子学会 广东省汽车行业协会 广东省机械行业协会

广东省电子信息行业协会 广东省测量控制技术与装备应用促进会 广东省仪器仪表行业协会

2024 年 12 月 30 日

荣誉证书

HONORARY CREDENTIAL

林彩霞 同志：

被评为2013年华南农业大学工程学院“优秀班主任”。特发此证，以资鼓励。

华南农业大学工程学院党委

二〇一四年一月十四日

荣誉证书

林彩霞 同志：

被评为工程学院“十二五”工作先进个人，特发此证，以资鼓励。

华南农业大学工程学院

二〇一六年元月

荣誉证书

林彩霞 同志：

被评为华南农业大学“优秀共产党员”。

特发此证，以资鼓励。

中共华南农业大学委员会

二〇一九年六月

荣誉证书

林彩霞同志：

在华南农业大学工程学院庆祝建党100周年表彰中，被评为：

优秀共产党员

特发此证，以资鼓励。

中共华南农业大学工程学院委员会

2021年7月